DISSERTATION

HYDROTHERMAL SURFACE MODIFICATIONS ON TITANIUM FOR BIOMEDICAL APPLICATIONS

Submitted by

Vignesh K. Manivasagam

Department of Mechanical Engineering

In partial fulfillment of the requirements

For the Degree of Doctor of Philosophy

Colorado State Univerity

Fort Collins, Colorado

Spring 2023

Doctoral Committee:

Advisor: Ketul C. Popat

Kimberly Cox-York
Sampath Walajabad
Zhijie Wang

ABSTRACT

HYDROTHERMAL SURFACE MODIFICATIONS ON TITANIUM FOR BIOMEDICAL APPLICATIONS

Titanium and its alloys are widely used in different biomaterial applications due to their remarkable mechanical properties and bio-inertness. However, titanium-based materials still face some challenges, with an emphasis on hemocompatibility. Blood-contacting devices such as stents, heart valves, and circulatory devices are prone to thrombus formation, restenosis, and inflammation due to inappropriate blood–implant surface interactions. After implantation, when blood encounters these implant surfaces, a series of reactions takes place, such as protein adsorption, platelet adhesion and activation, and white blood cell complex formation as a defense mechanism. Currently, patients are prescribed anticoagulant drugs to prevent blood clotting, but these drugs can weaken their immune system and cause profound bleeding during injury. Extensive research has been done to modify the surface properties of titanium to enhance its hemocompatibility. Results have shown that the modification of surface morphology, roughness, and chemistry has been effective in reducing thrombus formation. A simple hydrothermal treatments with different acidic/basic medium were investigated in this dissertation. The first treatment with sodium hydroxide and the second treatment with sulfuric acid. Hemocompatability, cytocompatibility and antibacterial properties of these surfaces were investigated. The results indicated that sodium hydroxide surface is suitable for orthopedic application and sulfuric acid surface with silane coating is highly suitable for blood contacting implant surface.

ACKNOWLEDGEMENTS

First and foremost, I am extremely grateful to my advisor, Prof. Ketul C. Popat for his invaluable advice, continuous support, and patience during my PhD study. His insights and expertise have been instrumental in shaping my research and helping me develop as a scholar. I am deeply grateful for his encouragement, and belief in me. His approach towards research has encouraged me in all the time of my academic research and daily life. "Thank you, Professor Ketul, for everything".

Secondly, I would like to offer my sincerest gratitude to my committee members, Prof. Kimberely Cox-York, Prof. Sampath Walajabad and Prof. Zhijie Wang for their encouragement, support, and helpful insights. A special thanks to Prof. Harpreet Singh Arora, Prof. Prashanth Konda Gokuldoss and Prof. Paulo Soares for the opportunity to collaborate with them.

I would like to thank my lab mates for their assistance, friendship and for enriching this journey with great moments including Kirti Tiwari, Dr. Roberta Maia Sabino, Dr. Tara Wigmosta, Prem Kantam, Justin Gangwish, Abhishek Bhattacharjee, Aniruddha Savargaonkar, Sayudh Ghosh, James Michael, Harvinder Virk and Zachary Montgomerie.A special thanks to Brady Hine, Clark Yarbrough, and Yeilin Benitez for their great help in preparing our samples.

I would also like to thank Dr. Patrick McCurdy, Dr. Roy Geiss for their technical support/ training with microscopy/spectroscopy tools and Dr. Gopinath Perumal for his technical support with surface charaterization.

Finally, I would like to express my gratitude to my parents, and family.Without their tremendous understanding and encouragement in the past few years, it would be impossible for me to complete my PhD.

DEDICATION

This PhD Dissertation is dedicated to my parents

Mr. Manivasagam.K.S

and

Dr. Geetha Manivasagam

who have always believed in me and supported me in all my endeavors.

Thank you for your love and encouragement.

TABLE OF CONTENTS

ABSTRACT. ii

ACKNOWLEDGEMENTS. iii

DEDICATION. iv

OVERVIEW. 1

HYPOTHESIS AND SPECIFIC AIMS. 3

1 SURFACE MODIFICATION STRATERGIES TO IMPROVE TITANIUM HEMO-COMPATABILITY 5

1.1 Introduction 5

1.2 Titanium and titanium-based alloys 6

1.3 Hemocompatibility of titanium-based biomaterials 9

1.3.1 Blood-biomaterial surface interactions 10

1.3.2 Evaluation of hemocompatibility of titanium surfaces 13

1.4 Strategies for improving hemocompatibility of titanium-based implants 15

1.4.1 Surface properties and their influence in hemocompatibility 15

1.4.2 Surface modifications on titanium and titanium alloys 18

1.5 Conclusions and Future Perspectives 36

1.6 References 39

2 HEMOCOMPATABILITY OF HYDROTHERMALLY TREATED TITANIUM AND TITANIUM ALLOY SURFACES 54

2.1 Introduction 54

2.2 Materials and Methods 56

2.2.1 Fabrication of nanostructures on the different surfaces 56
2.2.2 Characterization of different surfaces. 57
2.2.3 Surface morphology 57
2.2.4 Contact angle measurements and surface energy calculations 57
2.2.5 Surface chemistry 58
2.2.6 Surface crystal structure 59
2.2.7 Surface preparation prior to biological studies 59
2.2.8 Protein adsorption on the different surfaces 59
2.2.9 Platelet-rich plasma (PRP) isolation from whole blood 60
2.2.10 Cytotoxicity of different surfaces 60
2.2.11 Fibrinogen binding from PRP on different surfaces 61
2.2.12 Cell adhesion on different surfaces 61
2.2.13 Identification of platelets and leukocytes adhered on different surfaces . . . 61
2.2.14 Platelet activation on different surfaces 62
2.2.15 Whole blood clotting on different surfaces 62
2.2.16 Statistical Analysis 63
2.3 Results and Discussion 63
2.4 Conclusion 82
2.5 References 84

3 IMPROVED HEMOCOMPATABILTY ON SUPERHEMOPHOBIC MICRO-NANO STRUCTURED TITANIUM SURFACES 92

3.1 Introduction 92
3.2 Materials and Methods 94
3.2.1 Fabrication of micro-nanoporous surfaces 94
3.2.2 Surface characterization 95
3.2.3 Surface preparation for hemocompatibility studies 95
3.2.4 Isolation of Platelet Rich Plasma (PRP) from human blood 95

3.2.5 Fibrinogen binding on different surfaces from PRP 96
3.2.6 Cell adhesion on different surfaces 96
3.2.7 Identification of platelet and WBCs on different surfaces 96
3.2.8 Platelet activation on different surfaces 97
3.2.9 Hemolysis of erythrocytes on different surfaces 97
3.2.10 Thrombin generation on different surfaces 98
3.2.11 Complement convertase on different surfaces 98
3.2.12 Whole blood clotting on different surfaces 98
3.2.13 Statistical Analysis 99
3.3 Results and discussion 99
3.4 Conclusions 110
3.5 References: 112

4 ENHANCED ANTIBACTERIAL PROPERTIES ON SUPERHYDROPHOBIC MICRO-NANO STRUCTURED TITANIUM SURFACE 116
4.1 Introduction 116
4.2 Materials and Methods 118
4.2.1 Fabrication of nanostructured topography and surface modification on titanium 118
4.2.2 Surface Characterization 119
4.2.3 Cytotoxicity of different surfaces 122
4.2.4 Bacteria culture 122
4.2.5 Bacteria growth inhibition by different surfaces 123
4.2.6 Bacteria adhesion and viability on different surfaces 123
4.2.7 Bacteria morphology 123
4.2.8 Statistical Analysis 124
4.3 Results and Discussion 124
4.4 Conclusion 141

4.5 References 142

5 CYTOCOMPATIBILITY OF HYDROTHERMALLY TREATED TITANAUM 151

5.1 Introduction 151

5.2 Materials and Methods 153

5.2.1 Fabrication of nanoporous titanium surfaces 153

5.2.2 Surface characterization 154

5.2.3 Adipose derived stem cell culture on different nanoporous surfaces 155

5.2.4 Cytotoxicity on different surfaces 156

5.2.5 Cell Viability on different surfaces 156

5.2.6 Cell adhesion and proliferation on different surfaces 157

5.2.7 Cell differentiation on different surfaces 158

5.2.8 Statistical Analysis 159

5.3 Results and Discussion 160

5.4 Conclusion 176

5.5 References 178

6 SELECTIVE IN-VITRO ENDOTHELIALIZATION ON HYDROTHERMALLY TREATED TITANIUM FOR CARDIOVASCULAR APPLICATION 188

6.1 Introduction 188

6.2 Materials and Methods 190

6.2.1 Fabrication of nanoporous structures on titanium surfaces 191

6.2.2 HUVEC and SMC culture 192

6.2.3 Cytocompatibility 192

6.2.4 Cell viability 193

6.2.5 Cell adhesion and Proliferation 193

6.2.6 Cell morphology 194

6.2.7 Cell differentiation 194

6.2.8 Statistical analysis 194
6.3 Results and Discussion 195
6.3.1 Endothelial cell interaction with modified surfaces 197
6.3.2 SMC toxicity interaction with modified surfaces 203
6.4 Conclusion 209
6.5 References 210

LIST OF TABLES

1.1 Hemocompatibility testing (adapted from ISO-10993-4:2002) [59] 14

2.1 Apparent Contact Angles of DI Water, Blood, and PRP on Different Surfaces. The values were rounded off to zero decimal places. There is a significant difference in the apparent contact angle ($p < 0.05$) between all surfaces except A1 and A3 and Ti and Ti3 (statistical differences are not shown in the table). 67
2.2 Advancing Contact Angle of DI Water and Hexadecane on All Surfaces. The values were rounded off to zero decimal places. There is a significant difference in surface energy ($p < 0.05$) between all surfaces except A1 and A3 and Ti and Ti3 68
2.3 XPS Elemental Composition Calculated from Survey Scans for Different Surfaces. 70
2.4 Statistical Comparison of Different Results on Unmodified and Modified Surfaces . 82

4.1 Advancing contact angle and surface energy of different surfaces. 127
4.2 Elemental composition of different surfaces obtained from the XPS survey scans . 128
4.3 Electrochemical corrosion parameter for different surfaces 132

5.1 XPS elemental composition calculated from the survey scans for different surfaces. 164
5.2 EDS elemental composition of the SEM images was calculated after 28 days of incubation. 175

LIST OF FIGURES

1.1 A) Thrombus formation around the heart valve frame and strut [9]. Reproduced with permission from ref. 9. Copyright 2016, Elsevier. Examples of HeartMate II device thrombosis [10]. B) Fibrin formation and C) Fibrin with thrombus formation. Reproduced with permission from ref. 10. Copyright 2014, Elsevier. . . 6
1.2 Crystal structure transformation of titanium [28]. Adapted with permission from ref. 28. Copyright 2013, Elsevier. 8
1.3 Schematic representation of medical device associated thrombosis [6]. The initial protein adsorption on the implant surface mediates all the subsequent phenomena. Reproduced with permission from ref. 6. Copyright 2019, Elsevier. 9
1.4 Platelet adhesion and activation on the biomaterial surface [57]. 13
1.5 Different strategies of surface modification on titanium-based surfaces to improve hemocompatibility. 19
1.6 A-B) SEM images of red blood cells on control surfaces and plasma oxidized surfaces at 280W for 30 mins, respectively [81]. SEM images indicating the interaction of platelets with C) titanium surfaces and D) oxygen PIII treated surfaces [85]. Reproduced with permission from ref. 85. Copyright 2016, Elsevier. 21
1.7 A) SEM images indicating surface morphology of hydrothermally treated nanograss surfaces. B-C) SEM images indicating platelet adhesion on control and nanograss Ti29Nb alloy surfaces, respectively [89]. Adapted with permission from ref. 89. Copyright 2020, Elsevier. D) SEM images indicating morphology of control and hydrothermally treated titanium surfaces, respectively. E-F) SEM images indicating platelets and leukocytes adhered on control and hydrothermally treated titanium surfaces, respectively [90]. 22
1.8 A) SEM images indicating surface morphology of zinc doped TiO_2 nanotubes. B-C) SEM images indicating platelet adhesion on control and zinc doped TiO_2 nanotubes, respectively [94]. Adapted with permission from ref. 94. Copyright 2020, American Chemical Society. D) SEM images indicating surface morphology of TiO_2 nanotube arrays anodized at 30V. E-F) SEM images indicating platelet adhesion on control and TiO_2 nanotube arrays (anodized at 30V) surfaces [95]. Adapted with permission from ref. 95. Copyright 2019, Elsevier. 24

1.9 A) SEM images indicating crater-like porous microstructure on the Ti-6Al-4V surface. B-C) SEM images indicating platelet adhesion on bare Ti-6Al-4V and superhydrophobic MAO+TFOS surfaces, respectively [100]. Adapted with permission from ref. 100. Copyright 2015, Elsevier. D) SEM image indicating superhydrophobic TiO_2 nanotube surfaces. E-F) SEM images indicating platelet adhesion on bare TiO_2 nanotube surface and PTES modified superhydrophobic surfaces, respectively, after 120 mins exposure [102]. Adapted with permission from ref. 102. Copyright 2010, Elsevier. G) SEM image indicating multifunctional 3D micro-nanostructures on the nickel-titanium surface. H-I) SEM images indicating platelet adhesion on pristine nickel-titanium surface and superhydrophobic multifunctional 3D micro-nanostructured surface [103]. Adapted with permission from ref. 103. Copyright 2020, American Chemical Society. J) SEM images indicating nano-flowered surfaces. K-L) SEM images indicating platelet adhesion on non-textured titanium and superhemophobic nanoflower titanium surfaces [104]. Adapted with permission from ref. 104. Copyright 2016, Wiley-VCH. 28

1.10 A) SEM image indicating surface microtopography of titanium surface modified with PTL/heparin. B-C) Fluorescence images indicating adhesion of platelets on bare titanium and titanium modified with PTL/heparin, respectively [119]. Adapted with permission from ref. 119. Copyright 2019, Elsevier. D) SEM images indicating morphology of titanium surfaces modified with heparin/chitosan. E-F) SEM images indicating platelet adhesion on titanium and titanium surfaces modified with heparin/chitosan, respectively [111]. Adapted with permission from ref. 111. Copyright 2018, Elsevier. G) SEM image indicating titania nanotube surfaces modified with tanfloc/heparin polyelectrolyte multilayers. H-I) SEM images indicating platelet adhesion on unmodified titania nanotube surfaces and titania nanotube surfaces modified with tanfloc/heparin, respectively [109]. Adapted with permission from ref. 109. Copyright 2020, Wiley-VCH. J-L) SEM images indicating platelet adhesion on pristine titanium, TA/SS 1, and TA/SS 2 coated surfaces – 1 and 2 indicating different volume ratios [125]. Adapted with permission from ref. 125. Copyright 2020, Elsevier. M-O) SEM images indicating platelet adhesion on non-treated, tannic acid-treated, and ulvan-coated Ti/TiO_2 surfaces, respectively [127]. Adapted with permission from ref. 127. Copyright 2020, Elsevier. 32

1.11 A-C) SEM images indicating TiO_2 NT, TiO_2 NT+PEM and TiO_2 NT+PEM+NO surfaces. D-G) SEM images indicating adhered cells on bare titanium, TiO, TiO_2 NT, TiO, TiO_2 NT+PEM and TiO, TiO_2 NT+PEM+NO surfaces [134]. Adapted with permission from ref. 134. Copyright 2017, American Chemical Society. H-J) SEM images indicating surface morphology of HA micro-patterned titanium surfaces modified with EC-ECM (ECMEC/HAP), SMC-ECM (ECMSMC/HAP), and modified by both SMC-ECM and EC-ECM (ECMSMC/EC/HAP) respectively [136]. K-N) SEM images indicating platelet adhesion on respective surfaces [136]. O-R) Fluorescence images indicating growth of HUVEC cells after 3 days on respective surfaces [136]. 35

1.12 (A - B) SEM images showing the surface morphology of rutile TiO_2 nanorod arrays (TNA).139 (C) SEM images showing the surface morphology of the ZrN film. (D and E) SEM images showing platelet adhesion on nickel–titanium SMA and ZrN film surfaces, respectively.141 Adapted with permission from ref. 141. Copyright 2010, Elsevier. 36

2.1 Representative SEM images of Ti and A surfaces treated by hydrothermal treatment. Images were taken at two different magnification (500X and 15000X). 66
2.2 XPS Survey scans for different surfaces. 69
2.3 XPS High resolution O1s scans for different surfaces. 71
2.4 XRD scans for different surfaces. 72
2.5 Fibrinogen adsorption on different surfaces measured using Micro BCA assay. The results indicate significantly lower fibrinogen adsorption on Ti2 compared to all the other surfaces ($* \rightarrow p < 0.05$) Other statistical differences are included in Table 4. Error bar represent standard deviation. (b) Albumin adsorption on different surfaces measured using Micro BCA assay. The results indicate significantly lower albumin adsorption on Ti2 compared to all the other surfaces ($* \rightarrow p < 0.05$). Error bar represent standard deviation. 74
2.6 Cell cytotoxicity for PRP exposed to different surfaces measured using LDH assay. The results indicate no significant differences in LDH activity on all the surfaces and positive control (100% live cells), whereas, the LDH activity for negative control (100% dead cells) was significantly different than all the other surfaces ($* \rightarrow p < 0.05$)). Error bar represent standard deviation. 75
2.7 Fibrinogen binding from PRP on different surfaces measured using ELISA. The results indicate significant reduction in fibrinogen binding on Ti2 when compared to all the surfaces except Ti1 ($* \rightarrow p < 0.05$)). Other statistical differences are included in Table 4. Error bar represent standard deviation. 76
2.8 Representative fluorescence microscope images of adhered live cells (platelets and leukocytes) stained with Calcein-AM stain on different surfaces. The results indicate lower cell adhesion on all modified surfaces when compared to unmodified surfaces. 77
2.9 Percentage of area covered by the cells adhered on the surface calculated using ImageJ. The results indicate significantly lower cell adhesion on all modified surfaces when compared to unmodified surfaces ($* \rightarrow p < 0.05$)). Other statistical differences are included in Table 4. Error bar represent standard deviation. 77

2.10 (a) Representative fluorescence microscope images of adhered platelets and leukocytes stained with DAPI and rhodamine-phalloidin on different surfaces. The results indicate lower cell adhesion on all modified surfaces when compared to unmodified surfaces.(b) Percentage of area covered by the cells adhered on the surface stained with DAPI calculated using ImageJ. The results indicate significantly lower cell adhesion on all modified surfaces when compared to unmodified surfaces ($* \rightarrow p < 0.05$)), except Ti3 ($\# \rightarrow p < 0.05$)). Error bar represent standard deviation. (c) Percentage of area covered by the cells adhered on the surface stained with rhodamine-phalloidin calculated using ImageJ. The results indicate significantly lower cell adhesion on all modified surfaces when compared to unmodified surfaces ($* \rightarrow p < 0.05$)). Other statistical differences are included in Table 1.4. Error bar represent standard deviation. 79
2.11 Representative SEM images of adhered platelets and leukocytes on different surfaces. Images show a higher degree of platelet activation and platelet-leukocyte complex formation on unmodified surfaces when compared to modified surface. Images were taken at two different magnification (500X and 15000X) 80
2.12 Whole blood clotting on different surfaces for up to 45 mins. The dotted line represents the absorbance of free hemoglobin in un-clotted blood. Statistics not shown in the graph. There is a significant increase in free hemoglobin present on all modified surfaces when compared to the unmodified surface at respective time interval. Ti2 has the highest free hemoglobin after 45 mins compared to all surfaces. Other statistical differences for 45 min study are included in Table 2.4. Error bar represent standard deviation. 81

3.1 a) Representative SEM images of different surfaces. Images were taken at 500X, and image inserts depict 5000X magnification. b) Apparent contact angle measurements using Milli-Q water, PRP, blood on different surfaces. c) XRD intensity peaks of different surfaces. (nmin = 9). 100
3.2 Fibrinogen adsorption from PRP on different surfaces measured using a microplate reader. ($^*p < 0.05$). (nmin = 9). 102
3.3 a) Fluorescence images of adhered live cells adhered (platelets and WBCs) on different surfaces. b) Percentage area covered by adhered platelets and WBCs on different surfaces. c) Fluorescence images of adhered platelets(red) and WBCs(purple) on different surfaces. d) Percentage of the areas covered by adhered platelets(red) on dif-ferent surfaces. e) Percentage area covered by adhered WBCs(blue) on different sur-faces. ($^*p < 0.05$). (nmin = 9). 104
3.4 Representative SEM images of adhered platelets and WBCs (purple – photoshop for better visibility) on different surfaces. Images were taken at 500X, and 2000X magnification. (nmin = 9). 106
3.5 Hemoglobin release from erythrocytes solution incubated with different sur-faces was measured using a microplate reader. (nmin = 9). 107
3.6 Highest thrombin generation velocity of plasma incubated with different surfaces between two points. (nmin = 9). 108

3.7 Complement activation of plasma incubated with different surfaces was measured as activation of complement convertase C5a. The lines indicate the regions of inactive/low (0.2), medium (>0.2 0.6), and high (>0.6) reactivity. (nmin = 9). . . . 108
3.8 Whole blood clotting on different surfaces for up to 45 min. The dotted line represents the absorbance of free hemoglobin in un-clotted blood. ($^{*}p < 0.05$ (nmin = 9). 109

4.1 SEM observation of different surfaces. Images were taken at two magnifications (500x and 5000x). 126
4.2 Apparent contact angle measurements using the sessile drop method for different surfaces. The results indicate significantly higher contact angle on nTi-S compared to other surfaces (*p < 0.05). The error bar represents the standard deviation. . . . 127
4.3 A) XPS survey scans of different surfaces. B)High resolution XPS scan for carbon peaks on different surfaces 129
4.4 Cyclic polarization curves for different surfaces. Potentiodynamic polarization tests was done on at least three different substrates of each surface (nmin = 3) . . . 130
4.5 Nyquist plot and Bode plot for different surfaces. Equivalent electrical circuit for two different cases 132
4.6 Mott Schottky curves of different surfaces 134
4.7 Cell cytotoxicity of PRP exposed different surfaces measured using the LDH assay. *p < .05 indicates statistical significance. The error bar represents the standard deviation. Cell cytotoxicity tests was done on at least six different substrates of each surface (n_{min} = 6) 135
4.8 Inhibition of Staphylococcus aureus and Escherichia coli growth in the media by different surfaces. *p < .05 indicates statistical significance, p > .05 indicates no statistical significance. The error bar represents the standard deviation. Bacterial inhibition studies was done on at least nine different substrates of each surface (n_{min} = 9) 136
4.9 (A) Fluorescence images of adhered Staphylococcus aureus live(green) and dead(red) bacteria on different surfaces. Insert images depict higher magnification. (B) Percentage of the areas covered by the live bacteria cells adhered on different surfaces. (C) Percentage of the areas covered by the dead bacteria cells adhered on different surfaces. *p < .05 indicates statistical significance. The error bar represents the standard deviation. Bacterial adhesion and proliferation studies were done on at least nine different substrates of each surface (n_{min} = 9) 138
4.10 (A) Fluorescence images of adhered Escherichia coli live(green) and dead(red) bacteria on different surfaces. Insert images depict higher magnification. (B) Percentage of the areas covered by the live bacteria cells adhered on different surfaces. (C) Percentage of the areas covered by the dead bacteria cells adhered on different surfaces. *p < .05 indicates statistical significance. The error bar represents the standard deviation. Bacterial adhesion and proliferation studies were done on at least 9 different substrates of each surface (n_{min} = 9) 139

5.1 Representative SEM images of the developed surface morphology after hydrothermal treatment. The images were taken at 500X and 10, 000X magnification. 162

5.2 Apparent contact angles measured with DI water on different surfaces. The result indicates that the modified surfaces are significantly hydrophilic compared to Ti ($*p < 0.05$). The error bar represents the standard deviation. 163
5.3 XPS survey scans for different surfaces. Survey spectra were collected from 0 to 1100 eV with a pass energy of 187.85 eV. 164
5.4 XRD scans for different surfaces. XRD scans were collected at θ = 1.5° and 2θ ranges were chosen based on significant peak intensities. 165
5.5 Cell cytotoxicity for ADSCs exposed to different surfaces measured using the LDH assay. The results indicate no significant differences in the LDH activity on all of the surfaces and positive control (100% live cells), whereas the LDH activity for the negative control (100% dead cells) was significantly different than other surfaces ($*p < 0.05$). The error bar represents the standard deviation. 167
5.6 Cell viability of ADSCs exposed to different surfaces measured using Cell-Titer assay. The results indicate no significant differences in the cell viability on all the surfaces. The error bar represents the standard deviation. 168
5.7 (a) Representative fluorescence microscope images of ADSCs stained with DAPI and rhodamine phalloidin on different surfaces. The results indicate cell adhesion and proliferation on all surfaces. (b) Number of cells adhered to the surface stained with DAPI calculated using ImageJ. The results indicate no significant differences in the cell viability on all the surfaces. The error bar represents the standard deviation. 169
5.8 Representative SEM images of adhered cell on different surfaces. Images show a higher cell spreading on Ti_{NaOH} surfaces when compared to other surfaces. Images were taken at 1000X magnifications. 171
5.9 ALP activity of different surfaces was quantified and normalized by total protein content. ALP and BCA assays were performed after 14 and 28 days of culture. . . . 172
5.10 Calcium deposition by ADSCs on different surfaces was quantified and normalized by total protein content. Calcium and BCA assays were performed after 14 and 28 days of culture. The results indicate Ti_{NaOH} surface has higher calcium deposition compared to other surfaces ($*p < 0.05$). The error bar represents the standard deviation. 173
5.11 (a) Representative fluorescence microscope images of ADSCs along with osteocalcin stained with FITC, DAPI and rhodamine phalloidin on different surfaces. The results indicate cell proliferation and osteocalcin expression (green stain) on all surfaces. (b) Percentage area coverage of osteocalcin normalized by number of nuclei after 14 and 28 days of culture. Number of cells adhered to the surface stained with DAPI calculated using ImageJ. The area covered by osteocalcin expression was calculated using ImageJ. The results indicate significant differences on both modified surfaces ($*p < 0.05$) after 28 days of incubation. The error bar represents the standard deviation. 175
5.12 Representative SEM images of adhered cell on different surfaces after 14 and 28 days of incubation. Images were taken at 500X magnifications. 176

6.1 FESEM Images of polished and modified surfaces at two different magnification. . 196
6.2 Advancing contact angle of different surfaces. The error bar represents the standard deviation. (*p < 0.05). 197

6.3 Cell cytotoxicity for HUVECs exposed to different surfaces after 24 hrs measured using the LDH assay. The error bar represents the standard deviation. (*p < 0.05) . 198
6.4 Cell viability for HUVECs exposed to different surfaces measured after day 1,3 and 5 using the cell viability assay. The error bar represents the standard deviation. (*p < 0.05) 199
6.5 a)Fluorescence microscope images HUVECs stained with DAPI and rhodamine–phalloidin on different surfaces after day 1,3 and 5 of incubation. b) Percentage area coverage of cells on different surfaces after 1,3 and 5 of incubation. c) Number of cells adhered to the surface stained with DAPI calculated using ImageJ. The error bar represents the standard deviation. (*p < 0.05) 201
6.6 SEM images of adhered cells on different surfaces after day 1,3 and 5 of incubation. Images were taken at 1000× magnifications. 202
6.7 a) Fluorescence microscope images of HUVECs along with VE-Cadherin after day 5,7 and 10 of incubation. (b) Fluorescence microscope images of HUVECs along with vWF after day 5,7 and 10 of incubation.. (c) Percentage area coverage of VE-cadherin after day 5,7 and 10 of incubation. (d) Percentage area coverage of vWF after day 5,7 and 10 of incubation. 204
6.8 Cell cytotoxicity for SMCs exposed to different surfaces after 24 hrs measured using the LDH assay. The error bar represents the standard deviation. 205
6.9 Cell viability for SMCs exposed to different surfaces measured after day 1,3 and 5 using the cell viability assay. The error bar represents the standard deviation. . . . 205
6.10 a)Fluorescence microscope images SMCs stained with DAPI and rhodamine–phalloidin on different surfaces after day 1,3 and 5 of incubation. b) Percentage area coverage of cells on different surfaces after 1,3 and 5 of incubation. c) Number of cells adhered to the surface stained with DAPI calculated using ImageJ. The error bar represents the standard deviation. (*p < 0.05) 206
6.11 SEM images of adhered cells on different surfaces after day 1,3 and 5 of incubation. Images were taken at 1000× magnifications. 207
6.12 a) Fluorescence microscope images of SMCs along with calponin after day 5,7 and 10 of incubation. b) Fluorescence microscope images of SMCs along with MYH after day 5,7 and 10 of incubation. (c) Percentage area coverage of calponin after day 5,7 and 10 of incubation. (d) Percentage area coverage of MYH after day 5,7 and 10 of incubation. 208

OVERVIEW

Titanium is a highly valued material in the field of orthopedics and cardiovascular implants due to its excellent bulk properties such as strength, biocompatibility, and corrosion resistance. Orthopedic implants such as hip and knee replacements are commonly made from titanium alloys, as the material can withstand stress and corrosion in a body environment. In the field of cardiovascular implant, titanium is widely used for stents, heart valves and other implantable devices due to its ability to resist corrosion and maintain structural integrity in the body. Additionally, titanium is a non-toxic and non-allergenic metal.However, there are several clinical challenges associated with the use of titanium implants. One of the main challenges is the risk of implant failure or rejection. Titanium is a strong and biocompatible material, but its polished/plain surface is not biocompatible, and there is a risk of implant failure due to bacterial infection, thrombus formation, or absence of osseointegration. Hence, there is a critical need to develop surface modified titanium implants.

Biomaterial interaction with the biological environment is directly influenced by its surface characteristics, such as its chemical composition, topography, and wettability. Studies have shown that modifying the surface of a biomaterial to the micro and nanoscale can improve the cellular response and hemocompatability. This is because cells in the body naturally interact with nanoscale extracellular matrix elements such as proteins and minerals. Thus a biomaterial's nanoscale topography can affect protein adsorption and cell adhesion. Research has shown that surface treatment of titanium using hydrothermal etching leads to the formation of micro/nano topography, enhance the biocompatibility by increasing cell adhesion and differentiation, resistance to bacterial adhesion, and prevents blood clotting.

Research has shown that nanofibrous hydrophilic surface on titanium developed using hydrothermal treatment can improve the biocompatibility of the implants. Nanofibrous hydrophilic surface can reduce thrombogenic effect of the implant by reducing available surface area of contact for cell and platelet to adhere, which can decrease the formation of blood clots and prevent thrombus formation on the surface of the implant. Nanofibrous hydrophilic titanium also mimic

the structure of bone tissue and can be used as scaffold for bone tissue engineering, promoting the cell adhesion, proliferation and differentiation. Further, hydrophilic surface can also promote the osteoblast (bone-forming cells) function and reduce the osteoclast (bone-resorbing cells) activity, which can improve the bone healing and repair.

In the other end of wettability spectrum, studies have shown superhydrophobic surface on an implant can also have several advantages. One of the main advantages is that it can reduce the risk of blood clotting and infection. Superhydrophobic surfaces are highly resistant to the attachment of platelets and leukocytes, and growth of bacteria. Hence, there is a significant reduction of platelet-leukocyte complex formation leading to less blood clotting and bacterial biofilm formation. Thus, topography and wettability plays a significant role on the biocompatability of an implant.

In this dissertation, two different surface modification on titanium using hydrothermal treatment is explored for orthopedic and cardiovascular application. Superhyrophilic nanofibrous titanium surface was developed using hydrothermal treatment with sodium hydroxide. Results showed that the surface reduced thrombus formation. The cytocompatibility studies using ADSC revealed that this surface promoted cell spreading, differentiation, and bone tissue formations thus demonstrating the feasibility of utilizing these treatments for orthopedic applications. Superhyrophobic microscale planar structure with nanopits titanium surface was developed using hydrothermal treatment with sulfuric acid and vapor phase silanization. Results showed that surface prevented platelet adhesion and activation, as well as bacterial adhesion. This behavior was attributed to the formation of micro-nano structures with the coating of low energy silane preventing liquid interaction. Additionally, these samples displayed high resistance to corrosion. Therefore, the saline treatment method is considered promising for use in blood-contacting devices made of titanium. Further this micro-nano titanium surface also showed to selectively prevent smooth muscle cell adhesion and promote endothelization compared to nanofibrous titanium and unmodified titanium.

HYPOTHESIS AND SPECIFIC AIMS

Hypothesis: Specific morphological and chemical modifications on titanium surface improve the biocompatibility/hemocompatability properties of implants surfaces, such as preventing thrombus formation and bacterial infection, as well as promoting cell adhesion and differentiation on the surface.

Specific Aim 1: The main aim of the study is to identify and develop a facile surface modification on Ti based materials to understand blood-material interaction and reduce the blood clotting on the surface and enhance the service period of an cardiovascular implant. This research is discussed in Chapters 2.

- Evaluation and optimization of hydrothermal treatment on CpTi and Ti-6Al-4V at different concentrations of NaOH (Alkali), solution temperature and duration and investigate the effect of the treatment parameters on various surface features of Ti.
- Evaluation the effect of hydrothermal treatment on wettability, oxidation and phase formation on the surface of the modified CpTi and Ti-6Al-4V.
- Evaluation of the protein adhesion, cytotoxicity, platelet adhesion and activation, Leukocyte adhesion and leukocyte-platelet complex formation and whole blood clotting.

Specific Aim 2: The main aim of this study is to investigate the hemocompatbility and anibacterial potential of the superhydrophbic sulfuric acid surface for cardiovascular implant application. This research is discussed in Chapter 3 and 4.

- Evaluation of bacterial adhesion and proliferation on the surfaces after 6 hrs and 24 hrs of bacterial incubation using fluorescence microscopy.
- Evaluation of bacterial morphology and biofilm formation on the surfaces after 6 hrs and 24 hrs of bacterial incubation using scanning electron microscopy.

- Fabrication of superhemophobic surfaces and characterization of surface chemistry, morphology, and wettability.
- Evaluation of the protein adsorption, hemolysis, complement convertase, and whole blood clotting on superhemophobic surfaces.

Specific Aim 3: The main aim of this study is to investigate the optimal sodium hydroxide surface and sulfuric acid surface for adipose-derived stem cell adhesion, proliferation and differentiation for orthopedic implant applications. This research is discussed in Chapters 5

- Evaluation of adipose-derived stem cell viability, adhesion and proliferation on the surfaces after 4 and 7 days of cell culture using CellTiter-Blue assay, fluorescence microscopy, and scanning electron microscopy.
- Evaluation of adipose-derived stem cell differentiation on the surfaces after 1 and 3 weeks of induced osteogenesis via total protein content assay, alkaline phosphatase (ALP) activity, calcium concentration, fluorescence microscopy, and scanning electron microscopy.

Specific Aim 4: The main aim of this study is to investigate the endothelialization potential of the superhemophobic NT surfaces and the NT surfaces modified with PEMs for cardiovascular implant applications. This research is discussed in Chapter 6.

- Evaluation of endothelial cell viability, adhesion, proliferation, and differentiation on different NT surfaces using CellTiter-Blue assay, scanning electron microscopy, fluorescence microscopy, and immunofluorescent staining,
- Evaluation of smooth muscle cell viability, adhesion, proliferation, and differentiation on different NT surfaces using CellTiter-Blue assay, scanning electron microscopy, fluorescence microscopy, and immunofluorescent staining

CHAPTER 1: SURFACE MODIFICATION STRATEGIES TO IMPROVE TITANIUM HEMOCOMPATABILITY[1]

1.1 Introduction

Titanium and its alloys have been widely used in blood-contacting devices, such as intra-osseous implants, prosthetic heart valves, cardiovascular stents, and circulatory assist devices [2]. However, improper implant surface interaction with blood are prone to cause to thrombosis, and this is a major complication that can lead to the device failure and other serious complications [3]. Thrombosis is an acute syndrome where the blood clots on the implant surface and, once the clotting cascade begins, it spreads rapidly, which can also increase the chances of mortality [4]. To prevent that, patients are prescribed blood thinners such as aspirin, vorapaxar, etc. [5]. However, overuse of these medications can weaken the immune system and, during injuries, there is profound bleeding of blood [6].

Thrombosis is initiated due to the contact of blood to a foreign surface, such as a metal implant surface, and it starts by the adsorption of blood proteins onto the biomaterial surface, which can lead to a series of complex reactions that ultimately form the thrombus [7]. Studies have shown that there can be thrombus formation and pannus growth in the base of the heart valve struts and apex of the cage, which leads to stenosis, and there was no central flow, which can damage the blood cells (**Figure 1.1A**) [8,9]. Another medical device that is usually made of titanium is left ventricular assisted device (LVAD), a mechanical pump that is implanted in a human's chest to assist weakened heart. The major limitation with these devices is thromboembolism, bleeding, hemolysis, infection, and renal failure. A case study on patients using Heart Mate II showed that 11% of the studied patients had thrombus formation in less than one year after implantation (**Figure 1.1B-C**) [10]. Infection was also commonly found due to thrombus formation [10].

[1]This work was published in RCS and is reproduced in modified form here with permission

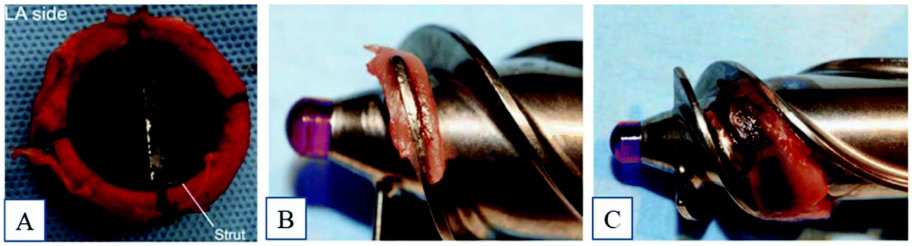

Figure 1.1: A) Thrombus formation around the heart valve frame and strut [9]. Reproduced with permission from ref. 9. Copyright 2016, Elsevier. Examples of HeartMate II device thrombosis [10]. B) Fibrin formation and C) Fibrin with thrombus formation. Reproduced with permission from ref. 10. Copyright 2014, Elsevier.

In recent years, efforts have been undertaken to reduce the thrombogenicity of biomaterials and therefore prevent these complications [11]. The thrombogenicity of a material is direct related to its surface properties and it can be influenced by modifying the surface characteristics such as topography, chemistry, charge, and mechanical properties [12,13]. Therefore, many research groups are focusing on modifying the titanium surfaces to improve its hemocompatibility and prevent failure of blood-contacting implants. The aim of this chapter is to provide an overview of surface modification strategies that are being applied to improve the blood-surface interaction of titanium-based materials. The chapter begins by highlighting the titanium properties (**Section 1.2**) and how its surface interacts with blood and its components (**Section 1.3**). Then, **Section 1.4** underlines the current progress in surface modification techniques on titanium to enhance its hemocompatibility. Finally, **Section 1.5** concludes the present research work and proposes scopes for future research.

1.2 Titanium and titanium-based alloys

Titanium-based implants have been largely used for biomedical applications due to their excellent mechanical properties, corrosion resistance, and great biocompatibility [14,15]. Titanium has replaced other implant materials such as stainless steel and cobalt-chromium mainly because it has the highest strength-density ratio when compared to all metals, which makes it a lightweight

implant for the required strength [16]. In addition, titanium can have its properties easily modified by forming alloys, making it suitable for a wide range of biomedical applications [17,18].

Titanium is also well accepted by different body tissues without inducing any negative hypersensitivity, toxicity to the cells, or inflammatory reactions [19–21]. This inert characteristics of titanium is due to its low electrical conductivity [22]. Clinically it has been shown that the body fluids are highly corrosive and many metals like stainless steel, magnesium and chromium-cobalt are degraded quickly due to pitting or fretting corrosion inside human body [23]. However, metals like titanium oxidizes easily, forming a stable thin passivating layer which is self-limiting and protects the implant from further oxidization [24]. These titanium oxide layers are formed at very fast rate when exposed to moisture in air or water and are usually few nanometers thick [25]. This oxide layer is shown to be more biologically inert because of its less reactive nature when compared to the $\alpha-$ Ti [26]. Titanium (Ti) is an allotropic metal [27]. Titanium along with its alloys are classified as α (low-temperature), $\alpha+\beta$, and β (high-temperature), based on the crystal structures present in the substrate. $\alpha-$ Ti is equated to hexagonal closed pack (HCP) structure, which makes the alloy stronger, high fracture toughness and low forgeability [28]. In contrast, β-Ti is when the HCP structure is transformed to body centered cube (BCC) structure, which makes the metal more ductile (**Figure 1.2**). The temperature at which titanium gets converted from HCP to BCC is 882°C and this is called beta transus temperature. There are many alloying agents that can change the stabilizing temperature, and based on the application, one can change the proportion of α stabilizing elements (O, Al, N, C) and β stabilizing elements (V, Nb, Mo, Ta, Fe, Mn, Cr, Co, Ni, Cu, Si, H). Addition of alloying agents to pure titanium changes the phase transformation temperatures and stability of alpha and beta phases. The volume fractions, size, and morphology of the α and β phases is changed to produce Ti alloys superplastically formable with the potential to design unitized structures for significant weight reduction [29]. This aspect of Ti alloys makes it easy to modify the mechanical properties based on the application. Ti-6Al-4V is a $\alpha+\beta$ alloy that is ductile and stronger than α type Ti alloy or β type Ti alloy. It is important to have both strength and ductility for implants as that will give them long life under the fatigue conditions [30].

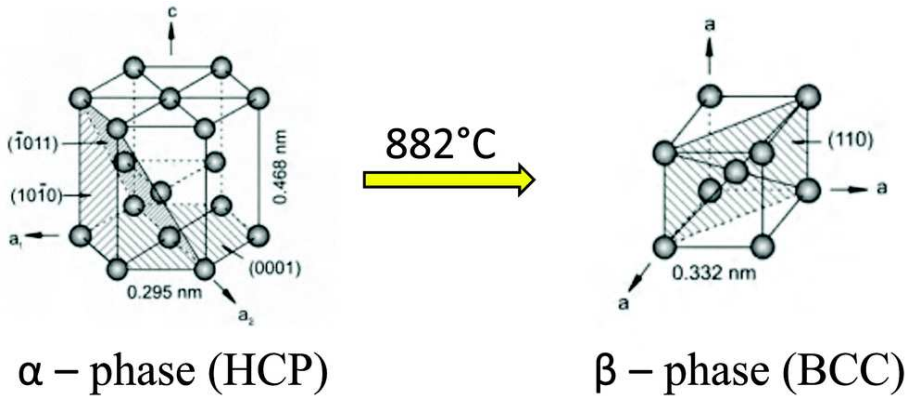

Figure 1.2: Crystal structure transformation of titanium [28]. Adapted with permission from ref. 28. Copyright 2013, Elsevier.

Titanium is often used for medical application in its pure form or with alloying agents such as vanadium, aluminum, tantalum, nickel, and zirconium [31]. There are four different grades of commercially pure titanium (cpTi) according to the ASTM standards, and these are based on the amounts of oxygen, nitrogen, hydrogen, iron, and carbon during the purification procedures [32]. Among various titanium and its alloys, the mainly used materials in the biomedical field are cpTi (Grade 2), nickel-titanium and Ti-6Al-4V alloy because of their excellent corrosion resistance, low modulus of elasticity, good biocompatibility and high strength [31]. Nickel-titanium alloy has received great attention due to its shape memory feature, which makes it suitable for self-expanding stents. Even though titanium has outstanding properties required for applications in blood-contacting implants, there are still some complications caused by its surface, such as thrombosis and restenosis [33]. Titanium surface has shown to be highly modifiable at both micro and nano level with simple techniques such as laser treatment, anodization, and hydrothermal treatment, and several studies have shown that these modification can improve biocompatibility [20,34,35]. Therefore, recent research has focused on tuning different surface modification strategies on titanium and titanium alloys to improve the biomaterial interaction with blood and its components, thus enhancing their hemocompatibility.

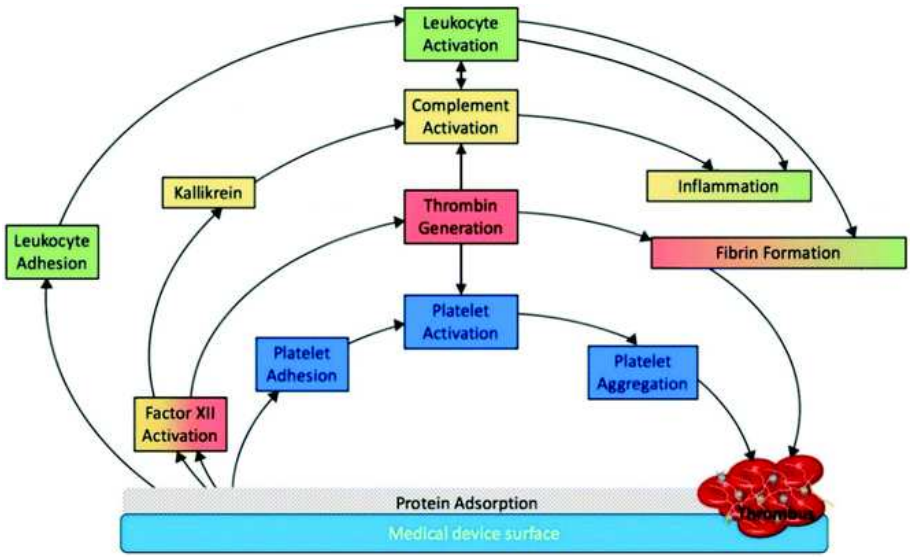

Figure 1.3: Schematic representation of medical device associated thrombosis [6]. The initial protein adsorption on the implant surface mediates all the subsequent phenomena. Reproduced with permission from ref. 6. Copyright 2019, Elsevier.

1.3 Hemocompatibility of titanium-based biomaterials

Hemocompatibility (i.e. blood compatibility) is an essential characteristic for any biomaterial used for blood-contacting medical devices [36]. Blood compatibility is the ability of a material to keep under control the thrombotic and inflammatory responses induced by the foreign surface when in contact with blood [37,38]. These responses correspond to a series of interconnected events that happen on the surface as shown in **Figure 1.3**. Since the interaction between implant and blood happens only on the implant surface, intensive research has been carried out to develop novel surfaces that are hemocompatible. Modifying the device's surface is effective because it can prevent the blood reactions without altering the favorable bulk material properties [39].

1.3.1 Blood-biomaterial surface interactions

Protein adsorption

When blood comes in contact with a biomaterial surface, the first event that happens is the adsorption of blood plasma proteins [40]. These blood proteins rapidly form a layer on the biomaterial surface that have a thickness of 2-10 nm and a concentration of proteins that is 1000-fold higher than in blood plasma [41]. This mechanism of protein adsorption is complex and dynamic, and involves electrostatic interactions, van der Waals, and hydrogen bonding [42]. The composition and concentration of adsorbed proteins depends on the physical and chemical properties of the surface and they might change over time, which is known as the "Vroman effect" [43]. Vroman effect is a reversible process where the early adsorbed proteins are replaced by proteins that possess higher surface affinity and usually are in relative lower concentration in blood [44]. These proteins, once adsorbed to the artificial surface, mediate all the subsequent reactions, such as adhesion and activation of platelets, thrombin generation, complement activation, and adhesion of leukocytes and red blood cells (**Figure 1.3**) [4]. The most abundant proteins in plasma are albumin, immunoglobulins, and fibrinogen [45]. Fibrinogen is a central protein in the coagulation cascade and one of the first to adsorb on biomaterials [46]. Once adsorbed to the artificial surface, it is responsible for platelet and leukocyte adhesion and activation [37]. Albumin is generally considered to be inert toward thrombosis, although some studies have shown that platelets and leukocytes can adhere to adsorbed albumin layers [44]. Another key protein involved in thrombus formation is factor XII, that once activated, trigger a series of complex interconnected reactions [6].

Factor XII activation

Factor XII, also called Hageman Factor, is a plasma protein that autoactivates by adsorption to the biomaterial surface [47]. This autoactivation occurs upon binding with the surface, presumably due to a conformational change, which forms the enzyme FXIIa [48]. FXIIa is then responsible for

initiating the intrinsic pathway of coagulation cascade and the complement activation.

1.3.1.3 Coagulation cascade

The coagulation cascade is the process by which the blood thrombus is formed, and it is divided into two pathways: intrinsic and extrinsic. The extrinsic pathway is triggered by damaged cells in the endothelial tissue, while the intrinsic pathway (also called contact activation) is due to the biomaterial surface interactions with adsorbed proteins [49]. These two pathways are not independent of each other, and both can be involved in the biomaterial-associated thrombosis [37]. The four proteins involved in the activation of the intrinsic pathway are: factor XII (FXII), prekallikrein, factor XI (FXI), and the high-molecular weight kininogen (HMWK). After FXII activation, FXIIa converts prekallikrein into kallikrein, and together with HMWK activates FXI, producing FXIa [50]. After FXI activation, factor IX is converted to its activated form factor IXa, leading to a cascade of proteolytic reactions that results in thrombin generation by cleavage of prothrombin [37]. Thrombin then converts fibrinogen to fibrin monomers, which polymerize to form the fibrin mesh [51]. The extrinsic pathway of the coagulation cascade is initiated by tissue factor (TF) expression from damaged cells at the site of vascular injury [37]. Factor VII (FVII) then binds to TF, and after its activation to FVIIa, they form the extrinsic tenase complex: TF-VIIa complex. TF–FVIIa complex, in the presence of calcium, cleaves factor X to form factor Xa. After that, both pathways lead to the common pathway where thrombin will be generated, and the fibrin mesh will be formed.

1.3.1.4 Complement activation

In addition, FXII and kallikrein are also involved in triggering the complement activation. The complement system is made up from more than 30 proteins and plays a vital role in body's immune response [46,52]. The activation of the complement system induced by biomaterials is part of the inflammatory response and is also interconnected to the coagulation cascade [37]. For example, complement activation is known to occur with vascular grafts, catheters, and during hemodialysis

and cardiopulmonary bypass [37]. The complement activation can be initiated by three different pathways: classical, lectin and alternative [53]. Biomaterial surfaces are responsible for triggering both classical and alternative pathways via cleavage of FXIIa by kallikrein to produce β-FXIIa [4]. β-FXIIa then activates the classical pathway, and kallikrein activates C3 and C5, generating the reactive fragments C3a and C5a [6]. C3a and C5a might then influence the leukocytes adhesion and activation on the implant surface. These enzymes and reactive fragments generated upon complement activation are also responsible for cell lysis.

1.3.1.5 Platelet adhesion

As mentioned, the adsorbed protein layer plays a vital role in platelet response to biomaterials. Adsorbed fibrinogen mediate the platelet adhesion to the surface, and it varies with the protein conformation changes and the availability of platelet binding domains [51]. Following the platelet adhesion to the implant surface, they undergo a morphological change, resulting in its activation and aggregation. The platelet activation consists of a shape change that produce granule contents and dendrites [44]. These activated platelets then release agonists, such as thromboxane A2 and ADP, that intensify platelet adhesion, activation, and aggregation on the medical device.

These platelet-mediated reactions are critical events in thrombus formation and are also interconnected to the intrinsic pathway of blood coagulation [54]. The thrombin generated by the intrinsic pathway also induces more platelet activation and aggregation, which accelerates the coagulation cascade [55]. These platelet aggregates deposited on the implant surface are trapped by the fibrin mesh to form a fibrin-platelet thrombus (**Figure 1.4**) [56]. Platelet activation is also known to occur following hemodialysis and cardiopulmonary bypass, and with catheters and vascular grafts [37].

1.3.1.6 Leukocyte adhesion

Besides the coagulation of blood plasma and the platelet-related reactions, the hemocompat-

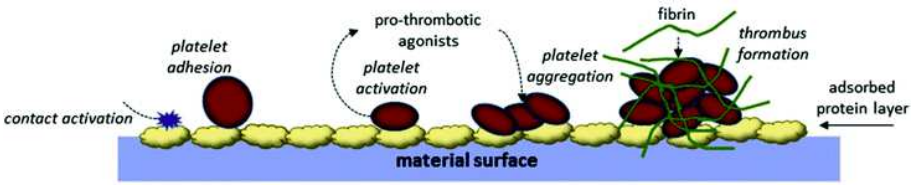

Figure 1.4: Platelet adhesion and activation on the biomaterial surface [57].

ibility of biomaterial surfaces is also influenced by leukocyte activation. Similar to platelets, the leukocytes, such as monocytes and neutrophils, can also adhere and activate upon binding to the surface. Fibrinogen is also primarily involved in leukocyte adhesion to biomaterials, and, following activation, the leukocytes can further assist both coagulation and inflammatory processes [52]. The activation of leukocytes has been commonly identified in cardiovascular devices, such as stents and vascular grafts, as well as during cardiopulmonary bypass, angioplasty, and hemodialysis [37]. Eventually, the monocytes adhered to the implant surface can differentiate into macrophages. These macrophages, once activated, produce pro-inflammatory cytokines that attract more leucocytes [58]. Ultimately, it can lead to the fusion of macrophages to form the giant cells and the recruitment of fibroblasts to form a fibrous capsule. This encapsulation prevents the implant to interact with the surrounding tissue and can cause the device failure.

1.3.2 Evaluation of hemocompatibility of titanium surfaces

To achieve good standardization, the methods and models for hemocompatibility tests are described in the ISO 10993-4/2002. Based on the primary process, the hemocompatibility evaluation can be classified into 5 different categories: blood coagulation, immunology, thrombosis, hematology, and platelets (**Table 1**) [36,39]. The evaluation of blood compatibility should also consider that these processes are not isolated and interfere in the other responses.

The coagulation category takes into account the contact activation system (i.e., intrinsic pathway of clotting cascade). The assays related to it investigate the specific coagulation factors and protein adsorption, as well as the thrombin generation. Previous study has developed a mathematical model

Table 1.1: Hemocompatibility testing (adapted from ISO-10993-4:2002) [59]

ISO 10993.4 categories	**Primary process**	**Assays**
Coagulation	Contact activation	Specific coagulation; factor Thrombin generation
Immunology	Complement activation	C3a; C5a; iC3;, C4d; SC5b-9; C3 convertase; C5 convertase
Thrombosis	Fibrinogen–fibrin conversion	Percent occlusion and flow reduction
Hematology	Hemolysis	Hemolysis; leukocyte adhesion/activation
Platelets	Platelet activation	Platelet count/adhesion; Platelet-activation and aggregation

that relates coagulation time to FXIIa concentration [47]. It is important to investigate the Factor XII activation on titanium biomaterial surfaces as it is responsible for initiating the intrinsic pathway of coagulation cascade and the complement activation. The immunology category covers the study of the complement system, and usually focuses on the release of peptide anaphylatoxins (such as C3a, C4a and C5a) [60]. The study of thrombosis focuses on the fibrinogen–fibrin conversion and the fibrin mesh formation, while the hematology evaluates leukocyte activation and hemolysis. Hemolysis is the release of hemoglobin from damaged red blood cells (i.e. erythrocytes), and it should be below 5%, according to ISO-993-5-10:1992 [61]. Another testing method that could be employed to investigate the biomaterial surface' hemocompatibility is the evaluation of whole blood clotting by a fast hemolysis assay as described elsewhere [62]. The platelet category includes the characterization of platelet adhesion, activation, and agglomeration, as well as its function in the thrombogenic potential of biomaterials.

1.4 Strategies for improving hemocompatibility of titanium-based implants

In blood-contacting implants, such as artificial heart valves, cardiovascular stents, and ventricular assist devices, hemocompatibility is crucial. Several studies have established that surface characteristics, such as chemistry, charge, wettability, and topography, play a major role in enhancing blood compatibility [63–66]. Proper surface modification techniques not only maintain the excellent bulk attributes of titanium and its alloys, such as relatively low modulus, good fatigue strength, machinability, and formability, but also improve specific surface properties demanded by different applications to improve the surface interaction with blood.

1.4.1 Surface properties and their influence in hemocompatibility

Over the last decades, intensive research has been conducted to understand the physical chemistry behind the biomaterial-blood interaction and how it leads to thrombosis and inflammation. This has promoted significant progress in developing novel surfaces for blood-contacting medical devices. Strategies to enhance blood compatibility of titanium are based on two main approaches: changing the surface chemistry and topography. By combining both strategies, it is possible to tailor the surface characteristics, such as roughness, wettability, and surface charge, to make the surface more hemocompatible.

When changing the topography, the surface roughness will get affected although roughness is not an exact definition of surface topography since it does not indicate if the roughness dimension is at the macroscale, microscale or nanoscale [38]. The micro/nano-scale architecture attracts great interest in the biomedical field due to the enhanced cellular response and biocompatibility [25]. Surface roughness Ra is the measure of the finely spaced micro-irregularities on the surface texture and is determined by calculating Ra and Rz. While Ra gives the average surface roughness, Rz can give information for any pore, hole, or surface deformities detrimental to strength [67].

In vivo/In vitro results have shown that surface roughness can influence the protein adsorption, platelet adhesion and activation, and thrombus formation.

While roughness is an important surface property for biomaterial interactions, it is important to understand the influence of roughness in wetting of the surface. The traditional R_a and R_z does not fit well statistically or fractal for superhydrophobic surfaces, which are commonly investigated for blood-contacting applications. In superhydrophobic surfaces there are other phenomenon such as pinning of the triple phase line, interface destabilization and wetting transition. Hence, it is essential to study the wettability of the surface.

Surface wettability is an important factor that quantifies how a liquid behaves when it interacts with a solid surface, and this is dictated by the intermolecular interaction of the liquid and solid surface and the cohesive force between the liquid molecules. The surface topography, chemistry, and charge, along with the liquid properties such as polarity can influence the wettability. Taking the water contact angle () into consideration, surfaces are termed superhydrophilic ($\theta \approx 0$), hydrophilic ($0° < \theta < 90°$), hydrophobic ($\theta > 90°$), and superhydrophobic ($\theta > 150°$). Designing hydrophilic surfaces is desirable as lower amount of blood plasma proteins adsorb on it in comparison with hydrophobic surfaces [46]. Due to the higher water-surface interaction, hydrophilic surfaces tend to reduce the blood protein adsorption [68]. The wettability of a liquid droplet on a textured surface differs from a smooth surface. The measure of macroscopic contact angle on a textured surface is defined as the apparent contact angle which is denoted by θ^*. When the liquid droplet comes into contact with a textured surface, it adapts either the Wenzel state or Cassie Baxter state to minimize its overall free energy [69]. In Wenzel state, the liquid droplet completely penetrates the nano/micro texture of the titanium surface, thereby having a completely wetted interface and the apparent contact angles are determined by using the relation:

$$\cos(\theta^*) = r\cos(\theta) \tag{1.1}$$

where r is the surface roughness of the features, which is the ratio of actual solid liquid interfacial

area to the projected surface area [70]. Due to the roughness factor, Wenzel state enhances wetting or de-wetting based on the young's contact angle. If θ <90°, then θ^* <<90°, and if θ >90 °, then θ^* >>90°.

As opposed to Wenzel state, in the Cassie Baxter state, the droplet does not penetrate the nano/micro features due to the pockets of air trapped between the features and the liquid droplet. In Cassie state the apparent contact angle is determined by using the relation:

$$\cos(\theta^*) = f_{sl}\cos(\theta) + f_{lv}\cos(\pi) = f_{sl}\cos(\theta) - f_{lv} \tag{1.2}$$

where f_{lv} is the area fraction of liquid-vapour interface and f_{sl} is the area fraction of solid-liquid interface [71].

Super-repellent surfaces are surfaces which display high apparent contact angles and low contact angle hysteresis and can be classified into superhydrophobic and superoleophobic surfaces [69]. Superhydrophobic surfaces normally display high apparent contact angles θ^* >150° and low contact angle hysteresis ($\Delta\theta < 5°$) for high surface tension liquids [69]. Super-repellent surfaces are achieved by attaining a Cassie Baxter state of wetting. Once the air is released due to the pressure of the liquid, there is a complete wetting, transitioning from Cassie state to the Wenzel state which is governed by breakthrough pressure [72]. This transition can make the surface more hydrophilic than the unmodified substrates due to the increase in overall roughness.

The chemical modification of implant surfaces for altering the wettability to reduce thrombus has also been extensively explored. Superhemophobic surfaces (i.e. surfaces that repel blood) were developed in recent times to reduce thrombogenicity of blood-contacting devices. These surfaces repel blood via a combination of nano/micro scale topographies and low surface energy silane coating. The surfaces are coated with various functional groups like CF_3, CF_2, CF_2H to lower the overall surface energy of the material, which increases the repellency towards blood. Fluorinated and per-fluorinated materials like per-fluorinated silanes, per-fluorinated phosphates, fluorinated

monomers, polymers, and copolymers which have low surface energy have been used to develop hemocompatible materials to reduce thrombosis and improve blood compatibility [73].

Studies have also explored hydrophilic coating with improved hemocompatibility. Hydrophilic polymers such as poly (ethylene glycol) (PEG) have been used for biomedical applications including bioconjugation, surface modification, and tissue engineering, due to critical properties such as good biocompatibility, non-immunogenicity, and resistance to non-specific binding of proteins [74,75]. PEG is very hydrophilic in nature and biochemically inert. PEG chains can be synthesized by controlled polymerization of ethylene glycol or ethylene oxide in aqueous solution [76]. The hydroxyl end groups of the PEG can be replaced with a variety of functional groups to improve surface properties and enhance hemocompatibility [45]. The crystallinity is another surface property that can influence blood-surface interaction [77]. The TiO_2 on the surface exists in different polymorphs. The phases which have shown major role in biomedical applications are anatase (tetragonal) and rutile (tetragonal) [78]. The phase transformation from anatase to rutile leads to a change in electron structure and therefore modifying the chemical properties of titanium surface. The rutile phase facets 100 and 110 are thermodynamically stable and hydrophilic due to the molecular adsorption at the O vacancies sites [79]. However, the crystalline TiO_2 is shown to be stable and that is required for a constant biological performance [80].

1.4.2 Surface modifications on titanium and titanium alloys

As explained in the previous section, the optimization of surface chemistry with micro/nanoscale topography leads to new biomaterials with enhanced hemocompatibility [38]. According to the different clinical needs, various surface modification techniques have been proposed, and this section will focus on these strategies developed in the past years to improve the hemocompatibility of titanium-based surfaces. An overview on these different strategies is given in **Figure 1.5**.

1.4.2.1 Plasma treatment

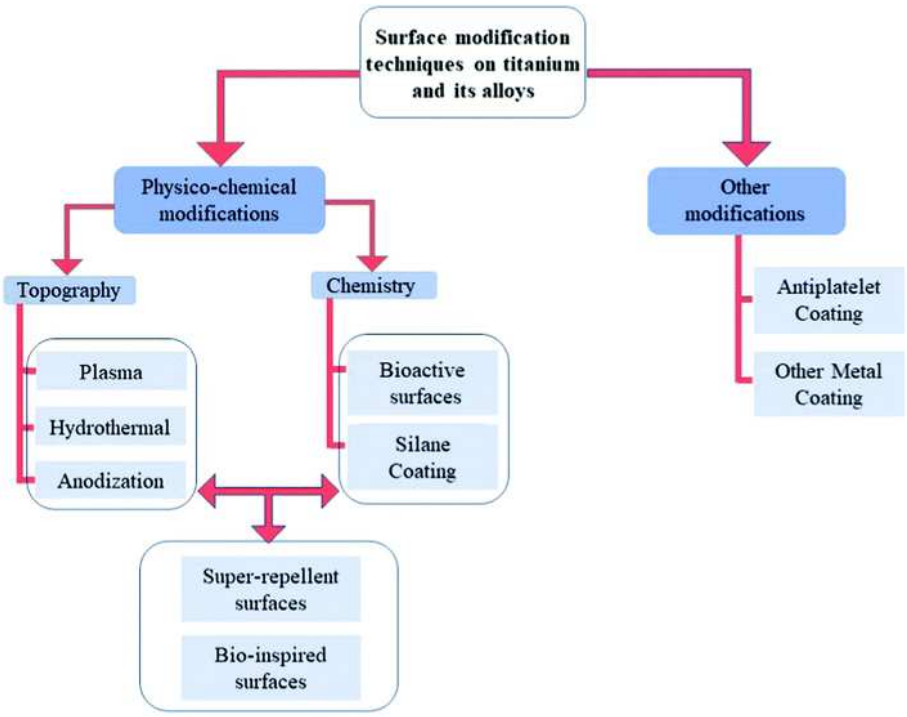

Figure 1.5: Different strategies of surface modification on titanium-based surfaces to improve hemocompatibility.

A simple technique used to treat titanium surfaces is plasma oxidation. The plasma oxidation treatment is used to generate oxide layers and is considered a green process due to low costs, lower water consumption, and no waste generation [81]. Plasma treatment generally transfer the additional energy in the plasma to the surface increasing the material surface energy and makes the surface more reactive [82]. Göttlicher et al. investigated the mechanisms required for the formation of nanocrystalline stoichiometric TiO_2 oxide layers using plasma oxidation [83]. Previous studies have shown that the presence of rutile TiO_2 phase can reduce thrombosis on the surfaces [84,85]. In addition, the ability to increase the roughness of the oxide layer via plasma treatment is also used to modulate the surface hydrophilicity. Chiang et al. showed that the plasma-oxidized samples with rough dimple-like oxide layer and nanostructured rutile TiO_2 phase possess enhanced hemocompatibility [81]. They used oxygen plasma with different treatment powers and durations to modify pure titanium surfaces by oxygen plasma to deposit a titanium oxide layer [81]. The microstructure analysis indicated formation of island like nanostructured rutile TiO_2

layer and dimple like nanostructured rutile TiO_2 layer on the plasma oxidized titanium surface. The presence of a rough dimple-like oxide layer with nanostructured rutile TiO_2 indicated better hemocompatibility when compared to control surfaces (**Figure 1.6A-B**). Hung et al. deposited TiO_2 layers using oxygen plasma immersion ion implantation (oxygen PIII). The oxygen PIII treated surfaces indicated the presence of Ti^{4+} chemical state which consisted of nanocrystalline TiO2 with a rutile structure [85]. The biological studies indicated delayed clotting time on the oxygen PIII treated surfaces which was associated with decreased fibrinogen adsorption. The oxygen PIII treated surfaces also showed lower platelet adhesion indicating the blood compatibility of the titanium implants can be improved by oxygen PIII (**Figure 1.6C-D**).

Klein et al. investigated the plasma electrolytic oxidation (PEO) on titanium surfaces by different phosphate-based electrolytes for use in ventricular assist devices (VADs) [86]. The PEO coating technique builds up TiO_2 oxide layers on the surface and is a process similar to alternating current anodizing. Although both processes use a counter electrode and a power supply, the PEO requires higher voltage conditions than in anodization, which leads to the development of different surface morphologies [86]. This PEO coatings can generate a variety of nanostructures that were able to prevent platelet adhesion and reproduce good hemocompatibility observed in modern VADs, as well as improve the wear resistance of the material.

1.4.2.2 Hydrothermal treatment

Hydrothermal treatment (HT) is a simple process where titanium substrates are treated in an elevated temperature and pressure, mostly in a liquid medium (acidic/alkaline) [15]. This treatment is highly tunable, and the reaction rate and kinetics can be altered by varying the concentration, temperature and pressure. Substrates are chemically etched and studies have shown that various surface features such as nanofibers, nanopores, nanoflowers, nanoneedles, and nanotubes can be developed on titanium surface without altering the bulk properties [87,88]. These nanostructures provide higher surface area and similar environment to the natural biological system [34]. Since the

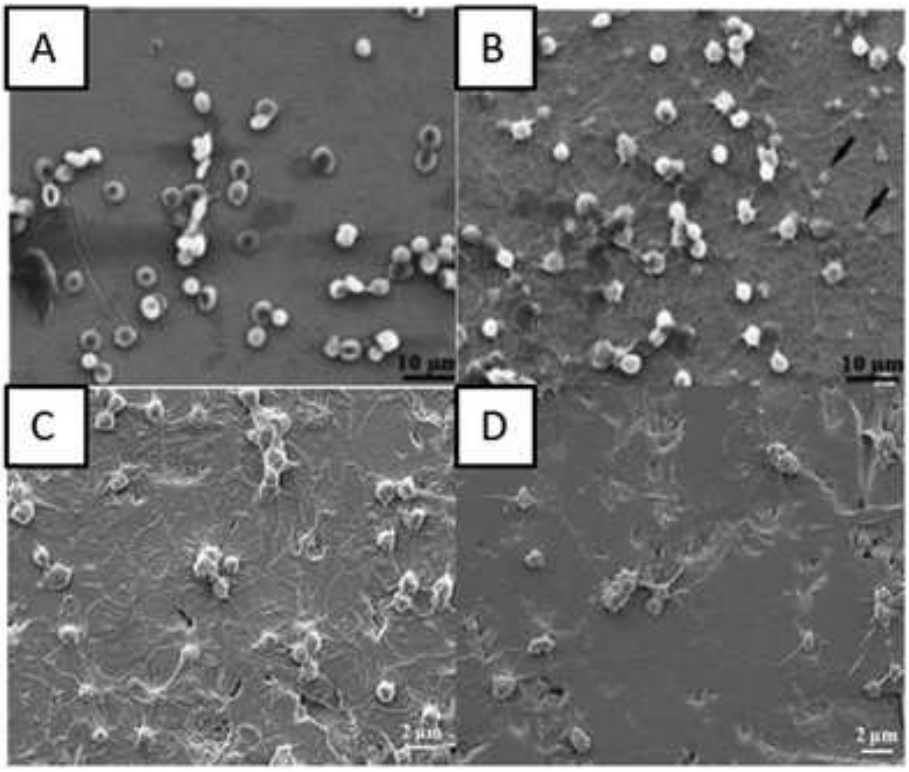

Figure 1.6: A-B) SEM images of red blood cells on control surfaces and plasma oxidized surfaces at 280W for 30 mins, respectively [81]. SEM images indicating the interaction of platelets with C) titanium surfaces and D) oxygen PIII treated surfaces [85]. Reproduced with permission from ref. 85. Copyright 2016, Elsevier.

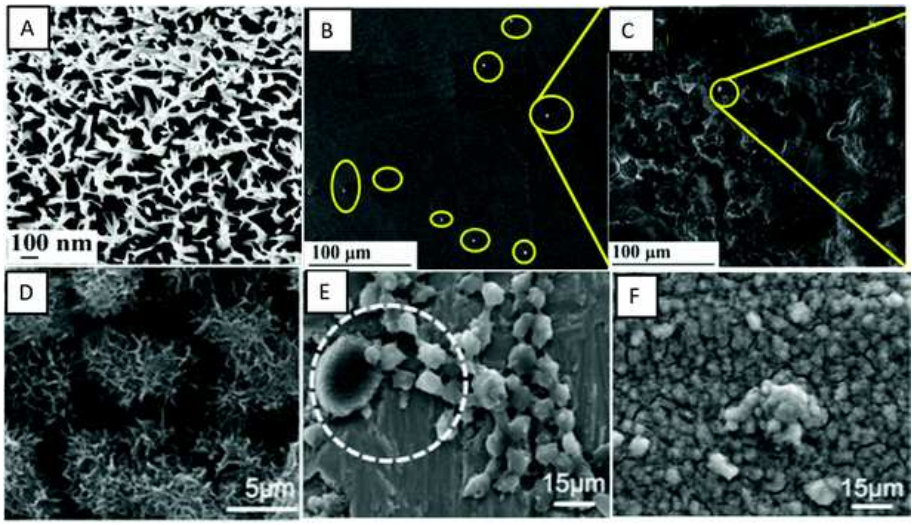

Figure 1.7: A) SEM images indicating surface morphology of hydrothermally treated nanograss surfaces. B-C) SEM images indicating platelet adhesion on control and nanograss Ti29Nb alloy surfaces, respectively [89]. Adapted with permission from ref. 89. Copyright 2020, Elsevier. D) SEM images indicating morphology of control and hydrothermally treated titanium surfaces, respectively. E-F) SEM images indicating platelets and leukocytes adhered on control and hydrothermally treated titanium surfaces, respectively [90].

blood cells and its components, such as protein and minerals, interact with nanoscale extracellular matrix elements, the surface nanotopography can modulate biological responses and stimulate physiological responses [35,64]. Vishnu et al. developed nanoneedles/nanograss on Ti-29Nb substrates using HT with NaOH solution [89]. The surface was superhydrophilic in nature and has shown reduced platelet adhesion and reduced hemolysis rates, thus improved hemocompatibility (**Figure 1.7A-C**). Manivasagam et al. have shown that the hydrothermally developed nanopore and nanoneedle surfaces that are hydrophilic in nature have improved hemocompatibility when compared to unmodified surfaces [90]. The nanopores surface which showed superhydrophilicity had the lowest protein adsorption and significantly decreased the platelet and leukocyte adhesion (**Figure 1.7D-F**).

1.4.2.3 Anodization

Anodization is an electrochemical treatment where the substrate to be treated is the anodic part

of the electrolytic cell in an electrolytic solution. This treatment is highly tunable, the reaction rate and kinetics can be altered by varying the anodization potential, electrolytic composition and concentration [91]. Anodization is a quick and inexpensive electrochemical technique to produce an array of TiO_2 nanotubes on currently implanted titanium-based devices [92]. TiO_2 nanotubes have attracted considerable attention due to high biocompatibility and osseointegration properties. Recently they have emerged as good approach for use in cardiovascular applications, such as stents [35]. Various studies have shown TiO_2 nanotubes can be produced with ordered alignment using anodization process on titanium substrates. The dimensions of the nanotubes such as thickness, diameter and length are controllable by altering the pH, voltage, electrolyte composition, and the time of experiment. The diameter of the nanotubes can be varied between 15 nm to 150 nm, and these structures usually make the surface hydrophilic in nature. The size of the nanotubes plays a key role in platelet adhesion. The 15 nm rods lead to higher platelet adhesion when compared to 100 nm rods [48].

Junkar et al. developed nanotubes for stent applications using anodization in hydrofluoric acid solution and further treatment with highly reactive oxygen plasma [93]. Results show that TiO_2 nanotubes developed are hydrophilic and has better hemocompatibility compared to unmodified titanium surface [93]. TiO_2 nanotubes treated with plasma decreased platelet and smooth muscle cells adhesion as well as enhanced endothelial cell growth. However, over time the nanotube surfaces were naturally oxidized, which made the surface hydrophobic, thus reducing the hemocompatibility. Pan et al. fabricated TiO_2 nanotube arrays of varying diameters via anodization and further doped them with zinc using hydrothermal treatment to improve biocompatibility [94]. The TiO_2 nanotube arrays were hydrophilic, whereas, the zinc doped TiO_2 nanotube arrays were superhydrophilic in nature. The hydrophilic and superhydrophilic surfaces increased the albumin adsorption and decreased the fibrinogen adsorption when compared to bare titanium. The results also indicated lower platelet adhesion on the superhydrophilic surfaces (Zn coated TiO_2 nanotube arrays) when compared to hydrophilic surfaces (TiO_2 nanotube arrays) and bare titanium (**Figure 1.8A-C**). The zinc coating also reduced the hemolysis rate and enhanced cell compatibility in-

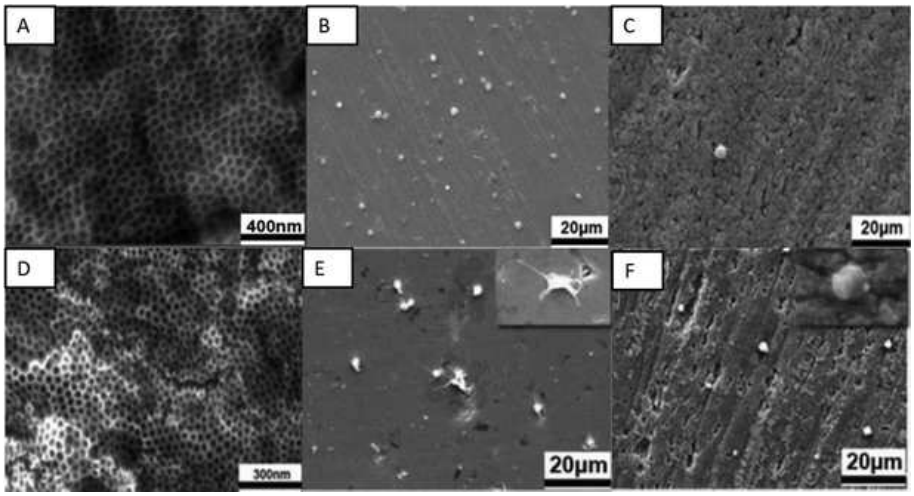

Figure 1.8: A) SEM images indicating surface morphology of zinc doped TiO_2 nanotubes. B-C) SEM images indicating platelet adhesion on control and zinc doped TiO_2 nanotubes, respectively [94]. Adapted with permission from ref. 94. Copyright 2020, American Chemical Society. D) SEM images indicating surface morphology of TiO_2 nanotube arrays anodized at 30V. E-F) SEM images indicating platelet adhesion on control and TiO_2 nanotube arrays (anodized at 30V) surfaces [95]. Adapted with permission from ref. 95. Copyright 2019, Elsevier.

dicating that modified hydrophilic and superhydrophilic surfaces can be used to improve blood compatibility and enhance cell endothelialization.

Gong et al. also developed in situ TiO_2 nanotube arrays by anodic oxidation and their crystal structures were further changed by annealing treatment. The effects of TiO_2 nanotube arrays with different diameters and crystal structures on endothelial cell behavior and blood compatibility were investigated [95]. The results indicated that the TiO_2 nanotube arrays with smaller diameter and anatase crystal had good blood and cell compatibility. There was a decrease in the platelet adhesion and hemolysis rate while also there was an increase in endothelial cell adhesion and proliferation (**Figure 1.8D-F**).

1.4.2.4 Super-repellent surfaces

Super-repellent surfaces are surfaces that repel most liquids as their surface energy is significantly lower [96]. Although hydrophilicity has been widely employed for blood-contacting

medical devices, recent research has shown even lower protein adsorption and platelet adhesion on superhydrophobic surfaces [97]. Superhydrophobicity can be achieved by combination of surface texture (e.g., micro and/or nanoscale texture) and coating with low surface energy compounds [98]. Studies have shown that nanotubes which are chemically coated can lead to varied surface interactions. Sabino et al. showed that when coated with a fluorinated silane the surface was superhydrophobic and when coated with PEG the surface superhydrophilic [48]. The superhydrophobic surface reduced the amount of protein adsorption and significantly delayed whole blood clotting when compared to other surfaces. Similarly, Xu et al. were able to produce superhydrophobic surface by coating the nanotube surface with self-assembled monolayers of octadecyl phosphonic acid (ODPA) [99]. Jiang et al. fabricated superhydrophobic titanium oxide coatings on Ti-6Al-4V alloys by micro arc oxidation (MAO) treatment and subsequent coating with 1 wt.% alcohol solution of 1H, 1H, 2H, 2H-perfluorooctyl-tricholorosilane (PFOTS) [100]. The resulted crater-like porous microstructured superhydrophobic surfaces displayed apparent water contact angle of 153°. The superhydrophobic surfaces displayed higher corrosion resistance when compared to uncoated Ti-6Al-4V. The superhydrophobic surfaces also showed low hemolysis ratio and no platelet adhesion, hence improving the blood compatibility of the Ti-6Al-4V alloy (**Figure 1.9A-C**).

Chen et al. fabricated superhydrophobic surface on Ti-6Al-4V alloy using hydrothermal treatment with NaOH and subsequent coating with PFOTS [101]. Various concentration of NaOH was used to analyze the difference in surface properties. The treatment developed feather-like or grass-like nanostructures on the surface based on the concentration. The coating made the grass-like structure surface superhydrophobic with highest apparent water contact angle of 159°. The superhydrophobic surface showed decreased hemolysis ratio, platelet adhesion and prolonged coagulation time, hence improving the in vitro hemocompatibility of Ti-6Al-4V alloy [101].

Yang et al. fabricated superhydrophobic TiO_2 nanotubes via electrochemical anodization in 0.5 wt.% HF electrolyte and subsequent coating with a methanolic solution of hydrolyzed 1 wt.% 1H, 1H, 2H, 2H-perfluorooctyl-triethoxysilane (PTES) [102]. The PTES modified TiO_2 nanotubes

displayed apparent water contact angle of 156°. The superhydrophobic nanotube surfaces displayed lower platelet adhesion and activation when compared to bare titanium and superhydrophilic surfaces, thus exhibiting enhanced hemocompatibility (**Figure 1.9D-F**).

Ma et al. fabricated multifunctional 3D microstructures on nickel-titanium alloys using femtosecond laser ablation combined with further fluorination of these microstructures to form superhydrophobic coating [103]. These fluorinated microstructures displayed apparent contact angles of 167° for water droplet indicating superhydrophobicity. The biocompatibility studies have shown low hemolysis ratio, low platelet adhesion and 100 % cell viability on these surfaces (**Figure 1.9G-I**). The surfaces have also shown excellent stability over time. Further, these surfaces have significantly reduced microbial adhesion and biofilm formation indicating antimicrobial properties.

Movafaghi et al. fabricated titania nanotube surfaces via electrochemical anodization and titanium nanoflowers via hydrothermal treatment [104]. These surfaces were further treated with (heptadecafluoro-1,1,2,2-tetrahydrodecyl)trichlorosilane to make them superhemophobic (i.e., surfaces that display contact angles > 150° with blood). These surfaces upon fluorination displayed an apparent contact angle of 150° and low roll off angles for human blood plasma indicating superhemophobicity. These surfaces displayed significant lower adhesion and activation of platelets when compared to hemophobic and hemophilic surfaces (**Figure 1.9J-L**). Bartlet et al. also developed superhemophobic titania nanotube surfaces [105]. The titania nanotube arrays were developed by anodizing technique and these surfaces were made superhemophobic by vapor phase silanization. These surfaces showed lower protein adsorption and lower platelet adhesion/activation, indicating a promising approach to design hemocompatible materials.

Montgomerie et al. fabricated superhydrophobic titania nanoflowers via hydrothermal process and silanization using Ti-6Al-4V alloy [106]. These surfaces showed significantly reduced protein adsorption and platelet adhesion and activation. The superhydrophobic titania nanoflowers indicated improved hemocompatibility and reduced bacterial adhesion when compared to both

non-textured and unmodified Ti-6Al-4V surfaces.

1.4.2.5 Bioactive surfaces

The modification of titanium surfaces using bioactive molecules or biopolymers, such as polysaccharides, peptides, and antibodies has received great attention to enhance their hemocompatibility properties. Biopolymers, such as heparin, chitosan, and some zwitterionic polymers, have been widely used to prevent protein and platelet attachments. Heparin is a naturally occurring polysaccharide and the most used antithrombogenic agent [57]. It possesses a very similar structure to heparan sulfate, a proteoglycan present on the endothelial cell surface that provides the natural anticoagulant surface property of the endothelium [108]. Heparin is responsible for binding to antithrombin and inhibiting the fibrin mesh formation. Because it is highly negative charged molecule, heparin is usually incorporated to titanium surfaces via electrostatic interactions with positive charged polymers to avoid the reduction of its biological activity [109]. Heparin has been combined with different polycations such as chitosan, tanfloc, and collagen to coat titanium using the layer-by-layer (LbL) self-assembly technique [110,111].

Zhang et al. showed that collagen/heparin coating on titanium surface decreases the platelet adhesion and activation and improves the endothelization process of the implant [112]. Collagen is the major component of extracellular matrix (ECM) and has been used to modify the surface of cardiovascular implants to enhance biocompatibility and induce cell-biomaterial interactions [110]. Cherng et al. coated pure titanium surfaces with heparin/dopamine and heparin/collagen via LbL techniques [113]. The heparin/dopamine was a porous polymer structure and heparin/collagen was a multilayer constructed by electrolytes. Both these surfaces promoted anticoagulation effect when compared to actual surfaces. However, the anticoagulation effects was better on the heparin/dopamine coated surfaces due to its long-term stability [114].

Yang et al. loaded TiO_2 nanotubes arrays with a 5-layer of polydopamine and further coated the surface with anticoagulant drug bivalirudin. The polydopamine coating controlled the release kinetics of bivalirudin and bivalirudin activity was seen for more than 300 days compared to the 40

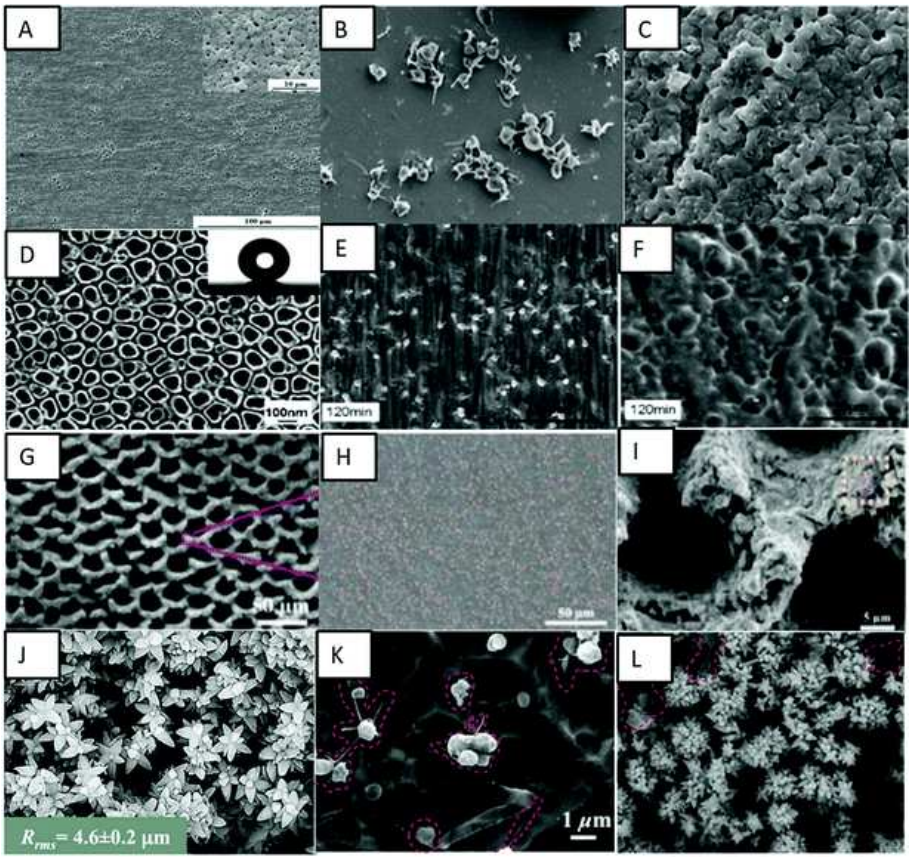

Figure 1.9: A) SEM images indicating crater-like porous microstructure on the Ti-6Al-4V surface. B-C) SEM images indicating platelet adhesion on bare Ti-6Al-4V and superhydrophobic MAO+TFOS surfaces, respectively [100]. Adapted with permission from ref. 100. Copyright 2015, Elsevier. D) SEM image indicating superhydrophobic TiO_2 nanotube surfaces. E-F) SEM images indicating platelet adhesion on bare TiO_2 nanotube surface and PTES modified superhydrophobic surfaces, respectively, after 120 mins exposure [102]. Adapted with permission from ref. 102. Copyright 2010, Elsevier. G) SEM image indicating multifunctional 3D micro-nanostructures on the nickel-titanium surface. H-I) SEM images indicating platelet adhesion on pristine nickel-titanium surface and superhydrophobic multifunctional 3D micro-nanostructured surface [103]. Adapted with permission from ref. 103. Copyright 2020, American Chemical Society. J) SEM images indicating nano-flowered surfaces. K-L) SEM images indicating platelet adhesion on non-textured titanium and superhemophobic nanoflower titanium surfaces [104]. Adapted with permission from ref. 104. Copyright 2016, Wiley-VCH.

days activity from TiO_2 nanotubes loaded with bivalirudin substrates. In vitro and ex vivo studies showed the modified surface improved hemocompatibility by reducing adhesion and denature of fibrinogen and platelets and effectively reducing thrombus formation [115].

Li et al. developed co-immobilization to form heparin and fibronectin films on aminosilanized titanium surfaces [116]. The technique combines electrostatic interaction and the co-immobilized films showed to be stable after immersion in phosphate-buffered saline (PBS) for five days and enhance the hemocompatibility of titanium surfaces. Fibronectin is an adhesive glycoprotein that promotes endothelial cell attachment and spreading [117]. The films reduced the hemolysis rate, prolonged the blood coagulation time, and increased the ATIII binding density. The co-immobilized surfaces also showed less platelets activation and aggregation, and less fibrinogen conformational change in comparison with unmodified titanium surface. Similarly, Li et al. fabricated titanium surfaces with heparin/fibronectin complexes. The heparin and fibronectin mixture was covalently immobilized on a titanium substrate and showed improved hemocompatibility and endothelialization [118]. The surfaces reduced the blood hemolysis rate, prolonged blood coagulation time, decreased platelets activation and aggregation, and induced less fibrinogen conformational change when compared with unmodified titanium surface.

Xu Cai prepared a bioactive coating by self-assembling phase transited lysozyme (PTL) and heparin to improve the biocompatibility of titanium [119]. PTL has been shown to have excellent biocompatibility and antibacterial properties, and in this study it was used positively charged PTL for strong electrostatic interactions with heparin. The PTL/heparin coated surfaces were hydrophilic in nature. The results indicated that these surfaces showed lower number of platelets adhered and delayed blood clotting time when compared to other surfaces (**Figure 1.10A-C**). These surfaces also showed low hemolysis ratio indicating better hemocompatibility compared to other surfaces.

Another biopolymer largely employed to introduce cell recognition sites to the biomaterial surface is chitosan. Chitosan has excellent biocompatibility properties, and its positive charges allows it to be combined with heparin via LbL technique. Zhang et al. investigated the immobilization of

heparin and chitosan on titanium to improve hemocompatibility and antibacterial activities (**Figure 1.10D-F**) [111]. They showed that these surfaces were able to prevent protein absorption, platelet adhesion, and blood clot mass. Vyas et al. also developed a biofunctionalization of titanium with chitosan/hydroxyapatite via silanization [120]. Hydroxyapatite is a bioactive ceramic largely used for biomaterial applications due to its similarity with natural bone [121]. These surfaces were able to significant decrease in hemolysis percentage in comparison with CpTi [120].

Zwitterionic polymers are known to be resistant to protein adsorption due to ionic interactions that rapidly creates a hydration layer on the surface [68]. Zwitterionic molecules have equal anion and cation groups on its chains, which make them highly hydrophilic and with natural antifouling properties [122]. Sabino et al. showed that the combination of a cationic tannin derivative (tanfloc) with heparin by LbL assembly significant decrease factor XII activation, and platelet adhesion and activation [109]. The zwitterionic-like properties of tanfloc are able to prevent blood protein adsorption and heparin acts to inhibit the coagulation cascade activation [123]. They developed tanfloc/heparin polyelectrolyte multilayers on titania nanotubes array surfaces to enhance blood compatibility and antibacterial properties [109]. The tanfloc/heparin coated nanotube arrays were hydrophilic in nature and displayed significant decrease in fibrinogen adsorbed, Factor XII activation and platelet adhesion and activation (**Figure 1.10G-I**). These surfaces also reduced bacterial adhesion and proliferation further indicating no biofilm formation. These surfaces hence enhanced blood compatibility and antibacterial properties on titanium surfaces.

Jia et al. modified TiO_2 nanotubes with two types of zwitterionic polymers, poly(sulfobetaine methacrylate) and poly(carboxybetaine methacrylate), using atom transfer radical polymerization technique [124]. Both polymer brushes reduced adsorption of albumin and fibrinogen protein to the surface compared to TiO_2 nanotubes. The FITR results showed that the adsorbed albumin on the polymer coated surface had a significantly different secondary structure, which reduced platelet adhesion and activation, In contrary, the TiO_2 nanotubes surface adsorbed albumin showed no structure change [124]. Cheng et al. conjugated natural tannic acid (TA) and silk sericin

(SS) via hydrogen bonding interactions and the resulting TA/SS conjugates were deposited on the titanium surfaces through surface adhesive trihydroxyphenyl groups in TA [125]. TA and its derivatives are widely used as a primer for immobilization of other molecules due to the presence of phenolic hydroxyl groups that could act hydrogen bond donor [126]. The TA/SS coated surfaces were hydrophilic in nature. These surfaces were repellent to proteins, showed lower platelet adhesion and anti-adhesive bacterial properties (**Figure 1.10J-L**). These surfaces further showed low cytotoxicity towards fibroblast cells indicating overall biocompatibility.

Lee Kang used a green seaweed derived polysaccharide ulvan to enhance blood compatibility of Ti/TiO_2 surfaces [127]. Tannic acid was used for surface coating and subsequent grafting of ulvan onto to the surface. Ulvan is a sulfated polysaccharide that has recently attracted attention due to its antioxidant, antiviral, and anti-adhesive properties [128]. The results indicated that the ulvan coated surfaces were superhydrophilic in nature and resulted in significant reduction in fibrinogen adsorption and platelet adhesion, thus enhancing hemocompatibility (**Figure 1.10M-O**).

Chen et al. prepared functional titanium surfaces with carboxylic terminated PEG600/PEG400 and CD34 antibodies and evaluated such surfaces for hemocompatibility [129]. The titanium surfaces were initially hydroxylated and further aminosilanized which was further used for covalently grafting of polyethylene glycol and the antibody. The CD34 antibody were immobilized on the surface to attract endothelial progenitor cells (EPCs) directly from the bloodstream [129]. The in vitro platelet adhesion tests confirmed superior hemocompatibility and enhanced endothelialization when compared to control surfaces.

Wu et al. fabricated quercetin-loaded chitosan nanoparticles and using LbL self-assembly technique coated titanium substrates with five and ten bilayers of hyaluronan and quercetin-loaded chitosan nanoparticles [130]. Quercetin is a naturally occurring flavonoid that has been shown to have anticoagulants effects similar to heparin. The 10-bilayer modified surface with quercetin-loaded chitosan as the top layer reduced platelet adhesion compared to control titanium surface and

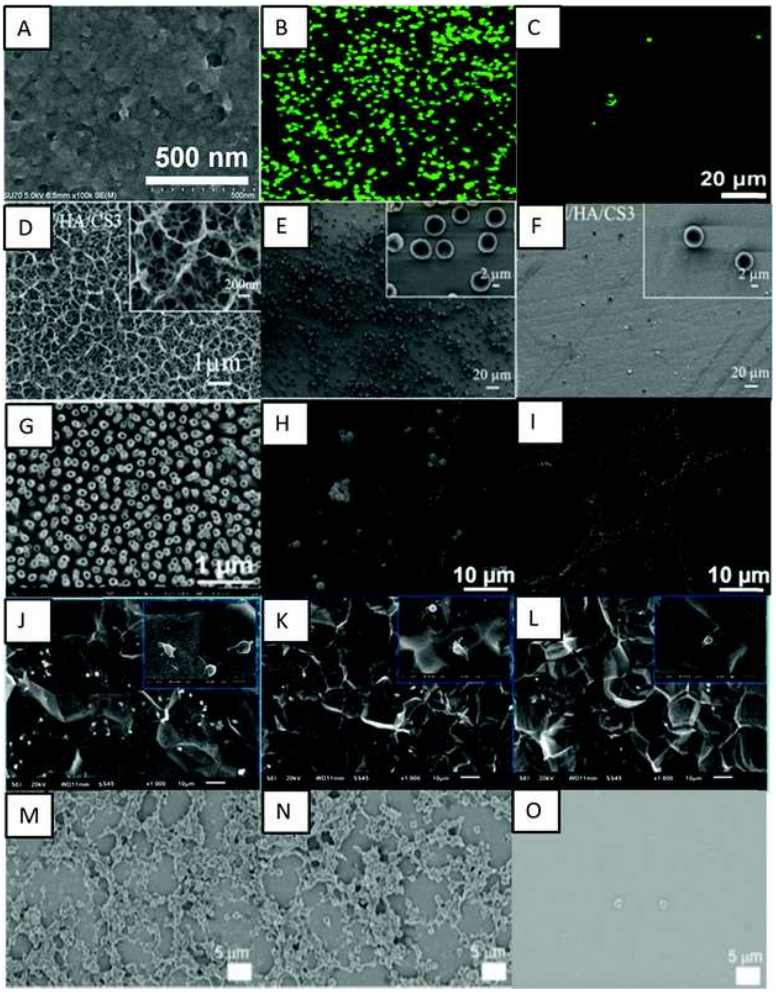

Figure 1.10: A) SEM image indicating surface microtopography of titanium surface modified with PTL/heparin. B-C) Fluorescence images indicating adhesion of platelets on bare titanium and titanium modified with PTL/heparin, respectively [119]. Adapted with permission from r ef. 119. Copyright 2019, Elsevier. D) SEM images indicating morphology of titanium surfaces modified with heparin/chitosan. E-F) SEM images indicating platelet adhesion on titanium and titanium surfaces modified w ith h eparin/chitosan, r espectively [111]. A dapted w ith p ermission f rom ref. 111. Copyright 2018, Elsevier. G) SEM image indicating titania nanotube surfaces modified with tanfloc/heparin polyelectrolyte m ultilayers. H-I) SEM images indicating platelet adhesion on unmodified titania nanotube surfaces and titania nanotube surfaces modified with tanfloc/heparin, respectively [109]. Adapted with permission from ref. 109. Copyright 2020, Wiley-VCH. J-L) SEM images indicating platelet adhesion on pristine titanium, TA/SS 1, and TA/SS 2 coated surfaces – 1 and 2 indicating different volume ratios [125]. Adapted with permission from r ef. 125. Copyright 2020, Elsevier. M-O) SEM images indicating platelet adhesion on non-treated, tannic acid-treated, and ulvan-coated Ti/TiO_2 surfaces, respectively [127]. Adapted with permission from ref. 127. Copyright 2020, Elsevier.

5-bilayer surface with hyaluronan as the top layer. This indicates that quercetin-loaded chitosan improved anticoagulation [130].

Llopis-Grimalt et al. modified the titanium surface to improve tissue response to stents using two different approaches, the use of nanostructuration by electrochemical anodization and the addition of quercitrin to the titanium surface [131]. Quercitrin, a glycoside formed from the flavonoid quercetin, has shown enhanced cell differentiation and anti-inflammatory activity when immobilized on titanium surfaces [132]. The surfaces were investigated for cell adhesion, cytotoxicity, nitic oxide production and metabolic activity using primary human umbilical cord endothelial cell. Platelet adhesion, hemolysis rate, and bacterial adhesion were also analyzed. The results indicated all surfaces were biocompatible, with no hemolysis rate, and the nanostructured surfaces displayed lower platelet adhesion. The nanostructure surfaces coated with quercitrin also showed enhanced endothelialization and lower bacterial adhesion as well as able to prevent thrombosis, thus being a promising approach to improve biocompatibility of bare metal stents.

1.4.2.6 Bio-inspired surfaces

The endothelial monolayer in blood vessels provides the perfect environment of blood compatibility. Blood flows inside them without any attraction or thrombus formation. The endothelial cells that line the interior surface of healthy blood vessels prevent blood clotting by several mechanisms, such as nitric oxide (NO) release or recruitment of heparan sulfate [133]. The endothelial inner lining is composed by a layer called glycocalyx, which is rich in proteoglycans bearing glycosaminoglycan (GAG). Recent research has been focusing on creating multifunction surfaces that can mimic the endothelium environment. Simon-Walker et al. coated TiO_2 nanotubes (TiO_2NT) with heparin-chitosan polyelectrolyte multilayers (PEM) to provide a glycosaminoglycan functionalization [134]. These surfaces when then modified with a NO-donor chemistry to provide an important antithrombotic signal. Combination of surface nanotopography, GAG-based surfaces, with NO-donor chemistry demonstrated substantial reduction in platelet adhesion and activation compared to unmodified TiO_2 surfaces (**Figure 1.11A-G**).

Liu et al. developed a multifunctional titanium surface for simultaneous enhancement of endothelial cell selectivity and hemocompatibility. The surface was prepared by conjugation of REDV peptide to a surface grafted PEGMA polymer brushes via surface-initiated atom transfer radical polymerization on a dopamine-modified titanium surface [135]. This surface showed improved endothelial cell selectivity and hemocompatibility, with reduced platelet adhesion when compared to pristine titanium.

Han et al. prepared a nature inspired extracellular matrix (ECM) coating on titanium surface by culturing/deculturizing smooth muscle cells (SCM) and endothelial cells (EC) controlled by hyaluronic acid (HA) micro-pattern [136]. This double deck ECM coating showed higher ECM density, different wettability's and larger pore sizes which lead to better hemocompatibility, anti-inflammation, tissue compatibility and pro-endothelialization (**Figure 1.11H-R**). The ECM coating maximized the reproducibility of structure and functionality of vascular basement membrane.

Wang et al. also prepared an ECM inspired surface by functionalization with heparin, fibronectin, and VEGF on titanium surface to construct a multifunctional microenvironment to inhibit thrombus formation [137]. The modified surfaces significantly enhanced the AT III binding density and prolonged clotting time. The in vitro platelet study also indicated favorable anticoagulant properties thus indicating the heparin/fibronectin/VEGF multifunctional coating was successfully constructed with desirable anticoagulant properties. In addition, these surfaces promoted enhanced proliferation of EPCs and ECs, thus accelerating endothelialization.

1.4.2.7 Other surface modifications

Several other agents have also been incorporated on the titanium surface to enhance its hemocompatibility [60]. Some cardiovascular implants, such as mechanical heart valves and stents, have been coated with pyrolytic carbon, which is known to decrease platelet adhesion and activation [3]. Chen et al. fabricated TiO_2 nanorod arrays (TNA) and used magnetic filtered cathodic vacuum arc deposition (FCVAD) to deposit carbon plasma nanocoating with sp^3-C bonding on these nanorod

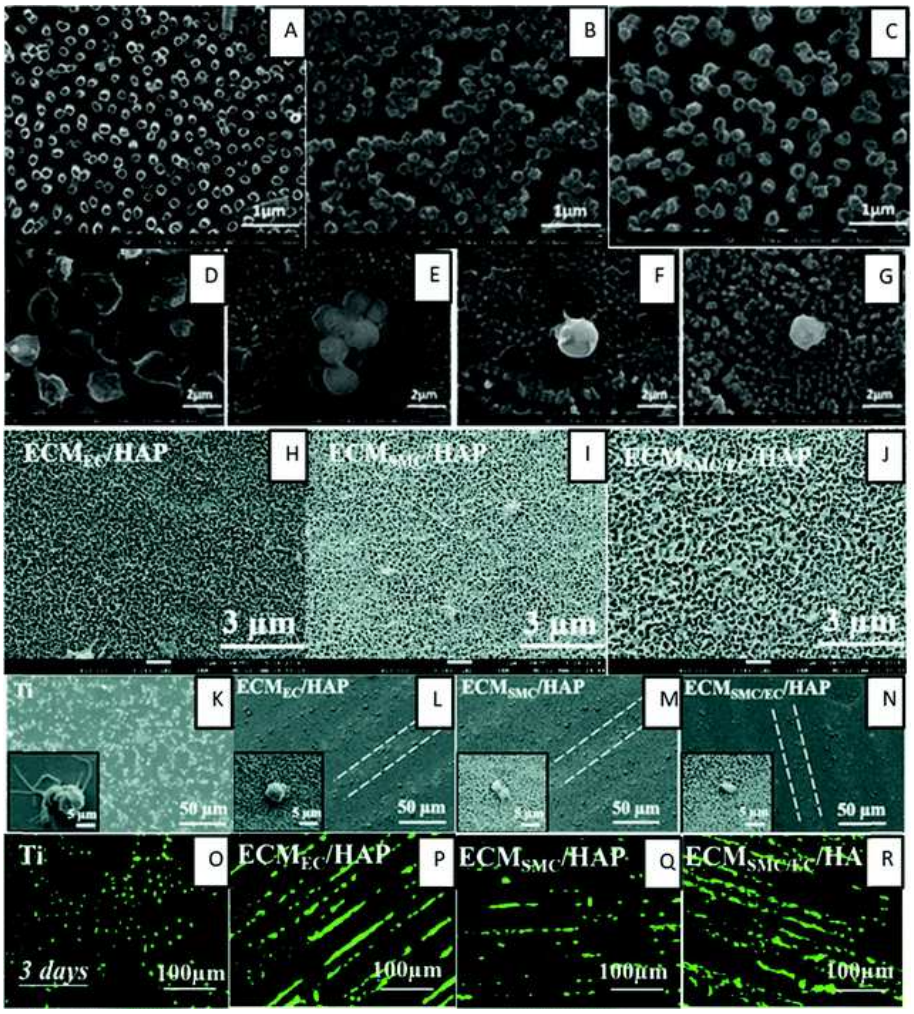

Figure 1.11: A-C) SEM images indicating TiO_2 NT, TiO_2 NT+PEM and TiO_2 NT+PEM+NO surfaces. D-G) SEM images indicating adhered cells on bare titanium, TiO, TiO_2 NT, TiO, TiO_2 NT+PEM and TiO, TiO_2 NT+PEM+NO surfaces [134]. Adapted with permission from ref. 134. Copyright 2017, American Chemical Society. H-J) SEM images indicating surface morphology of HA micro-patterned titanium surfaces modified with EC-ECM (ECMEC/HAP), SMC-ECM (ECMSMC/HAP), and modified by both SMC-ECM and EC-ECM (ECMSMC/EC/HAP) respectively [136]. K-N) SEM images indicating platelet adhesion on respective surfaces [136]. O-R) Fluorescence images indicating growth of HUVEC cells after 3 days on respective surfaces [136].

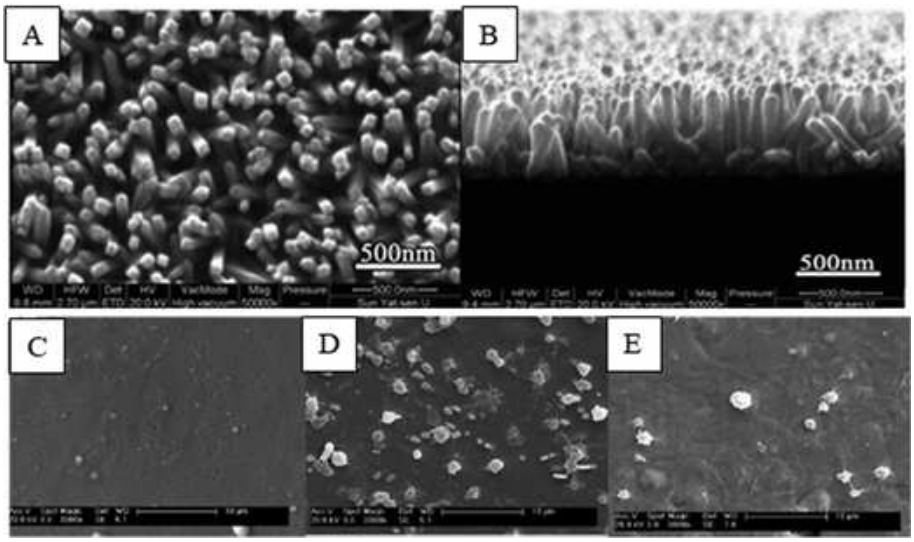

Figure 1.12: (A - B) SEM images showing the surface morphology of rutile TiO_2 nanorod arrays (TNA).139 (C) SEM images showing the surface morphology of the ZrN film. (D and E) SEM images showing platelet adhesion on nickel–titanium SMA and ZrN film surfaces, respectively.141 Adapted with permission from ref. 141. Copyright 2010, Elsevier.

arrays (**Figure 12A-B)**. [139] The TNA nanocomposites were investigated for hemocompatibility and cell endothelialization. The carbon nanocoatings improved cell viability and possessed higher hemocompatibility. Their previous work also indicated that these TNAs showed excellent blood compatibility, showing drastically reduced platelet adhesion and activation due to hydrophobicity and surface topography [140].

1.5 Conclusions and Future Perspectives

Blood is a complex smart liquid which can perform various necessary functions needed for our body functionality. However, one of its main properties is to clot when exposed to a foreign environment/material and this property poses a major concern when an implant is introduced into human body. Hence, researchers have been exploring different techniques to enhance hemocompatibility of implant surfaces. Design of hemocompatible titanium surfaces can be achieved by understanding the blood kinetics and the series of reactions taking place due to blood proteins, cells, and platelets

which leads to thrombus formation and inflammation. The influence of implant surface properties such as chemistry, morphology, crystallinity, charge, and wettability has shown to be significant, and various studies have been carried out to develop surfaces with improved hemocompatibility.

Different techniques for surface modification reviewed in this chapter has shown that hemocompatibility can be improved with surfaces imitating the vascular environment with surface morphology/chemistry, repelling blood protein interaction, anticoagulant drug loading and NO release. However, it is noticed that the combination of these properties enhances hemocompatibility significantly. The key aspect to be more focused is durability and longevity of the surface modification, commercialization potential and more realistic testing methods.

Hundreds of new surface modification techniques are proposed, studied, and published annually. However, most of the studies focuses on the evaluation of platelet adhesion and activation, protein adsorption, and hemolysis and coagulation tests. It is critical that researchers also investigate the contact and complement activation of the surfaces as they are important aspects of blood compatibility. In addition, most of the surface are evaluated in in vitro conditions with isolated blood components for a short duration of time. In reality, implants are present inside human body, with blood constantly flowing over the surface for longer periods. Hence, it is important to evaluate surfaces under dynamic conditions and more in vivo evaluations need to be done to understand the surface hemocompatibility. Besides that, implant surfaces are generally evaluated using human blood from healthy donors. In the current era, with advancement in biomedical sciences, implants are used by patients from different age groups and these humans also possess other diseases or complications that can alter immune reactions to implants. Hence, it is important to perform hemocompatibility studies considering different scenarios.

Titanium will continue to play an important role in blood-contacting implants for the foreseeable future. Although titanium has proven to be an excellent material for implants, there are still significant problems such thrombosis and restenosis due to undesirable blood-surface interactions. Over the years several approaches have been proposed to enhance the surface properties of titanium-

based materials to prevent thrombus formation. Some of them are based on creating micro/nano-scale topography meanwhile others proposed the surface chemistry modification. The combination of both strategies, which makes possible the tailoring the surface characteristics, such as wettability, roughness, surface charge, and crystallinity, has been shown to make the surface more compatible with blood and its components. Another promising approach is the immobilization of bioactive molecules on titanium surface, such as polysaccharides, peptides, and antibodies, which improves the blood-biomaterial response by using agents that are similar to the ones present in the body.

Recent research has also focused on the development of multifunctional titanium surfaces with the aim to mimic the endothelium environment. By modifying these surfaces through physical, chemical, and biological processes, the biomaterial would be able to not only prevent thrombogenic and inflammatory responses, but also stimulate endothelial cell adhesion, migration, and proliferation, and eventually build an endothelial layer on the titanium surfaces. In the near future, the new generation of titanium-based biomaterials should take advantage of the current state of the art to further improve the blood-surface interaction and develop a truly hemocompatible titanium surface. We believe that this review contributed to provide guidelines for the development of new and enhanced titanium-based surfaces for blood-contacting implants.

1.6 References

[1] V.K. Manivasagam, R.M. Sabino, P. Kantam, K.C. Popat, Surface modification strategies to improve titanium hemocompatibility: a comprehensive review, Mater. Adv. 2 (2021) 5824–5842. doi:10.1039/d1ma00367d.

[2] A.M. Khorasani, M. Goldberg, E.H. Doeven, G. Littlefair, Titanium in biomedical applications—properties and fabrication: A review, J. Biomater. Tissue Eng. 5 (2015) 593–619. doi:10.1166/jbt.2015.1361.

[3] M.T. Kalathottukaren, J.N. Kizhakkedathu, Mechanisms of blood coagulation in response to biomaterials: Extrinsic factors, in: Hemocompatibility Biomater. Clin. Appl. Blood-Biomaterials Interact., Elsevier, 2018: pp. 29–49. doi:10.1016/B978-0-08-100497-5.00003-3.

[4] I.H. Jaffer, J.C. Fredenburgh, J. Hirsh, J.I. Weitz, Medical device-induced thrombosis: what causes it and how can we prevent it?, J. Thromb. Haemost. 13 (2015) S72–S81. doi:10.1111/jth.12961.

[5] X.R. Xu, N. Carrim, M.A. Dias Neves, T. Mckeown, T.W. Stratton, R. Matos, P. Coelho, X. Lei, P. Chen, J. Xu, X. Dai, B.X. Li, H. Ni, Platelets and platelet adhesion molecules: novel mechanisms of thrombosis and anti-thrombotic therapies, Thromb. J. 14 (2016) 29. doi:10.1186/s12959-016-0100-6.

[6] I.H. Jaffer, J.I. Weitz, The blood compatibility challenge. Part 1: Blood-contacting medical devices: The scope of the problem, Acta Biomater. 94 (2019) 2–10. doi:10.1016/j.actbio.2019.06.021.

[7] J.L. Brash, T.A. Horbett, R.A. Latour, P. Tengvall, The blood compatibility challenge. Part 2: Protein adsorption phenomena governing blood reactivity, Acta Biomater. 94 (2019) 11–24. doi:10.1016/j.actbio.2019.06.022.

[8] L.P. Dasi, H.A. Simon, P. Sucosky, A.P. Yoganathan, Fluid mechanics of artificial heart valves, Clin. Exp. Pharmacol. Physiol. 36 (2009) 225–237. doi:10.1111/j.1440-1681.2008.05099.x.

[9] G.H. Kim, D.H. Yang, J.W. Kang, D.H. Kim, S.H. Jung, T.H. Lim, Subvalvular pannus and thrombosis in a mitral valve prosthesis, J. Cardiovasc. Comput. Tomogr. 10 (2016) 191–192. doi:10.1016/j.jcct.2015.09.004.

[10] N. Uriel, J. Han, K.A. Morrison, N. Nahumi, M. Yuzefpolskaya, A.R. Garan, J. Duong, P.C. Colombo, H. Takayama, S. Thomas, Y. Naka, U.P. Jorde, Device thrombosis in HeartMate II continuous-flow left ventricular assist devices: A multifactorial phenomenon, J. Hear. Lung Transplant. 33 (2014) 51–59. doi:10.1016/j.healun.2013.10.005.

[11] M. Bakir, Haemocompatibility of titanium and its alloys, J. Biomater. Appl. 27 (2012) 3–15. doi:10.1177/0885328212439615.

[12] S.A. Smith, R.J. Travers, J.H. Morrissey, How it all starts: Initiation of the clotting cascade, Crit. Rev. Biochem. Mol. Biol. 50 (2015) 326–336. doi:10.3109/10409238.2015.1050550.

[13] N. Mackman, Triggers, targets and treatments for thrombosis, Nature. 451 (2008) 914–918. doi:10.1038/nature06797.

[14] V.K. Manivasagam, K.C. Popat, Hydrothermally treated titanium surfaces for enhanced osteogenic differentiation of adipose derived stem cells, Mater. Sci. Eng. C. 128 (2021) 112315. doi:10.1016/J.MSEC.2021.112315.

[15] J. Vishnu, V. K Manivasagam, V. Gopal, C. Bartomeu Garcia, P. Hameed, G. Manivasagam, T.J. Webster, Hydrothermal treatment of etched titanium: A potential surface nano-modification technique for enhanced biocompatibility, Nanomedicine Nanotechnology, Biol. Med. 20 (2019) 102016. doi:10.1016/j.nano.2019.102016.

[16] H.J. Rack, J.I. Qazi, Titanium alloys for biomedical applications, Mater. Sci. Eng. C. 26 (2006) 1269–1277. doi:10.1016/j.msec.2005.08.032.

[17] F. Zhang, Z. Zhang, X. Zhu, E.T. Kang, K.G. Neoh, Silk-functionalized titanium surfaces for enhancing osteoblast functions and reducing bacterial adhesion, Biomaterials. 29 (2008) 4751–4759. doi:10.1016/j.biomaterials.2008.08.043.

[18] S. Lee, Y.Y. Chang, J. Lee, S.K. Madhurakkat Perikamana, E.M. Kim, Y.H. Jung, J.H. Yun, H. Shin, Surface engineering of titanium alloy using metal-polyphenol network coating with magnesium ions for improved osseointegration, Biomater. Sci. 8 (2020) 3404–3417. doi:10.1039/d0bm00566e.

[19] M. Kulkarni, A. Mazare, E. Gongadze, Perutkova, V. Kralj-Iglic, I. Milošev, P. Schmuki,

A. Iglič, M. Mozetič, Titanium nanostructures for biomedical applications, Nanotechnology. 26 (2015) 062002. doi:10.1088/0957-4484/26/6/062002.

[20] M. Kaur, K. Singh, Review on titanium and titanium based alloys as biomaterials for orthopaedic applications, Mater. Sci. Eng. C. 102 (2019) 844–862. doi:10.1016/J.MSEC.2019.04.064.

[21] A. Dehghanghadikolaei, H. Ibrahim, A. Amerinatanzi, M. Hashemi, N.S. Moghaddam, M. Elahinia, Improving corrosion resistance of additively manufactured nickel–titanium biomedical devices by micro-arc oxidation process, J. Mater. Sci. 54 (2019) 7333–7355. doi:10.1007/s10853-019-03375-1.

[22] A.T. Sidambe, Biocompatibility of advanced manufactured titanium implants-A review, Materials (Basel). 7 (2014) 8168–8188. doi:10.3390/ma7128168.

[23] N. Eliaz, Corrosion of Metallic Biomaterials: A Review, Materials (Basel). 12 (2019) 407. doi:10.3390/ma12030407.

[24] R. Zhang, X. Ai, Y. Wan, Z. Liu, D. Zhang, S. Feng, Surface Corrosion Resistance in Turning of Titanium Alloy, Int. J. Corros. 2015 (2015) 1–8. doi:10.1155/2015/823172.

[25] J.C.M. Souza, M.B. Sordi, M. Kanazawa, S. Ravindran, B. Henriques, F.S. Silva, C. Aparicio, L.F. Cooper, Nano-scale modification of titanium implant surfaces to enhance osseointegration, Acta Biomater. 94 (2019) 112–131. doi:10.1016/j.actbio.2019.05.045.

[26] G. Wang, J. Li, K. Lv, W. Zhang, X. Ding, G. Yang, X. Liu, X. Jiang, Surface thermal oxidation on titanium implants to enhance osteogenic activity and in vivo osseointegration, Sci. Rep. 6 (2016) 1–13. doi:10.1038/srep31769.

[27] M.L. Teffo, N.E. Nyakane, M. Seerane, M.B. Shongwe, R. Machaka, The effect of alloying elements on densification and mechanical behaviour of titanium based alloy, in: Mater. Today Proc., Elsevier, 2021: pp. 1203–1208. doi:10.1016/j.matpr.2020.09.280.

[28] D. Banerjee, J.C. Williams, Perspectives on titanium science and technology, Acta Mater. 61 (2013) 844–879. doi:10.1016/j.actamat.2012.10.043.

[29] E. Alabort, D. Barba, M.R. Shagiev, M.A. Murzinova, R.M. Galeyev, O.R. Valiakhmetov, A.F. Aletdinov, R.C. Reed, Alloys-by-design: Application to titanium alloys for optimal superplasticity,

Acta Mater. 178 (2019) 275–287. doi:10.1016/j.actamat.2019.07.026.

[30] Y. Oshida, Materials Classification, in: Biosci. Bioeng. Titan. Mater., Elsevier, 2013: pp. 9–34. doi:10.1016/b978-0-444-62625-7.00002-9.

[31] Y. Li, C. Yang, H. Zhao, S. Qu, X. Li, Y. Li, New developments of ti-based alloys for biomedical applications, Materials (Basel). 7 (2014) 1709–1800. doi:10.3390/ma7031709.

[32] M. Özcan, C. Hämmerle, Titanium as a reconstruction and implant material in dentistry: Advantages and pitfalls, Materials (Basel). 5 (2012) 1528–1545. doi:10.3390/ma5091528.

[33] B.S. Smith, S. Yoriya, L. Grissom, C.A. Grimes, K.C. Popat, Hemocompatibility of titania nanotube arrays, J. Biomed. Mater. Res. - Part A. 95 A (2010) 350–360. doi:10.1002/jbm.a.32853.

[34] V.B. Damodaran, D. Bhatnagar, V. Leszczak, K.C. Popat, Titania nanostructures: A biomedical perspective, RSC Adv. 5 (2015) 37149–37171. doi:10.1039/c5ra04271b.

[35] Y. Cheng, H. Yang, Y. Yang, J. Huang, K. Wu, Z. Chen, X. Wang, C. Lin, Y. Lai, Progress in TiO 2 nanotube coatings for biomedical applications: a review, J. Mater. Chem. B. 6 (2018) 1862–1886. doi:10.1039/C8TB00149A.

[36] V. Balan, L. Verestiuc, Strategies to improve chitosan hemocompatibility: A review, Eur. Polym. J. 53 (2014) 171–188. doi:10.1016/j.eurpolymj.2014.01.033.

[37] M.B. Gorbet, M. V. Sefton, Biomaterial-associated thrombosis: Roles of coagulation factors, complement, platelets and leukocytes, Biomater. Silver Jubil. Compend. 25 (2004) 219–241. doi:10.1016/B978-008045154-1.50025-3.

[38] L. Chen, D. Han, L. Jiang, On improving blood compatibility: From bioinspired to synthetic design and fabrication of biointerfacial topography at micro/nano scales, Colloids Surfaces B Biointerfaces. 85 (2011) 2–7. doi:10.1016/J.COLSURFB.2010.10.034.

[39] H.S. Lee, N. Tomczyk, J. Kandel, R.J. Composto, D.M. Eckmann, Hemocompatibility of chitosan/poly(acrylic acid) grafted polyurethane tubing, J. Mater. Chem. B. 1 (2013) 6382–6391. doi:10.1039/c3tb21218a.

[40] L.C. Xu, J.W. Bauer, C.A. Siedlecki, Proteins, platelets, and blood coagulation at biomaterial

interfaces, Colloids Surfaces B Biointerfaces. 124 (2014) 49–68. doi:10.1016/j.colsurfb.2014.09.040.

[41] C.J. Wilson, R.E. Clegg, D.I. Leavesley, M.J. Pearcy, Mediation of biomaterial-cell interactions by adsorbed proteins: A review, Tissue Eng. 11 (2005) 1–18. doi:10.1089/ten.2005.11.1.

[42] P. Roach, D. Farrar, C.C. Perry, Interpretation of protein adsorption: Surface-induced conformational changes, J. Am. Chem. Soc. 127 (2005) 8168–8173. doi:10.1021/ja042898o.

[43] S.Y. Jung, S.M. Lim, F. Albertorio, G. Kim, M.C. Gurau, R.D. Yang, M.A. Holden, P.S. Cremer, The Vroman Effect: A Molecular Level Description of Fibrinogen Displacement, J. Am. Chem. Soc. 125 (2003) 12782–12786. doi:10.1021/ja037263o.

[44] X. Liu, L. Yuan, D. Li, Z. Tang, Y. Wang, G. Chen, H. Chen, J.L. Brash, Blood compatible materials: state of the art, J. Mater. Chem. B. 2 (2014) 5709–5926. www.rsc.org/MaterialsB (accessed July 10, 2018).

[45] L.C. Xu, J.W. Bauer, C.A. Siedlecki, Proteins, platelets, and blood coagulation at biomaterial interfaces, Colloids Surfaces B Biointerfaces. 124 (2014) 49–68. doi:10.1016/j.colsurfb.2014.09.040.

[46] C. Sperling, M. Fischer, M.F. Maitz, C. Werner, Blood coagulation on biomaterials requires the combination of distinct activation processes, Biomaterials. 30 (2009) 4447–4456. doi:10.1016/J.BIOMATERIALS.2009.05.044.

[47] Z. Guo, K.M. Bussard, K. Chatterjee, R. Miller, E.A. Vogler, C.A. Siedlecki, Mathematical modeling of material-induced blood plasma coagulation, Biomaterials. 27 (2006) 796–806. doi:10.1016/j.biomaterials.2005.06.021.

[48] R.M. Sabino, K. Kauk, S. Movafaghi, A. Kota, K.C. Popat, Interaction of blood plasma proteins with superhemophobic titania nanotube surfaces, Nanomedicine Nanotechnology, Biol. Med. 21 (2019) 102046. doi:10.1016/J.NANO.2019.102046.

[49] A. De Mel, B.G. Cousins, A.M. Seifalian, Surface modification of biomaterials: A quest for blood compatibility, Int. J. Biomater. (2012) 1–8. doi:10.1155/2012/707863.

[50] K. Chatterjee, Z. Guo, E.A. Vogler, C.A. Siedlecki, Contributions of contact activation pathways of coagulation factor XII in plasma, J. Biomed. Mater. Res. - Part A. 90 (2009) 27–34.

doi:10.1002/jbm.a.32076.

[51] J.L. Brash, T.A. Horbett, R.A. Latour, P. Tengvall, The blood compatibility challenge. Part 2: Protein adsorption phenomena governing blood reactivity, Acta Biomater. 94 (2019) 11–24. doi:10.1016/j.actbio.2019.06.022.

[52] M. Gorbet, C. Sperling, M.F. Maitz, C.A. Siedlecki, C. Werner, M. V. Sefton, The blood compatibility challenge. Part 3: Material associated activation of blood cascades and cells, Acta Biomater. 94 (2019) 25–32. doi:10.1016/j.actbio.2019.06.020.

[53] F. Poppelaars, B. Faria, M.G. da Costa, C.F.M. Franssen, W.J. van Son, S.P. Berger, M.R. Daha, M.A. Seelen, The complement system in dialysis: A forgotten story?, Front. Immunol. 9 (2018) 71. doi:10.3389/fimmu.2018.00071.

[54] Y. Yan, L.C. Xu, E.A. Vogler, C.A. Siedlecki, Contact activation by the intrinsic pathway of blood plasma coagulation, in: Hemocompatibility Biomater. Clin. Appl. Blood-Biomaterials Interact., Elsevier, 2018: pp. 3–28. doi:10.1016/B978-0-08-100497-5.00001-X.

[55] A. Thor, L. Rasmusson, A. Wennerberg, P. Thomsen, J.-M. Hirsch, B. Nilsson, J. Hong, The role of whole blood in thrombin generation in contact with various titanium surfaces, Biomaterials. 28 (2007) 966–974. doi:10.1016/J.BIOMATERIALS.2006.10.020.

[56] X.R. Xu, N. Carrim, M.A.D. Neves, T. McKeown, T.W. Stratton, R.M.P. Coelho, X. Lei, P. Chen, J. Xu, X. Dai, B.X. Li, H. Ni, Platelets and platelet adhesion molecules: Novel mechanisms of thrombosis and anti-thrombotic therapies, Thromb. J. 14 (2016) 29. doi:10.1186/s12959-016-0100-6.

[57] R. Biran, D. Pond, Heparin coatings for improving blood compatibility of medical devices, Adv. Drug Deliv. Rev. 112 (2017) 12–23. doi:10.1016/j.addr.2016.12.002.

[58] Y.K. Kim, E.Y. Chen, W.F. Liu, Biomolecular strategies to modulate the macrophage response to implanted materials, J. Mater. Chem. B. 4 (2016) 1600–1609. doi:10.1039/c5tb01605c.

[59] U.T. Seyfert, V. Biehl, J. Schenk, In vitro hemocompatibility testing of biomaterials according to the ISO 10993-4, in: Biomol. Eng., Elsevier, 2002: pp. 91–96. doi:10.1016/S1389-0344(02)00015-1.

[60] V. Balan, L. Verestiuc, Strategies to improve chitosan hemocompatibility: A review, Eur. Polym. J. 53 (2014) 171–188. doi:10.1016/j.eurpolymj.2014.01.033.

[61] L.Y.C. Madruga, R.M. Sabino, E.C.G. Santos, K.C. Popat, R. de C. Balaban, M.J. Kipper, Carboxymethyl-kappa-carrageenan: A study of biocompatibility, antioxidant and antibacterial activities, Int. J. Biol. Macromol. 152 (2020) 483–491. doi:10.1016/j.ijbiomac.2020.02.274.

[62] R. Sabino, K. Popat, Evaluating Whole Blood Clotting in vitro on Biomaterial Surfaces, BIO-PROTOCOL. 10 (2020) e3505. doi:10.21769/bioprotoc.3505.

[63] P. Gill, V. Musaramthota, N. Munroe, A. Datye, R. Dua, W. Haider, A. McGoron, R. Rokicki, Surface modification of Ni-Ti alloys for stent application after magnetoelectropolishing, Mater. Sci. Eng. C. 50 (2015) 37–44. doi:10.1016/j.msec.2015.01.009.

[64] B.S. Smith, K.C. Popat, Titania Nanotube Arrays as Interfaces for Blood-Contacting Implantable Devices, (2012) 642–658.

[65] J.L. Chen, Q.L. Li, J.Y. Chen, C. Chen, N. Huang, Improving blood-compatibility of titanium by coating collagen-heparin multilayers, Appl. Surf. Sci. 255 (2009) 6894–6900. doi:10.1016/j.apsusc.2009.03.011.

[66] S. Nie, H. Qin, C. Cheng, W. Zhao, S. Sun, B. Su, C. Zhao, Z. Gu, Blood activation and compatibility on single-molecular-layer biointerfaces, J. Mater. Chem. B. 2 (2014) 4911–4921. doi:10.1039/c4tb00555d.

[67] S. Kumar, Selective Laser Sintering/Melting, in: Compr. Mater. Process., Elsevier Ltd, 2014: pp. 93–134. doi:10.1016/B978-0-08-096532-1.01003-7.

[68] X. Liu, L. Yuan, D. Li, Z. Tang, Y. Wang, G. Chen, H. Chen, J.L. Brash, Blood compatible materials: state of the art Xiaoli, J. Mater. Chem. B. 2 (2014) 5709–5926.

[69] A.K. Kota, G. Kwon, A. Tuteja, The design and applications of superomniphobic surfaces, NPG Asia Mater. 6 (2014) 109. doi:10.1038/am.2014.34.

[70] K.Y. Yeh, L.J. Chen, J.Y. Chang, Contact angle hysteresis on regular pillar-like hydrophobic surfaces, Langmuir. 24 (2008) 245–251. doi:10.1021/la7020337.

[71] B.M.L. Koch, A. Amirfazli, J.A.W. Elliott, Modeling and measurement of contact angle hysteresis on textured high-contact-angle surfaces, J. Phys. Chem. C. 118 (2014) 18554–18563. doi:10.1021/jp504891u.

[72] S. Movafaghi, W. Wang, D.L. Bark, L.P. Dasi, K.C. Popat, A.K. Kota, Hemocompatibility of super-repellent surfaces: Current and future, Mater. Horizons. 6 (2019) 1596–1610. doi:10.1039/c9mh00051h.

[73] D.L. Bark, H. Vahabi, H. Bui, S. Movafaghi, B. Moore, A.K. Kota, K. Popat, L.P. Dasi, Hemodynamic Performance and Thrombogenic Properties of a Superhydrophobic Bileaflet Mechanical Heart Valve, Ann. Biomed. Eng. 45 (2017) 452–463. doi:10.1007/s10439-016-1618-2.

[74] K.M. Hansson, S. Tosatti, J. Isaksson, J. Wetterö, M. Textor, T.L. Lindahl, P. Tengvall, Whole blood coagulation on protein adsorption-resistant PEG and peptide functionalised PEG-coated titanium surfaces, Biomaterials. 26 (2005) 861–872. doi:10.1016/j.biomaterials.2004.03.036.

[75] C.J. Pan, Y.H. Hou, B. Bin Zhang, Y.X. Dong, H.Y. Ding, Blood compatibility and interaction with endothelial cells of titanium modified by sequential immobilization of poly (ethylene glycol) and heparin, J. Mater. Chem. B. 2 (2014) 892–902. doi:10.1039/c3tb21403f.

[76] J. Herzberger, K. Niederer, H. Pohlit, J. Seiwert, M. Worm, F.R. Wurm, H. Frey, Polymerization of ethylene oxide, propylene oxide, and other alkylene oxides: Synthesis, novel polymer architectures, and bioconjugation, Chem. Rev. 116 (2016) 2170–2243. doi:10.1021/acs.chemrev.5b00441.

[77] A. Rosengren, S. Oscarsson, The influence of plasma proteins on bone cell adhesion, in: Cell. Response to Biomater., Elsevier Ltd., 2008: pp. 538–559. doi:10.1533/9781845695477.3.538.

[78] D.A.H. Hanaor, C.C. Sorrell, Review of the anatase to rutile phase transformation, J. Mater. Sci. 46 (2011) 855–874. doi:10.1007/s10853-010-5113-0.

[79] F. Parrino, F.R. Pomilla, G. Camera-Roda, V. Loddo, L. Palmisano, Properties of titanium dioxide, in: Titan. Dioxide Its Appl., Elsevier, 2021: pp. 13–66. doi:10.1016/b978-0-12-819960-2.00001-8.

[80] H.N. Pantaroto, J.M. Cordeiro, L.T. Pereira, A.B. de Almeida, F.H. Nociti Junior, E.C. Rangel, N.F. Azevedo Neto, J.H.D. da Silva, V.A.R. Barão, Sputtered crystalline TiO2 film drives improved

surface properties of titanium-based biomedical implants, Mater. Sci. Eng. C. 119 (2021) 111638. doi:10.1016/j.msec.2020.111638.

[81] H.-J. Chiang, H.-H. Chou, K.-L. Ou, E. Sugiatno, M. Ruslin, R.A. Waris, C.-F. Huang, C.-M. Liu, P.-W. Peng, Evaluation of Surface Characteristics and Hemocompatibility on the Oxygen Plasma-Modified Biomedical Titanium, Metals (Basel). 8 (2018) 513. doi:10.3390/met8070513.

[82] M. Erofeev, V. Ripenko, M. Shulepov, V. Tarasenko, Surface treatment of metals in the plasma of a nanosecond diffuse discharge at atmospheric pressure, Eur. Phys. J. D. 71 (2017) 1–5. doi:10.1140/epjd/e2017-70636-6.

[83] M. Göttlicher, M. Rohnke, A. Kunz, J. Thomas, R.A. Henning, T. Leichtweiß, T. Gemming, J. Janek, Anodization of titanium in radio frequency oxygen discharge - Microstructure, kinetics transport mechanism, Solid State Ionics. 290 (2016) 130–139. doi:10.1016/j.ssi.2016.04.013.

[84] D. Xie, G. Wan, M.F. Maitz, Y. Lei, N. Huang, H. Sun, Characterization and mechanical investigation of Ti-O 2-x film prepared by plasma immersion ion implantation and deposition for cardiovascular stents surface modification, Nucl. Instruments Methods Phys. Res. Sect. B Beam Interact. with Mater. Atoms. 289 (2012) 91–96. doi:10.1016/j.nimb.2012.07.033.

[85] W.C. Hung, F.M. Chang, T. Sen Yang, K.L. Ou, C.T. Lin, P.W. Peng, Oxygen-implanted induced formation of oxide layer enhances blood compatibility on titanium for biomedical applications, Mater. Sci. Eng. C. 68 (2016) 523–529. doi:10.1016/j.msec.2016.06.024.

[86] M. Klein, Y. Kuhn, E. Woelke, T. Linde, C. Ptock, A. Kopp, T. Bletek, T. Schmitz-Rode, U. Steinseifer, J. Arens, J.C. Clauser, In vitro study on the hemocompatibility of plasma electrolytic oxidation coatings on titanium substrates, Artif. Organs. 44 (2020) 419–427. doi:10.1111/aor.13592.

[87] P. Hameed, V.K. Manivasagam, M. Sankar, K.C. Popat, G. Manivasagam, Nanofibers and Nanosurfaces, in: Springer, Singapore, 2021: pp. 107–130. doi:10.1007/978-981-33-6252-9_4.

[88] C.L. Wong, Y.N. Tan, A.R. Mohamed, A review on the formation of titania nanotube photocatalysts by hydrothermal treatment, J. Environ. Manage. 92 (2011) 1669–1680. doi:10.1016/j.jenvman.2011.03.006.

[89] J. Vishnu, M. Calin, S. Pilz, A. Gebert, B. Kaczmarek, M. Michalska-Sionkowska, V. Hoff-

mann, G. Manivasagam, Superhydrophilic nanostructured surfaces of beta Ti[sbnd]29Nb alloy for cardiovascular stent applications, Surf. Coatings Technol. 396 (2020) 125965. doi:10.1016/j.surfcoat.2020.125965.

[90] V.K. Manivasagam, K.C. Popat, In Vitro Investigation of Hemocompatibility of Hydrothermally Treated Titanium and Titanium Alloy Surfaces, ACS Omega. (2020) acsomega.0c00281. doi:10.1021/acsomega.0c00281.

[91] Y. Cheng, H. Yang, Y. Yang, J. Huang, K. Wu, Z. Chen, X. Wang, C. Lin, Y. Lai, Progress in TiO2 nanotube coatings for biomedical applications: A review, J. Mater. Chem. B. 6 (2018) 1862–1886. doi:10.1039/c8tb00149a.

[92] K.M. Kummer, E. Taylor, T.J. Webster, Biological applications of anodized TiO 2 nanostructures: A review from orthopedic to stent applications, Nanosci. Nanotechnol. Lett. 4 (2012) 483–493. doi:10.1166/nnl.2012.1352.

[93] I. Junkar, M. Kulkarni, M. Benčina, J. Kovač, K. Mrak-Poljšak, K. Lakota, S. Sodin-Šemrl, M. Mozetič, A. Iglič, Titanium Dioxide Nanotube Arrays for Cardiovascular Stent Applications, ACS Omega. 5 (2020) 7280–7289. doi:10.1021/acsomega.9b04118.

[94] C. Pan, Y. Hu, Z. Gong, Y. Yang, S. Liu, L. Quan, Z. Yang, Y. Wei, W. Ye, Improved Blood Compatibility and Endothelialization of Titanium Oxide Nanotube Arrays on Titanium Surface by Zinc Doping, ACS Biomater. Sci. Eng. 6 (2020) 2072–2083. doi:10.1021/acsbiomaterials.0c00187.

[95] Z. Gong, Y. Hu, F. Gao, L. Quan, T. Liu, T. Gong, C. Pan, Effects of diameters and crystals of titanium dioxide nanotube arrays on blood compatibility and endothelial cell behaviors, Colloids Surfaces B Biointerfaces. 184 (2019) 110521. doi:10.1016/j.colsurfb.2019.110521.

[96] S. Movafaghi, W. Wang, D.L. Bark, L.P. Dasi, K.C. Popat, A.K. Kota, Hemocompatibility of super-repellent surfaces: Current and future, Mater. Horizons. 6 (2019) 1596–1610. doi:10.1039/c9mh00051h.

[97] V. Jokinen, E. Kankuri, S. Hoshian, S. Franssila, R.H.A. Ras, Superhydrophobic Blood-Repellent Surfaces, Adv. Mater. 30 (2018) 1705104. doi:10.1002/adma.201705104.

[98] W. Wang, K. Lockwood, L.M. Boyd, M.D. Davidson, S. Movafaghi, H. Vahabi, S.R. Khetani,

A.K. Kota, Superhydrophobic Coatings with Edible Materials, ACS Appl. Mater. Interfaces. 8 (2016) 18664–18668. doi:10.1021/acsami.6b06958.

[99] X. Gu, Y. Zheng, Y. Cheng, S. Zhong, T. Xi, In vitro corrosion and biocompatibility of binary magnesium alloys, Biomaterials. 30 (2009) 484–498. doi:10.1016/j.biomaterials.2008.10.021.

[100] J.Y. Jiang, J.L. Xu, Z.H. Liu, L. Deng, B. Sun, S.D. Liu, L. Wang, H.Y. Liu, Preparation, corrosion resistance and hemocompatibility of the superhydrophobic TiO 2 coatings on biomedical Ti-6Al-4V alloys, Appl. Surf. Sci. 347 (2015) 591–595. doi:10.1016/j.apsusc.2015.04.075.

[101] J. Chen, J.L. Xu, J. Huang, P. Zhang, J.M. Luo, L. Lian, Formation mechanism and hemocompatibility of the superhydrophobic surface on biomedical Ti–6Al–4V alloy, J. Mater. Sci. 2021 5612. 56 (2021) 7698–7709. doi:10.1007/S10853-020-05696-Y.

[102] Y. Yang, Y. Lai, Q. Zhang, K. Wu, L. Zhang, C. Lin, P. Tang, A novel electrochemical strategy for improving blood compatibility of titanium-based biomaterials, Colloids Surfaces B Biointerfaces. 79 (2010) 309–313. doi:10.1016/j.colsurfb.2010.04.013.

[103] Y. Ma, L. Jiang, J. Hu, H. Liu, S. Wang, P. Zuo, P. Ji, L. Qu, T. Cui, Multifunctional 3D Micro-Nanostructures Fabricated through Temporally Shaped Femtosecond Laser Processing for Preventing Thrombosis and Bacterial Infection, ACS Appl. Mater. Interfaces. 12 (2020) 17155–17166. doi:10.1021/acsami.9b20766.

[104] S. Movafaghi, V. Leszczak, W. Wang, J.A. Sorkin, L.P. Dasi, K.C. Popat, A.K. Kota, Hemocompatibility of Superhemophobic Titania Surfaces, Adv. Healthc. Mater. 6 (2017) 1600717. doi:10.1002/adhm.201600717.

[105] K. Bartlet, S. Movafaghi, A. Kota, K.C. Popat, Superhemophobic titania nanotube array surfaces for blood contacting medical devices, RSC Adv. 7 (2017) 35466–35476. doi:10.1039/C7RA03373G.

[106] Z. Montgomerie, K.C. Popat, Improved hemocompatibility and reduced bacterial adhesion on superhydrophobic titania nanoflower surfaces, Mater. Sci. Eng. C. 119 (2021) 111503. doi:10.1016/j.msec.2020.111503.

[107] S. Moradi, N. Hadjesfandiari, S.F. Toosi, J.N. Kizhakkedathu, S.G. Hatzikiriakos, Effect of

Extreme Wettability on Platelet Adhesion on Metallic Implants: From Superhydrophilicity to Superhydrophobicity, ACS Appl. Mater. Interfaces. 8 (2016) 17631–17641. doi:10.1021/acsami.6b03644.

[108] H.D.M. Follmann, A.F. Naves, A.F. Martins, O. Félix, G. Decher, E.C. Muniz, R. Silva, Advanced fibroblast proliferation inhibition for biocompatible coating by electrostatic layer-by-layer assemblies of heparin and chitosan derivatives, J. Colloid Interface Sci. 474 (2016) 9–17. doi:10.1016/j.jcis.2016.04.008.

[109] R.M. Sabino, K. Kauk, L.Y.C. Madruga, M.J. Kipper, A.F. Martins, K.C. Popat, Enhanced hemocompatibility and antibacterial activity on titania nanotubes with tanfloc/heparin polyelectrolyte multilayers, J. Biomed. Mater. Res. Part A. 108 (2020) 992–1005. doi:10.1002/jbm.a.36876.

[110] J. Chen, C. Chen, Z. Chen, J. Chen, Q. Li, N. Huang, Collagen/heparin coating on titanium surface improves the biocompatibility of titanium applied as a blood-contacting biomaterial, J. Biomed. Mater. Res. Part A. 95A (2010) 341–349. doi:10.1002/jbm.a.32847.

[111] X. Zhang, G. Zhang, H. Zhang, J. Li, X. Yao, B. Tang, Surface immobilization of heparin and chitosan on titanium to improve hemocompatibility and antibacterial activities, Colloids Surfaces B Biointerfaces. 172 (2018) 338–345. doi:10.1016/J.COLSURFB.2018.08.060.

[112] K. Zhang, J. ying Chen, W. Qin, J. an Li, F. xia Guan, N. Huang, Constructing bio-layer of heparin and type IV collagen on titanium surface for improving its endothelialization and blood compatibility, J. Mater. Sci. Mater. Med. 27 (2016) 81. doi:10.1007/s10856-016-5693-6.

[113] W.J. Cherng, Y.H. Pan, T.C. Wu, C.C. Chou, C.H. Yeh, J.J. Ho, Hemocompatibility and adhesion of heparin/dopamine and heparin/collagen self-assembly multilayers coated on a titanium substrate, Appl. Surf. Sci. 463 (2019) 732–740. doi:10.1016/j.apsusc.2018.08.217.

[114] Y. Liu, K. Ai, L. Lu, Polydopamine and its derivative materials: Synthesis and promising applications in energy, environmental, and biomedical fields, Chem. Rev. 114 (2014) 5057–5115. doi:10.1021/cr400407a.

[115] Y. Yang, X. Li, H. Qiu, P. Li, P. Qi, M.F. Maitz, T. You, R. Shen, Z. Yang, W. Tian, N. Huang, Polydopamine Modified TiO2 Nanotube Arrays for Long-Term Controlled Elution of Bivalirudin and Improved Hemocompatibility, ACS Appl. Mater. Interfaces. 10 (2017)

7649–7660. doi:10.1021/ACSAMI.7B06108.

[116] G. Li, P. Yang, W. Qin, M.F. Maitz, S. Zhou, N. Huang, The effect of coimmobilizing heparin and fibronectin on titanium on hemocompatibility and endothelialization, Biomaterials. 32 (2011) 4691–4703. doi:10.1016/j.biomaterials.2011.03.025.

[117] R. Daum, D. Visser, C. Wild, L. Kutuzova, M. Schneider, G. Lorenz, M. Weiss, S. Hinderer, U.A. Stock, M. Seifert, K. Schenke-Layland, Fibronectin Adsorption on Electrospun Synthetic Vascular Grafts Attracts Endothelial Progenitor Cells and Promotes Endothelialization in Dynamic In Vitro Culture, Cells. 9 (2020) 778. doi:10.3390/cells9030778.

[118] G. Li, P. Yang, Y. Liao, N. Huang, Tailoring of the titanium surface by immobilization of heparin/fibronectin complexes for improving blood compatibility and endothelialization: An in vitro study, Biomacromolecules. 12 (2011) 1155–1168. doi:10.1021/bm101468v.

[119] K. Xu, K. Cai, Self-assembled phase-transited lysozyme/heparin coating on titanium surfaces for improved hemocompatibility, Mater. Lett. 247 (2019) 95–98. doi:10.1016/j.matlet.2019.03.110.

[120] V. Vyas, T. Kaur, S. Kar, A. Thirugnanam, Biofunctionalization of commercially pure titanium with chitosan/hydroxyapatite biocomposite via silanization: evaluation of biological performances, J. Adhes. Sci. Technol. 31 (2017) 1768–1781. doi:10.1080/01694243.2016.1278070.

[121] R.M. Sabino, G. Mondini, M.J. Kipper, A.F. Martins, K.C. Popat, Tanfloc/heparin polyelectrolyte multilayers improve osteogenic differentiation of adipose-derived stem cells on titania nanotube surfaces, Carbohydr. Polym. 251 (2021) 117079. doi:10.1016/j.carbpol.2020.117079.

[122] W. Lin, J. Zhang, Z. Wang, S. Chen, Development of robust biocompatible silicone with high resistance to protein adsorption and bacterial adhesion, Acta Biomater. 7 (2011) 2053–2059. doi:10.1016/J.ACTBIO.2011.02.001.

[123] P.C.F. da Câmara, L.Y.C. Madruga, R.M. Sabino, J. Vlcek, R.C. Balaban, K.C. Popat, A.F. Martins, M.J. Kipper, Polyelectrolyte multilayers containing a tannin derivative polyphenol improve blood compatibility through interactions with platelets and serum proteins, Mater. Sci. Eng. C. 112 (2020) 110919. doi:10.1016/j.msec.2020.110919.

[124] E. Jia, B. Liang, Y. Lin, Z. Su, Hemocompatibility of polyzwitterion-modified titanium

dioxide nanotubes, Nanotechnology. 32 (2021) 305704. doi:10.1088/1361-6528/ABF0CB.

[125] Y.F. Cheng, Y.H. Mei, G. Sathishkumar, Z.S. Lu, C.M. Li, F. Wang, Q.Y. Xia, L.Q. Xu, Tannic acid-assisted deposition of silk sericin on the titanium surfaces for antifouling application, Colloids Interface Sci. Commun. 35 (2020) 100241. doi:10.1016/j.colcom.2020.100241.

[126] L. Meng, K. Pan, Y. Zhu, W. Wei, X. Li, X. Liu, Zwitterionic-Based Surface via the Coelectrodeposition of Colloid Particles and Tannic Acid with Bacterial Resistance but Cell Adhesion Properties, ACS Biomater. Sci. Eng. 4 (2018) 4122–4131. doi:10.1021/acsbiomaterials.8b01239.

[127] A. Lee, S.M. Kang, Ultralow fouling of fibrinogen and human platelets on ulvan multilayer-coated solid surfaces, J. Ind. Eng. Chem. 82 (2020) 228–233. doi:10.1016/j.jiec.2019.10.017.

[128] M.J. Stadnik, M.B. de Freitas, Algal polysaccharides as source of plant resistance inducers, Trop. Plant Pathol. 39 (2014) 111–118. doi:10.1590/S1982-56762014000200001.

[129] J. Chen, J. Cao, J. Wang, M.F. Maitz, L. Guo, Y. Zhao, Q. Li, K. Xiong, N. Huang, Biofunctionalization of titanium with PEG and anti-CD34 for hemocompatibility and stimulated endothelialization, J. Colloid Interface Sci. 368 (2012) 636–647. doi:10.1016/j.jcis.2011.11.039.

[130] X. Wu, C. Liu, H. Chen, Y. Zhang, L. Li, N. Tang, Layer-by-Layer Deposition of Hyaluronan and Quercetin-Loaded Chitosan Nanoparticles onto Titanium for Improving Blood Compatibility, Coatings 2020, Vol. 10, Page 256. 10 (2020) 256. doi:10.3390/COATINGS10030256.

[131] M.A. Llopis-Grimalt, M.A. Forteza-Genestra, V. Alcolea-Rodriguez, J.M. Ramis, M. Monjo, Nanostructured titanium for improved endothelial biocompatibility and reduced platelet adhesion in stent applications, Coatings. 10 (2020) 907. doi:10.3390/COATINGS10090907.

[132] A. Córdoba, M. Satué, M. Gómez-Florit, M. Hierro-Oliva, C. Petzold, S.P. Lyngstadaas, M.L. González-Martín, M. Monjo, J.M. Ramis, Flavonoid-Modified Surfaces: Multifunctional Bioactive Biomaterials with Osteopromotive, Anti-Inflammatory, and Anti-Fibrotic Potential, Adv. Healthc. Mater. 4 (2015) 540–549. doi:10.1002/adhm.201400587.

[133] R. Luo, J. Zhang, W. Zhuang, L. Deng, L. Li, H. Yu, J. Wang, N. Huang, Y. Wang, Multifunctional coatings that mimic the endothelium: Surface bound active heparin nanoparticles with: In situ generation of nitric oxide from nitrosothiols, J. Mater. Chem. B. 6 (2018) 5582–5595.

doi:10.1039/c8tb00596f.

[134] R. Simon-Walker, R. Romero, J.M. Staver, Y. Zang, M.M. Reynolds, K.C. Popat, M.J. Kipper, Glycocalyx-inspired nitric oxide-releasing surfaces reduce platelet adhesion and activation on titanium, ACS Biomater. Sci. Eng. 3 (2017) 68–77. doi:10.1021/acsbiomaterials.6b00572.

[135] Y. Liu, T.T. Yang Tan, S. Yuan, C. Choong, Multifunctional P(PEGMA)-REDV conjugated titanium surfaces for improved endothelial cell selectivity and hemocompatibility, J. Mater. Chem. B. 1 (2013) 157–167. doi:10.1039/c2tb00014h.

[136] C. Han, X. Luo, D. Zou, J. Li, K. Zhang, P. Yang, N. Huang, Nature-inspired extracellular matrix coating produced by micro-patterned smooth muscle and endothelial cells endows cardiovascular materials with better biocompatibility, Biomater. Sci. 7 (2019) 2686–2701. doi:10.1039/c9bm00128j.

[137] X. Wang, T. Liu, Y. Chen, K. Zhang, M.F. Maitz, C. Pan, J. Chen, N. Huang, Extracellular matrix inspired surface functionalization with heparin, fibronectin and VEGF provides an anticoagulant and endothelialization supporting microenvironment, Appl. Surf. Sci. 320 (2014) 871–882. doi:10.1016/j.apsusc.2014.09.004.

CHAPTER 2: HEMOCOMPATIBILITY OF HYDROTHERMALLY TREATED TITANIUM AND TITANIUM ALLOY SURFACES[1]

2.1 Introduction

Different types of blood contacting medical devices such as mechanical heart valves, stents, vascular grafts, catheters, etc. are implanted in patients worldwide to treat cardiovascular diseases. It is estimated that the number of coronary procedures carried out in USA to implant these medical devices in the year 2019 is approximately 1,055,000, out of which 335,000 (approximately 31) are recurring procedures [1]. Most of the recurring procedures are due to inappropriate interaction of the implant material with blood and its components which results in infection, inflammation and thrombosis [2,3]. Thrombosis is one of the major reasons for implant failure, where blood clot forms on the implant surface, thus obstructing the flow of the blood. Fibrinogen is adhered on the surface immediately after blood comes in contact with the surface and this induces platelet adhesion, activation and aggregation on the surface. Simultaneously, factor XII also adsorbs to the surface and gets autoactivated resulting in conversion of prekallikrein to kallikrein, thus initiating coagulation and thrombin formation on the surface [4]. Thrombin converts fibrinogen to fibrin and traps red blood cells and forms the blood clot. Hence it is important to understand the blood-implant surface interactions and modify the implant surface characteristics to improve its compatibility with blood and its components, i.e. hemocompatibility [5].

Several clinical approaches have been employed to prevent blood clotting on implant surfaces. The most common approach is to prescribe patients with blood thinners such as Aspirin, Clopidogrel and Vorapaxar to avoid clotting of the blood [6]. However, there are significant risks associated with internal bleeding and weakened immune response that may compromise the overall health of these patients [7]. Implants coated with anticoagulants such as warfarin and heparin has also been

[1]This work was published in ACS Omega and is reproduced in modified form here with permission

widely used [8–10], however there are risks associated with decrease in plate count, inflammation and internal bleeding 11. Several other research approaches have also been investigated to prevent blood clotting such as surface modification of implant surfaces with antithrombotic agents like polyethylene oxide and albumin protein. However, studies have shown that there is no significant difference in blood clotting compared to unmodified surfaces [2,10,12,13]. Different surface nano features with varied roughness and wettability have also been investigated, and the results have shown significant differences in blood plasma protein adsorption [14–16]. However, the effect of the size and shape of nano features on protein adsorption and whole blood clotting is not well established. Different approaches on modifying the surface chemistry and topography combined have also been investigated. For example, superhydrophobic surfaces have shown significant reduction in adsorption of blood plasma proteins and whole blood clotting [17–19]. Nevertheless, these surfaces may not be stable for prolonged duration when exposed to blood. Also, superhydrophobic surfaces will not adhere endothelial cells which plays a major role in the integration of many blood contacting medical devices with the native tissue [19]. Thus, there is a need to develop robust surfaces that prevents fibrinogen adsorption, controls blood clotting, and also have potential to interact appropriately with the native tissue without compromising the implant integration.

Titanium (Ti) and its alloys have been established as a material of choice for different implantable medical devices such as heart valves, stents, dental and orthopedic implants [20–22]. Even though, titanium implants interact appropriately with the native tissue, they are prone to thrombosis when in contact with blood. In this study, Ti and its alloy Ti-6Al-4V were hydrothermally treated to form nanostructured surfaces with the aim to enhance their hemocompatibility. The hydrothermal treatment modified the surface of Ti and Ti-6Al-4V with different nanotopographies and wettability properties. Previous studies have shown that nanostructured titanium surfaces have led to better hemocompatibility when compared nontextured surfaces [21–24]. However, it is not well established whether it is the alteration of surface wettability or the nanostructure that majorly contributes to the difference in hemocompatible response. In this study, we have developed three different types of nanostructured surfaces by hydrothermal treatment on Ti and TI-6Al-4V. The surfaces

were characterized for their wettability, surface morphology, surface chemistry and crystallinity. The hemocompatibility of these surfaces was characterized by evaluating blood plasma protein adsorption, platelet adhesion and activation, platelet-leukocyte complex formation and whole blood clotting. The results indicate that surface topography and the size of nanostructure plays a major role in determining the hemocompatible response on hydrothermally treated surfaces.

2.2 Materials and Methods

2.2.1 Fabrication of nanostructures on the different surfaces

The materials used in this study were sheets of 0.05 mm thick commercially pure Ti (Grade 2) and Ti-6Al-4V alloy. Square substrates of dimension 6 mm X 6 mm were cut from the sheets. The surfaces were polished using SiC abrasive sheets up to grade 1400. Polished substrates were then cleaned ultrasonically with acetone and deionized (DI) water for 10 mins each. Three different fabrication processes were used to hydrothermally treat the substrates to form nanostructures on the surface and are explained below:

Substrates were immersed in 75 ml of 1M NaOH solution inside an inert PTFE bottle and hydrothermally treated for 4 hrs at 200°C inside an oven. The treated substrates were rinsed with DI water and were annealed for 1 hr at 300°C.

Substrates were immersed in 50 ml of 5M NaOH solution inside an inert PTFE bottle and hydrothermally treated for 24 hrs at 60°C inside an oven. The treated substrates were rinsed with DI water and were annealed for 1 hr at 300°C.

Substrates were immersed in 75 ml of 1M NaOH solution inside an inert PTFE bottle and hydrothermally treated for 2.5 hrs at 200°C inside an oven. The treated substrates were rinsed with DI water and were annealed for 1 hr at 300°C. After annealing they were again rinsed with DI water and immersed in 50 ml of 0.6M HCl solution inside an inert PTFE bottle for 1 hr inside an oven. The treated substrates were rinsed with DI water and were annealed for 2 hrs at 600°C.

After the treatments, all substrates were ultrasonically cleaned with DI water for 10 mins and dried using nitrogen gas. Following notation will be used in the manuscript for different surfaces: Ti for unmodified Ti, A for unmodified Ti-6Al-4V. The modified surfaces are abbreviated as Ti1, Ti2, Ti3, A1, A2, A3; where the number corresponds to the hydrothermal treatment used.

2.2.2 Characterization of different surfaces.

The modified surfaces were characterized using different techniques to evaluate their surface energy, morphology, chemistry and crystal structure.

2.2.3 Surface morphology

The surface morphology was characterized using a JEOL 6500 field emission scanning electron microscopy (SEM) operated at an accelerating voltage of 15KV. The surfaces were coated with 5 nm gold before imaging. The surfaces were imaged at a magnification of 5000X and 30000X. The images were processed using ImageJ software.

2.2.4 Contact angle measurements and surface energy calculations

The surface hydrophobicity/hydrophilicity was characterized by measuring apparent contact angle θ^* and advancing contact angle (θ_{adv}) at room temperature using sessile drop method (Ramé-hart 260F4 goniometer). Images were captured 3 secs after 5 µl droplet of DI water (polar) and hexadecane (non-polar) was placed on the substrate. The errors in apparent and advancing contact angles were ±4º and ±3º respectively. The images were analyzed using the manufacturer provided software to measure the contact angles. Apparent contact angles for blood and platelet-rich plasma (PRP) (see section 2.2.5 for isolation of blood and PRP) were also measured using the same method. The advancing contact angles for water and hexadecane were used to calculate the solid-vapor surface energy. The polar and dispersive components of the surface energy was calculated using the equation Young's (equation 2.1) and Owens-Wendt equation (equation 2.2).

$$\gamma_{lv} cos\theta = \gamma_{sv} - \gamma_{sl} \tag{2.1}$$

$$\gamma_{sl} = \gamma_{sv} + \gamma_{lv} - 2(\sqrt{\gamma_{s^D}\gamma_{l_v^D}} + \sqrt{\gamma_{s_v}^P \gamma_{l_v}^P}) \tag{2.2}$$

where γ_{lv} is the liquid (water)vapor interfacial tension (72.8 mN/M) and hexadecane (27.5 mN/M), θ is the advancing contact angle, γ_{sv} is the solid surface free energy, γ_{sl} is the solid-liquid interfacial free energy, γ_{sD} and γ_{lD} is the dispersive components and γ_{sP} and γ_{lP} is the polar components of the solid and liquid free surface energy respectively. The above two equations were solved to get the final equations to calculate the dispersive (equation 2.3) and polar (equation 2.4) components of the solid-vapor surface energy. The overall solid-vapor surface energy is the sum of the dispersive and polar components (equation 2.5) [25].

$$\gamma_{s_v}^d = \gamma_{L_v}^d((1 + cos(\theta_\gamma^d)/2)^2 \tag{2.3}$$

$$\gamma_{s_v}^p = 1/(\gamma_{L_V}^p)(\gamma_l v(1 + cos\theta_\gamma^d))/2 - \sqrt{(}\gamma_{L_v}^d \gamma_{s_v}^d))^2 \tag{2.4}$$

$$\gamma_{sv} = \gamma_{s_v}^d + \gamma_{s_v}^p \tag{2.5}$$

2.2.5 Surface chemistry

The surface chemistry was characterized using a PE-5800 X-ray Photoelectron spectrometer (XPS). Survey spectra were collected from 0 to 1100 eV with a pass energy of 187.85 eV. High resolution

spectra were collected for oxygen (O1s) using a pass energy of 10 eV. Surface elemental composition was calculated using peak fit analysis in the Multipack and Origin software.

2.2.6 Surface crystal structure

The presence of anatase and rutile crystal phases was characterized using Bruker D8 GAXRD Glancing Angle X-ray Diffraction (GAXRD). XRD scans were collected at = 1.5° and 2 ranges were chosen based on significant peak intensities. Detector scans were run at a step size of 0.01 with a time per step of 1 s. Peaks were filtered and correlated to crystal structures using DIFFRACT.EVA software.

2.2.7 Surface preparation prior to biological studies

Prior to biological studies, the surfaces were sonicated in acetone for 10 mins followed by rinsing with DI water and phosphate buffered saline (PBS) solution. The surfaces were sterilized by exposing to UV light for 15 mins inside a biosafety cabinet.

2.2.8 Protein adsorption on the different surfaces

Albumin and fibrinogen adsorption were characterized using a micro-BCA assay. The surfaces were incubated for 2 hrs in a 48-well plate on a horizontal shaker (100rpm) at 37°C and 5% CO2 with 300 µl of protein solution (concentration 100 µg/ml in PBS). After 2 hrs, the protein solution was aspirated, and surfaces were rinsed 3 times with PBS. To measure the amount of protein adhered on different surfaces, the substrates are incubated for 1 hr in a 48-well plate on a horizontal shaker (100rpm) at 37°C and 5% CO2 with 200 µl of 1% sodium dodecyl sulfate (SDS). This was repeated twice, and the SDS solution with the desorbed protein was pooled. The pooled SDS was used with micro-BCA assay to measure the absorbance of the resulting solution at a wavelength of 562 nm using a plate reader. The protocol given by the manufacturer was followed to plot the standard curve and the protein concentration from the absorbance values was calculated.

2.2.9 Platelet-rich plasma (PRP) isolation from whole blood

Whole blood was isolated through venipuncture from healthy donors who refrained from having drugs that may have affected their blood. The isolation procedure was in accordance with the protocol approved by the Colorado State University Institutional Review Board. Procedures were performed in compliance with the National Institutes of Health's "Guiding Principles for Ethical Research". Informed consents were obtained from human participants prior to enrolling in this study. The blood was collected in 6 ml tubes coated with the anticoagulant, ethylenediaminetetraacetic acid (EDTA). The first tube of blood was discarded to account for the platelet plug and locally activated platelets resulting from the needle insertion. The PRP was isolated by centrifuging the blood tubes at 150 g for 15 mins. The centrifugation results into two layers, the top layer which is PRP and the bottom layer which are the red blood cells. After centrifugation, the tubes were let to rest for another 15 mins before the PRP was used. All the biological studies were repeated at least three times with blood drawn from at least three different donors. However, for each experiment, the PRP was only pooled from the same donor. This is because there is donor-to-donor variability in the number of platelets and it is not possible to compare the absolute values from different donors.

2.2.10 Cytotoxicity of different surfaces

Cytotoxicity of different surfaces was evaluated using commercially available Lacate dehydrogenase (LDH) assay kit. The surfaces along with positive (provided with the assay) and negative controls (PRP treated with Triton-X provided with the assay) were incubated with 300 µl of PRP in a 48-well plate on a horizontal shaker (100rpm) for 2 hrs at 37°C and 5% CO2. After the incubation, the PRP solution was aspirated and surfaces were rinsed 3 times with PBS to remove any nonadherent cells. 100 µl of surface-exposed PRP was pipetted to the 96-well plate and protocol provided by the manufacturer was followed. The absorbance of the resulting solution was measured at a wavelength of 490 nm using a plate reader.

2.2.11 Fibrinogen binding from PRP on different surfaces

Fibrinogen binding was measured using commercially available ELISA kit for human fibrinogen. The surfaces were incubated in 300 µl of PRP in a 48-well plate on a horizontal shaker (100rpm) for 2 hrs at 37°C and 5% CO2. The surface exposed PRP was then diluted to 1/10,000 with the diluent provided with the ELISA kit. This diluted PRP was pipetted to the 96-well plate and protocol provided by the manufacturer was followed. The absorbance of the resulting solution was measured at a wavelength of 450 nm using a plate reader.

2.2.12 Cell adhesion on different surfaces

Cell adhesion on different surfaces was imaged using fluorescence microscopy. The surfaces were incubated in 300 µl of PRP in a 48-well plate on a horizontal shaker (100rpm) for 2 hrs at 37°C and 5% CO2. After the incubation, the PRP was aspirated and surfaces were rinsed 3 times with PBS to remove any unadhered cells. The surfaces were then incubated in dark with 1 ml of 5% calcein-AM solution in PBS for 20 mins at room temperature. The stain solution was aspirated, and the surfaces were rinsed 2 times with PBS. The surfaces were imaged using a fluorescence microscope (Zeiss Axiovision) at 20X. All images were further processed using ImageJ to calculate the surface coverage of cells.

2.2.13 Identification of platelets and leukocytes adhered on different surfaces

Identification of platelets and leukocytes adhered on different surfaces was imaged using fluorescence microscopy. The surfaces were incubated in 300 μl of PRP in a 48-well plate on a horizontal shaker (100rpm) for 2 hrs at 37°C and 5% CO_2. After the incubation, the PRP was aspirated and surfaces were rinsed 3 times with PBS to remove any unadhered cells. The surfaces were fixed in a 3.7% formaldehyde solution diluted with PBS for 15 min. The fixed surfaces were rinsed twice in PBS for 5 mins each. Subsequently the surfaces were incubated in a solution of 1% Triton X diluted with PBS for 3 min. The surfaces were again rinsed twice in PBS and moved to a new

48-well plate. 200 μl of 0.05% rhodamine phalloidin (actin) solution in PBS was added to each well and incubated for 25 mins. 21 μl of 3% DAPI (4', 6 – diamidino – 2 – phenylindole) stain stock solution was added to each well and incubated for 5 more mins. The surfaces were then rinsed twice in PBS and imaged using a fluorescence microscope. ImageJ was used to calculate the actin cell coverage and number of nuclei on the substrates. The DAPI will stain the nucleus of leukocytes blue, whereas the rhodamine – phalloidin will stain the cytoskeleton of both the platelets and leukocytes red.

2.2.14 Platelet activation on different surfaces

Platelet activation on different surfaces was characterized using SEM. The surfaces were incubated in 300 μl of PRP in a 48-well plate on a horizontal shaker (100rpm) for 2 hrs at 37°C and 5% CO_2. After the incubation, the PRP was aspirated and surfaces were rinsed 3 times with PBS to remove any unadhered cells. The cells adhered on the surface were fixed by incubating the surfaces in a solution containing 6% glutaraldehyde, 0.1M sodium cacodylate and 0.1M sucrose in DI water for 45 mins. The surfaces were then incubated in a buffer solution containing 0.1M sodium cacodylate and 0.1M sucrose for 10 mins. This was followed by incubating the surfaces in a 35%, 50%, 70% and 100% ethanol for 10 mins each. The surfaces were air-dried and imaged using an SEM as discussed in Section 2.2.1.

2.2.15 Whole blood clotting on different surfaces

Whole blood clotting on different surfaces was characterized by indirectly measuring the amount of free hemoglobin in un-clotted blood after exposure of surfaces to whole human blood using a plate reader. For this study, blood was drawn in a vacuum tube without any anticoagulant and was used immediately after drawing. 5 μl of blood was pipetted on top of different surfaces in 24-well plate and the blood was allowed to clot for up to 45 mins. After every 15 mins, the surfaces were evaluated for presence of free hemoglobin. 500 μl of DI water was added to the surfaces and gently shaken for 30 secs to lyse red blood cells that were not trapped in the clot on the surface.

The absorbance of free hemoglobin released by the lysed red blood cells was measured at 540 nm wavelength using a plate reader.

2.2.16 Statistical Analysis

Surface characterization was repeated for at least 3 different samples of each surface. SEM images and contact angle measurements were taken at 3 different locations on each sample ($n_{min} = 9$). Protein adsorption were carried out on at least 3 different samples of each surface and was repeated at least 3 times ($n_{min} = 9$). The LDH assay, fluorescence microscopy, platelet activation and whole blood clotting was repeated at least 2 times (with PRP from different donors) with at least 3 different samples of each surface ($n_{min} = 6$). The quantitative results were analyzed using two-way ANOVA test using R software. Results were considered statistically significant with a $p - value < 0.05$. The data presented (i.e., the arithmetic mean and standard deviation) is only from one donor as it is not appropriate to compare values between different donors due to the variability in the platelet counts for each donor. However, similar trends were observed for blood from different donors for all the results presented indicating the reproducibility of the data.

2.3 Results and Discussion

Despite extensive research carried out to understand the interaction of blood and its components with the surface of implantable medical devices 26–30, implants fail majorly due to blood clotting. This is major concerns with blood contacting biomaterials where protein absorption, platelet adhesion and activation which causes blood clotting that could be fatal for patients. In this study, Ti and its alloy, Ti-6Al-4V were exposed to an alkaline solution (NaOH) which leads to a corrosive reaction on the surface along with oxidization of the element(s) present **(Equation 2.6)**.

$$Ti + 2NaOH + H_20 \longrightarrow Na_2TiO_3 + TiO_2 + 2H_2 \tag{2.6}$$

The rate of the reaction is influenced by various factors such as the concentration of NaOH, reaction temperature and time [31]. These corrosive reactions lead to unique nanostructures on the material surface [32]. The modified surfaces were characterized for surface morphology, surface energy, surface chemistry and crystal structure. The possible oxides states of titanium formed during the reaction in a NaOH solution according to the Pourbaix diagram [33] for titanium are TiO_2 [34] and Ti_2O_3 (Ti1, Ti2, A1, A2). These titanium oxides when further treated with HCl (Ti3, A3) develops titanate structures (equation 2.7) and this modification lead to unique surface topography that is different than the treatment with just NaOH.

$$Na_2TiO_3 + 2HCl \longrightarrow H_2TiO_3 + 2NaCl \tag{2.7}$$

In this study, hemocompatibility of the treated surfaces was characterized by protein absorption, cell cytotoxicity, cell adhesion, platelet adhesion and platelet activation, and whole blood clotting. Improved hemocompatibility may lead to less implant failures, thus increasing the implant life and decreasing recurring procedures in patients.

The morphology of different surfaces was visualized using SEM. The results indicate that the unmodified surfaces as expected do not have any unique surface features. Whereas after the treatment with NaOH, the surfaces have developed unique nanostructures. Ti1 and A1 when exposed to 1M NaOH for 4 hours have developed nanoporous surface **(Figure 2.1)**. There are also nanosized protrusions present on A1 with the length of single protrusions approximately 250-430 nm. These protrusions are not present on Ti1. Ti2 and A2 when exposed to 5M NaOH for 24 hrs have developed interconnected web like nanoporous surface. The grain boundaries are also visible on the surface since they get etched faster than the rest of the surface. The web like nanoporous architecture is more clearly visible on the A2 (approximate pore size 150-280 nm) as compared to that on Ti2 (approximate pore size 70-170 nm). Ti3 and A3 were exposed to 1M NaOH for 2.5 hrs and later were further exposed to 0.6M HCl for 1 hr. This led to dramatically different

nanostructured surface, almost similar to nanosized granules. The average size of granules is approximately 160-220 nm for Ti3 and 90-120 nm for A3. All the surfaces fabricated had respective uniform morphology (Figure 1). The mechanism for the formation of different nanostructures on surfaces is not well established. However, it is likely that titanium when exposed to NaOH solution at specific temperatures will start reacting to form TiO_2 and Na+-O-Ti. The charge repulsion within Na+-O-Ti leads to protrusions in Ti1 and A1 (Figure 2.1). When the reaction time is significantly increased (Ti2 and A2), the TiO_2 and Na+-O-Ti is denser on the surfaces and hence results in absence of protrusions but a nanoporous surface. When the NaOH treated surfaces are exposed to HCl, the surface becomes neutral due to absence of Na+-O-Ti resulting in formation of denser granule like structures on the surface (**Figure 2.1**).

Contact angle on different surfaces was measured using a goniometer. There are two different configurations that defines contact angle on a nanostructured surface, namely Wenzel and Cassie-Baxter [35]. In Wenzel state, there is a complete wetting of the surface. Whereas, Cassie-Baxter is a meta stable state where air is trapped in between the surface and the liquid. Therefore, the contact angle is influenced by the area fraction of liquid in contact with solid and air. The apparent contact angles (θ^*) for different surfaces were measured with DI water, blood and PRP (Table 2.1). DI water is commonly used to characterize the surface wettability [36]. However, the goal in this study is to understand how blood and its components interact with different surfaces, therefore contact angles with blood and PRP were also measured. Blood is a very viscous fluid that includes PRP [37] (water, proteins, platelets, white blood cells, other biological factors) and red blood cells. However, when PRP is separated from blood, it is less viscous than blood, almost similar to DI water. All modified surfaces were hydrophilic ($\theta^* \leq 90^{\circ}$) with DI water (Table 2.1). The following trend for (θ^*) was observed: $Ti > A > Ti3 > A3 > A1 > Ti1 > A2 > Ti2$. Ti2 and A2 are more hydrophilic compared to all the other surfaces, almost close to being superhydrophilic ((θ^*) < 10). This is mainly due to the etched grain boundaries that increases the surface area and thus more wetting on the surface. A1 and A3 had almost similar contact angle despite different surface features and this

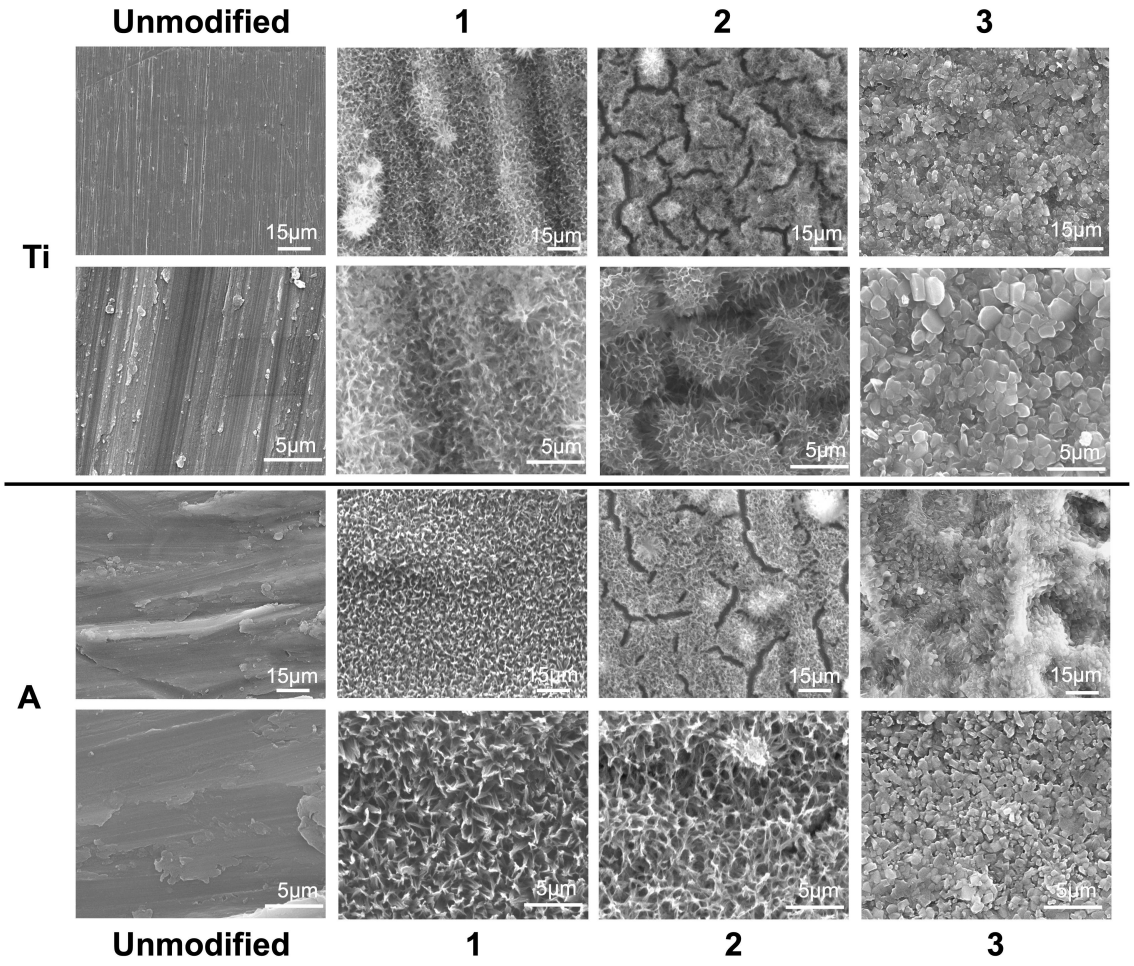

Figure 2.1: Representative SEM images of Ti and A surfaces treated by hydrothermal treatment. Images were taken at two different magnification (500X and 15000X).

could be due to the difference in surface chemistries that lead to similar polar interactions. Ti3 was least hydrophilic compared to all modified surfaces. In summary, titanium surfaces Ti, Ti1 and Ti2 are more hydrophilic than alloy surfaces A, A1, A2; whereas, A3 is more hydrophilic than Ti3 (**Table 2.1**). The surface wettability with PRP and blood is more influential for blood clotting [38]. All the modified surfaces are hydrophilic/hemophilic ($\theta^* < 90$) with PRP (Table 2.1). The following trend for (θ^*) was observed: $Ti > A > Ti2 > A3 > A2 > Ti3 > Ti1 > A1$. Further, surface wettability characteristics were completely different with blood when compared to DI water and PRP (Table 2.1). The following trend for θ^* was observed: $A > Ti > Ti3 > Ti2 > A3 > A2 > Ti1 > A1$. This could be due to the difference in the liquid properties specifically the viscosity and surface tension [39–42]. The results indicate that the interactions between different surfaces with different liquids were always in Wenzel state which is more stable than the Cassie-Baxter state [43].

Table 2.1: Apparent Contact Angles of DI Water, Blood, and PRP on Different Surfaces. The values were rounded off to zero decimal places. There is a significant difference in the apparent contact angle ($p < 0.05$) between all surfaces except A1 and A3 and Ti and Ti3 (statistical differences are not shown in the table).

Surface	DI Water	Blood	PRP
Ti	86	82	96
A	79	87	94
Ti1	31	25	12
A1	46	22	8
Ti2	13	41	29
A2	17	38	18
Ti3	64	47	16
A3	46	39	28

The advancing contact angle (θ_{adv}) for different surfaces with DI water (polar) and hexadecane (non-polar) were measured (**Table 2.2**). The trend for θ_{adv} with DI water were similar to θ^*. The (θ_{adv}) values were used to further calculate the surface energy using Owen-Wendt equation. Higher surface energy relates to higher hydrophilicity, whereas lower surface energy relates to higher hydrophobicity of the surface. The following trend for surface energy was observed:

$Ti2 > A2 > Ti1 > A1 > Ti3 > A3 > Ti > A$. Ti and A have non zero θ^* with hexadecane unlike all the modified surfaces. This is because of their low surface energy compared to other surfaces.

Table 2.2: Advancing Contact Angle of DI Water and Hexadecane on All Surfaces. The values were rounded off to zero decimal places. There is a significant difference in surface energy ($p < 0.05$) between all surfaces except A1 and A3 and Ti and Ti3

Surface	DI Water	Hexadecane	Surface energy (mJ/m^2)
Ti	92	19	27.75
A	98	24	25.85
Ti1	40	0	57.56
A1	63	0	42.07
Ti2	18	0	69.36
A2	30	0	63.07
Ti3	76	0	34.7
A3	65	0	40.81

The surface chemistry was analyzed using XPS. Survey scans were obtained and processed using MultiPak and Origin software (Figure 2.2). All the surfaces showed peaks for O1s (529–530eV for metal oxides), Ti_2p (458.5eV for TiO_2) and C1s (284.eV). Carbon is present on the surface due to impurities in the XPS chamber or on the surface. Ti1, Ti2 and A1, A2 have lower C_1s peaks compared to Ti and A respectively **(Table 2.3)**, indicating that the NaOH treatment removes some of the carbon impurities from the surfaces. Ti1 and A1 have higher Ti_2p peaks compared to Ti and A respectively. This is due to the etching process that exposes more surface titanium. However, Ti2 and A2 have lower Ti_2p peaks compared to A1 and Ti1 respectively due to longer etching process that oxidizes the titanium on the surface. In contrast, Ti3 and A3 have higher Ti_2p peaks compared to all the other surfaces due to acidic environment that etches the oxide exposing more surface titanium **(Table 2.3)**.

High resolution O1s scans were obtained to evaluate the oxidation of titanium on different surfaces **(Figure 2.3)**. The O-Ti and O-H peaks were present on all surfaces and H_2O peaks were

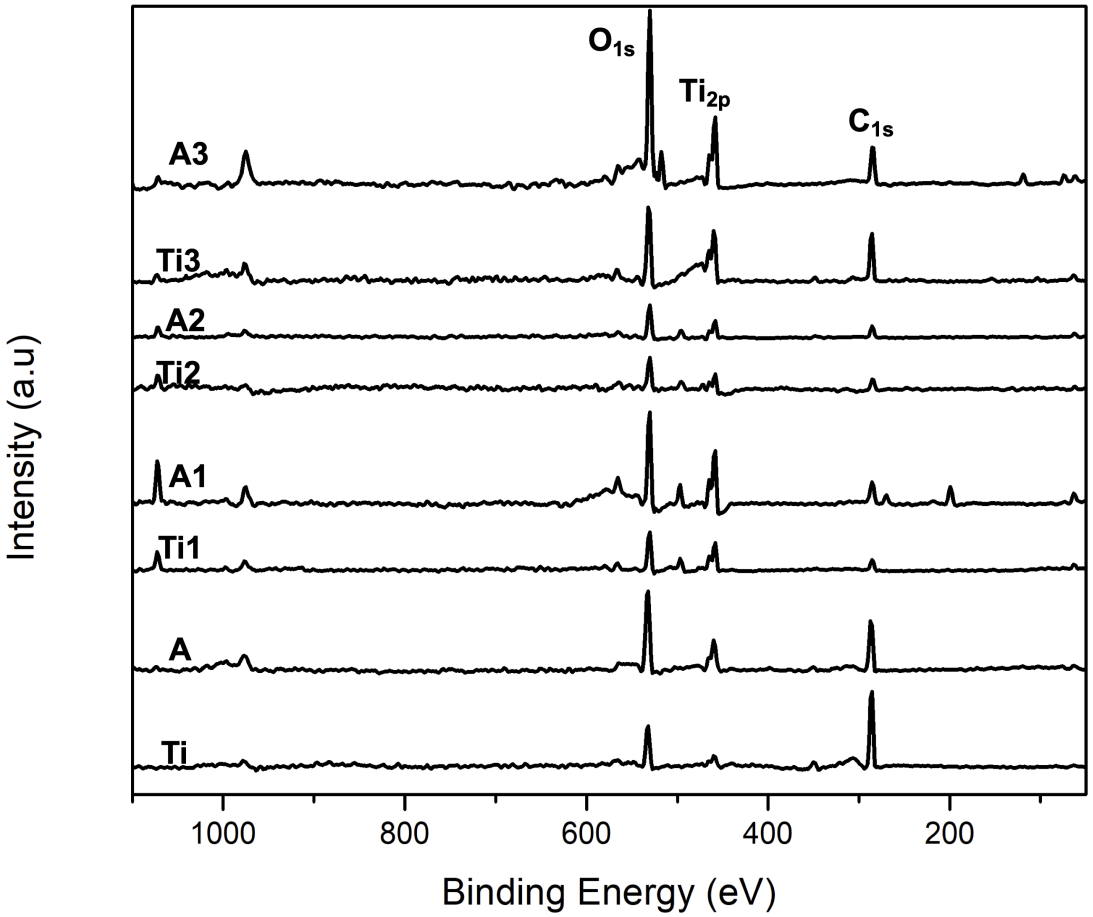

Figure 2.2: XPS Survey scans for different surfaces.

Table 2.3: XPS Elemental Composition Calculated from Survey Scans for Different Surfaces.

Surface	O 1s	Ti 2p	C 1s
Ti	20.8	2.8	76.4
A	39.0	7.0	54.0
Ti1	52.1	16.1	31.8
A1	51.5	16.8	31.7
Ti2	45.2	12.2	42.4
A2	50.3	12.1	37.6
Ti3	37.1	17.7	45.2
A3	38.9	20.1	41.0

present only on Ti1 and A1. Ti1 and A1 surfaces have higher O-Ti when compared to Ti and A respectively. However, with longer exposure to NaOH, Ti2 and A2 have no presence of H_2O, lower O-H peak, and higher O-Ti peaks compared to Ti and A respectively due to increase in oxidation on the surface. In contrast, Ti3 and A3 have higher O-H peaks and lower O-Ti peaks when compared to all the other substrates as the acid etches the oxide formed on the surface.

Surface crystallinity of different surfaces was analyzed using XRD (**Figure 2.4**). Different peaks relevant to surfaces here are as follows:

- Intensity peaks at 24° (101) and 62° (204) correspond to anatase phase (JCPDS No. 21-1272).
- Intensity peaks at 27° (110) and 76° (110) correspond to rutile phase of TiO_2 (JCPDS No. 21-1276).
- Intensity peaks at 38.1° (002) and 39.9° (101) planes correspond to metallic Ti (JCPDS No. 89-5009).
- Intensity peak at 48.7° (030) correspond to titanate structure (JCPDS No. 37-951) which suggests the presence of $Na_2Ti_3O_7$.

Ti1 and A1 show similar results with lower metallic Ti peaks compared to Ti and A respectively since both of these surfaces are oxidized. Ti2 and A2 also have higher TiO_2 rutile and metallic Ti

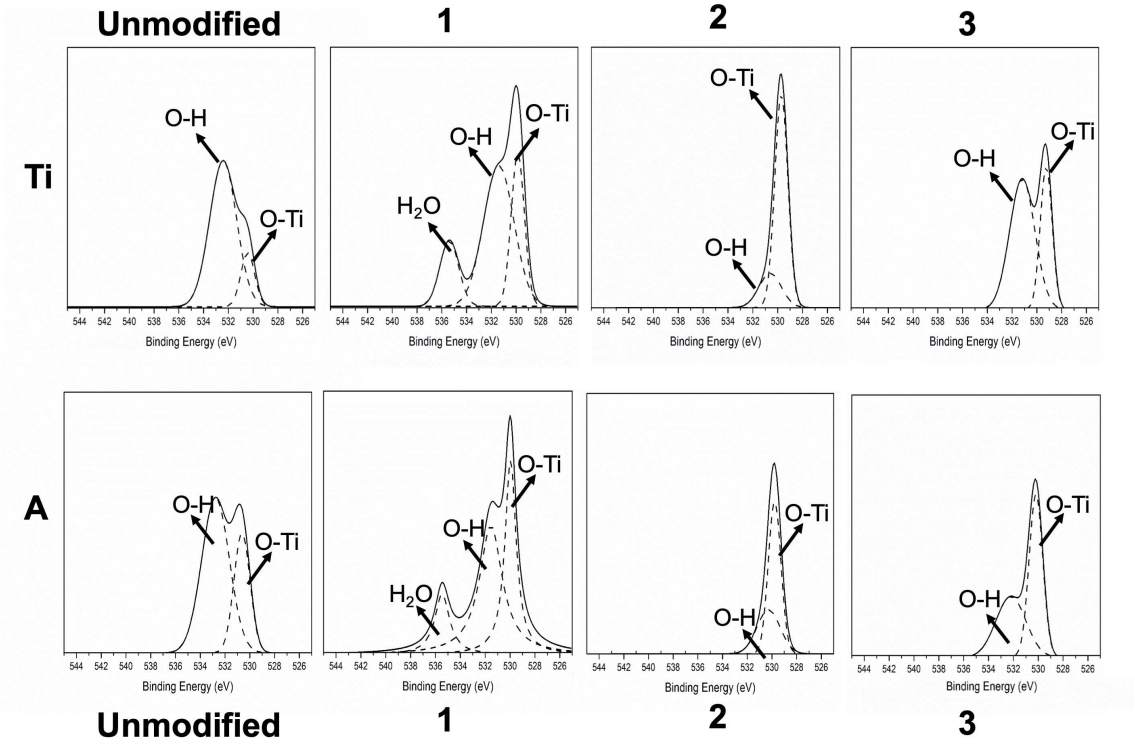

Figure 2.3: XPS High resolution O1s scans for different surfaces.

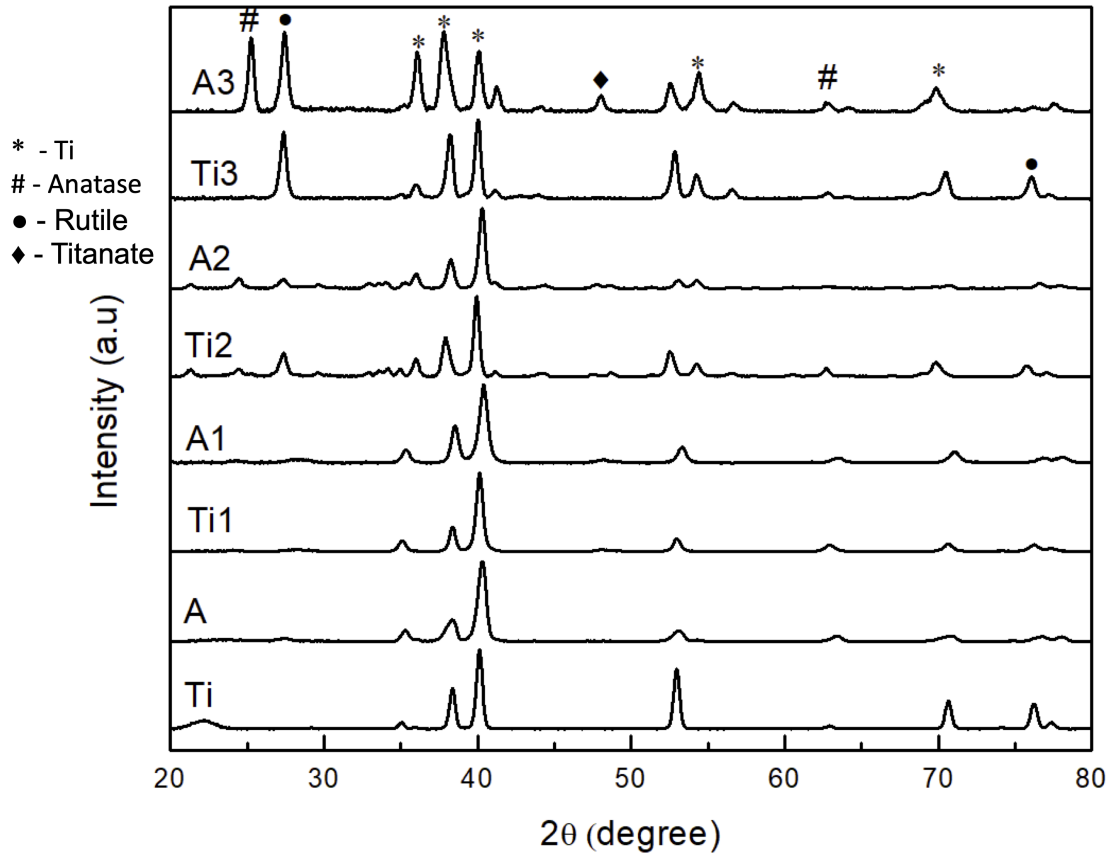

Figure 2.4: XRD scans for different surfaces.

peaks compared to Ti1 and A1 due to higher oxidation and etching during prolonged exposure to NaOH. Ti3 and A3 have higher TiO_2 rutile and Ti compared to all the surfaces 44. A3 also showed titanate peak.

Protein adsorption was characterized on different surfaces using a micro-BCA assay **(Figure 2.5)**. Protein adsorption to a surface is influenced by surface properties such as chemistry, topography, charge and roughness [45–47]. Fibrinogen is an inflammatory protein, directly influences the platelet adhesion and activation. It is excreted by the liver and is present in blood. It is a planar protein that has a trinodular structure linked by two coiled-coil regions with molecular weight of 340kDa [48]. When fibrinogen interacts with a unfamiliar surface (e.g. implant surface) it releases fibrinopeptides which drive the kinetics of thrombin formation [49]. Hence, it is impor-

tant to understand the amount of protein adsorbed to the surface. Albumin is the most abundant protein in the blood. It's a passivating protein which prevents blood thrombosis [50,51]. It is a globular protein with molecular weight 66.5 kDa [52]. However, more albumin doesn't directly correlate to less blood clotting as it is just one of many factors [53]. In this study, all modified surfaces are more hydrophilic than unmodified surfaces. More hydrophilicity is equated with less protein adsorption on the surface due to the energy barrier created by the liquid adsorbed to the surface [24,54]. The results for fibrinogen adsorption follow the following trend **(Figure 2.5a)**: $A3 > A1 > A2 > Ti3 > Ti2 > Ti > A > Ti2$ which doesn't follow the apparent contact angle trend **(Table 1.1)**. Ti2 has significantly lower fibrinogen adsorption compare to all the other surfaces since it is the most hydrophilic and has the densest porous structure compared to other surfaces **(Figure 2.1)**. However, A2 with almost similar contact angle and less dense porous structure has significantly higher fibrinogen adsorption compare to Ti2. Further, Ti1, Ti2 and Ti3 has lower protein adhesion compared to A1, A2 and A3 respectively in spite of similar nanostructure but different feature size. This is because the protein adsorption is also not merely influenced by contact angle but also majorly by surface topography [55]. Other statistical differences between different surfaces are included in **Table 1.4**. In contrast, the results for albumin adsorption follows the following trend **(Figure 1.5b)**: $A2 > Ti1 > A1 > Ti3 > Ti > A > A3 > Ti2$. Similar to fibrinogen adsorption, Ti2 has significantly lower albumin adsorption compare to all the other. Further, there is no significant differences in albumin adsorption on other surfaces irrespective of changes in contact angle and surface topography. The surface interaction with albumin is different than that of fibrinogen due to its globular shape and different charge [56].

Cytotoxicity of different surfaces was evaluated using LDH assay. Surface modification changes the topography and chemistry and it's important to evaluate if these changes induces any toxicity to the cells in contact with the surface. Cells when influenced by any toxic element stop growing and eventually die. When a cell begins to breakdown, they lose membrane integrity and release components from the cytoplasm into the medium and one of the stable enzymes excreted during this process is LDH [57]. Hence the presence of this LDH enzyme is a marker for cytotoxicity

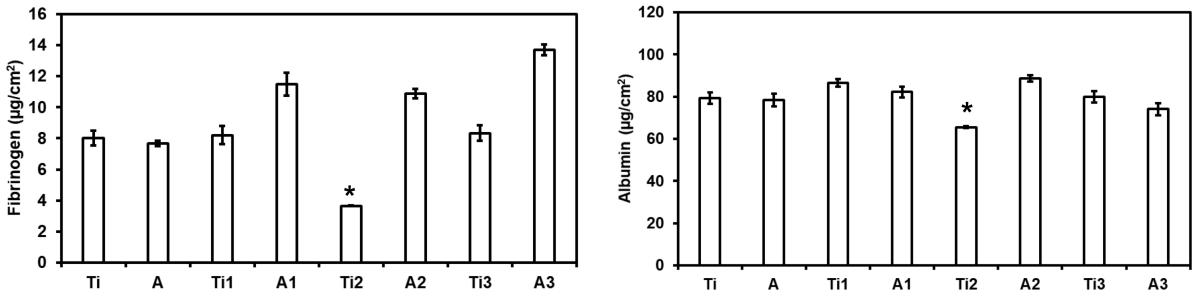

Figure 2.5: Fibrinogen adsorption on different surfaces measured using Micro BCA assay. The results indicate significantly lower fibrinogen adsorption on Ti2 compared to all the other surfaces ($* \rightarrow p < 0.05$) Other statistical differences are included in Table 4. Error bar represent standard deviation. (b) Albumin adsorption on different surfaces measured using Micro BCA assay. The results indicate significantly lower albumin adsorption on Ti2 compared to all the other surfaces ($* \rightarrow p < 0.05$). Error bar represent standard deviation.

[58]. The host body should be able to tolerate the implant while maintaining stability, without any exclusion and destruction [59]. The results indicate that all the substrates have similar amount of LDH expression compared to the positive control (100% live cells) indicating that none of the surfaces are inducing toxicity to the cells present in the PRP **(Figure 2.6)**. LDH expression from the negative control (100% dead cells) was significantly higher when compared to the all the surfaces and the positive control **(Figure 2.6)**. Thus, the results indicate that none of the surfaces demonstrate short term cytotoxic effects on the cells present in the PRP.

Fibrinogen binding from PRP on different surfaces was evaluated using an ELISA assay. Fibrinogen binding from PRP is a realistic environment since it is also influenced by other components that are present in PRP (other proteins, platelets, thrombin, leukocytes, etc.). Fibrinogen when in contact with thrombin gets converted to fibrin. This fibrin fibers form the blood clot on the surface. Hence it is important to evaluate fibrinogen binding directly from the PRP on different surfaces. The surface exposed PRP was assayed to measure the indirect amount of fibrinogen that was adsorbed on the surface. Higher fibrinogen in the surface exposed PRP indicates less fibrinogen adsorbed on the surface. The results indicate that all the surfaces have significantly higher amount of fibrinogen in the surface exposed PRP indicating lower fibrinogen adsorption on the surface when compared to

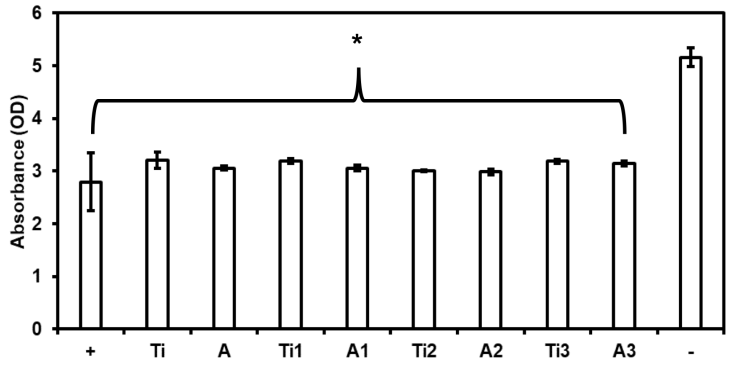

Figure 2.6: Cell cytotoxicity for PRP exposed to different surfaces measured using LDH assay. The results indicate no significant differences in LDH activity on all the surfaces and positive control (100% live cells), whereas, the LDH activity for negative control (100% dead cells) was significantly different than all the other surfaces ($* \rightarrow p < 0.05$)). Error bar represent standard deviation.

the Ti and A **(Figure 2.7)**. Further, Ti2 has significantly higher amount of fibrinogen in the surface exposed PRP indicating significantly lower fibrinogen adsorption on the surface when compared to all surfaces except Ti1. This is because Ti1 and Ti2 have similar nanostructures, however, Ti1 has less dense porous structure than Ti2 and when these surfaces are in contact with PRP, the fibrinogen binding may be influenced. Other statistical differences between different surfaces are included in Table 4. These results are similar to that of fibrinogen adsorption measured by micro-BCA assay.

Cell adhesion from PRP (platelets and leukocytes adhesion) on different surfaces was evaluated using fluorescence microscopy **(Figure 2.8a)**. The surfaces with adhered cells were stained with Calcein-AM [60]. Platelet and leukocyte adhesion plays a vital role in stimulation of the coagulation factors for hemostasis [61]. Leukocytes can impact coagulation directly by producing anticoagulant molecules or procoagulant or indirectly acting on platelets, other leukocytes or endothelial cells [62]. Hence it is important to understand the influence of surface modification on cell adhesion. The fluorescence microscopy images show that Ti and A have higher cell adhesion when compared to all the other surfaces (Figure 8a). The area covered by the cells adhered on the surface was calculated using ImageJ (Figure 2.8b). The results indicate significant decrease in cell adhesion

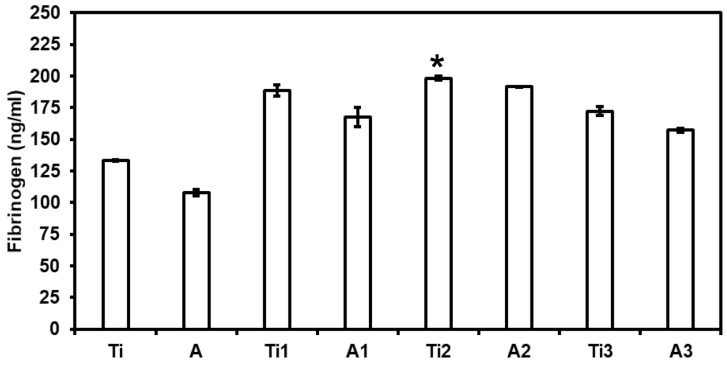

Figure 2.7: Fibrinogen binding from PRP on different surfaces measured using ELISA. The results indicate significant reduction in fibrinogen binding on Ti2 when compared to all the surfaces except Ti1 ($* \rightarrow p < 0.05$)). Other statistical differences are included in Table 4. Error bar represent standard deviation.

on the modified surfaces when compared to the Ti and A (Figure 2.8b), with Ti1 and Ti2 having least cell adhesion. Further, Ti1, Ti2 and Ti3 showed less cell adhesion when compared to A1, A2 and A3 respectively. Surface area is a key factor that influences cell adhesion. In general, higher surface area results in higher cell adhesion [63]. However, nanotopography of surfaces also influences cell adhesion. In porous surface like Ti2, dense porous structure majorly influences cell adhesion [64,65]. Results indicate lower cell adhesion on Ti2 due to its dense porous structure that drastically reduces area of contact with the cells. Cell adhesion through penetration into porous structure is also not possible as the size of the pores are smaller than the size of the cells [65]. Other statistical differences between different surfaces are included in **Table 2.4**.

Identification of different cell types (platelets and leukocytes) adhered on the surface from PRP was evaluated using fluorescence microscopy (Figure 9a). The surfaces with adhered cells were stained with DAPI and rhodamine-phalloidin. DAPI stains the nucleus of the cells whereas rhodamine-phalloidin stains the cytoskeleton of the cells. Since platelets do not have nucleus, they will not stain positive for DAPI, whereas both platelet and leukocytes will stain positive of rhodamine-phalloidin. Thus, by staining the cells with DAPI and rhodamine-phalloidin, leukocytes

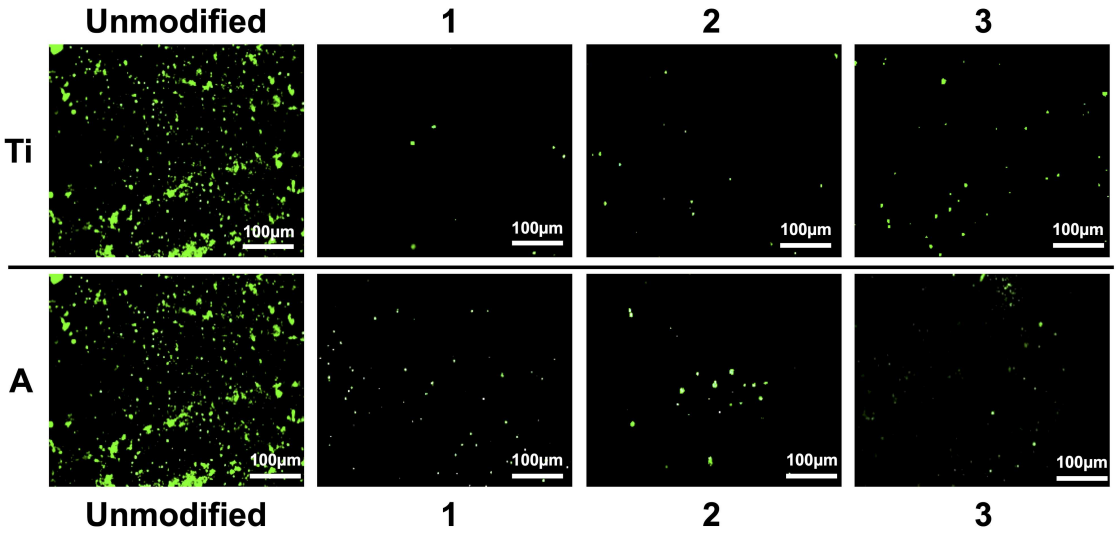

Figure 2.8: Representative fluorescence microscope images of adhered live cells (platelets and leukocytes) stained with Calcein-AM stain on different surfaces. The results indicate lower cell adhesion on all modified surfaces when compared to unmodified surfaces.

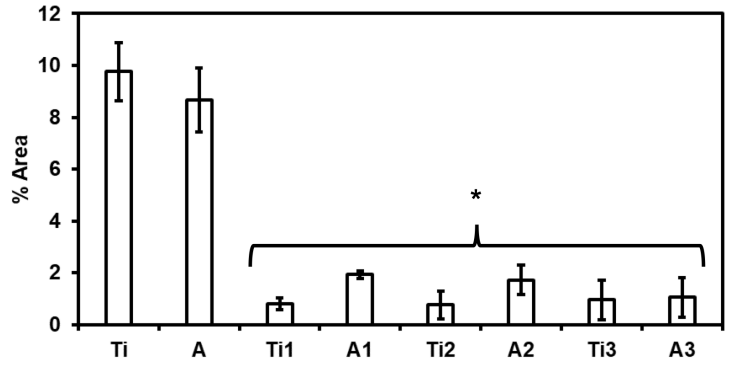

Figure 2.9: Percentage of area covered by the cells adhered on the surface calculated using ImageJ. The results indicate significantly lower cell adhesion on all modified surfaces when compared to unmodified surfaces ($* \rightarrow p < 0.05$)). Other statistical differences are included in Table 4. Error bar represent standard deviation.

adhered on the surface can be identified. During thrombosis, once the platelets are activated they interact with leukocytes and further enhance platelets activation rate 66,67. Hence, it is important to identify and evaluate platelet and leukocytes adhesion on the surface. The fluorescence microscopy images show that Ti and A have higher leukocytes and platelets adhered on the surface when compared to all the other surfaces (**Figure 2.9a**). The area covered by the leukocytes and platelets on the surface was calculated using ImageJ. The results from DAPI images indicate significant decrease in leukocyte adhesion on all the modified surfaces (**Figure 2.9b**), except Ti3, when compared to Ti and A. Results from rhodamine-phalloidin images indicate that platelet and leukocyte count from rhodamine-phalloidin stains **(Figure 2.9c)** is significantly lower on all modified surfaces when compared to Ti and A, with Ti1 and Ti2 having least cell adhesion. Further, Ti1, Ti2 and Ti3 showed less cell adhesion when compared to A1, A2 and A3 respectively. Other statistical differences between different surfaces are included in **Table 2.4**. Similar trends as to that of cell adhesion study were observed in this study.

Platelet activation and platelet-leukocyte complex formation on different surfaces was visualized using SEM. Platelets when activated change shapes, form dendrites and start aggregating [22]. Activated platelet may assist leukocyte localization during thrombosis and modulate their function [62]. Leukocyte-platelet interaction thus initiates biosynthesis of cytokines and inflammatory reactions which leads to several heart conditions [68]. Therefore, it is crucial to evaluate if the surfaces induce platelet activation and platelet-leukocyte complex formation. The SEM images shows activated platelets with dendrites on Ti and A **(Figure 2.10)**. Further, leukocyte-platelet interactions are also observed on Ti and A **(Figure 2.10, dotted circle)**. However, there is drastic reduction in platelet activation and absence of leukocyte-platelet interactions on all the other surfaces. Further, platelets seem to aggregate on modified surfaces. However, the platelets are not activated as no dendrite extensions are present.

Whole blood clotting was evaluated on different surfaces by measuring the free hemoglobin present on the surface that was in contact with blood. The un-clotted blood when diluted with DI

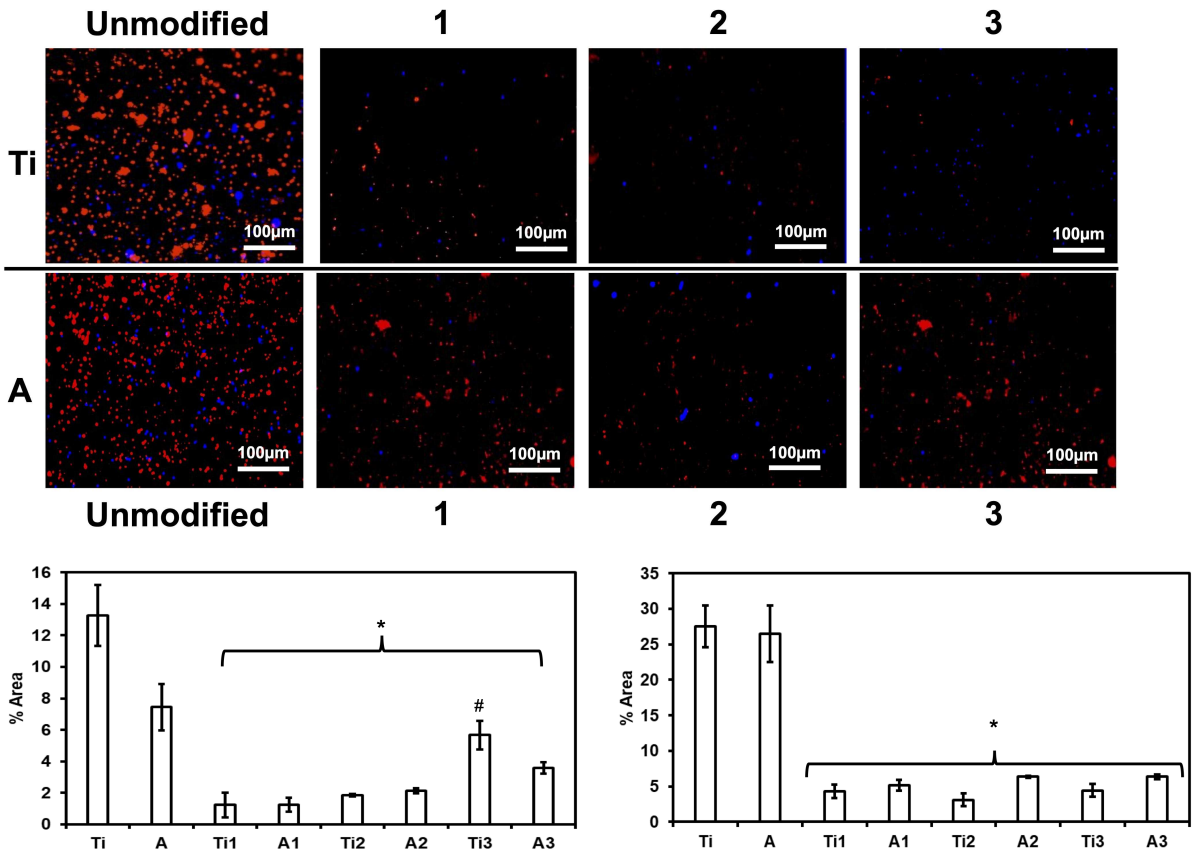

Figure 2.10: (a) Representative fluorescence microscope images of adhered platelets and leukocytes stained with DAPI and rhodamine-phalloidin on different surfaces. The results indicate lower cell adhesion on all modified surfaces when compared to unmodified surfaces.(b) Percentage of area covered by the cells adhered on the surface stained with DAPI calculated using ImageJ. The results indicate significantly lower cell adhesion on all modified surfaces when compared to unmodified surfaces ($* \rightarrow p < 0.05$)), except Ti3 ($\# \rightarrow p < 0.05$)). Error bar represent standard deviation. (c) Percentage of area covered by the cells adhered on the surface stained with rhodamine-phalloidin calculated using ImageJ. The results indicate significantly lower cell adhesion on all modified surfaces when compared to unmodified surfaces ($* \rightarrow p < 0.05$)). Other statistical differences are included in Table 1.4. Error bar represent standard deviation.

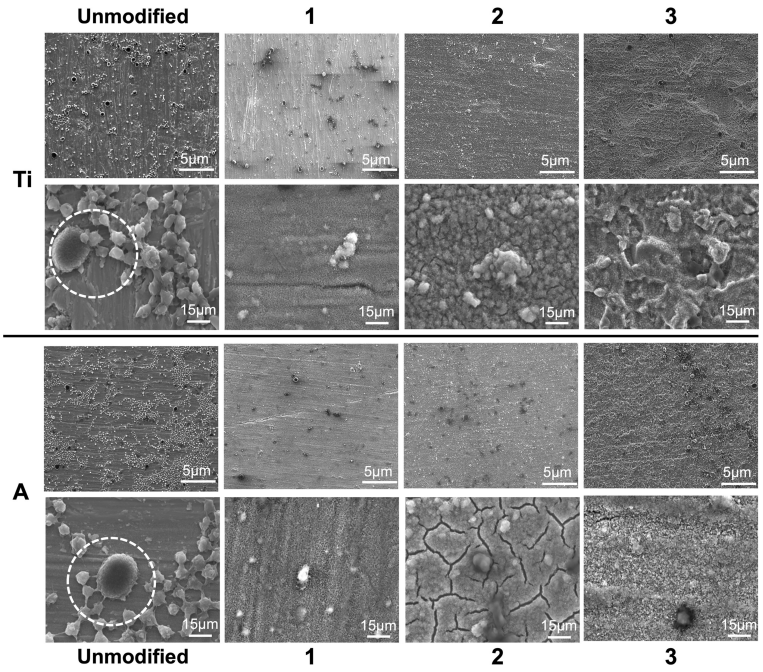

Figure 2.11: Representative SEM images of adhered platelets and leukocytes on different surfaces. Images show a higher degree of platelet activation and platelet-leukocyte complex formation on unmodified surfaces when compared to modified surface. Images were taken at two different magnification (500X and 15000X)

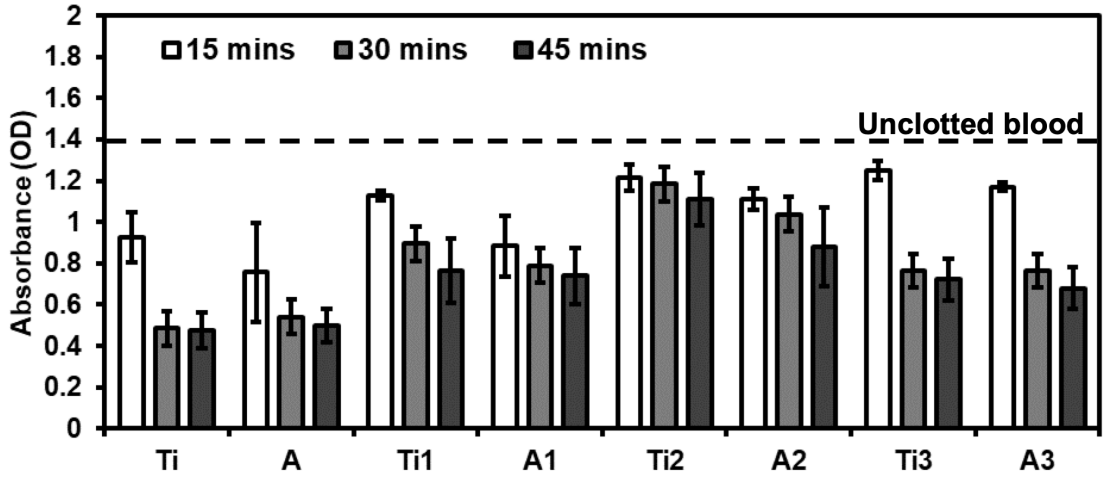

Figure 2.12: Whole blood clotting on different surfaces for up to 45 mins. The dotted line represents the absorbance of free hemoglobin in un-clotted blood. Statistics not shown in the graph. There is a significant increase in free hemoglobin present on all modified surfaces when compared to the unmodified surface at respective time interval. Ti2 has the highest free hemoglobin after 45 mins compared to all surfaces. Other statistical differences for 45 min study are included in Table 2.4. Error bar represent standard deviation.

water results in lysis of red blood cells thus releasing hemoglobin. Hence, higher hemoglobin in the diluted solution indicates less blood clotting on the surface. The blood was allowed to clot for 45 mins on all the surfaces and the amount of free hemoglobin was measured after every 15 mins **(Figure 2.11)**. During the three-time points evaluated, the blood clotting was significantly lower on all the modified surfaces when compared to Ti and A. The amount of free hemoglobin on Ti and A decreased drastically from 15 to 45 mins indicating that the blood is clotting on the surface. However, Ti1, A1, Ti2 and A2 surfaces did not show significant reduction in free hemoglobin from 15 to 45 mins. Further, Ti3 and A3 did not show significant differences in free hemoglobin after 15 mins, however showed a significant reduction in free hemoglobin after 30 and 45 mins. After 45 mins, Ti2 and A2 showed the highest free hemoglobin when compared to all surfaces indicating minimum blood. clotting. Other statistical differences between different surfaces are included in **Table 2.4**. In summary, Ti1, Ti2 and Ti3 showed less blood clotting when compared to A1, A2 and A3 respectively at all time points.

Table 2.4: Statistical Comparison of Different Results on Unmodified and Modified Surfaces

	Surface energy (mJ/m^2)	Fibrinogen adsorption - MicroBCA	Fibrinogen Binding - ELISA	Cell Adhesion- Calcein / F-Actin	Whole Blood Clotting – 45 mins
Ti	27.75	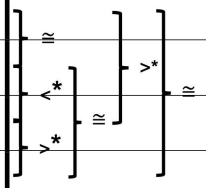	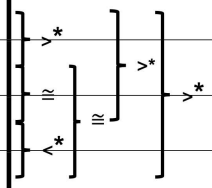	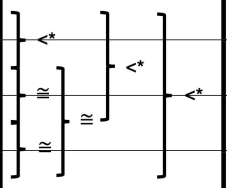	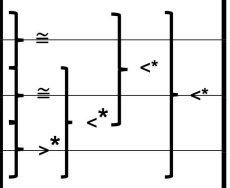
Ti1	57.56				
Ti2	69.36				
Ti3	34.70				
A	25.85	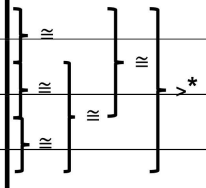	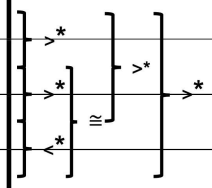	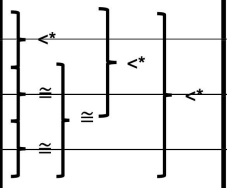	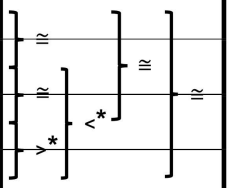
A1	42.07				
A2	63.07				
A3	40.81				

2.4 Conclusion

Improving hemocompatibility of medical devices is still a major concern. In this study, Ti and its alloy Ti-6Al-4V were hydrothermally treated to form nanostructured surfaces with the aim to enhance their hemocompatibility. After treatment with NaOH, the surfaces developed a unique nanopororus structure. With increase in concentration of NaOH, the surface had denser nanoporous structure. However, the surface was uniquely different for Ti versus Ti-6Al-4V. Further treatment with HCl, had dramatic effect on the surface morphology. The surface had nanogranular structure with no significant differences between Ti and Ti-6Al-4V. However, all the surfaces fabricated had respective uniform morphologies. All the modified surfaces were also hydrophilic when compared to unmodified surfaces. As discussed earlier, blood clotting is influenced by the various components of blood and their interaction with material surface, and thus the surface topography and surface chemistry may have long-term implications in success of blood-contacting medical devices. The results indicate that nanoporous surface Ti2 is more hemocompatible than nanogranular surface Ti3.

The hemocompatibility studies indicate significant lower fibrinogen adsorption and cell adhesion on Ti2 compare to all the other surfaces. The results from whole blood clotting study indicate that after 45 mins, Ti2 had significantly higher free hemoglobin on the surface when compared to all surfaces. Hence, this indicates that denser porous structure may be better for blood contact medical devices when compared to all other modified and unmodified surfaces. The final analysis and comparisons between different surfaces elucit three main conclusions: Ti is more hemocompatible than Ti-6Al-4V alloy. Ti and Ti3 have similar surface energy. But, the results show significant reduction in protein adsorption and platelet adhesion on Ti3 compared to Ti indicating that Ti3 is more hemocompatible than Ti. This may be due to the presence of nanogranular topography. Hence, this shows that the surface morphology plays a major role in protein adsorption and cell adhesion. Nanoporous surfaces Ti2 are more hemocompatible than granular surfaces Ti3. The pore size plays also influence cell and platelet adhesion. Ti1 and Ti2 are both nanoporous, but Ti2 is denser than Ti1, and hence has significantly improved hemocompatibility. Thus, in summary the hydrothermal treatment may be a promising approach towards modifying surface topography that may interact appropriately with blood and its components for different blood contacting medical devices.

2.5 References

[1] Benjamin, E. J.; Muntner, P.; Alonso, A.; Bittencourt, M. S.; Callaway, C. W.; Carson, A. P.; Chamberlain, A. M.; Chang, A. R.; Cheng, S.; Das, S. R.; et al. Heart Disease and Stroke Statistics-2019 Update: A Report From the American Heart Association. Circulation 2019, 139 [10], e56–e66. https://doi.org/10.1161/CIR.0000000000000659.

[2] Gorbet, M. B.; Sefton, M. V. Biomaterial-Associated Thrombosis: Roles of Coagulation Factors, Complement, Platelets and Leukocytes. Biomaterials. November 2004, pp 5681–5703. https://doi.org/10.1016/j.biomaterials.2004.01.023.

[3] Nezafati, M. Analyzing Biomaterial Surfaces and Blood-Surface Interactions. In Hemocompatibility of Biomaterials for Clinical Applications: Blood-Biomaterials Interactions; Elsevier Inc., 2018; pp 107–117. https://doi.org/10.1016/B978-0-08-100497-5.00014-8.

[4] Jaffer, I. H.; Fredenburgh, J. C.; Hirsh, J.; Weitz, J. I. Medical Device-Induced Thrombosis: What Causes It and How Can We Prevent It? Journal of Thrombosis and Haemostasis. Blackwell Publishing Ltd June 1, 2015, pp S72–S81. https://doi.org/10.1111/jth.12961.

[5] Hemocompatibility of Biomaterials for Clinical Applications; Elsevier, 2018. https://doi.org/10.1016/c2014-0-04140-8.

[6] Jneid, H.; Bhatt, D. L.; Corti, R.; Badimon, J. J.; Fuster, V.; Francis, G. S. Aspirin and Clopidogrel in Acute Coronary Syndromes: Therapeutic Insights from the CURE Study. Archives of Internal Medicine. May 26, 2003, pp 1145–1153. https://doi.org/10.1001/archinte.163.10.1145.

[7] Torosian, M.; Michelson, E. L.; Morganroth, J.; MacVaugh, H. Aspirin- and Coumadin -Related Bleeding after Coronary-Artery Bypass Graft Surgery. Ann. Intern. Med. 1978, 89 [3], 325–328. https://doi.org/10.7326/0003-4819-89-3-325.

[8] Callahan, B. C.; Lisecki, E. J.; Banks, R. E.; Dalton, J. E.; Cook, S. D.; Wolff, J. D. The Effect of Warfarin on the Attachment of Bone to Hydroxyapatite-Coated and Uncoated Porous Implants. J. Bone Joint Surg. Am. 1995, 77 [2], 225–230. https://doi.org/10.2106/00004623-199502000-00008.

[9] Wang, A.; McAllister, J. P.; Finlayson, P.; Li, J.; Brabant, K.; Tang, H.; Black, C.; Cao, T.; Liang, X.; Salley, S. O.; et al. Short-and Long-Term Neural Biocompatibility of Heparin Coated Sapphire Implants. Mater. Sci. Eng. C 2007, 27 [2], 237–243. https://doi.org/10.1016/j.msec.2006.05.011.

[10] Levy, M.; Hartman, A. R. Heparin-Coated Bypass Circuits in Cardiopulmonary Bypass: Improved Biocompatibility or Not. Int. J. Cardiol. 1996, 53 [SUPPL.]. https://doi.org/10.1016/0167-5273[96]02611-3.

[11] Krishnamurthy, M.; Freedman, M. L. Complications of Anticoagulation with Heparin. Virtual Mentor 2005, 7 [4], 297–300. https://doi.org/10.1001/virtualmentor.2005.7.4.cprl1-0504.

[12] Defraigne, J. O.; Pincemail, J.; Larbuisson, R.; Blaffart, F.; Limet, R. Cytokine Release and Neutrophil Activation Are Not Prevented by Heparin- Coated Circuits and Aprotinin Administration. Ann. Thorac. Surg. 2000, 69 [4], 1084–1091. https://doi.org/10.1016/S0003-4975[00]01093-6.

[13] Sheppard, J. I.; McClung, W. G.; Feuerstein, I. A. Adherent Platelet Morphology on Adsorbed Fibrinogen: Effects of Protein Incubation Time and Albumin Addition. J. Biomed. Mater. Res. 1994, 28 [10], 1175–1186. https://doi.org/10.1002/jbm.820281008.

[14] Rechendorff, K.; Hovgaard, M. B.; Foss, M.; Zhdanov, V. P.; Besenbacher, F. Enhancement of Protein Adsorption Induced by Surface Roughness. Langmuir 2006, 22 [26], 10885–10888. https://doi.org/10.1021/la0621923.

[15] Akkas, T.; Citak, C.; Sirkecioglu, A.; Güner, F. S. Which Is More Effective for Protein Adsorption: Surface Roughness, Surface Wettability or Swelling? Case Study of Polyurethane Films Prepared from Castor Oil and Poly[Ethylene Glycol]. Polym. Int. 2013, 62 [8], 1202–1209. https://doi.org/10.1002/pi.4408.

[16] Cai, N.; Wong, C. C.; Gong, Y. X.; Tan, S. C. W.; Chan, V.; Liao, K. Modulating Cell Adhesion Dynamics on Carbon Nanotube Monolayer Engineered with Extracellular Matrix Proteins. ACS Appl. Mater. Interfaces 2010, 2 [4], 1038–1047. https://doi.org/10.1021/am9008117.

[17] Khanmohammadi Chenab, K.; Sohrabi, B.; Rahmanzadeh, A. Superhydrophobicity: Advanced Biological and Biomedical Applications. Biomaterials Science. Royal Society of Chemistry August

1, 2019, pp 3110–3137. https://doi.org/10.1039/c9bm00558g.

[18] Neto, A. I.; Levkin, P. A.; Mano, J. F. Patterned Superhydrophobic Surfaces to Process and Characterize Biomaterials and 3D Cell Culture. Materials Horizons. Royal Society of Chemistry May 1, 2018, pp 379–393. https://doi.org/10.1039/c7mh00877e.

[19] Falde, E. J.; Yohe, S. T.; Colson, Y. L.; Grinstaff, M. W. Superhydrophobic Materials for Biomedical Applications. https://doi.org/10.1016/j.biomaterials.2016.06.050.

[20] Ratner, B. D. A Perspective on Titanium Biocompatibility; 2001; pp 1–12. https://doi.org/10.1 978-3-642-56486.4.1.

[21] Vishnu, J.; K Manivasagam, V.; Gopal, V.; Bartomeu Garcia, C.; Hameed, P.; Manivasagam, G.; Webster, T. J. Hydrothermal Treatment of Etched Titanium: A Potential Surface Nano-Modification Technique for Enhanced Biocompatibility. Nanomedicine Nanotechnology, Biol. Med. 2019, 20. https://doi.org/10.1016/j.nano.2019.102016.

[22] Bartlet, K.; Movafaghi, S.; Kota, A.; Popat, K. C. Superhemophobic Titania Nanotube Array Surfaces for Blood Contacting Medical Devices. 2017. https://doi.org/10.1039/c7ra03373g.

[23] Leszczak, V.; Popat, K. C. Improved in Vitro Blood Compatibility of Polycaprolactone Nanowire Surfaces. ACS Appl. Mater. Interfaces 2014, 6 [18], 15913–15924.
https://doi.org/10.1021/am503508r.

[24] Rabinow, B. E.; Ding, Y. S.; Qin, C.; McHalsky, M. L.; Schneider, J. H.; Ashline, K. A.; Shelbourn, T. L.; Albrecht, R. M. Biomaterials with Permanent Hydrophilic Surfaces and Low Protein Adsorption Properties. J. Biomater. Sci. Polym. Ed. 1995, 6 [1], 91–109. https://doi.org/10.1163/
156856295X00788.

[25] Annamalai, M.; Gopinadhan, K.; Han, S. A.; Saha, S.; Park, H. J.; Cho, E. B.; Kumar, B.; Patra, A.; Kim, S.-W.; Venkatesan, T. Surface Energy and Wettability of van Der Waals Structures. Nanoscale 2016, 8 [10], 5764–5770. https://doi.org/10.1039/C5NR06705G.

[26] Seyfert, U. T.; Biehl, V.; Schenk, J. In Vitro Hemocompatibility Testing of Biomaterials According to the ISO 10993-4. In Biomolecular Engineering; 2002; Vol. 19, pp 91–96. https://doi.org

/10.1016/S1389-0344[02]00015-1.

[27] Tanzi, M. C. Bioactive Technologies for Hemocompatibility. Expert Review of Medical Devices. July 2005, pp 473–492. https://doi.org/10.1586/17434440.2.4.473.

[28] Werner, C.; Maitz, M. F.; Sperling, C. Current Strategies towards Hemocompatible Coatings. J. Mater. Chem. 2007, 17 [32], 3376–3384. https://doi.org/10.1039/b703416b.

[29] Fischer, M.; Maitz, M. F.; Werner, C. Coatings for Biomaterials to Improve Hemocompatibility. In Hemocompatibility of Biomaterials for Clinical Applications: Blood-Biomaterials Interactions; Elsevier Inc., 2018; pp 163–190. https://doi.org/10.1016/B978-0-08-100497-5.00007-0.

[30] Huang, N.; Yang, P.; Leng, Y. X.; Chen, J. Y.; Sun, H.; Wang, J.; Wang, G. J.; Ding, P. D.; Xi, T. F.; Leng, Y. Hemocompatibility of Titanium Oxide Films. Biomaterials 2003, 24 [13], 2177–2187. https://doi.org/10.1016/S0142-9612[03]00046-2.

[31] Mentus, S.; Pjescic, J.; Blagojevic, N. Investigation of Titanium Corrosion in Concentrated NaOH Solutions. Mater. Corros. 2002, 53 [1], 44–50.
https://doi.org/10.1002/1521-4176[200201]53:1¡44::AID-MACO44¿3.0.CO;2-R.

[32] Guo, Z.; Jiang, N.; Chen, C.; Zhu, S.; Zhang, L.; Li, Y. 2. Surface Bioactivation through the Nanostructured Layer on Titanium Modified by Facile HPT Treatment. Sci. Rep. 2017, 7 [1], 4155. https://doi.org/10.1038/s41598-017-04395-0.

[33] POURBAIX, M. Atlas of Electrochemical Equilibria in Aqueous Solutions; Pergamon Press, Oxford, 1974; pp 214–218.

[34] Wang, P.; Yi, X.; Lu, Y.; Yu, H.; Yu, J. 5. In-Situ Synthesis of Amorphous H2TiO3-Modified TiO2 and Its Improved Photocatalytic H2-Evolution Performance. J. Colloid Interface Sci. 2018, 532, 272–279. https://doi.org/10.1016/j.jcis.2018.07.139.

[35] Giacomello, A.; Meloni, S.; Chinappi, M.; Casciola, C. M. Cassie-Baxter and Wenzel States on a Nanostructured Surface: Phase Diagram, Metastabilities, and Transition Mechanism by Atomistic Free Energy Calculations. Langmuir 2012, 28 [29], 10764–10772. https://doi.org/10.1021/la3013.

[36] Pereira, M. M.; Kurnia, K. A.; Sousa, F. L.; Silva, N. J. O.; Lopes-Da-Silva, J. A.; Coutinho, J. A. P.; Freire, M. G. Contact Angles and Wettability of Ionic Liquids on Po-

lar and Non-Polar Surfaces. Phys. Chem. Chem. Phys. 2015, 17 [47], 31653–31661. https://doi.org/10.1039/c5cp05873b.

[37] Boswell, S. G.; Cole, B. J.; Sundman, E. A.; Karas, V.; Fortier, L. A. Platelet-Rich Plasma: A Milieu of Bioactive Factors. Arthrosc. - J. Arthrosc. Relat. Surg. 2012, 28 [3], 429–439. https://doi.org/10.1016/j.arthro.2011.10.018.

[38] Carter, A. M.; Standeven, K. F.; Grant, P. J. 9. Common Genetic Determinants of Coagulation and Fibrinolysis. In Emery and Rimoin's Principles and Practice of Medical Genetics; Elsevier Ltd, 2013; pp 1–20. https://doi.org/10.1016/B978-0-12-383834-6.00060-4.

[39] Pirofsky, B. THE DETERMINATION OF BLOOD VISCOSITY IN MAN BY A METHOD BASED ON POISEUILLE'S LAW. J. Clin. Invest. 1953. https://doi.org/10.1172/JCI102738.

[40] Hrnčíř, E.; Rosina1, J. Surface Tension of Blood; 1997; Vol. 46.

[41] Vargaftik, N. B.; Volkov, B. N.; Voljak, L. D. International Tables of the Surface Tension of Water ARTICLES YOU MAY BE INTERESTED IN. J. Phys. Chem. Ref. Data 1983, 12, 817. https://doi.org/10.1063/1.555688.

[42] Krishnan, A.; Wilson, A.; Sturgeon, J.; Siedlecki, C. A.; Vogler, E. A. Liquid-Vapor Interfacial Tension of Blood Plasma, Serum and Purified Protein Constituents Thereof. Biomaterials 2005, 26 [17], 3445–3453. https://doi.org/10.1016/j.biomaterials.2004.09.016.

[43] Giacomello, A.; Meloni, S.; Chinappi, M.; Casciola, C. M. 10. Cassie-Baxter and Wenzel States on a Nanostructured Surface: Phase Diagram, Metastabilities, and Transition Mechanism by Atomistic Free Energy Calculations. Langmuir 2012, 28 [29], 10764–10772. https://doi.org/10.1021/la3018453.

[44] Kasuga, T.; Hiramatsu, M.; Hoson, A.; Sekino, T.; Niihara, K. 7. Titania Nanotubes Prepared by Chemical Processing. Adv. Mater. 1999, 11 [15], 1307–1311. https://doi.org/10.02/[SICI]1521-4095[199910]11:15¡1307::AID-ADMA13073.0.CO;2-H.

[45] Michiardi, A.; Aparicio, C.; Ratner, B. D.; Planell, J. A.; Gil, J. The Influence of Surface Energy on Competitive Protein Adsorption on Oxidized NiTi Surfaces. Biomaterials 2007, 28 [4], 586–594. https://doi.org/10.1016/j.biomaterials.2006.09.040.

[46] Wahlgren, M.; Arnebrant, T. Protein Adsorption to Solid Surfaces. Trends Biotechnol. 1991, 9 [1], 201–208. https://doi.org/10.1016/0167-7799[91]90064-O.

[47] Jansen, B.; Ellinghorst, G. Modification of Polyetherurethane for Biomedical Application by Radiation Induced Grafting. II. Water Sorption, Surface Properties, and Protein Adsorption of Grafted Films. J. Biomed. Mater. Res. 1984, 18 [6], 655–669. https://doi.org/10.1002/jbm.820180607.

[48] Matsuda, M.; Sugo, T. 12. Structure and Function of Human Fibrinogen Inferred from Dysfibrinogens. International journal of hematology. 2002, pp 352–360. https://doi.org/10.1007/BF03165284.

[49] Blombäck, B.; Hessel, B.; Hogg, D.; Therkildsen, L. 13. A Two-Step Fibrinogen–Fibrin Transition in Blood Coagulation. Nature 1978, 275 [5680], 501–505. https://doi.org/10.1038/275501a0.

[50] Mulvihill, J. N.; Faradji, A.; Oberling, F.; Cazenave, J. -P. Surface Passivation by Human Albumin of Plasmaperesis Circuits Reduces Platelet Accumulation and Thrombus Formation. Experimental and Clinical Studies. J. Biomed. Mater. Res. 1990, 24 [2], 155–163. https://doi.org/10.1002/jbm.820240203.

[51] Sweryda-Krawiec, B.; Devaraj, H.; Jacob, G.; Hickman, J. J. A New Interpretation of Serum Albumin Surface Passivation. Langmuir 2004, 20 [6], 2054–2056. https://doi.org/10.1021/la034870g.

[52] Abildgaard, U. 11. Purification of Two Progressive Antithrombins of Human Plasma. Scand. J. Clin. Lab. Invest. 1967, 19 [2], 190–195. https://doi.org/10.3109/00365516709093501.

[53] Niemi, T. T.; Suojaranta-Ylinen, R. T.; Kukkonen, S. I.; Kuitunen, A. H. Gelatin and Hydroxyethyl Starch, but Not Albumin, Impair Hemostasis After Cardiac Surgery. Anesth. Analg. 2006, 102 [4], 998–1006. https://doi.org/10.1213/01.ane.0000200285.20510.b6.

[54] Vogler, E. A. Protein Adsorption in Three Dimensions. Biomaterials 2012, 33 [5], 1201–1237. https://doi.org/10.1016/j.biomaterials.2011.10.059.

[55] Wilson, C. J.; Clegg, R. E.; Leavesley, D. I.; Pearcy, M. J. Mediation of Biomaterial-Cell Interactions by Adsorbed Proteins: A Review. Tissue Engineering. January 2005, pp 1–18. https://doi.org/10.1089/ten.2005.11.1.

[56] Kulkarni, M.; Mazare, A.; Park, J.; Gongadze, E.; Killian, M. S.; Kralj, S.; von der Mark, K.; Iglič, A.; Schmuki, P. Protein Interactions with Layers of TiO2 Nanotube and Nanopore Arrays: Morphology and Surface Charge Influence. Acta Biomater. 2016, 45, 357–366. https://doi.org/10.1016/j.actbio.2016.08.050.

[57] Korzeniewski, C.; Callewaert, D. M. An Enzyme-Release Assay for Natural Cytotoxicity. J. Immunol. Methods 1983, 64 [3], 313–320. https://doi.org/10.1016/0022-1759[83]90438-6.

[58] Legrand, C.; Bour, J. M.; Jacob, C.; Capiaumont, J.; Martial, A.; Marc, A.; Wudtke, M.; Kretzmer, G.; Demangel, C.; Duval, D.; et al. Lactate Dehydrogenase [LDH] Activity of the Number of Dead Cells in the Medium of Cultured Eukaryotic Cells as Marker. J. Biotechnol. 1992, 25 [3], 231–243. https://doi.org/10.1016/0168-1656[92]90158-6.

[59] Kunzmann, A.; Andersson, B.; Thurnherr, T.; Krug, H.; Scheynius, A.; Fadeel, B. Toxicology of Engineered Nanomaterials: Focus on Biocompatibility, Biodistribution and Biodegradation. Biochimica et Biophysica Acta - General Subjects. March 2011, pp 361–373. https://doi.org/10.1016/j.bbagen.2010.04.007.

[60] Zan, X.; Fang, Z.; Wu, J.; Xiao, F.; Huo, F.; Duan, H. 4. Freestanding Graphene Paper Decorated with 2D-Assembly of Au@Pt Nanoparticles as Flexible Biosensors to Monitor Live Cell Secretion of Nitric Oxide. Biosens. Bioelectron. 2013, 49, 71–78. https://doi.org/10.1016/J.BIOS.2013.05.006.

[61] Periayah, M. H.; Halim, A. S.; Saad, A. Z. M. Mechanism Action of Platelets and Crucial Blood Coagulation Pathways in Hemostasis. International Journal of Hematology-Oncology and Stem Cell Research. Tehran University of Medical Sciences [TUMS] 2017, pp 319–327.

[62] Elstad, M. R.; McIntyre, T. M.; Prescott, S. M.; Zimmerman, G. A. The Interaction of Leukocytes with Platelets in Blood Coagulation. Curr. Opin. Hematol. 1995, 2 [1], 47–54. https://doi.org/10.1097/00062752-199502010-00007.

[63] Chen, H.; Song, W.; Zhou, F.; Wu, Z.; Huang, H.; Zhang, J.; Lin, Q.; Yang, B. The Effect of Surface Microtopography of Poly[Dimethylsiloxane] on Protein Adsorption, Platelet and Cell Adhesion. Colloids Surfaces B Biointerfaces 2009, 71 [2], 275–281.

https://doi.org/10.1016/j.colsurfb.2009.02.018.

[64] Ferraz, N.; Ott, M. K.; Hong, J. Time Sequence of Blood Activation by Nanoporous Alumina: Studies on Platelets and Complement System. Microsc. Res. Tech. 2010, 73 [12], 1101–1109. https://doi.org/10.1002/jemt.20854.

[65] Asthana, A.; White, C. M.; Douglass, M.; Kisaalita, W. S. Evaluation of Cellular Adhesion and Organization in Different Microporous Polymeric Scaffolds. Biotechnol. Prog. 2018, 34 [2], 505–514. https://doi.org/10.1002/btpr.2627.

[66] McEver, R. P. Adhesive Interactions of Leukocytes, Platelets, and the Vessel Wall during Hemostasis and Inflammation. Thrombosis and Haemostasis. 2001, pp 746–756. https://doi.org/10.1055/s-0037-1616128.

[67] Ogura, H.; Kawasaki, T.; Tanaka, H.; Koh, T.; Tanaka, R.; Ozeki, Y.; Hosotsubo, H.; Kuwagata, Y.; Shimazu, T.; Sugimoto, H. Activated Platelets Enhance Microparticle Formation and Platelet-Leukocyte Interaction in Severe Trauma and Sepsis. J. Trauma - Inj. Infect. Crit. Care 2001, 50 [5], 801–809. https://doi.org/10.1097/00005373-200105000-00005.

[68] Cerletti, C.; Tamburrelli, C.; Izzi, B.; Gianfagna, F.; De Gaetano, G. Platelet-Leukocyte Interactions in Thrombosis. Thrombosis Research. March 2012, pp 263–266. https://doi.org/10.1016/j.thromres.2011.10.010.

CHAPTER 3: IMPROVED HEMOCOMPATIBILITY ON SUPERHEMOPHOBIC MICRO-NANO STRUCTURED TITANIUM SURFACES[1]

3.1 Introduction

In recent times, a considerable increase in demand for cardiovascular implants to repair and replace damaged tissues has been noted [1,2]. Titanium and titanium alloys are preferred as an implant material owing to its suitable mechanical properties, corrosion resistance, and bio/hemocompatibility [3,4]. Titanium and titanium alloys have been preferred for several cardiovascular implants such as endovascular stents, neurovascular flow diverters, structural heart devices and heart valve casing [5–7]. However, these implants may fail due to inappropriate interactions at surface level with blood and its components leading to initiation of the coagulation cascade followed by thrombus formation and inflammation [8,9]. Clinically, patients with cardiovascular implants are prescribed use of systemic anticoagulant drugs and anti-platelet to avoid thrombus formation on the implant surface [10,11]. However, studies have shown that overuse of these drugs can lead to internal bleeding complications, notably in patients that are already prone to high bleeding risks and elderly patients [11,12]. In addition, anticoagulant therapy also shown variable responses due to poor adherence and genetic variability [13,14]. Hence, the critical need to develop cardiovascular implants with suitable surface properties that prevents thrombus formation.

Implant surfaces are prone to thrombus formation due to the hemodynamic alteration of blood flow and improper interactions by the implant compared to the native endothelial layer covered arteries [15]. Once the blood flows over the implant surface, there is a rapid increase in plasma protein (fibrinogen and von Willebrand factor) adsorption on the surface [16,17]. These proteins alleviate coagulation cascade and thrombin formation. Fibrinogen adsorption further promotes adhesion and activation of platelets. Simultaneously, there is contact activation of intrinsic coagulation pathway

[1]This work was published in MDPI Bioengineering and is reproduced in modified form here with permission

by adsorbing factor XII and its subsequent change in confrontation and activation. Activated FXIIa initiates activation of other factors leading to formation of thrombin and complement activation on the surface. Thrombin reacts with fibrinogen and forms mesh to trap activated platelets and red blood cells (RBCs) to form blood clot. Additionally, activation of coagulation cascade is greatly interconnected with platelets and leukocytes (WBCs) adhesion and activation [4,18,19]. Thus, it is essential to understand the cardiovascular implant surface interaction with blood and its components and develop sur-faces that can prevent protein adsorption and thrombus formation. Several approaches have been investigated to develop surfaces of cardiovascular implants with improved blood compatibility. Studies have shown that biocompatibility can depend on the implant surface topography, chemistry, crystallinity, and charge[20–24]. Surface passivation techniques such as mechanical treatment, plasma treatment, anodization, and thermochemical treatments modify the surface micro/nanoscale topography and chemistry[24–26]. These surfaces are normally hydrophilic and have shown to influence hemocompatibility. While hydrophilic surface-induced interaction have proven to be highly advantageous for other implants, surface interaction for blood contacting implants could also pose a great challenge due to thrombus formation [27,28]. Biopolymers, such as chitosan, heparin, and few zwitterionic polymers, are used to prevent protein adsorption and platelet adhesions but they have not been found in the clinical market [29,30]. Further, recent studies have explored superhydrophobic surfaces for cardiovascular implants. Superhydrophobicity is achieved only with the combination of surface roughness/topography (e.g., micro, nano or micro-nano topography) and surface chemistry (e.g., aminopropyltriethoxysilane, 3-acryloxypropyltrimethoxysilane + bis-1,2-(triethoxysilyl) ethane, heptadecafluoro-1,1,2,2-tetrahydrodecyl tri-chlorosilane). These surfaces have shown significant reduction in platelet and WBCs adhesion [31–35]. However, nanotubes and nanoflowers developed on titanium surface are shown to be instable and can easily delaminate. Hence, there is a need to develop a stable surface morphology which can lead to superhydrophobic surface. Researchers have developed superhydrophobic titanium surface using laser-hydrothermal treatment and PDMS/silane coating for anti-icing [36,37]. However, hemocompatibility of these surfaces are not evaluated and the process on micro-nano surface is complicated compared to the

method reported in this manuscript.

In this study, a novel micro-nano surface topography was developed on titanium surface using thermochemical technique with sulfuric acid. The surfaces were further modified with a fluoro-silane to reduce the surface energy and make the surface superhemophobic. The surfaces were characterized for morphology using a Scanning Electron Microscope (SEM); wettability with water, platelet rich plasma and whole blood using a goniometer; and crystallinity using an X-ray Diffraction (XRD). The hemocompatibility of surfaces were characterized by evaluating fibrinogen adsorption, blood cell adhesion, platelet activation, hemolysis, thrombin generation, complement activation, and whole blood clotting. Results implied that superhydrophobic micro-nano surface prevented platelet and WBCs adhesion significantly (> 90 %) and prevented thrombus formation. Thus, this novel surface modification can be a potential cardiovascular implant surface with enhanced hemocompatibility.

3.2 Materials and Methods

3.2.1 Fabrication of micro-nanoporous surfaces

The micro-nanoporous surfaces on Grade 2 titanium foils were fabricated using thermochemical process and were further modified to be superhydrophobic with a silane as described in our previous work [38]. In brief, polished and cleaned titanium foils were thermochemically treated with 0.5 M sulfuric acid in a polytetrafluoroethylene container inside an 80 °C hot air oven for 8 hrs. After the treatment, surfaces were ultrasonically clean and annealed at 300 °C for 1 hr. Modified surfaces were washed with Milli-Q water, air-dried and kept in a sealed petri dish inside a desiccator until further use.

The micro-nanoporous surfaces was made superhydrophobic by grating with low energy silane. Prior to grafting, the micro-nanoporous surfaces were plasma etched at 200V in 10 cm3/min in an oxygen gas chamber for 5 min. Subsequently, the surfaces were modified by grafting with 150μl of

heptadecafluoro-1,1,2,2-tetrahydrodecyl tri-chlorosilane (silane) inside a closed chamber at 120°C for 1 hr.

The following notations are used for different surfaces in this manuscript: un-modified titanium surfaces: Ti; micro-nanoporous titanium surfaces: nTi; superhydrophobic micro-nanoporous surfaces: nTi-S.

3.2.2 Surface characterization

The topography of control and modified surfaces was visualized using a JEOL 6500 scanning electron microscopy (SEM). The apparent contact angle (θ^*) of different sur-face with Milli-Q water, platelet rich plasma (PRP) and human blood was calculated using the images taken with a ramé-hart goniometer. The presence of crystal structures on surfaces was characterized using a Bruker D8 discover DaVinci Powder X-ray dif-fraction (XRD) machine equipped with Cu K radiation. XRD scans were collected at = 1.5°.

3.2.3 Surface preparation for hemocompatibility studies

Surfaces were cleaned in 24-well plates with Milli-Q water and phosphate-buffered saline (PBS), each for 5 mins. They were further sterilized by exposure to Ultra Violet light present in a biosafety cabinet for 15 mins.

3.2.4 Isolation of Platelet Rich Plasma (PRP) from human blood

Whole blood from healthy individuals who have refrained from using any medi-cation that may affect the blood clotting in past 7 days was collected in a blood collection tube containing ethylenediaminetetraacetic acid (EDTA). The procedure to collect blood was performed as per the standard protocol authorized by the Institutional Review Board of Colorado State University and National Institutes of Health's "Guiding Principles for Ethical Research". prior to the blood draw, consents were obtained from hu-man participants. The first tube of blood was discarded to avoid the use of

locally activated platelets due to needle insertion. Collected blood was centrifuged at 150 g for 15 mins. The upper layer and buffy coat (platelet rich plasma) from the tubes were pooled prior to using with different surfaces after resting it for another 15mins.

3.2.5 Fibrinogen binding on different surfaces from PRP

Fibrinogen binding on different surfaces from the pooled PRP was measured using a commercially available enzyme linked immunoassay (ELISA). Sterilized surfaces were incubated with PRP for 2 hrs on a flat shaker at 100 rpm, 37 °C and 5% CO_2. The PRP incubated with the surfaces was diluted 1/10,000 folds and the manufacturer provided protocol was followed to determine the fibrinogen binding on different surfaces. Absorbance of the final solution was measured using a microplate reader at 450 nm wavelength. Results presented are calculated after subtracting the positive control (total fibrinogen present after incubation with empty well).

3.2.6 Cell adhesion on different surfaces

Cell adhesion from PRP on different surface was visualized using fluorescence microscopy. Sterilized surfaces were incubated with PRP for 2 hrs on a flat shaker at 100 rpm, 37 °C and 5% CO_2. After incubation, surfaces were isolated and rinsed thrice with PBS. The surfaces were then incubated with 5% Calcein-AM stain for 20 mins. The stain solution was aspirated, and the surfaces were rinsed thrice with PBS. Surfaces were imaged using Zeiss fluorescence microscope. All images were processed, and the area covered by the live cells were measured using ImageJ.

3.2.7 Identification of platelet and WBCs on different surfaces

Identification of platelet and WBCs on different surface was visualized using fluorescence microscopy. Sterilized surfaces were incubated with PRP for 2 hrs on a flat shaker at 100 rpm, 37 °C and 5% CO_2. After incubation, the surfaces isolated and rinsed thrice with PBS. Rinsed surfaces were fixed using formaldehyde (3.7%) and were rinsed thrice with PBS. The cells were

further permeabilized using triton (1%) and were rinsed four times with PBS. The surfaces were then incubated with 0.05% rhoda-minephalloidin (actin)stain solution and incubated for 25 mins. Later, 4,6-diamidino-2- phenylindole (DAPI) stain solution (3%) was added and incubated for 5 mins. The stain solution was aspirated, and the surfaces were rinsed thrice with PBS. Surfaces were imaged using Zeiss fluorescence microscope. All images were further processed and the number of cells using ImageJ.

3.2.8 Platelet activation on different surfaces

Platelet activation and platelets-WBCs complex formation on different surface was visualized using SEM. Sterilized surfaces were incubated with PRP for 2 hrs on a flat shaker at 100rpm, 37 °C and 5% CO_2. After incubation, the PRP solution was aspirated, and the surfaces were rinsed thrice with PBS. The surfaces were then fixed using a fixative solution containing glutaraldehyde (6%), 0.1 M sodium cacodylate, and 0.1 M sucrose for 45 mins. Later, the surfaces were then incubated in a buffer solution containing 0.1 M sodium cacodylate and 0.1 M sucrose for 10 mins. This was followed by dehydration of surfaces by incubation in 35, 50, 70 and 100% ethanol for 10 mins each. The surfaces were dried and imaged using SEM.

3.2.9 Hemolysis of erythrocytes on different surfaces

The hemolytic activity on different surfaces was measured using a commercially available hemolysis assay kit (HaemoScan), which is in accordance the international standard ISO 10993/Part 4 and ASTM F756-08 standards [39] to evaluate the hemocompatibility of biomaterials. Sterilized surfaces and control surfaces (Buna-S and silicon elastomer, provided with the assay) were incubated with manufacturer provided erythrocyte suspension for 24 hrs on a flat shaker at 100 rpm, 37°C and 5% CO_2. The protocol provided by the manufacturer was followed to determine the hemolytic activity on different surfaces. Absorbance of the resulting solution was measured at different wavelengths (415/450/380 nm) wavelength using a microplate reader.

3.2.10 Thrombin generation on different surfaces

Thrombin generation on different surfaces was measured using a commercially available thrombin generation assay (HaemoScan), which is in accordance the international standard ISO 10993/Part 4 to evaluate the biocompatibility of biomaterials. Sterilized surfaces and manufacturer provided control surfaces (low-density polyethylene and medical steel, provided with the assay) were incubated with manufacturer provided plasma for 15 mins at 37 °C. Manufacturer provided protocol was followed to determine the maximum thrombin generation over a time interval and average thrombin generation over a period of 4 mins from the solution incubated with different surfaces. Absorbance of the resulting solution was measured at different wavelength (405/540 nm) using a microplate reader.

3.2.11 Complement convertase on different surfaces

The complement activation on different surfaces was measured using a commercially available complement convertase kit (HaemoScan), which is in accordance the international standard ISO 10993/Part 4 to evaluate the biocompatibility of biomaterials. Sterilized surfaces and manufacturer provided control surfaces (medical steel, polydimethylsiloxane, and low-density polyethylene, provided with the assay) were incubated with manufacturer provided plasma for 24 hrs at 37 °C and 5% CO_2. Manufacturer provided protocol was followed to determine the complement generated due to inter-action with different surfaces. Absorbance of the resulting solution was measured at 405 nm wavelength using a microplate reader.

3.2.12 Whole blood clotting on different surfaces

Whole blood clotting on different surfaces was assessed by quantify the free hemoglobin in unclotted blood after exposure of whole human blood to the surfaces. Blood was collected in a tube without any anticoagulant coating and study was per-formed immediately after the blood draw. 5 μl of whole blood was pipetted on top of different surfaces, and the blood was allowed to clot for up

to 45 mins. After every 15 min, the surfaces were evaluated for the presence of free hemoglobin. Milli-Q water was added to the surfaces and gently shaken for 30 s to lyse RBCs that were not trapped in the clot on the surface. The absorbance of free hemoglobin released by lysed RBCs was measured using a microplate reader at 540 nm.

3.2.13 Statistical Analysis

Surface characterization was performed at 3 different samples of each surface. Surface morphology using SEM and wettability using goniometer were taken at 3 different locations on each sample (nmin = 9). Different hemocompatibility studies were repeated at least 3 different times with blood from at least 2 healthy individuals (nmin = 6). The result presented is from a single study with blood drawn from single individual. This is because there is a significant difference in platelet count from each individual and it's not appropriate to compare the absolute value. However, similar trends were observed for blood from different donors/assay kits for Results presented, indicating the reproducibility of the data. The quantitative data were processed using R software and the p value was determined using a two-way analysis of variance (ANOVA) test. For a p-value < 0.05, the data set was considered significant. The error bar represents the standard deviation.

3.3 Results and discussion

Even though extensive research has been carried out for enhancing implants surface interaction with blood and its component, to this day, a truly hemocompatible implant surface that can prevent blood clotting has not been developed. Studies have shown implant surface interaction with blood stimulates protein adsorption (fibrinogen), platelet adhesion, platelet activation and inflammatory reactions. These improper reactions affect implant functionality and life. Hence, in this study, a novel superhydrophobic surface was developed and its hemocompatibility was characterized by quantifying fibrinogen protein adsorption, hemolysis, thrombin generation, complement activation, platelet adhesion/activation. Previous studies have demonstrated shown that these surfaces have

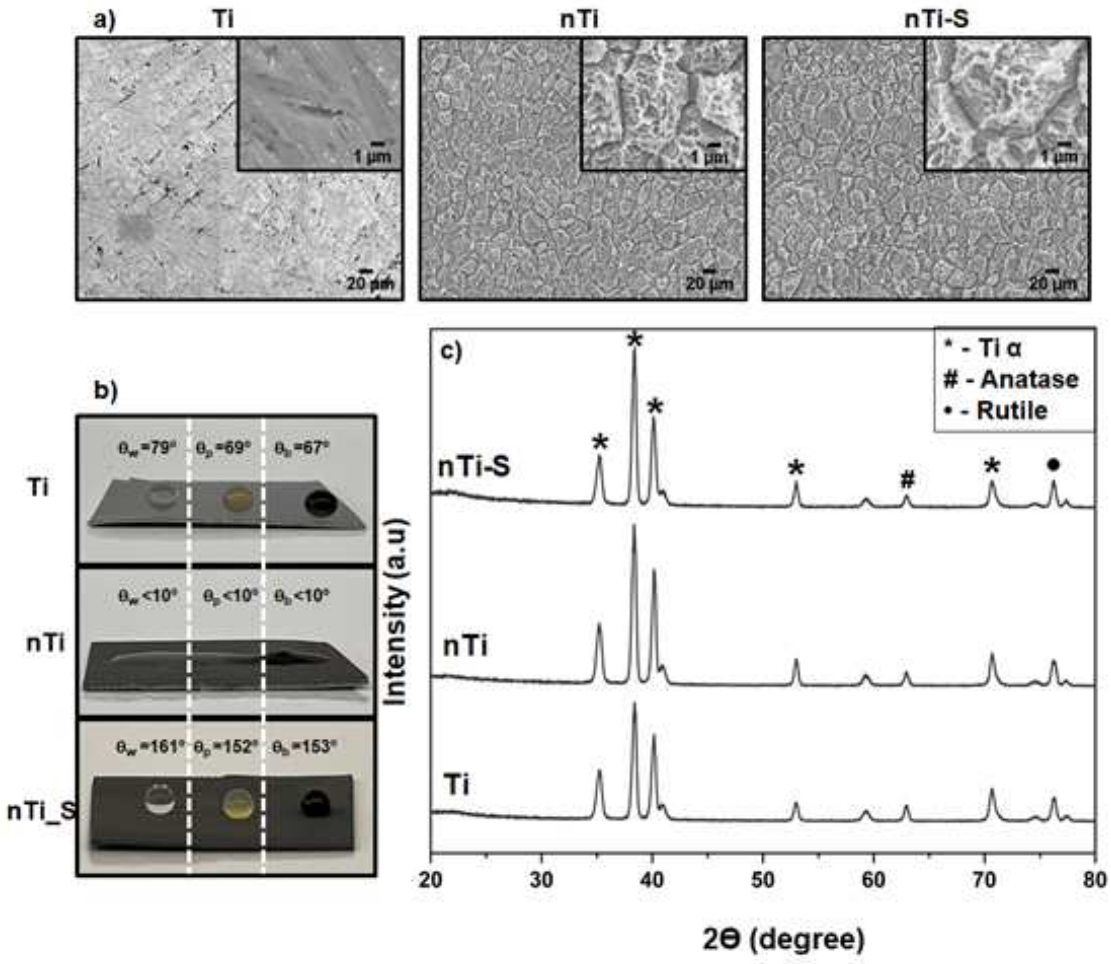

Figure 3.1: a) Representative SEM images of different surfaces. Images were taken at 500X, and image inserts depict 5000X magnification. b) Apparent contact angle measurements using Milli-Q water, PRP, blood on different surfaces. c) XRD intensity peaks of different surfaces. (nmin = 9).

good corrosion resistance and anti-bacterial properties [38].

The topography of different surfaces was imaged using SEM. Surface topography is an important property that determines the biological responses to a foreign material. The thermochemical treatment alters the surface properties such as topography, chemistry, and wettability without altering the bulk properties of the titanium substrate [40]. Results (**Figure 3.1a**) indicated that Ti surfaces were smooth and did not have any unique surface topography. nTi surfaces had microscale topography formed because of quicker etching near the grain boundaries. Faster etching is due to

the disordered atomic arrangement at the grain boundaries. Further, etching on the grain surfaces led to the formation of nano-pits. Thus, the results indicate that the thermochemical treatment led to a micro-nano topography. Further, after silane modification, nTi-S surfaces did not show any significant difference in the surface topography when compared to nTi surfaces. The presence of silane after deposition was confirmed with XPS results in the author's previous publication[41].

The wettability of different surfaces was quantified by measuring the apparent contact angle with Milli-Q water (θ_w), PRP (θ_p), and whole blood (θ_b) using a goniometer. Studies have shown that blood is mostly made up of water. Wettability can be broadly classified into three categories, superhemo/hydrophobic when θ_w and θ_b >150°, hemo/hydrophobic if θ_w and θ_b > 90°, and hemo/hydrophilic if θ_w and θ_b < 90°. Liquid interaction with a textured surface can adapt two configurations to reduce the total liquid-solid free energy, Wenzel, and Cassie-Baxter state. At wenzel state, the fluid permeates into the surface topography and increases the liquid-solid interfacial area. This reduces the apparent contact angle compared to the surface without surface features. In contrary, in the meta stable Cassie-Baxter state the liquid doesn't interact with the surface topography creating air pockets between the liquid and surface topography. This leads to high apparent contact angle. Studies have shown that Cassie-Baxter state can be achieved with a combination of low energy surface chemistry and appropriate surface topography [27].Previous studies have shown that silane coating on plain polished titanium surface is not superhydrophobic. Results (**Figure 3.1b**) indicated that as expected the Ti surface is hydro/hemophilic, this is because of absence of any unique topography on the surface and high apparent contact angle compared to the Milli-Q water, PRP and whole blood [6,33]. nTi surface is super-hemo/hydrophilic because of combination of micro-nano surface topography and higher titanium oxide as confirmed with the XPS results in previous publication[41]. Studies have shown that surface oxide layer attracts water molecules. However, nTi-S surface is super-hemo/hydrophobic surface in Cassie-Baxter state as confirmed advancing contact angle studies from wettability studies in previous publication [41]. This due to presence of low energy silane on the surface and the micro-nano topography. The apparent contact angle with blood was lower compared to PRP because blood is denser liquid.

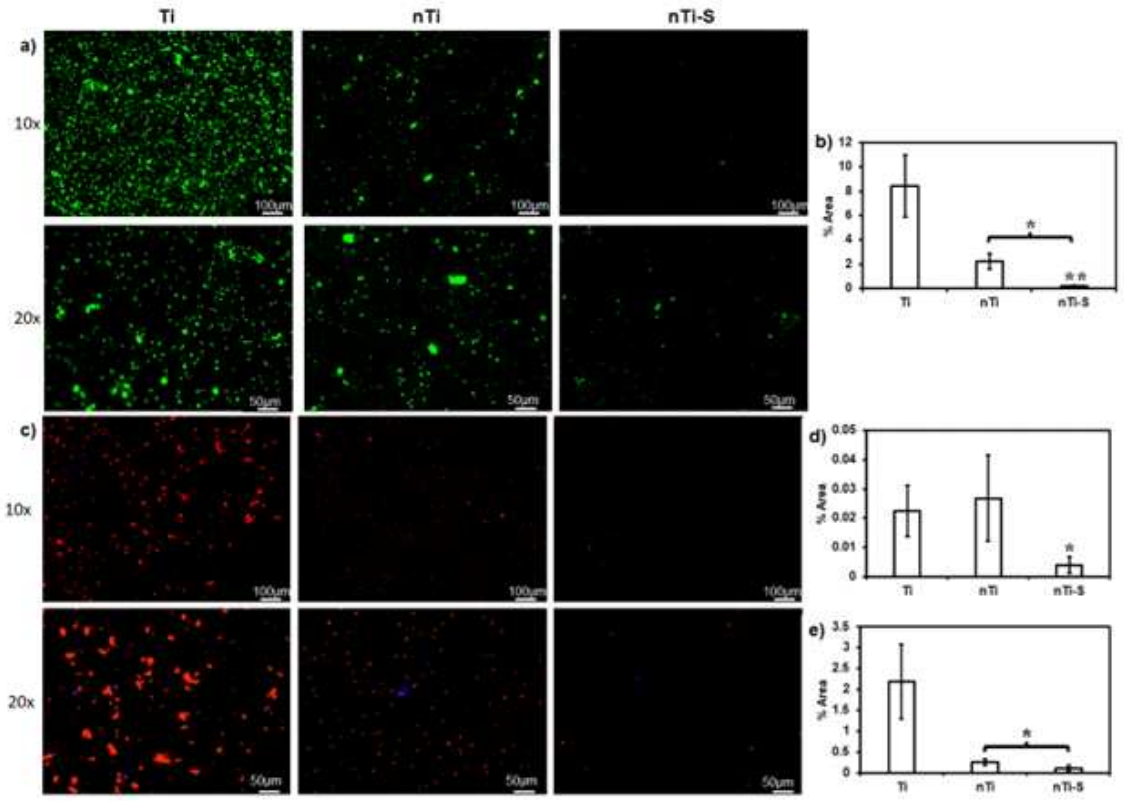

Figure 3.2: Fibrinogen adsorption from PRP on different surfaces measured using a microplate reader. ($^{*}p < 0.05$). (nmin = 9).

The phase analysis of different surfaces was assessed using an XRD. Studies have shown that surface crystallinity plays a major role in wettability and cellular interaction [42,43]. The rutile and anatase phase of TiO_2 was present on all surfaces and these phases have shown to be more cytocompatible. Results (**Figure 3.1c**) indicate that the surfaces have the following metallic alpha phase titanium intensity peaks at 32° (002)35° (100), 40° (101) and 53° (102). TiO_2 anatase phase Intensity peaks at 62° (204). TiO_2 rutile phase intensity peaks at 27° (110) and 76° (110). nTi and nTi-S had higher presence of metallic alpha phase titanium on the surface because the treatment removed the impurities and oxide layer on the Ti surface. The surface modification of nTi-S did not alter the crystal structure when compared to nTi surface.

Fibrinogen adsorption from PRP on different surfaces was quantified using a commercially available enzyme linked immunoassay (ELISA) for human fibrinogen. Most abundant proteins present in human blood are albumin and fibrinogen. Albumin is a passivating protein; it doesn't actively promote blood clotting. However, fibrinogen is a key protein in the development of surface-induced thrombosis, through binding integrin receptor IIb3 (GPIIb/IIIa) of platelet. This leads to platelet immobilization, activation, and aggregation, and this is also a precursor for fibrin formation. Fibrin is a leading structural component in blood clotting coagulation cascade. Various studies have demonstrated that nano, micro or micro-nano surface topography influences protein adsorption and alter protein conformation and spatial distribution on the surface [17,44]. The size of the proteins are in nanometer range and studies have shown the surface topography and its feature size can influence protein adsorption and nucleation inside the topography [45]. PRP mostly contains blood proteins (fibrinogen), platelets, and white blood cells. The surface exposed PRP was analyzed to evaluate the protein content in the solution and the amount of protein adsorbed on the surface was calculated by subtracting the protein content in the positive control. Results (**Figure 3.2**) indicate no significant difference in fibrinogen adsorption on nTi and Ti surfaces. In contrary, nTi-S surfaces had significantly lower fibrinogen adsorption compared to nTi and Ti surface. This is because the lower surface energy nTi-S surface prevents interaction with liquid reducing protein adsorption. In addition, studies have shown that fibrinogen adhered to hydrophobic surfaces have a specific conformation which prevents fibrinogen fiber formation [46].

Live cell adhesion (platelet and WBCs) on different surfaces was assessed after incubation with PRP. The surfaces with adhered live cells were stained with calcein-AM. Platelet and WBCs adhesion is the immediate step in the coagulation cascade after fibrinogen adsorption on the surface [47,48]. Activated platelets further promote platelet adhesion and activation. Simultaneously, interact with WBCs (**Figure 3.3a**) leading to platelet-WBCs complex formation. Results (**Figure 3.3b**) indicate the Ti surface adhered significantly higher cells compared to nTi and nTi-S surface. nTi surface showed lower cell adhesion compared to Ti surface because the surface has significantly

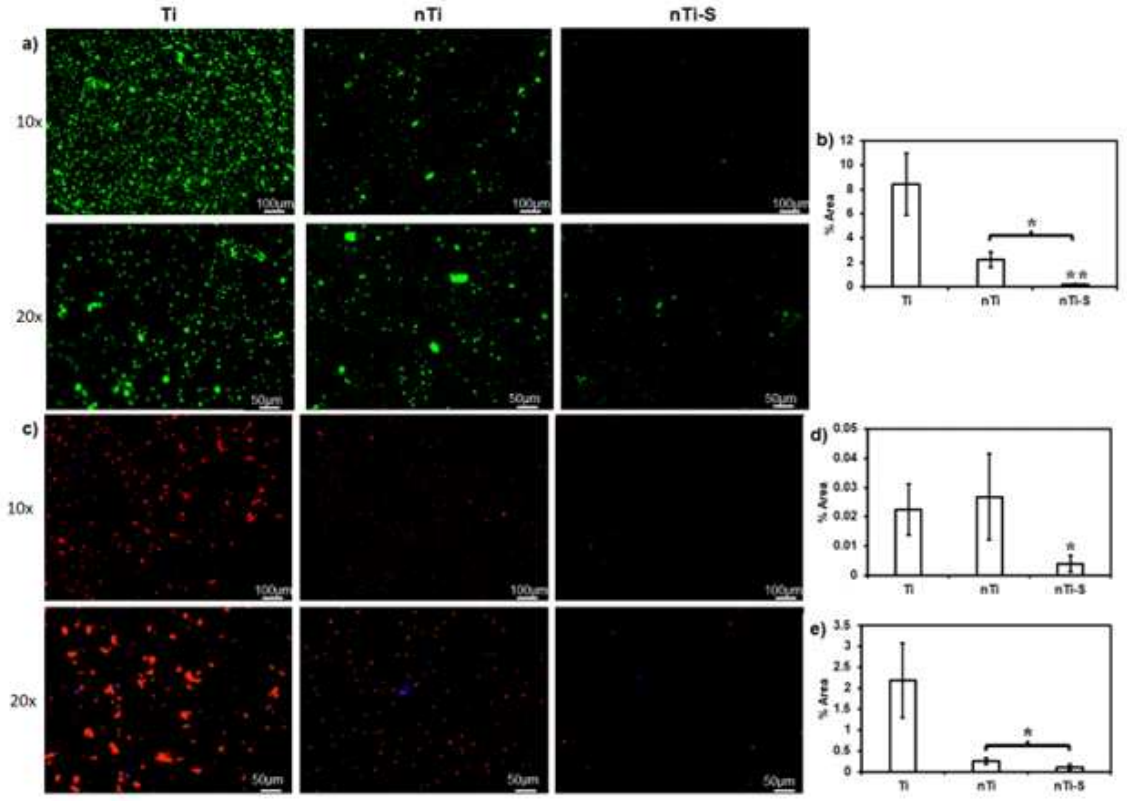

Figure 3.3: a) Fluorescence images of adhered live cells adhered (platelets and WBCs) on different surfaces. b) Percentage area covered by adhered platelets and WBCs on different surfaces. c) Fluorescence images of adhered platelets(red) and WBCs(purple) on different surfaces. d) Percentage of the areas covered by adhered platelets(red) on dif-ferent surfaces. e) Percentage area covered by adhered WBCs(blue) on different sur-faces. ($^*p < 0.05$). (nmin = 9).

lower surface area of contact due to presence of nano-pits, thus preventing platelet/WBCs from adhering to the surface. However, the Ti surface is a simple planar surface which alleviates platelet/WBCs adhesion. nTi-S surface had the lowest platelet/WBCs adhesion. This is because the superhemophobic nature of the surface prevents any interaction of the liquid with the surface.

Identification of platelet and WBCs on different surface was assessed after incubation with PRP by staining with rhodamine phalloidin and DAPI. DAPI purple stains nucleus of the cells, whereas rhodamine–phalloidin red stains the cytoskeleton of the cells. Since, platelet don't have nucleus, they are stained red. Platelets play a crucial role in the extrinsic pathway of the coagulation cascade while WBCs play a crucial role in intrinsic pathway by secreting anticoagulant molecules and indirectly activating platelets. WBCs and platelet complex formation can accelerate thrombus formation [49]. Rhodamine phalloidin stains positive for cytoskeleton of both platelet and WBCs. DAPI stains positive for nucleus of WBCs and negative for platelets, as they are anuclear (**Figure 3.3c**). WBCs adhesion results (**Figure 3.3d**) showed that both Ti and nTi had significantly higher WBCs adhesion compared to nTi-S. Platelet adhesion results (**Figure 3.3e**) indicate the Ti surface had significantly higher platelet adhesion compared to nTi and nTi-S surfaces. nTi showed lower platelet adhesion compared to Ti surface because the micro-nano surface topography had localized platelet adhesion and prevented platelet aggregation. nTi-S surface had the lowest platelet/WBCs adhesion. This is because the superhemophobic surface prevents blood component interaction significantly.

Platelet and WBCs adhesion, activation and complex aggregate formation on different surfaces were visualized after incubation with PRP using SEM. Platelets when activated go through a morphology change and form dendrites and initiate aggregation. The activated platelet indirectly supports WBCs localization during thrombosis. Simultaneously, platelet-WBCs complex formation promotes inflammation reactions. Activated platelet alter their morphology and have dendrite developed on the peripheral[50]. Results (**Figure 3.4**) indicate that Ti surface has significantly promoted platelet adhesion and activation (dendrite formation) and the planar surface assists easy

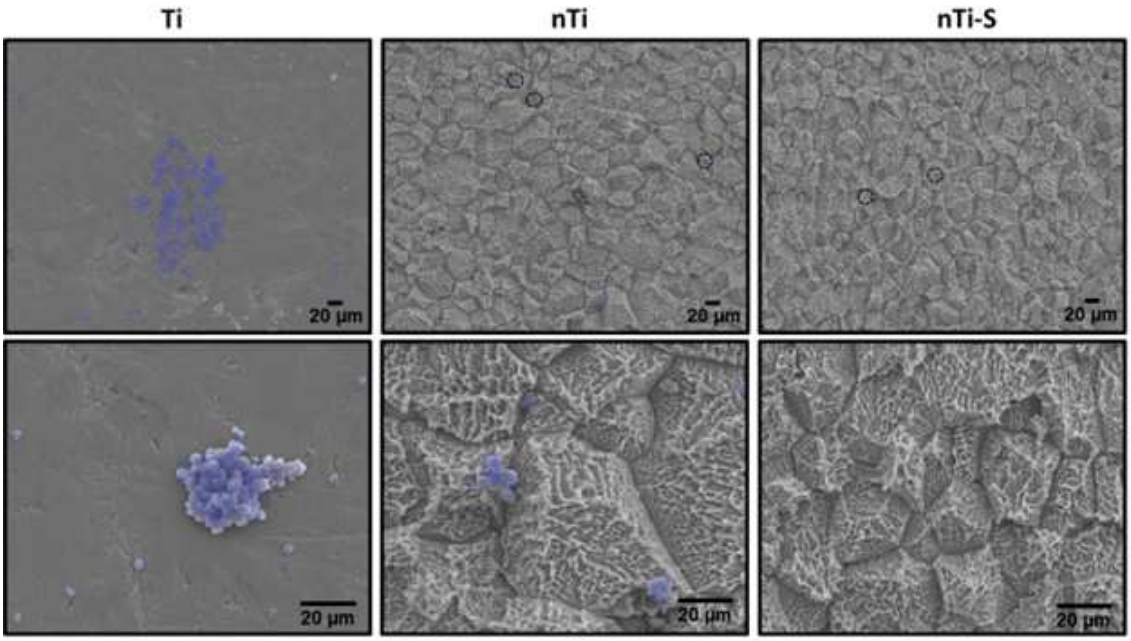

Figure 3.4: Representative SEM images of adhered platelets and WBCs (purple – photoshop for better visibility) on different surfaces. Images were taken at 500X, and 2000X magnification. (nmin = 9).

platelet aggregation and platelet-WBCs formation (highlighted in purple). nTi surface shows lower platelet adhesion and aggregate formation compared to Ti surface. nTi have platelet adhesion; however, the surface morphology has prevented well spread platelet aggregation and platelet activation (dendrite formation). nTi-S surface had the least platelet adhesion, and neither platelet aggregation nor platelet activation is observed on the surface.

The hemolytic activity of different surface was assessed after incubation with erythrocytes using a commercially available hemolysis assay. Studies have shown that erythrocyte lysis can be induced due to contact with implant surface due to its surface chemistry, surface charge and topography [6]. Erythrocyte's lysis induced by surface interactions leads to release of hemoglobin [51,52]. Therefore, presence of hemoglobin is a marker of hemolysis. Results (**Figure 3.5**) indicate that the hemoglobin release from the erythrocytes incubated with different surfaces was not significantly different from the two FDA approved Buna N (control 1) and silicon elastomer (control 2). Hence, neither the micro-nano surface topography nor the silane chemistry does not induce hemolysis.

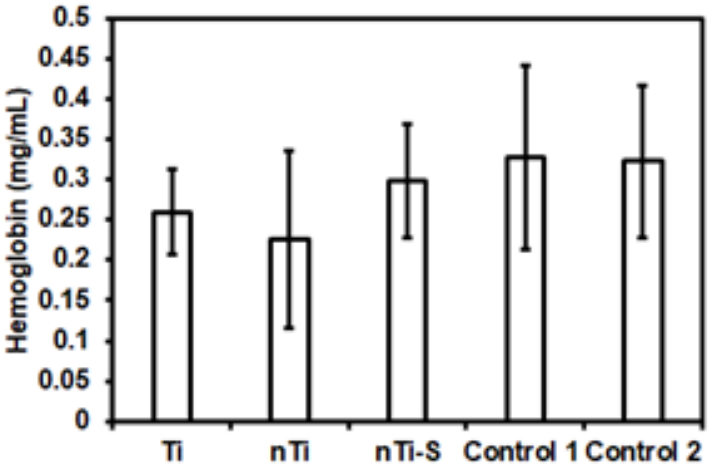

Figure 3.5: Hemoglobin release from erythrocytes solution incubated with different sur-faces was measured using a microplate reader. (nmin = 9).

The thrombin formation of different surfaces was assessed using a commercially available thrombin generation assay. Studies have shown that thrombin plays a vital role in converting fibrinogen to fibrin, which is an integral step in clot formation. Thrombin is formed from prothrombin due to the coagulation cascade formation from both intrinsic and extrinsic pathway activation[4]. Thrombin generation also activate platelets and inflammatory cell chemotaxis. Thrombin has a short half-life, making it complicated to quantify its activity [53]. The surface exposed manufacturer provided plasma was activated, and thrombin generation was measured at different time points. The assay is developed to measure the thrombin generation velocity at different time points and the highest velocity is reported. standard deviation is applicable for this assay. Results (**Figure 3.6**) indicate that the rate at which thrombin was generated was significantly higher with medical steel compared to low-density polyethylene, titanium, and other modified surfaces over a period of 4 mins. nTi surface had the lowest thrombin generation velocity compared to Ti, nTi-S, low density polyethylene (control 1) and medical steel (control 2) surfaces. This may be because the nTi surface is hydrophilic and there is constant thrombin generation.

Complement convertase activation of different surfaces was assessed using a commercially available complement convertase assay. Thrombus formation is due to the initiation of the coagu-

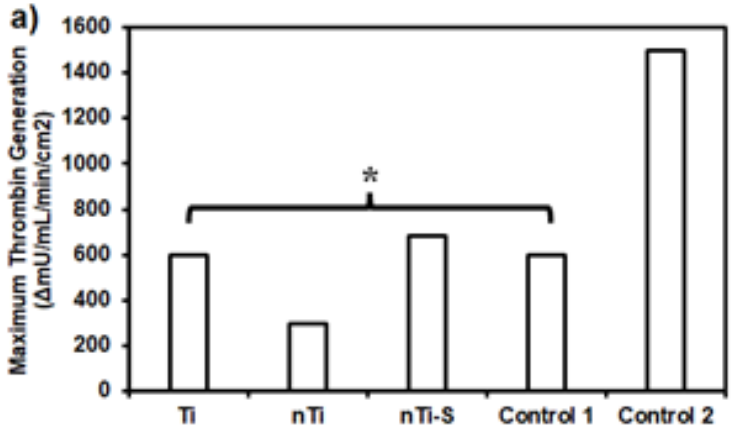

Figure 3.6: Highest thrombin generation velocity of plasma incubated with different surfaces between two points. (nmin = 9).

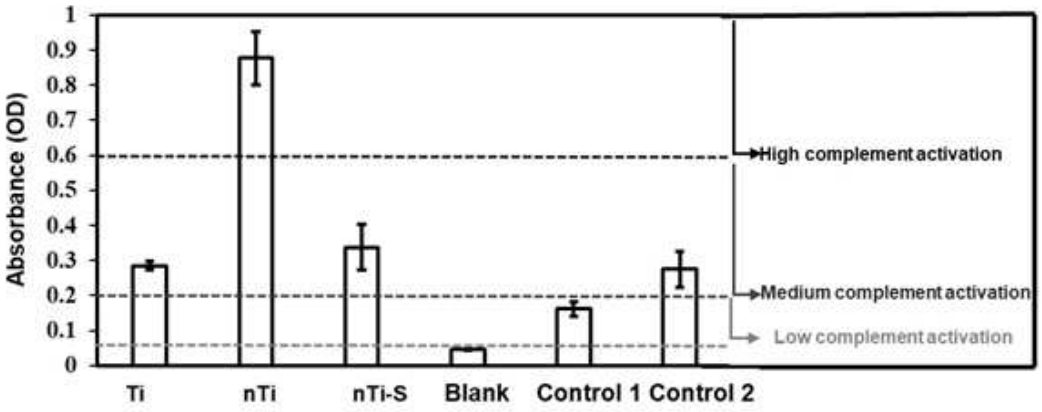

Figure 3.7: Complement activation of plasma incubated with different surfaces was measured as activation of complement convertase C5a. The lines indicate the regions of inactive/low (0.2), medium (>0.2 0.6), and high (>0.6) reactivity. (nmin = 9).

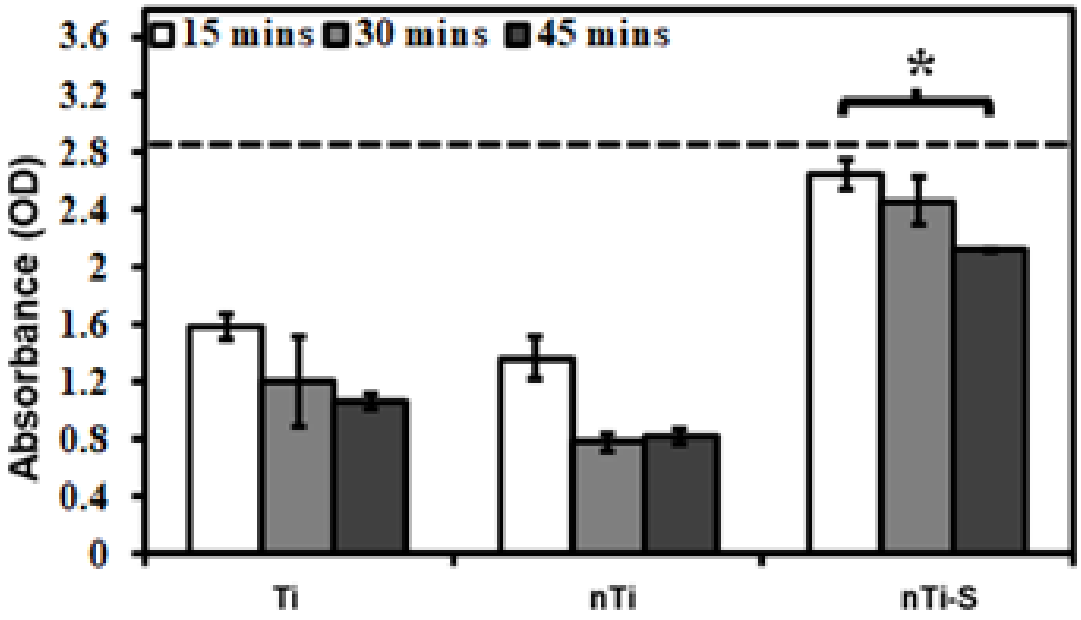

Figure 3.8: Whole blood clotting on different surfaces for up to 45 min. The dotted line represents the absorbance of free hemoglobin in un-clotted blood. ($^{*}p < 0.05$ (nmin = 9).

lation cascade, and this cascade is divided into two categories, intrinsic and extrinsic pathway. The intrinsic pathway (contact activation) is because of the interaction between the adsorbed proteins and the implant surface. Complement activation is a part of the intrinsic inflammatory response and simultaneously influences blood clotting. Complement activation alleviates WBCs adhesion and activation on the implant surface [54,55]. Different surfaces were incubated with manufacturer provided plasma and the adhered complement factors on the surface was measured. Results (**Figure 3.7**) indicate that nTi surface had significantly higher complement activation compared to other modified, low-density polyethylene (control 1) and medical steel (control 2) surfaces. However, there was no significant difference between medical steel, Ti and nTi-S surfaces and the values were in the lower spectrum of medium complement activation.

Blood clotting kinetics on different surface was assessed after incubation with whole blood by quantifying the free hemoglobin in the blood interacting with the surface. Previous studies evaluated the influence of proteins, enzymes, and cells individually with the modified surfaces.

However, when an implant is placed inside human body, whole blood comes in contact. Hence, the whole blood clotting kinetics is studied. After 15 mins, 30 mins, and 45 mins of incubation, different surfaces were immersed in Milli-Q water to measure the hemoglobin on live RBCs. RBCs, in presence of Milli-Q water rupture because of osmosis releasing hemoglobin. Thus, higher concentration of hemoglobin in Milli-Q water indirectly indicated less blood clotting at the surface. Results (**Figure 3.8**) indicate that after 45 mins, nTi-S surface has significantly higher hemoglobin compared to Ti and nTi surfaces thus evidently prevents blood clotting significantly. Similar trends were observed over the entire duration of study. Over time there was steady decrease in free hemoglobin, a part of this is due to the exposure of blood to the atmosphere.

3.4 Conclusions

Blood contacting implants are highly susceptible to thrombosis and bacterial infection as the planar surface properties alleviates improper interactions. In the quest of developing hemocompatible surfaces, a thermochemical method was explored for modifying implant surfaces, this technique is very elementary and is easily scalable. In this present study, titanium substrates were thermochemically treated with sulfuric acid under controlled atmosphere. The treatment etched the surface at micron and nano scale.

- Treatment led to a novel micro-nano surface topography, further coating with silane made the surface super-hemophobic.
- Hemolysis studies shows that there was no significant hemolysis due to the surface modifications compared to the reference materials. The fibrinogen adhesion from PRP shows that super-hemophobic surface adhered significantly lower fibrinogen compared to other surfaces. Studies have shown that reduced fibrinogen adhesion prevents platelet adhesion and activation.
- Ti and modified surfaces showed significantly lower thrombus generation kinetics compared

to medical grade steel. The modified superhemophobic surface didn't activate higher complement, thus preventing any inflammatory reactions. However, the micro-nano surface showed higher complement activation.

- The superhemophobic surface significantly prevented platelet/WBCs adhesion compared to other surfaces. However, micro-nano surface had similar WBCs adhesion and lower platelet adhesion compared to Ti. The planar Ti surface had significantly high platelet adhesion, activation, and platelet-WBCs complex formation. However, the micro-nano surface shows localized platelet adhesion and aggregate formation, but the micro-nano surface prevents platelet-WBCs complex formation due to its surface topography. In contrary, superhemophobic proves to be the most hemocompatible surface as it significantly prevented platelet and WBCs adhesion.

- The whole blood clotting kinetics shows that the super-hemophobic surface had significantly lower whole blood clotting after 45 mins of incubation compared to other surfaces. Thus, the micro-nano surface coated with silane is a promising candidate for blood contacting implant application.

Further studies are directed towards analyzing the mechanisms causing the improved hemocompatibility of micro/nano surface features and stability by investigating the influence of superhemophobic surface dynamic in-vitro and in-vivo conditions.

3.5 References:

1] David Yaffee MD, Mathew Williams, Journal of American College of Cardiology (2015).

[2] S.H. Woolf, H. Schoomaker, JAMA 322 (2019) 1996–2016.

[3] M. Kaur, K. Singh, Materials Science and Engineering: C 102 (2019) 844–862.

[4] V. K. Manivasagam, R. M. Sabino, Prem Kantam, K. C. Popat, Mater Adv 2 (2021) 5824–5842.

[5] N. Huang, P. Yang, Y.X. Leng, J.Y. Chen, H. Sun, J. Wang, G.J. Wang, P.D. Ding, T.F. Xi, Y. Leng, Biomaterials 24 (2003) 2177–2187. [6] V.K. Manivasagam, K.C. Popat, ACS Omega (2020).

[7] H.-J. Chiang, H.-H. Chou, K.-L. Ou, E. Sugiatno, M. Ruslin, R.A. Waris, C.-F. Huang, C.-M. Liu, P.-W. Peng, Metals (Basel) 8 (2018) 513.

[8] J. Yang, Y. Zhou, F. Wei, Y. Xiao, Clin Oral Implants Res 27 (2016) 1031–1038.

[9] M. Weber, H. Steinle, S. Golombek, L. Hann, C. Schlensak, H.P. Wendel, M. Avci-Adali, Front Bioeng Biotechnol 6 (2018) 99.

[10] D.L. Bhatt, J.S. Hulot, D.J. Moliterno, R.A. Harrington, Circ Res 114 (2014) 1929–1943.

[11] Z. Shah, V. Jeevanantham, R. Masoomi, P. Tadros, J Atr Fibrillation 8 (2015).

[12] E.J. Pirozzi, B.K. Wills, StatPearls (2021).

[13] P.T. Chen, T.J. Wang, M.H. Hsieh, J.C. Liu, C.Y. Liu, K.Y. Wang, W.C. Laio, BMJ Open 9 (2019).

[14] S. Park, I. Jang, Int J Environ Res Public Health 18 (2021).

[15] B.B. Lieber, A.P. Stancampiano, A.K. Wakhloo, Annals of Biomedical Engineering 1997 25:3 25 (1997) 460–469.

[16] J.M. Grunkemeier, W.B. Tsai, C.D. McFarland, T.A. Horbett, Biomaterials 21 (2000) 2243–2252.

[17] T.A. Horbett, J Biomed Mater Res A 106 (2018) 2777.

[18] I.H. Jaffer, J.C. Fredenburgh, J. Hirsh, J.I. Weitz, Journal of Thrombosis and Haemostasis 13 (2015) S72–S81.

[19] C.A. Labarrere, A.E. Dabiri, G.S. Kassab, Front Bioeng Biotechnol 8 (2020) 123.

[20] P. Hameed, V.K. Manivasagam, M. Sankar, K.C. Popat, G. Manivasagam, in: Springer Series in Biomaterials Science and Engineering, Springer Science and Business Media Deutschland GmbH, 2021, pp. 107–130.

[21] J. Vishnu, V. K Manivasagam, V. Gopal, C. Bartomeu Garcia, P. Hameed, G. Manivasagam, T.J. Webster, Nanomedicine 20 (2019).

[22] V.K. Manivasagam, K.C. Popat, Materials Science and Engineering: C (2021) 112315.

[23] S. Nastyshyn, Y. Stetsyshyn, J. Raczkowska, Y. Nastishin, Y. Melnyk, Y. Panchenko, A. Budkowski, Polymers (Basel) 14 (2022) 4245.

[24] V.K. Manivasagam, M. Sankar, · Caterina, B. Garcia, J. Vishnu, · Kaushik Chatterjee, · Satyam Suwas, G. Manivasa-gam, · Thomas, J. Webster, C.B. Garcia, K. Chatterjee, S. Suwas, T.J. Webster, In Vitro Models 2022 1:3 1 (2022) 273–288.

[25] R.M. Sabino, G. Mondini, M.J. Kipper, A.F. Martins, K.C. Popat, Carbohydr Polym 251 (2021) 117079.

[26] R.M. Sabino, K. Kauk, L.Y.C. Madruga, M.J. Kipper, A.F. Martins, K.C. Popat, J Biomed Mater Res A 108 (2020) 992–1005.

[27] S. Movafaghi, W. Wang, D.L. Bark, L.P. Dasi, K.C. Popat, A.K. Kota, Mater Horiz 6 (2019) 1596.

[28] X.H. Wu, Y.K. Liew, C.W. Mai, Y.Y. Then, International Journal of Molecular Sciences 2021, Vol. 22, Page 3341 22 (2021) 3341.

[29] B.K.D. Ngo, M.A. Grunlan, ACS Macro Lett 6 (2017) 992–1000.

[30] J. Fang, J. Zhang, J. Du, Y. Pan, J. Shi, Y. Peng, W. Chen, L. Yuan, S.H. Ye, W.R. Wagner, M. Yin, X. Mo, ACS Appl Mater Interfaces 8 (2016) 14442–14452.

[31] K. Khanmohammadi Chenab, B. Sohrabi, A. Rahmanzadeh, Biomater Sci 7 (2019) 3110–3137.

[32] V. Jokinen, E. Kankuri, S. Hoshian, S. Franssila, R.H.A. Ras, Advanced Materials 30 (2018) 1705104.

[33] Z. Montgomerie, K.C. Popat, Materials Science and Engineering C 119 (2021) 111503.

[34] A.I. Neto, P.A. Levkin, J.F. Mano, Mater Horiz 5 (2018) 379–393.

[35] J.L. 1, X.L. 2, C.Z. 1, H.Y. 2 Tian Shi 1, Polymers, MDPI (2022).

[36] J. Lu, C.-V. Ngo, S.C. Singh, J. Yang, W. Xin, Z. Yu, C. Guo, Langmuir 35 (2019) 3562–3567.

[37] R. Liu, Z. Chi, L. Cao, Z. Weng, L. Wang, L. Li, S. Saeed, Z. Lian, Z. Wang, Appl Surf Sci 534 (2020) 147576.

[38] V.K. Manivasagam, — Gopinath Perumal, — Harpreet, S. Arora, — Ketul, C. Popat, J Biomed Mater Res A (2022).

[39] [40] R.M. Sabino, K. Kauk, S. Movafaghi, A. Kota, K.C. Popat, Nanomedicine 21 (2019) 102046.

[41] V.K. Manivasagam, G. Perumal, H.S. Arora, K.C. Popat, J Biomed Mater Res A (2022).

[42] H. Cui, P.J. Sinko, Frontiers of Materials Science 2012 6:1 6 (2011) 47–59.

[43] M.M. Shirolkar, D. Phase, V. Sathe, J. Rodrguez-Carvajal, R.J. Choudhary, S.K. Kulkarni, J Appl Phys 109 (2011) 123512.

[44] J.I. Sheppard, W.G. McClung, I.A. Feuerstein, J Biomed Mater Res 28 (1994) 1175–1186.

[45] P.E. Scopelliti, A. Borgonovo, M. Indrieri, L. Giorgetti, G. Bongiorno, R. Carbone, A. Podestà, P. Milani, PLoS One 5 (2010) e11862.

[46] L. Zhang, B. Casey, D.K. Galanakis, C. Marmorat, S. Skoog, K. Vorvolakos, M. Simon, M.H. Rafailovich, Acta Biomater 54 (2017) 164–174.

[47] C. Cerletti, C. Tamburrelli, B. Izzi, F. Gianfagna, G. de Gaetano, Thromb Res 129 (2012) 263–266.

[48] L.C. Xu, J.W. Bauer, C.A. Siedlecki, Colloids Surf B Biointerfaces 124 (2014) 49–68.

[49] M.R. Elstad, T.M. McIntyre, S.M. Prescott, G.A. Zimmerman, Curr Opin Hematol 2 (1995) 47–54.

[50] V.B. Damodaran, V. Leszczak, K.A. Wold, S.M. Lantvit, K.C. Popat, M.M. Reynolds, RSC Adv 3 (2013) 24406–24414.

[51] A.R. Franco, E.M. Fernandes, M.T. Rodrigues, F.J. Rodrigues, M.E. Gomes, I.B. Leonor, D.L. Kaplan, R.L. Reis, Acta Biomater 99 (2019) 236–246.

[52] K. v. Nemani, K.L. Moodie, J.B. Brennick, A. Su, B. Gimi, Materials Science and Engineering: C 33 (2013) 4453–4459.

[53] J.G. EA Vogler, JG Nadeau,

[54] M.B. Gorbet, M. v. Sefton, The Biomaterials: Silver Jubilee Compendium 25 (2004) 219–241.

[55] N. Ferraz, M.K. Ott, J. Hong, Microsc Res Tech 73 (2010) 1101–1109.

CHAPTER 4: ENHANCED ANTIBACTERIAL PROPERTIES ON SUPERHYDROPHOBIC MICRO-NANO STRUCTURED TITANIUM SURFACE[1]

4.1 Introduction

Implantable medical devices such as cardiovascular or orthopedic implants are commonly used in patients as it improves the quality of life by replacing damaged human tissue. In the United States alone, more than three million orthopedic implants [1]and one million cardiac implants surgeries are performed annually [2]. These numbers are expected to increase exponentially across all different age groups due to increased average life expectancy and advancements in surgical procedures. However, infection remains a major reason for implant failure [3,4]. In the United States, implant related infections accounts for almost 25 % of the total health care associated infections. The Centers for Disease Control and Prevention (CDC) and the National Institutes of Health (NIH) estimate that biofilm phenotype bacteria cause 65 to 80 % of all human infectious diseases [5]. Studies have shown that 99 % of biofilm forming bacteria are gram positive Staphylococcus species (*S. aureus* and *S. epidermis*) and 15 % of implant infection are gram negative bacilli species (*E. coli* and *P. aeruginosa*) [6–8].

Implant associated infection is due to the complex interactions between the implant surface, pathogen (bacteria), and the patient's immune system. Normally, the host immune response is stronger on pathogens, and it is instinctively cleared. However, after bacteria adheres on implant surface, they proliferate and form a protective biofilm. Bacteria biofilm is a complex three-dimensional extracellular polymeric substance which hold the cluster of bacteria together [9,10]. It also acts as a protective layer against effects of antibiotics, immune response, nutrient deprivation, and pH changes. The bacteria cells at the periphery of the biofilm also detached and spreads the infection further into different parts of the body [11,12]. The tissue response for the bacteria

[1]This work was published in Journal of Biomedical Materials Research Part A and is reproduced in modified form here with permission

biofilm also leads to inflammation, formation of granulation tissue, and a fibrous encapsulation of the implant [13]. Typically, revision implant surgeries are required to treat this type of infection [14]. Studies have also shown that there has been an overuse of antibiotics to which bacteria have developed a biochemical resistance to them. This resistance may have been acquired by random mutation and gene transfers during the bacteria reproduction [15]. For example, Staphylococcus aureus has a mutated variant which is resistant to methicillin, and Enterococcus has a mutated variant resistant to vancomycin [16,17]. Some bacteria have also developed tolerance towards ethanol-based disinfectants, which makes it difficult to eradicate them completely in a clinical setting [18]. Thus, the possibility of implant infections during surgical procedures are increasing rapidly. Hence, there is a critical need to develop implant surfaces that have antibacterial properties against different strains of bacteria.

Bacteria adhesion and biofilm formation on an implant surface is influenced by the implant properties such as surface topography (roughness, porosity, etc.), physio-chemical properties (wettability, chemistry, charge, etc.)[19,20]. Other environmental conditions such as pH, temperature, bacteria type (gram positive/gram negative), bacteria shape and size also influence the infection rate, however these are not controllable [21,22]. Hence, researchers have attempted to modulate the implant properties by various techniques to make the surface antibacterial for different bacteria species. Implant surfaces doped with varying amounts of bactericidal materials such as silver, copper and zinc have been investigated [23–25], however the major limitation is that these ions may diffuse into the surrounding tissues over time causing toxicity and necrosis [26]. Photocatalytic materials have been shown to have antibacterial properties when exposed to UV light [27,28], however, these materials have shown poor long-term stability. Recently, studies have shown that surface with sharp features and hydrophilic chemistry has improved antibacterial properties [29–31], and superhydrophobic surfaces have reduced protein adsorption and bacterial adhesion [32–34].

In this study, a simple thermochemical treatment was used to develop micro-nano surface topography on titanium surface[2,35,36]. Titanium based materials are commonly used for car-

diac implants due to their favorable biocompatibility and mechanical properties [37–39]. The surfaces were further modified using heptadecafluoro-1,1,2,2-tetrahydrodecyl trichlorosilane and poly-ethyleneglycol 2-[methoxy(polyethyleneoxy)propyl] trimethoxysilane to alter the chemistry and wettability of the surface. The combined micro-nano surface topography and modification with PEG and silane led to a superhydrophilic and a superhydrophobic surface, respectively. All the surfaces were characterized for morphology, wettability, chemistry, corrosion resistance and surface charge as these properties can influence bacteria adhesion and biofilm formation. Bacteria cell (*S. aureus* and *E. coli*) growth inhibition in the physiological environment, their adhesion and proliferation, and biofilm formation were evaluated on different surfaces for up to 24 hrs of incubation. The results indicated that the superhydrophobic micro-nano modified surface decreased bacterial adhesion significantly (> 90 %) and prevented biofilm formation. Thus, this novel surface modification can be a potential implant surface with high antibacterial properties.

4.2 Materials and Methods

4.2.1 Fabrication of nanostructured topography and surface modification on titanium

The micro-nano surface topography was fabricated on commercially pure titanium (Grade 2) surfaces using thermochemical process. Prior to modification, the surfaces (50 mm X 20 mm X 0.25 mm) were mechanically polished using silicon carbide sheets of different grit sizes (400, 600, 800, 100 and 1200) and cleaned with acetone in a sonicator for 10 mins. The cleaned surfaces were rinsed with DI water and air dried. They were then immersed in 0.5 M sulfuric acid in a polytetrafluoroethylene (PTFE) container and placed inside a hot air oven at 80 °C for 8 hrs for thermochemical treatment. After the thermochemical treatment, the surfaces were further cleaned with acetone in a sonicator for 10 mins. The surfaces were then annealed at 300 °C for 1 hr and stored until further modification.

The micro-nanostructured surfaces were further modified to be superhydrophobic and superhydrophilic. Prior to this modification, the micro-nanostructured surfaces were etched with plasma at 200V in 10cm^3/min of oxygen gas for 5mins. The surfaces were modified by placing them in a closed chamber either with 150 μl of heptadecafluoro-1,1,2,2-tetrahydrodecyl trichlorosilane (referred as silane in this chapter) at 120°C for 1hr to make the surfaces superhydrophobic; or with 10 ml of 2 vol% of poly-ethyleneglycol 2-[methoxy(polyethyleneoxy)propyl] trimethoxysilane (referred as PEG in this manuscript) in ethanol solution at room temperature for 24 hrs to make the surface superhydrophilic.

All modified surfaces were rinsed with DI water, dried with air, and stored in a desiccator until further use. In this manuscript, unmodified titanium surfaces are referred as Ti; micro-nanostructured titanium surfaces are referred as nTi; superhydrophobic micro-nanostructured titanium surfaces are referred as nTi-S; superhydrophilic micro-nanostructured titanium surfaces are referred as nTi-PEG.

4.2.2 Surface Characterization

Surface morphology

The surface morphology of different surfaces was visualized using a JEOL 6500 field emission scanning electron microscopy (SEM). The surfaces were imaged after coating with 10 nm gold for improved conductivity. The parameters for the SEM were optimized and chosen as follows: accelerating voltage of 15 kV, working distance range: 7 – 12 mm, and vacuum pressure below 3 X 10^{-4} Pa. The working distance, brightness and contrast was adjusted for each surface to ensure similar quality of images. The SEM images were acquired using the secondary electron detector and back scattered detector at different magnifications ranging from 500 X – 5000 X magnification.

Surface wettability

The surface wettability of different surfaces was characterized using a Rame-hart 260F4 goniometer. The apparent contact angle was measured 3 secs after a 10 μl drop of DI water (polar) or hexadecane (non-polar) was placed on the surface using the DROPimage software. The advancing contact angle was measured by continuously increasing the droplet volume using a micrometer syringe. The surface energy of different surfaces was calculated using the advancing contact angles and Young's and Owens-Wendt equations [2,32].

Surface chemistry

The surface chemistry of different surfaces was characterized using a PE-5800 X-ray photoelectron spectroscopy (XPS) equipped with an Al K x-ray source. The overall atomic composition of different surface was computed by obtaining the survey scan spectra that were collected from 0 to 1100 eV. The scan was done using a pass energy of 160 eV and a 0.05 eV step for 15 cycles. The data was analyzed using Multipak and the graphs were normalized, stacked, and plotted using OriginLab software. The percentage of elements present on each surface was calculated from the survey scan using the Multipak software. The high-resolution spectra scans were collected for carbon ($C1_s$) on different surfaces. The scan was done using a pass energy of 100 eV and a 0.05 eV step for 50 cycles. All C1s peaks were recalibrated by shifting the maximum peak at binding energy of 284.8 eV. The peaks were fitted and plotted using OrginLab software.

Electrochemical behavior

Electrochemical behavior of different surfaces was characterized using standard three electrode cell with graphite rod as counter electrode, saturated calomel electrode (SCE) as reference electrode and specimen as working electrode using a Gamry Interface 1000 E electrochemical setup. Prior to the experiment, the surfaces were polarized cathodically at –1 V vs. SCE for 10 min to clean the native oxide layer. Later, OCP measurements were conducted until the system attained stable open circuit potential (E_{OCP}) for 3600 s. Potentiodynamic polarization were collected at a scan rate of 0.166

mV/s from –0.4 V to +1.0 V vs E_{OCP}P and Tafel exploration were done to obtain the corrosion rate in mpy (mils per year). Electrochemical impedance spectroscopy (EIS) measurements were obtained at E_{OCP} over a frequency range of 0.01 Hz to 100 kHz with a set AC voltage amplitude of 10 mV. The electrochemical parameters obtained by electrical equivalent circuit (EEC) fitting are R_s (solution resistance), R_p (polarization resistance), CPE (constant phase element), n value (measure of passive layer homogeneity). CPE was used instead of pure capacitor to account the deviations produced by surface inhomogeneities. Impedance of CPE is given by the relation

$$Z_{CPE} = 1/(Q(j\omega)^n) \tag{4.1}$$

where Q is the Capacitance, ω is the angular frequency given by 2, f is the frequency, j is an imaginary root, and n was used to predict the surface heterogeneities of the formed passive layer(= 1 for nearly smooth electrode) [40,41].

Mott–Schottky analysis was done to determine the flat band potential on a potentiostatically grown oxide layer at 3V for 1000s with a negative scan from 1.5 V to -0.5 V. Gamry E-chem analyst 7.03 was used to model the electrical equivalent circuits and to analyze the obtained data. Mott–Schottky analysis was characterized to determine the flat band potential on a potentiostatically grown oxide layer at 3 V for 1000 s with a negative scan from 0.4 V to -0.6 V.

The electronic properties of the metal in a metal-electrolyte environment were determined using Mott Schottky (M-S) analysis, a capacitive measurement technique. Neglecting Helmholtz capacitance, the space charge capacitance, Csc, can be related to the charge carrier density N (donor, Nd or acceptor, Na in terms of n-type or p-type semiconductor respectively) by [40,42]

$$1/(C_{sc}^2) = ((2/(q\epsilon\epsilon_0 NA^2)))/((E - E_{fb} - kT/q)) \tag{4.2}$$

where, ϵ is the dielectric constant of the passive film (usually 60 for titanium) [43], ϵ_0 is the vacuum permittivity (8.85 × 1012 F/m), A is the area of the working electrode (0.5 cm2), E is the applied potential, E_{fb} is the flat band potential, q is the electron charge (1.602×1019 C), T is the

absolute temperature (K), and k is the Boltzmann constant (1.38×1023 J/K). Nd for all specimen was determined from the slope of the respective M-S curves, whereas Efb was obtained by an extrapolation of the M-S curve to $C^2 = 0$.

4.2.3 Cytotoxicity of different surfaces

Cytotoxicity of different surfaces was evaluated using Platelet Rich Plasma (PRP). PRP was isolated from human blood as described in previous work [2,44]. Lactate dehydrogenase (LDH) presence was evaluated using commercially available Lactate dehydrogenase (LDH) Cytotoxicity Assay Kit. Different surfaces were incubated with 300 μl Platelet Rich Plasma (PRP) for 2 hrs at 37 °C in a 48 well plate. The surface exposed PRP was used to evaluate cytotoxicity of different surfaces as per the protocol given by the assay manufacturer and the absorbance was measured at 600 nm. Positive (PRP exposed to blank well) and negative controls (PRP treated with Triton-X) were used to determine the maximum and minimum value of LDH.

4.2.4 Bacteria culture

Bacteria strains of gram-positive Staphylococcus aureus (S. aureus) and gram-negative Escherichia coli (E. coli) were used to characterize the antibacterial properties of different surfaces. Bacteria grown in an agar plate were introduced into 5 ml of trypsin soy broth (TSB) used as a bacteria growth media and vortexed for 10 secs to properly mix the bacteria within the media. This media was subsequently incubated for 6 hrs at 37 °C. After incubation, three dilutions (25%, 50% and 75%) of the solution were made to create different bacteria concentrations in a 96 well plate, and the absorbance was read at a wavelength of 562 nm in a plate reader to determine optical density. A dilution was made until the solution with an average optical density of 0.52 was obtained, indicating a concentration of 109 bacteria cells/ml of TSB solution. Once the required dilution was achieved, the solution was further diluted with TSB to obtain final concentration of 106 bacteria cells/ml in TSB solution. Prior to bacteria studies, the surfaces were further cut into 0.5 mm X 0.5 mm samples and were cleaned by rinsing them with 500 μl of DI water and phosphate buffered saline

(PBS). The surfaces were then exposed to UV light for 15 mins for sterilization. 300 μl of bacteria solution (106 bacteria cells/ml of TSB solution) was pipetted on all the surfaces in a 48 well plate. The well plates were incubated at 37°C and 5% CO_2 for the duration of studies.

4.2.5 Bacteria growth inhibition by different surfaces

Bacteria inhibition on different surfaces was characterized using microplate reader by following guidelines of the Clinical and Laboratory Standards Institute using the broth microdilution method. After 6, 12 and 24 hrs of incubation with bacteria solution, 100 μl of aliquot solution was used to characterize bacteria inhibition by measuring the absorbance at 600 nm. Bacteria solution incubated in blank wells (polystyrene) were used as control.

4.2.6 Bacteria adhesion and viability on different surfaces

Bacteria adhesion on different surfaces was characterized using fluorescence microscopy. After 6, 12 and 24 hrs of incubation with bacteria solution, the bacteria adhesion and viability were characterized by using commercially available live/dead bacteria staining assay. In a dark environment, the surfaces were washed carefully using PBS, and 500 μl of stain solution (1.5 μl/ml of propidium iodide and 1.5 μl/ml Syto 9) was added to each well and incubated for 20 mins at room temperature. After the incubation, stain solution was removed, and the surfaces was again rinsed with PBS twice. The surfaces were fixed in a 3.7% formaldehyde PBS solution for 15 mins. Finally, the fixative was removed, and the surfaces was rinsed in PBS twice before imaging under a Zeiss fluorescence microscope. Live and dead bacteria adhesion area coverage was calculated using Image J software.

4.2.7 Bacteria morphology

Bacteria morphology and colonization on different surfaces was characterized using SEM. After 6, 12 and 24 hrs of incubation with bacteria solution, the surfaces were washed carefully using PBS. The surfaces were incubated for 45 mins in a primary fixative solution consisting of 3%

glutaraldehyde, 0.1 M sodium cacodylate, and 0.1 M sucrose in DI water. This was followed by further incubation for 10 mins in a buffer solution consisting of 0.1 M sodium cacodylate, and 0.1 M sucrose in DI water. The surfaces were then washed and dehydrated in subsequent solutions of 35, 50, 70, and 100% ethanol in DI water for 10 mins each. The surfaces were coated with 10 nm of gold before imaging. The SEM images were taken as described in the materials and methods section 2.2.1. The images were processed using Adobe Photoshop and S. aureus bacteria was colored blue, and E. Coli was colored green.

4.2.8 Statistical Analysis

Surface characterization techniques were repeated for at least three different samples of each surface (nmin = 3). Bacteria inhibition, adhesion, and morphology studies were carried out on at least three different samples of each surface and was repeated at least three times (nmin = 9). The quantitative results were analyzed using a two-way analysis of variance (ANOVA) test using the R software. The results were considered statistically significant with a p-value ¡0.05.

4.3 Results and Discussion

Implantable medical devices are commonly used to replace diseased or damaged tissues and have improved life expectancy and quality of life for millions of patients. However, this has also resulted in increased implant failure due to infection and mutated antibiotics resistant bacteria stain. Revision surgeries are usually performed to remove the infected implants [45,46]. Hence, there is a significant need to develop implant surface with antibacterial properties [47]. Studies have shown that modifying implant surface properties such as roughness, wettability, charge, and chemistry can enhance antibacterial properties [48]. In this study, a superhydrophilic and superhydrophobic titania micro-nano topography surfaces were developed and investigated for potential of being antibacterial for cardiovascular application.

SEM was used to analyze the morphology of different surfaces. The results indicate that Ti did

not have any distinguishable topography, however, at higher magnification the SEM images show surface irregularities due to the polishing (**Figure 4.1**). During the subsequent thermochemical treatment of Ti, following chemical reactions take place during thermochemical treatment:

$$TiO_2 + 2H_2SO_4 \longrightarrow Ti(SO_4)_2 + 2H_2O \tag{4.3}$$

$$Ti + 2H_2SO_4 \longrightarrow Ti(SO_4)_2 + 2H_2 \tag{4.4}$$

$$Ti + 2H_2O \longrightarrow TiO_2 + 2H_2 \tag{4.5}$$

$$Ti + H_2 \longrightarrow TiH_2 \tag{4.6}$$

The results indicate that nTi surface had developed micro-nano topography after the thermochemical treatment (**Figure 4.1**). The micron scale topography had formed due to faster etching at the grain boundaries. This is because grain boundaries have higher surface energy as there is disordered atomic arrangement. This leads to faster etching at the grain boundaries compared to the grain itself [2,36,49]. Further, nanoscale pits were also visible on the grain surface due to etching. Thus, the images indicate that the thermochemical treatment led to a micro-nano topography on Ti surface. Further, the SEM images nTi-S and nTi-PEG did not show any significant difference in the surface topography when compared to nTi surfaces.

A goniometer was used to determine the wettability of different surfaces. The wettability dictates the surface interaction with proteins, cells, and bacteria when implanted into the body and hence it was evaluated. The apparent contact angle (θ^*) was measured using DI Water. θ^* is defined as the angle made by the liquid droplet placed on a rough surface. The angle is measured between the liquid-air interface and the solid-liquid interface at the triple phase point passing through the liquid [50]. The results indicate that θ^* for different surfaces followed the following trend: nTi-PEG

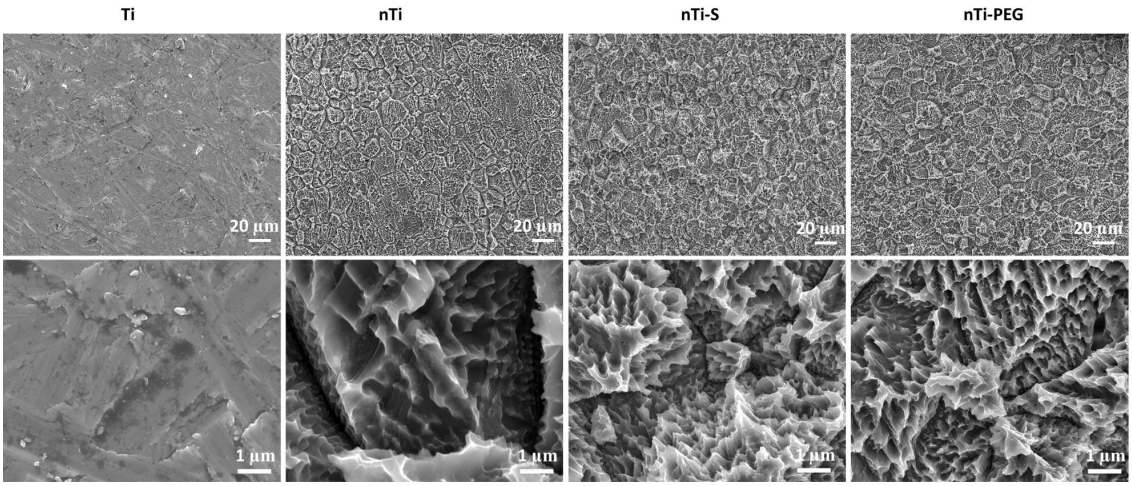

Figure 4.1: SEM observation of different surfaces. Images were taken at two magnifications (500x and 5000x).

< nTi < Ti < nTi-S. As expected, the Ti surface was hydrophilic (≈ 72º) since the surface had no specific topography. Whereas after the thermochemical treatment, nTi was superhydrophilic (≈ 8º). A surface is classified as superhydrophilic when (θ^*) is lesser than 10º [51]. This is due to the increased surface area created by the micro-nano topography. In contrast, nTi-S surface was superhydrophobic (≈ 160º). A surface is classified as superhydrophobic when (θ^*) is greater than 150º [51]. The surface is superhydrophobic due to the combination of nanoscale topography and low surface energy silane coating. This leads to formation of air pockets between the nano pits which further repel water. In contrary, nTi-PEG surface was superhydrophilic (≈ 0º). This is because the surface is grafted with PEG and the ether oxygen bonds readily bond with hydrogen present in the water molecules making them easy to spread [52].

The surface energy of different surfaces was calculated by measuring the advancing contact angle (θ_{adv}) with DI water (polar) and Hexadecane (non-polar). The surface energy was characterized to understand the surface properties (polar interaction and van der wall forces). Surface energy of a solid surface dictates the wetting with any liquid. The surface energy was calculated using the Young's and Owens-Wendt equation [53]. The surface energy had the similar trend as that of

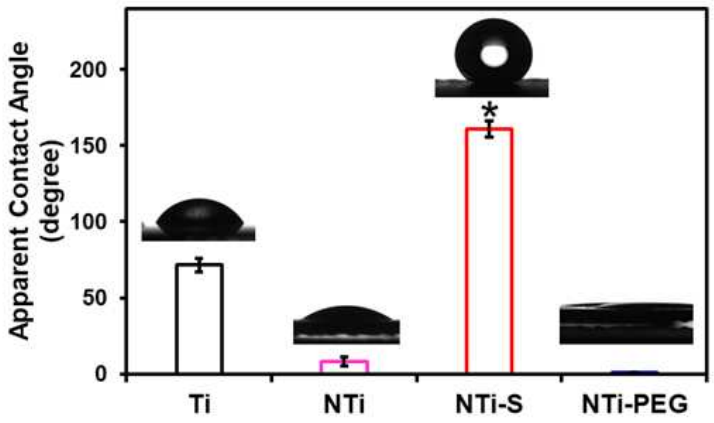

Figure 4.2: Apparent contact angle measurements using the sessile drop method for different surfaces. The results indicate significantly higher contact angle on nTi-S compared to other surfaces (*p < 0.05). The error bar represents the standard deviation.

Table 4.1: Advancing contact angle and surface energy of different surfaces.

	Advancing Contact Angle (DI Water)	Advancing Contact Angle (DI Water)	Surface Energy (mJ/M^2)
Ti	75.74	17.7	30.66
nTi	10	0	71.93
nTi-S	166.6	120.9	2.25
nTi-PEG	6.6	24.9	72.34

(θ^*) (nTi-PEG < nTi < Ti < nTi-S). nTi-S had significantly lower surface energy indicating that the surface will repel most liquids (**Table 4.1**). However, the nTi-PEG had significantly higher surface energy indicating that the most liquids will easily spread on the surface. [53].

XPS was used to analyze the surface chemistry. The surface chemistry dictates the interaction of proteins, cells, and bacteria with the surface, and certain elements can induce toxic effect when implanted, and hence it was evaluated. The survey scans were taken to analyze different elements present on the surfaces. The results (Figure 3) indicate presence of C_{1s} (≈ 284.8 eV), O1s (≈ 529 eV), and $Ti_{2p2/3}$ (≈ 458.5 eV) peaks on all the surfaces. The C_{1s} content was higher on polished Ti (Table 2) surface due to presence of impurities on the surface and in the XPS chamber. After

thermochemical treatment, some of the carbon impurities were removed as well as the native oxide layer was etched, thus increasing the $Ti_{2p2/3}$ peak on the nTi surface [2,54]. Simultaneously, the exposed $Ti_{2p2/3}$ reacts with the sulfuric acid and water which results in formation of titania (eq. 3, eq. 4, and eq. 5). Thus, the nTi surface had higher $Ti_{2p2/3}$ and O_{1s} peaks. After modification with silane, F_{1s} ($\approx$ 689 eV) peak was present on nTi-S confirming silane on the surface [44,55]. Similarly, nTi-PEG surface had higher C_{1s} peaks when compared to nTi confirming PEG on the surface.

Table 4.2: Elemental composition of different surfaces obtained from the XPS survey scans

	C	Ti	O	F	Others
Ti	61.2	4	27.4	4	27.4
nTi	43.4	9.4	36.6	0.7	9.9
nTi-S	20	12	41	23.9	3.1
nTi-PEG	53.6	7.8	36.5	0	2.1

High resolution C1s spectra were obtained to further confirm the presence of silane and PEG on the surfaces (**Figure 4.3b**). Studies have shown that surfaces exposed to ambient atmosphere has a small detectable amount of carbon, with three different chemical states (C-C ($\approx$ 284.8 eV), O-C=O ($\approx$ 288.5 eV) and C-O-C ($\approx$ 286.5 eV)) commonly present [56]]. The high-resolution scans on Ti and nTi surface showed all these three peaks and C-C was the dominant peak. After the silane modification, -CF2 ($\approx$ 292.0 eV) and -CF3 ($\approx$ 293–294 eV) peaks were present on nTi-S surface indicating the surface was successfully modified with silane. Similarly, after PEG modification, higher C-O-C peak was present on nTi-PEG, indicating the surface was successfully modified with PEG.

A three-electrode electrochemical setup was used to analyze the corrosion behavior and material degradation of different surfaces. Metal implants are prone to corrosion after implantation due to the physiological pH, temperature and electrolytes present in the body fluids. Implant corrosion leads to poor functionality, durability and adverse reactions on the tissue surrounding the

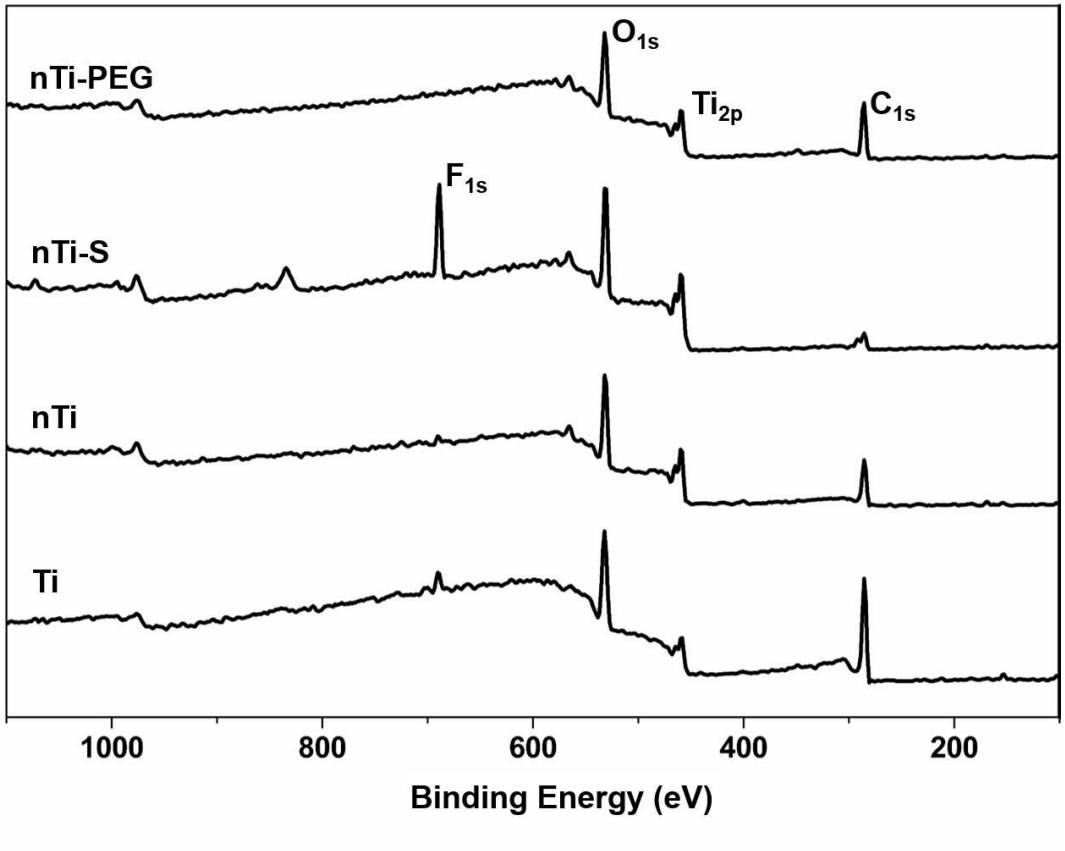

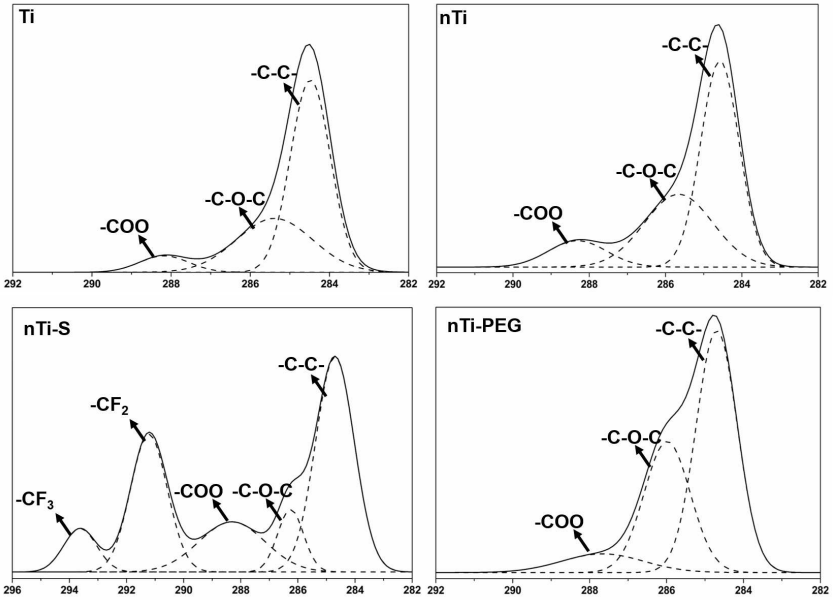

Figure 4.3: A) XPS survey scans of different surfaces. B)High resolution XPS scan for carbon peaks on different surfaces

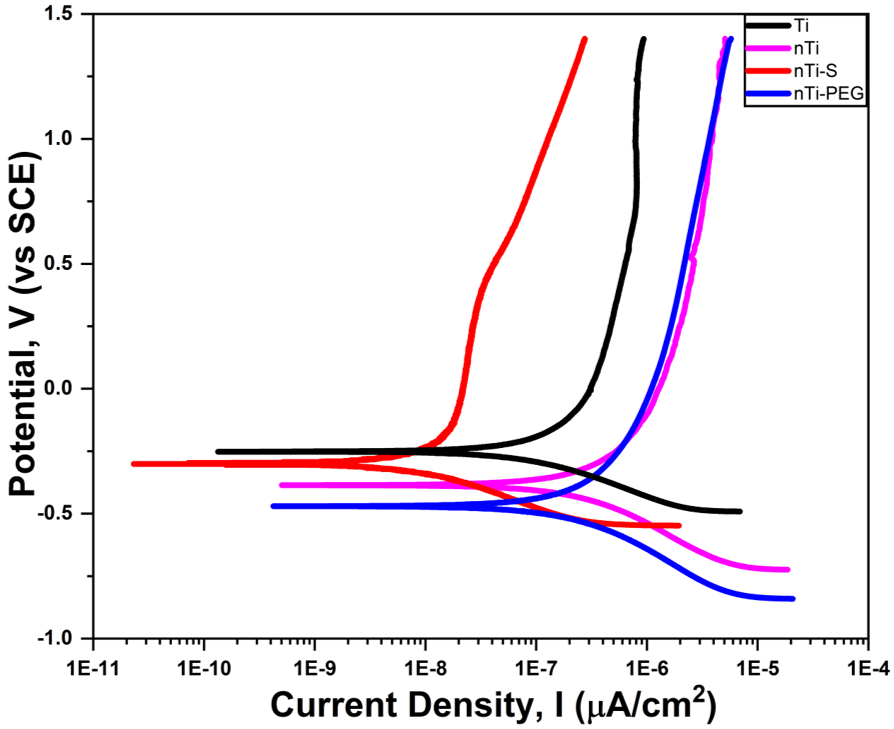

Figure 4.4: Cyclic polarization curves for different surfaces. Potentiodynamic polarization tests was done on at least three different substrates of each surface (nmin = 3)

implant [57,58]. Hence, the corrosion behavior was studied in simulated body fluid environment. Potentiodynamic polarization tests (**Figure 4.4**) were performed to determine the corrosion current density (I_{corr}), corrosion potential (E_{corr}) and corrosion penetration rate (CPY) using Faraday's expression [59]. The potentiodynamic polarization (Tafel) curves for different surfaces were simulated in Ringer solution at 37℃ (**Figure 4.4**). The results indicate that all the surfaces tend to passivate spontaneously in anodic region and no pitting corrosion was observed. This is due to the formation of TiO_2 and quick passivating nature of titanium [60]. The corrosion rate of different surfaces followed the following trend: nTi < nTi-PEG < Ti < nTi-S (Table 3). nTi and nTi-PEG showed higher Icorr and CPY compared to Ti surface. This may be due to the hydrophilic nature of the micro-nano surface topography on nTi and nTi-PEG that increases liquid interaction with the surface [52-55].

EIS was used to analyze the interface reactions of the passive layer formed on different surfaces. In this technique, impedance of the substrate/solution interface is measured over a variable frequency range. The interface reactions were modelled using electrical equivalent circuit (combination of resistors and capacitors) and simulated to replicate the processes that takes place in substrate-electrolyte interface. The results obtained from EIS were further analyzed to determine the polarization resistance (low-frequency region), solution resistance (high-frequency region), capacitance of the coating, and porosity. The polarization resistance is often used for calculating the corrosion rate [40]. Bode plot (**Figure 4.5a**) and Nyquist plot (**Figure 4.5b**) shows that the behavior of all surfaces was similar except that of nTi-S. The results shows that Ti, nTi and nTi-PEG surface had one-time step resistive behavior at high and low frequencies, whereas capacitive behavior was seen at intermediate frequencies. However, nTi-S surface shows three-time step resistive behavior indicating three different interactions due to its superhydrophobic nature and presence of multiple interfaces (Cassie-Baxter state, silane modification, and surface topography). The electrical equivalent circuits were designed to fit the nTi-S consisted of three constant phase elements (**Figure 4.5c**). The results indicate that polarization resistance, Rp obtained after curve fitting followed the following trend: nTi-PEG < nTi < Ti < nTi-S. Thus, the higher impedance spectra shown by nTi-S reflect the high corrosion resistance and effectiveness of the silane coating on the micro-nano topography. Further, higher n (measure of passive layer homogeneity) value arises from CPE element (eq. 4.1) suggests that relatively superior passive film was formed on nTi-S surface with less inhomogeneities and porosity [61].

Mott Schottky analysis was to analyze the surface charge of the passive layer formed on different surfaces [42]. Studies have shown that surface modifications can influence surface charge by altering charge carrier density and its Fermi level [62,63]. Surface charge plays major role in dictating the bacterial adhesion with the surface and hence was investigated. Although bacterial adhesion is a complex phenomenon, surface charge plays a major role in dictating the bacterial adhesion with the surface and hence it was particularly investigated. The significance of relative positioning of

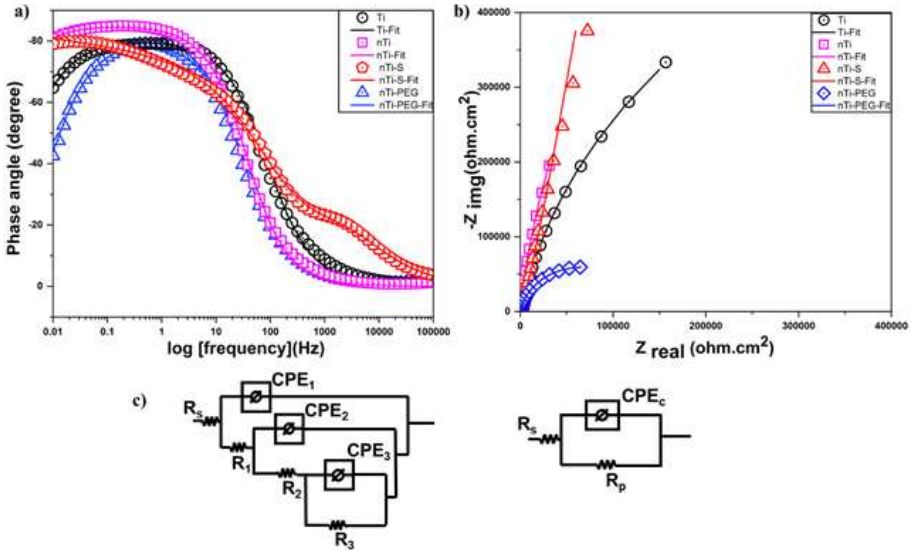

Figure 4.5: Nyquist plot and Bode plot for different surfaces. Equivalent electrical circuit for two different cases

Table 4.3 Electrochemical corrosion parameter for different surface

	Icorr (nA/cm^2)	Ecorr (mV)	CPY ($mpy \times 10^{-3}$)	Solution resistance, R_s (k ohm/cm^2)	Polarization resistance, R_p (k ohm/cm^2)	Constant Phase Element ($\times 10^{-6}\ \mu S\ s^n\ cm^2$)	Homogeneity factor (n)
Ti	135	-251	46.25	1340	1340	73.56	0.89
nTi	413	-386	141	2415	2415	64.80	0.93
nTi-S	15.8	-302	5.39	5679	5679	36.12	0.94
nTi-PEG	354	-470	121	143.8	143.8	95.77	0.89

flat-band potential with respect to OCP is key in predicting the surface charge of different surfaces. Thus, in this study, Mott Schottky curves ($1/C^2$ vs E) for the passive layer formed on different surfaces in ringer solution (**Figure 4.6**) were analyzed. The results indicate that the Mott Schottky curves look very similar for all surfaces. There was n-type behavior for the passive film in the –0.5 V to –0.1 V region and dielectric behavior above –0.1 V. The calculated donor density values (using eq. 2) for all surfaces were of the order of $1020/cm^3$. The results also indicated that the trend observed here was similar to the reported Mott Schottky behavior for titanium surfaces [40,64].

However, the nTi-S MS curve yields higher slope with lower donor density value compared to Ti, whereas both n-Ti and nTi-PEG had higher donor density value. Studies have shown that decrease in donor density helps in increase in corrosion resistance due to lesser number of oxygen vacancies and interstitials titanium [40,62]. Further, the Mott-Schottky results are in good agreement with potentiodynamic and EIS results. Thus, the superior corrosion resistance of nTi-S may be due to the less defective and thicker passive layer formation on the surface. Furthermore, the surface charge which is the difference between the location of flat band potential and rest potential on a surface affects the surface-bacteria interactions. The results indicate that the surface charge is highly negative on nTi-S compared to all the other surfaces. In physiological conditions, most of the bacteria membranes are negatively charged (within the pH range of 5-7) and they get repelled when they come in contact with a negatively charged surface [66]. Thus, nTi-S being highly negative will tend to repel bacteria compared to other surfaces. Further, the superhydrophobic nature of the nTi-S will prevent initial bacteria adhesion on the surface. Thus, the ability of nTi-S surface to reduce bacteria adhesion and biofilm formation may be due to a combine effect of repulsive negative surface charge and superhydrophobic nature.

Table 4.4 Electrochemical corrosion parameter for different surfaces

	E_{fb} (mV)	Nd donor density (cm^{-3}	OCP (mV)	Difference (E_{fb}-OCP)
Ti	-525	3.08	-420	-105
nTi	-627	11.8	-264	-363
nTi-S	-910	1.03	-136	-774
nTi-PEG	-594	7.33	-299	-295

Cytotoxicity of different surfaces was characterized after 2 hrs of incubation with PRP. PRP of human blood is made up of white blood cells and platelets is a simple model to study cytotoxicity [2]. When an implant surface is exposed to cells, the surface properties may be toxic, and cells die due to apoptosis or necrosis or through other form of cell damage. LDH is a stable enzyme present

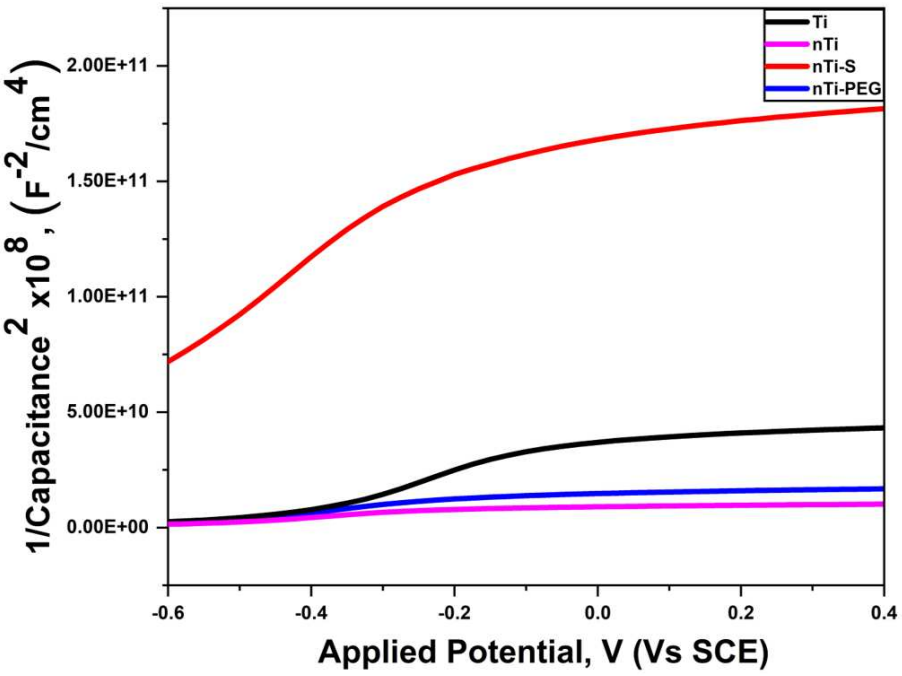

Figure 4.6: Mott Schottky curves of different surfaces

in the cytoplasm of cells and after cell death, LDH gets released into the cell culture supernatant. Hence, the LDH activity is marker for cytotoxicity. The results indicate that different surface showed no significant difference (**Figure 4.7**) in LDH activity compared to positive control (100% live cells). The LDH activity of the negative control (100% dead cells) was significantly higher compared to the positive control and different surfaces. Thus, the modified surface do not induce any toxicity to blood cells.

Inhibition of *S. aureus* and *E. coli* growth in presence of different surfaces was characterized after 6, 12 and 24 hrs of incubation in growth media. When an implant surface comes in contact with bacteria cells, the surface may inhibit the growth of bacteria present in the surrounding area prior to them adhering on the surface, and hence was investigated [67,68]. The results indicate that Ti and all modified surfaces inhibit S. aureus growth significantly in the media when compared to the control (empty well, no surfaces) at different time points (**Figure 4.8**). However, there was no significant difference in bacteria growth inhibition on all the surfaces. The presence of

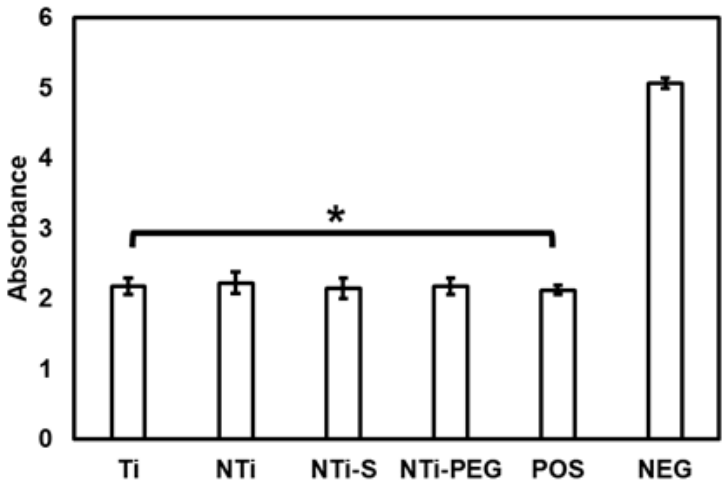

Figure 4.7: Cell cytotoxicity of PRP exposed different surfaces measured using the LDH assay. *p < .05 indicates statistical significance. The error bar represents the standard deviation. Cell cytotoxicity tests was done on at least six different substrates of each surface (n_{min} = 6)

TiO_2 on surfaces has shown to affect *S. aureus* membrane permeability and inhibit the synthesis of nucleic acid causing reduced expression of soluble protein; thereby inhibiting bacteria growth in the media [69,70]. In contrast, Ti and all modified surfaces did not show significant inhibition of *E. coli* growth in the media when compared to the control (empty well, no surfaces) for the entire duration of study. After 24 hours of incubation, no significant difference was seen in *E. coli* bacterial inhibition between different surfaces. However, when comparing the S. aureus with *E. coli*, all surfaces had significantly lower *E. coli* bacterial growth during the entire duration of the study. This may be due to the titanium ion preventing *E. coli* growth [71].

Adhesion and colonization of *S. aureus* and *E. coli* on different surfaces was evaluated after 6, 12 and 24 hrs of incubation in growth media using fluorescence microscopy. After the planktonic bacteria cells come in contact with an implant surface, depending on surface properties, they may adhere and proliferate eventually forming biofilm [72]. Once adhered, the bacteria cells will synthesize extracellular matrix on implant surface resulting into irreversible attachment on the surface. After adhering, the bacteria cells will proliferate and colonize on surface, and together with

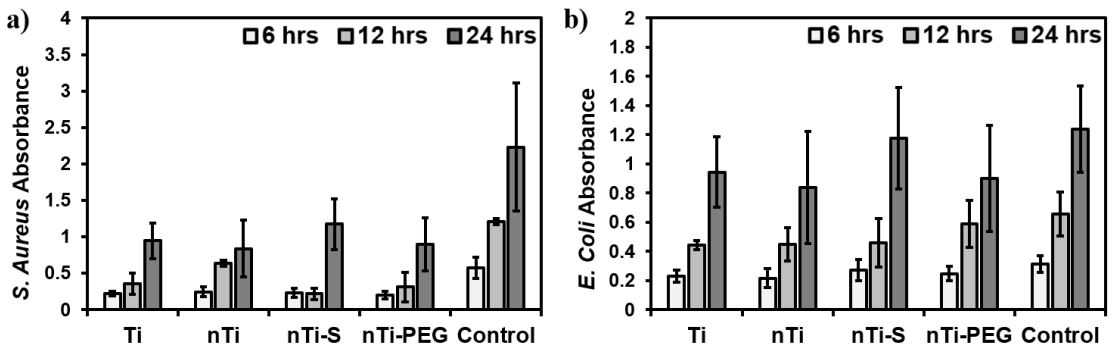

Figure 4.8: Inhibition of Staphylococcus aureus and Escherichia coli growth in the media by different surfaces. *p < .05 indicates statistical significance, p > .05 indicates no statistical significance. The error bar represents the standard deviation. Bacterial inhibition studies was done on at least nine different substrates of each surface (n_{min} = 9)

their extracellular matrix will form biofilm that may be resistant to different antibiotics. Further, bacteria cells in the periphery of the biofilm will detach, migrate and spread the infection [73,74]. Hence, it is important to evaluate whether bacteria adhesion and subsequent biofilm formation can be prevented on different surfaces. *S. aureus* and *E. coli* adhesion was evaluated at different time points to understand their growth kinetics on the surface. The adhered bacteria on different surfaces were stained using a live (green)/dead (red) stain kit and imaged using a fluorescence microscope.

After 6 hrs of *S. aureus* incubation (**Figure 4.9a**) with the different surface, the results indicate that there was significant reduction in live planktonic bacteria adhesion on nTi-S and nTi-PEG surface compared to Ti and nTi surface. After 12 hrs of incubation, live planktonic bacteria had formed colonies on the surface of Ti, nTi and nTi-PEG surfaces. In contrast, there was significant reduction in live bacteria adhesion with no colonization present on nTi-S surface. There was also a significantly higher number of dead bacteria on nTi and nTi-PEG surfaces. This may be due to the hydrophilic nature and higher energy on the surface that attracts the bacteria on to the surface features and induces strain to the cell membrane eventually rupturing it and killing the bacteria [75,76] .After 24 hrs of incubation, live colonized bacteria had formed on the Ti surface. Even though, the nTi surface had higher live bacteria adhesion compared to nTi-S and nTi – PEG, there

were no colonies present on the surface. This may be due to the nano-micro scale topography of nTi surface that resulted in uneven spreading of bacteria, thus preventing colonization. However, the nTi-S surface had significantly lower bacteria adhesion (>90%) compared to all the other surfaces (**Figure 4.9b/c**). This may be due to the combination of superhydrophobic nature of the surface that prevents any interaction with the growth media, as well as the negative charge on the surface that repels bacteria cells. nTi-PEG surfaces had significantly lower live bacteria adhesion when compared to Ti and nTi surface, however, significantly higher live bacterial adhesion when compared to nTi-S surface. This may be due to the superhydrophilic nature of the Ti-PEG surface, and just the negative charge is not sufficient to prevent bacterial adhesion. Simultaneously, there is significantly higher dead bacteria on nTi and nTi-PEG surface for the similar reason as explained previously. Thus, the results indicate that the nTi-S had significantly lower live bacteria adhesion when compared to other surfaces for the entire duration of the study proving the coating is stable.

After 6 hrs of *E. coli* incubation, the results (**Figure 4.10a**) indicated significantly lower live bacteria adhesion on nTi-S and nTi-PEG surfaces compared to large number of live planktonic bacteria found on Ti and nTi surfaces. After 12 hrs of incubation, higher live planktonic bacteria cells were adherent on Ti, nTi and nTi-PEG compared to nTi-S. Smaller colonies of live bacteria cells were seen on Ti surface. However, nTi had significantly higher dead bacteria due to the similar reason as explained previously. After 24 hrs of incubation, live colonized bacteria were found on the Ti surface. There is a significant reduction in live bacteria adhesion on nTi, nTi-S and nTi-PEG surfaces compared to Ti. There were significantly higher dead bacteria on nTi (**Figure 4.10b/c**) compared to other surfaces due to the similar reason as explained previously. Thus, the results indicate that nTi-S had significantly lower bacteria (<90%) adhesion when compared to other surfaces for the entire duration of the study proving the coating is stable and superhydrophobic preventing any interaction with the media and the negative charge is repelling bacteria adhesion

Morphology and biofilm formation of *S. aureus* (blue) and *E. coli* (green) on different surfaces was evaluated after 6, 12 and 24 hrs of incubation in growth media. The adhered bacteria were

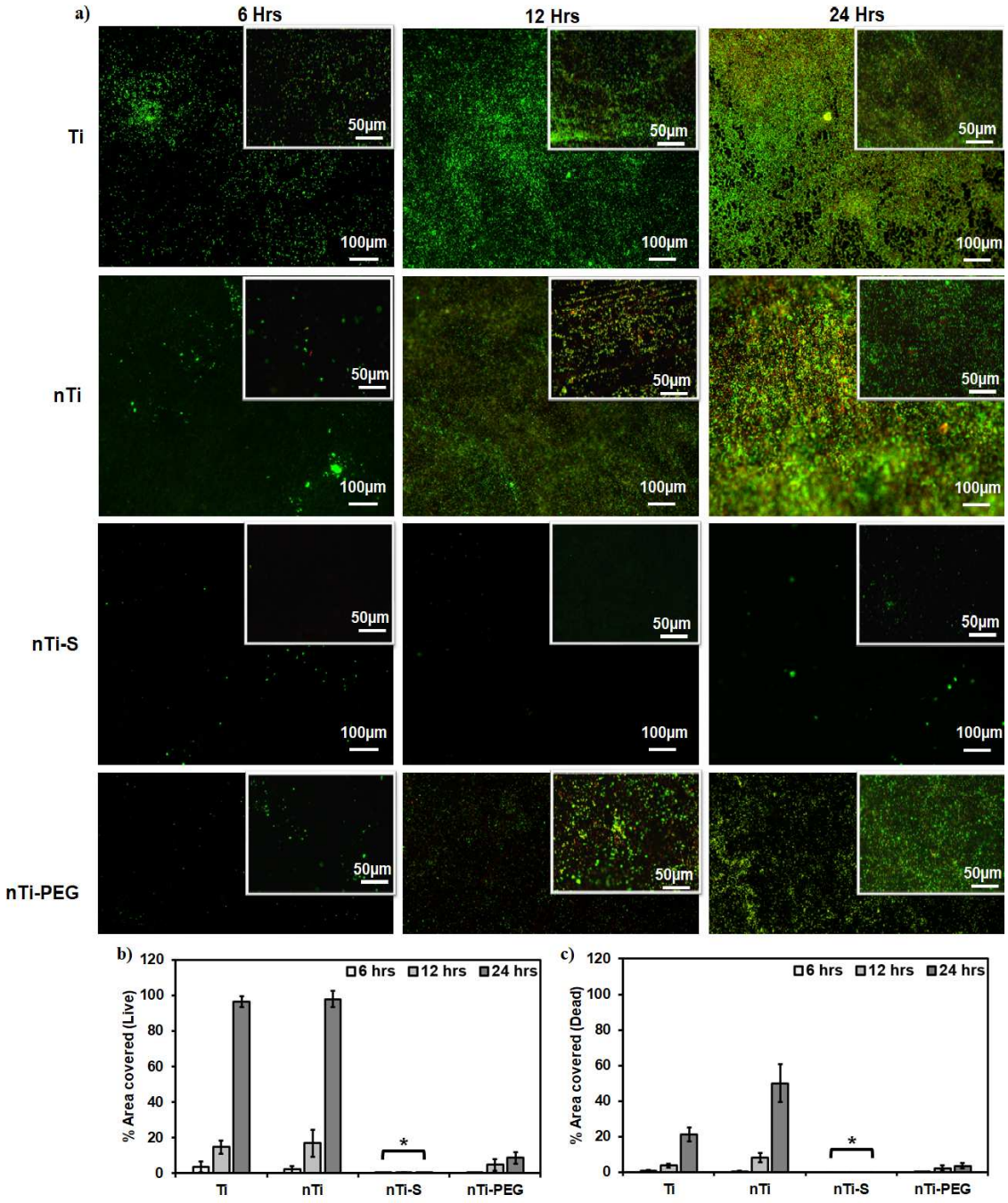

Figure 4.9: (A) Fluorescence images of adhered Staphylococcus aureus live(green) and dead(red) bacteria on different surfaces. Insert images depict higher magnification. (B) Percentage of the areas covered by the live bacteria cells adhered on different surfaces. (C) Percentage of the areas covered by the dead bacteria cells adhered on different surfaces. *p < .05 indicates statistical significance. The error bar represents the standard deviation. Bacterial adhesion and proliferation studies were done on at least nine different substrates of each surface ($n_{min} = 9$)

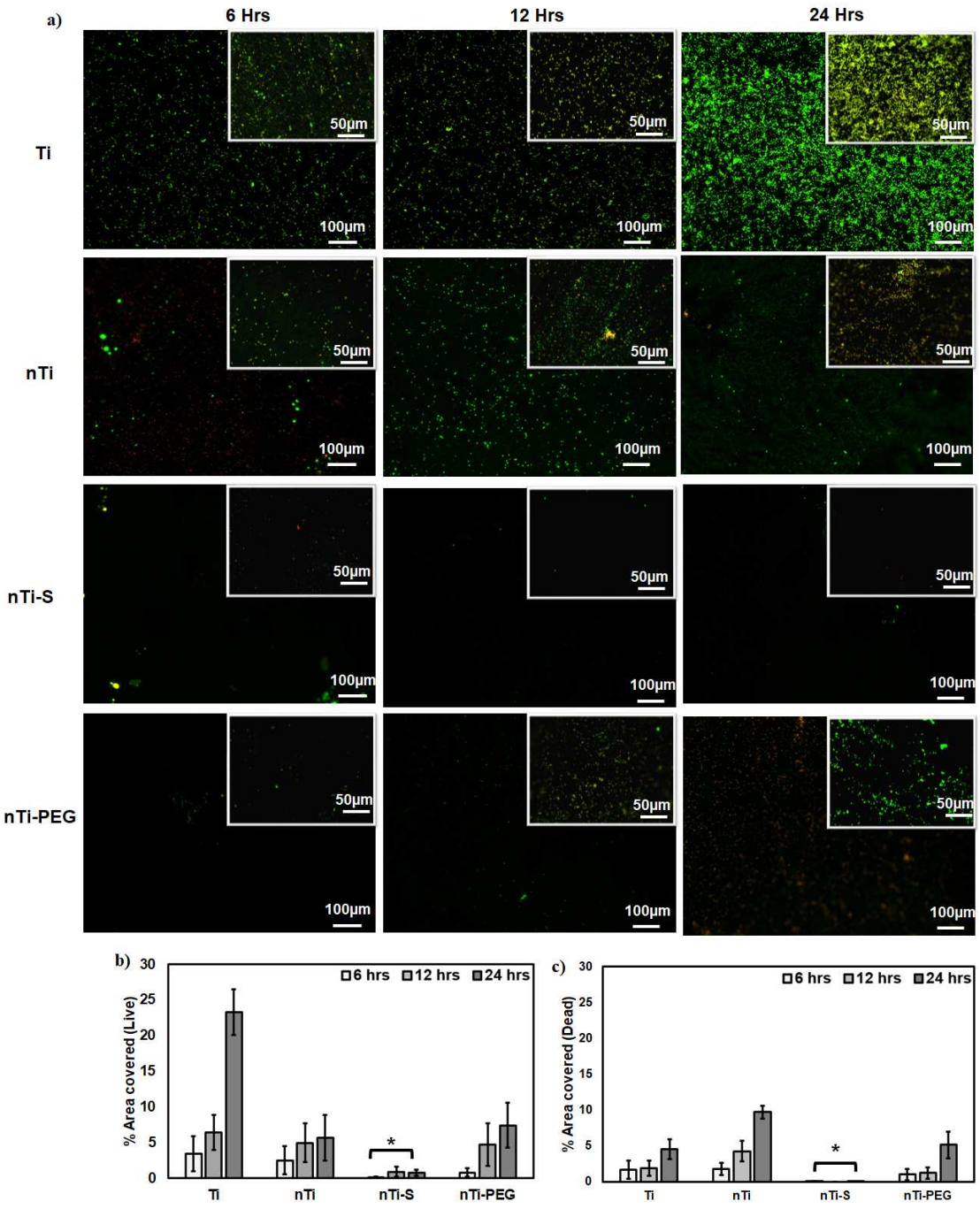

Figure 4.10: (A) Fluorescence images of adhered Escherichia coli live(green) and dead(red) bacteria on different surfaces. Insert images depict higher magnification. (B) Percentage of the areas covered by the live bacteria cells adhered on different surfaces. (C) Percentage of the areas covered by the dead bacteria cells adhered on different surfaces. *p < .05 indicates statistical significance. The error bar represents the standard deviation. Bacterial adhesion and proliferation studies were done on at least 9 different substrates of each surface (n_{min} = 9)

fixed and imaged using a SEM. The visualization of bacteria morphology and biofilm formation on different surfaces was investigated to understand the interaction of bacteria cells with surface topography. After 6 hrs of S. aureus incubation, the results (**Figure 4.11a**) indicate that the Ti surface had highest planktonic bacteria adhesion from the media as seen previously in fluorescence images. The nTi surface with micro-nano topography prevented bacteria adhesion because of reduced surface area for protein adsorption and bacteria adhesion. The nTi-S superhydrophobic surface prevented bacteria adhesion because of the combination effect as explained previously. The nTi-PEG superhydrophilic surface had lower bacteria adhesion showing that PEG chemistry prevents adhesion compared to the nTi surface. After 12 hrs of incubation, results indicate that Ti surface had higher bacteria adhesion and biofilm formation compared to other surfaces, nTi and nTi-PEG surface topography prevent complete biofilm formation and localized bacteria colonies between the micron scale structures. nTi-S surface had a significantly lower bacteria adhesion, and this is in accordance with the fluorescence results. After 24 hrs of incubation, the Ti surface was completely covered with bacteria cells with biofilm formation. The nTi and nTi-PEG surface had bacteria cells initially adhered in the valleys of the surface topography and divided further. However, the surface prevented complete biofilm formation when compared to Ti. The nTi-S surface had significantly lower bacteria adhered on the surface as seen in the fluorescence images.

After 6 hrs of *E. coli* incubation, the results indicate that the Ti surface had highest planktonic bacteria adhesion from the media as seen previously in fluorescence images. nTi-S surface had no bacteria adhesion. However, nTi and nTi-PEG surfaces had bacteria adhesion, with disintegrated cell membrane. This may be due to the surface topography, or the titanium ions present which is antibacterial by killing as mentioned previously. After 12 hrs of incubation (**Figure 4.11b**), colonized bacteria were found adherent to Ti surface. nTi surface had lower bacteria adhered on the surface compared to Ti. However, there was significant reduction in bacteria adhesion on nTi-S and nTi-PEG surface and adhered bacteria were disintegrated. After 24 hrs of incubation, the colonized bacteria had covered the surface with biofilm formation on the Ti surface. However, there is a significant reduction in bacteria adhesion on nTi, nTi-S and nTi-PEG surface compared

to Ti surface. nTi-S surface had significantly lower bacteria adhesion compared to all surfaces.

4.4 Conclusion

In this work, a simple thermochemical treatment was used to fabricate micro-nano surface topography on titanium surface and the surface was further modified with silane and PEG to make it superhydrophobic and superhydrophilic, respectively. The XPS results confirmed the oxidation after thermochemical treatment and the high-resolution results confirmed the presence of silane and PEG with the carbon-fluorine and etherpeaks, respectively. The electrochemical analysis using potentio-dynamic polarization study indicated lowest corrosion rate for nTi-S compared to other surface due to the combined effect of the surface topography, superhydrophobicity and formation of stable passive layer on the surface. In addition, electrochemical impedance spectroscopy results indicated that nTi-S surface has less defective and thick passive film formation on the surface. Furthermore, Mott-Schottky analysis indicated that nTi-S surface had relatively higher negative charge on the nTi-S surface compared to other surfaces. Cytotoxicity results shows that modified surfaces does not induce any toxicity to blood cells. Bacteria inhibition results shows that surfaces inhibit *S. aureus* growth compared to control. The bacteria adhesion results show that all modified surfaces prevented bacteria colonization formation compared to Ti. However, nTi-S surface significantly reduced *S. aureus* and *E. coli* bacteria adhesion ($< 90\%$) when compared to other surfaces. The SEM results showed that *S. aureus* bacteria formed biofilm within 24 hrs on Ti compared to other modified surfaces. nTi and nTi-PEG surfaces adhered higher bacteria due to its hydrophilic nature, but the surface topography localized colonization and thus prevented biofilm formation. However, the nTi-S did not adhere any bacteria after 24 hrs of incubation due to its superhydrophobicity and negative surface charge. Thus, these results conclude that superhydrophobic nTi-S surface has the potential of being antibacterial for implantable medical devices.

4.5 References

[1] H. Park, J.S. Temenoff, A.G. Mikos, Biodegradable Orthopedic Implants, in: Engineering of Functional Skeletal Tissues, Springer London, 2007: pp. 55–68. //https://doi.org/10.1007/978-1-84628-366-6_4.

[2] V.K. Manivasagam, K.C. Popat, In Vitro Investigation of Hemocompatibility of Hydrothermally Treated Titanium and Titanium Alloy Surfaces, ACS Omega. (2020). https://doi.org/10.1021/acsomega.0c00281.

[3] M. Quirynen, M. de Soete, D. van Steenberghe, Infectious risks for oral implants: A review of the literature, Clinical Oral Implants Research. 13 (2002) 1–19. https://doi.org/10.1034/j.1600-0501.2002.130101.x.

[4] H. Chouirfa, H. Bouloussa, V. Migonney, C. Falentin-Daudré, Review of titanium surface modification techniques and coatings for antibacterial applications, Acta Biomaterialia. 83 (2019) 37–54. https://doi.org/10.1016/j.actbio.2018.10.036.

[5] M. Haque, M. Sartelli, J. McKimm, M.A. Bakar, Health care-associated infections – An overview, Infection and Drug Resistance. 11 (2018) 2321–2333. https://doi.org/10.2147/IDR.S177247.

[6] M. Ribeiro, F.J. Monteiro, M.P. Ferraz, Infection of orthopedic implants with emphasis on bacterial adhesion process and techniques used in studying bacterial-material interactions., Biomatter. 2 (2012) 176–194. https://doi.org/10.4161/biom.22905.

[7] M. Otto, Staphylococcal biofilms, Current Topics in Microbiology and Immunology. 322 (2008) 207–228. https://doi.org/10.1007/978-3-540-75418-$3_1$0.

[8] A. Bhattacharjee, R. Clark, C. Gentry-Weeks, Y.V. Li, A novel receptor-free polydiacetylene nanofiber biosensor for detecting E. coli via colorimetric changes, Materials Advances. 1 (2020) 3387–3397. https://doi.org/10.1039/D0MA00619J.

[9] Z. Khatoon, C.D. McTiernan, E.J. Suuronen, T.F. Mah, E.I. Alarcon, Bacterial biofilm formation on implantable devices and approaches to its treatment and prevention, Heliyon. 4 (2018) 1067.

https://doi.org/10.1016/j.heliyon.2018.e01067.

[10] T.W. Mak, M.E. Saunders, Immunity to Pathogens, in: The Immune Response, Elsevier, 2006: pp. 641–694. https://doi.org/10.1016/b978-012088451-3.50024-7.

[11] R.M. Donlan, Biofilms: Microbial life on surfaces, Emerging Infectious Diseases. 8 (2002) 881–890. https://doi.org/10.3201/eid0809.020063.

[12] S. Singh, S.K. Singh, I. Chowdhury, R. Singh, Understanding the Mechanism of Bacterial Biofilms Resistance to Antimicrobial Agents, The Open Microbiology Journal. 11 (2017) 53–62. https://doi.org/10.2174/1874285801711010053.

[13] Z. Versey, W.S. da Cruz Nizer, E. Russell, S. Zigic, K.G. DeZeeuw, J.E. Marek, J. Overhage, E. Cassol, Biofilm-Innate Immune Interface: Contribution to Chronic Wound Formation, Frontiers in Immunology. 12 (2021). https://doi.org/10.3389/fimmu.2021.648554.

[14] S.M.J. Mortazavi, J. Schwartzenberger, M.S. Austin, J.J. Purtill, J. Parvizi, Revision total knee arthroplasty infection: Incidence and predictors, in: Clinical Orthopaedics and Related Research, Springer New York, 2010: pp. 2052–2059. https://doi.org/10.1007/s11999-010-1308-6.

[15] S.B. Hoffman, Mechanisms of Antibiotic Resistance, Compendium on Continuing Education for the Practicing Veterinarian. 23 (2001) 464–472. https://doi.org/10.1128/microbiolspec.vmbf-0016-2015.

[16] S. Lakhundi, K. Zhang, Methicillin-Resistant Staphylococcus aureus: Molecular Characterization, Evolution, and Epidemiology, Clinical Microbiology Reviews. 31 (2018). https://doi.org/10.1128/CMR.00020-18.

[17] K.A. Dubin, D. Mathur, P.T. McKenney, B.P. Taylor, E.R. Littmann, J.U. Peled, M.R.M. van den Brink, Y. Taur, E.G. Pamer, J.B. Xavier, Diversification and Evolution of Vancomycin-Resistant Enterococcus faecium during Intestinal Domination, Infection and Immunity. 87 (2019). https://doi.org/10.1128/IAI.00102-19.

[18] G. Mcdonnell, A.D. Russell, Antiseptics and disinfectants: Activity, action, and resistance, Clinical Microbiology Reviews. 12 (1999) 147–179. https://doi.org/10.1128/cmr.12.1.147.

[19] M. Yang, Y. Ding, X. Ge, Y. Leng, Control of bacterial adhesion and growth on honeycomb-like patterned surfaces, Colloids and Surfaces B: Biointerfaces. 135 (2015) 549–555. https://doi.org/10.1016/J.COLSURFB.2015.08.010.

[20] X. Ge, C. Ren, Y. Ding, G. Chen, X. Lu, K. Wang, F. Ren, M. Yang, Z. Wang, J. Li, X. An, B. Qian, Y. Leng, Micro/nano-structured TiO2 surface with dual-functional antibacterial effects for biomedical applications, Bioactive Materials. 4 (2019) 346. https://doi.org/10.1016/J.BIOACTMAT.2019.10.006.

[21] S. Zheng, M. Bawazir, A. Dhall, H.E. Kim, L. He, J. Heo, G. Hwang, Implication of Surface Properties, Bacterial Motility, and Hydrodynamic Conditions on Bacterial Surface Sensing and Their Initial Adhesion, Frontiers in Bioengineering and Biotechnology. 9 (2021) 82. https://doi.org/10.3389/fbioe.2021.643722.

[22] L. Damiati, M.G. Eales, A.H. Nobbs, B. Su, P.M. Tsimbouri, M. Salmeron-Sanchez, M.J. Dalby, Impact of surface topography and coating on osteogenesis and bacterial attachment on titanium implants, Journal of Tissue Engineering. 9 (2018). https://doi.org/10.1177/20417314190694.

[23] S. yi Shao, J. xi Chen, H. yan Tang, P. pan Ming, J. Yang, W. qing Zhu, S. mei Zhang, J. Qiu, A titanium surface modified with zinc-containing nanowires: Enhancing biocompatibility and antibacterial property in vitro, Applied Surface Science. 515 (2020) 146107. https://doi.org/10.1016/j.apsusc.2020.146107.

[24] A. Rodríguez-Contreras, D. Torres, B. Rafik, M. Ortiz-Hernandez, M.P. Ginebra, J.A. Calero, J.M. Manero, E. Ruperez, Bioactivity and antibacterial properties of calcium- and silver-doped coatings on 3D printed titanium scaffolds, Surface and Coatings Technology. 421 (2021) 127476. https://doi.org/10.1016/J.SURFCOAT.2021.127476.

[25] Y. Bao, W. Wang, W. Cui, G. Qin, Corrosion resistance and antibacterial activity of Ti-N-O coatings deposited on dental titanium alloy, Surface and Coatings Technology. 419 (2021) 127296. https://doi.org/10.1016/J.SURFCOAT.2021.127296.

[26] K. Hori, S. Matsumoto, Bacterial adhesion: From mechanism to control, Biochemical Engineering Journal. 48 (2010) 424–434. https://doi.org/10.1016/j.bej.2009.11.014.

[27] H.A. Foster, I.B. Ditta, S. Varghese, A. Steele, Photocatalytic disinfection using titanium dioxide: Spectrum and mechanism of antimicrobial activity, Applied Microbiology and Biotechnology. 90 (2011) 1847–1868. https://doi.org/10.1007/s00253-011-3213-7.

[28] V.K. Yemmireddy, Y.C. Hung, Using Photocatalyst Metal Oxides as Antimicrobial Surface Coatings to Ensure Food Safety—Opportunities and Challenges, Comprehensive Reviews in Food Science and Food Safety. 16 (2017) 617–631. https://doi.org/10.1111/1541-4337.12267.

[29] S.W.M.A.I. Senevirathne, J. Hasan, A. Mathew, M. Woodruff, P.K.D.V. Yarlagadda, Bactericidal efficiency of micro- And nanostructured surfaces: A critical perspective, RSC Advances. 11 (2021) 1883–1900. https://doi.org/10.1039/d0ra08878a.

[30] A. Velic, J. Hasan, Z. Li, P.K.D.V. Yarlagadda, Mechanics of Bacterial Interaction and Death on Nanopatterned Surfaces, Biophysical Journal. 120 (2021) 217–231. https://doi.org/10.1016/j.bpj.2020.12.003.

[31] J. Vishnu, V. K Manivasagam, V. Gopal, C. Bartomeu Garcia, P. Hameed, G. Manivasagam, T.J. Webster, Hydrothermal treatment of etched titanium: A potential surface nano-modification technique for enhanced biocompatibility, Nanomedicine: Nanotechnology, Biology, and Medicine. 20 (2019). https://doi.org/10.1016/j.nano.2019.102016.

[32] K. Bartlet, S. Movafaghi, A. Kota, K.C. Popat, Superhemophobic titania nanotube array surfaces for blood contacting medical devices, (2017). https://doi.org/10.1039/c7ra03373g.

[33] S.C. Vanithakumari, G. Jena, S. Sofia, C. Thinaharan, R.P. George, J. Philip, Fabrication of superhydrophobic titanium surfaces with superior antibacterial properties using graphene oxide and silanized silica nanoparticles, Surface and Coatings Technology. 400 (2020) 126074. https://doi.org/10.1016/J.SURFCOAT.2020.126074.

[34] S. Li, Y. Liu, Z. Tian, X. Liu, Z. Han, L. Ren, Biomimetic superhydrophobic and antibacterial stainless-steel mesh via double-potentiostatic electrodeposition and modification, Surface and Coatings Technology. 403 (2020) 126355. https://doi.org/10.1016/J.SURFCOAT.2020.126355.

[35] J. Vishnu, V. K Manivasagam, V. Gopal, C. Bartomeu Garcia, P. Hameed, G. Manivasagam, T.J. Webster, Hydrothermal treatment of etched titanium: A potential surface nano-modification

technique for enhanced biocompatibility, Nanomedicine: Nanotechnology, Biology, and Medicine. 20 (2019). https://doi.org/10.1016/j.nano.2019.102016.

[36] V.K. Manivasagam, K.C. Popat, Hydrothermally Treated Titanium Surfaces for Enhanced Osteogenic Differentiation of Adipose Derived Stem Cells, Materials Science and Engineering: C. (2021) 112315. https://doi.org/10.1016/J.MSEC.2021.112315.

[37] P. Hameed, V.K. Manivasagam, M. Sankar, K.C. Popat, G. Manivasagam, Nanofibers and nanosurfaces, in: Springer Series in Biomaterials Science and Engineering, Springer Science and Business Media Deutschland GmbH, 2021: pp. 107–130. https://doi.org/10.1007/978-981-33-6252-9_4.

[38] M. Geetha, A.K. Singh, R. Asokamani, A.K. Gogia, Ti based biomaterials, the ultimate choice for orthopaedic implants - A review, Progress in Materials Science. 54 (2009) 397–425. https://doi.org/10.1016/j.pmatsci.2008.06.004.

[39] V. K. Manivasagam, R. M. Sabino, Prem Kantam, K. C. Popat, Surface modification strategies to improve titanium hemocompatibility: a comprehensive review, Materials Advances. (2021). https://doi.org/10.1039/D1MA00367D.

[40] J.R. Macdonald, Impedance Spectroscopy, 1992.

[41] A. Lasia, Electrochemical Impedance Spectroscopy and its Applications, in: Electrochemical Impedance Spectroscopy and Its Applications, Springer New York, 2014: pp. 1–5. https://doi.org/10.1007/978-1-4614-8933-7_1.

[42] A. Fattah-alhosseini, M.A. Golozar, A. Saatchi, K. Raeissi, Effect of solution concentration on semiconducting properties of passive films formed on austenitic stainless steels, Corrosion Science. 52 (2010) 205–209. https://doi.org/10.1016/j.corsci.2009.09.003.

[43] A. Fattah-alhosseini, A.R. Ansari, Y. Mazaheri, M.K. Keshavarz, Effect of immersion time on the passive and electrochemical response of annealed and nano-grained commercial pure titanium in Ringer's physiological solution at 37 °C, Materials Science and Engineering C. 71 (2017) 771–779. https://doi.org/10.1016/j.msec.2016.10.057.

[44] R.M. Sabino, K. Kauk, S. Movafaghi, A. Kota, K.C. Popat, Interaction of blood plasma proteins

with superhemophobic titania nanotube surfaces, Nanomedicine: Nanotechnology, Biology and Medicine. 21 (2019) 102046. https://doi.org/10.1016/J.NANO.2019.102046.

[45] B. Li, T.J. Webster, Bacteria antibiotic resistance: New challenges and opportunities for implant-associated orthopedic infections, Journal of Orthopaedic Research. 36 (2018) 22–32. https://doi.org/10.1002/jor.23656.

[46] Z. Khatoon, C.D. McTiernan, E.J. Suuronen, T.F. Mah, E.I. Alarcon, Bacterial biofilm formation on implantable devices and approaches to its treatment and prevention, Heliyon. 4 (2018). https://doi.org/10.1016/j.heliyon.2018.e01067.

[47] A. Trampuz, A.F. Widmer, Infections associated with orthopedic implants, Current Opinion in Infectious Diseases. 19 (2006) 349–356. https://doi.org/10.1097/01.qco.0000235161.85925.e8.

[48] H. Amani, H. Arzaghi, M. Bayandori, A.S. Dezfuli, H. Pazoki-Toroudi, A. Shafiee, L. Moradi, Controlling Cell Behavior through the Design of Biomaterial Surfaces: A Focus on Surface Modification Techniques, Advanced Materials Interfaces. 6 (2019) 1900572. https://doi.org/10.1002/admi.201900572.

[49] P. Chauhan, V. Koul, N. Bhatnagar, Effect of acid etching temperature on surface physiochemical properties and cytocompatibility of Ti6Al4V ELI alloy, Materials Research Express. 6 (2019) 105412. https://doi.org/10.1088/2053-1591/ab3ac5.

[50] E. Fadeeva, S. Schlie-Wolter, B.N. Chichkov, G. Paasche, T. Lenarz, Structuring of biomaterial surfaces with ultrashort pulsed laser radiation, in: Laser Surface Modification of Biomaterials: Techniques and Applications, Elsevier Inc., 2016: pp. 145–172. https://doi.org/10.1016/B978-0-08-100883-6.00005-8.

[51] K.Y. Law, Definitions for hydrophilicity, hydrophobicity, and superhydrophobicity: Getting the basics right, Journal of Physical Chemistry Letters. 5 (2014) 686–688. https://doi.org/10.1021/jz402762h.

[52] M.P. Sikka, V.K. Midha, The role of biopolymers and biodegradable polymeric dressings in managing chronic wounds, in: Advanced Textiles for Wound Care, Elsevier, 2019: pp. 463–488. https://doi.org/10.1016/b978-0-08-102192-7.00016-3.

[53] A. Rudawska, E. Jacniacka, Analysis for determining surface free energy uncertainty by the Owen-Wendt method, International Journal of Adhesion and Adhesives. 29 (2009) 451–457. https://doi.org/10.1016/j.ijadhadh.2008.09.008.

[54] R. Zahran, J.I. Rosales Leal, M.A. Rodríguez Valverde, M.A. Cabrerizo Vílchez, Effect of hydrofluoric acid etching time on titanium topography, chemistry, wettability, and cell adhesion, PLoS ONE. 11 (2016). https://doi.org/10.1371/journal.pone.0165296.

[55] Z. Montgomerie, K.C. Popat, Improved hemocompatibility and reduced bacterial adhesion on superhydrophobic titania nanoflower surfaces, Materials Science and Engineering C. 119 (2021) 111503. https://doi.org/10.1016/j.msec.2020.111503.

[56] A. v. Shchukarev, D. v. Korolkov, XPS study of group IA carbonates, Central European Journal of Chemistry. 2 (2004) 347–362. https://doi.org/10.2478/BF02475578.

[57] G. Manivasagam, D. Dhinasekaran, A. Rajamanickam, Biomedical Implants: Corrosion and its Prevention-A Review, 2010.

[58] N. Eliaz, Corrosion of metallic biomaterials: A review, Materials. 12 (2019). https://doi.org/10.3390/ma12030407.

[59] Fundamentals of Electrochemical Corrosion - ASM International, (n.d.). https://www.asminternational.org /search/-/journal content/56/10192/06594G/PUBLICATION (accessed June 11, 2021).

[60] D.F. Williams, On the mechanisms of biocompatibility, Biomaterials. 29 (2008) 2941–2953. https://doi.org/10.1016/j.biomaterials.2008.04.023.

[61] G. Perumal, H.S. Grewal, H.S. Arora, Enhanced durability, bio-activity and corrosion resistance of stainless steel through severe surface deformation, Colloids and Surfaces B: Biointerfaces. 194 (2020). https://doi.org/10.1016/j.colsurfb.2020.111197.

[62] G. Perumal, A. Chakrabarti, H.S. Grewal, S. Pati, S. Singh, H.S. Arora, Enhanced antibacterial properties and the cellular response of stainless steel through friction stir processing, Biofouling. 35 (2019) 187–203. https://doi.org/10.1080/08927014.2019.1584794.

[63] S. Bahl, P. Shreyas, M.A. Trishul, S. Suwas, K. Chatterjee, Enhancing the mechanical and

biological performance of a metallic biomaterial for orthopedic applications through changes in the surface oxide layer by nanocrystalline surface modification, Nanoscale. 7 (2015) 7704–7716. https://doi.org/10.1039/c5nr00574d.

[64] R. Narayanan, S.K. Seshadri, Point defect model and corrosion of anodic oxide coatings on Ti-6Al-4V, Corrosion Science. 50 (2008) 1521–1529. https://doi.org/10.1016/j.corsci.2008.02.023.

[65] A. Fattah-alhosseini, O. Imantalab, G. Ansari, The role of grain refinement and film formation potential on the electrochemical behavior of commercial pure titanium in Hank's physiological solution, Materials Science and Engineering C. 71 (2017) 827–834. https://doi.org/10.1016/j.msec.2016.10.072.

[66] A.T. Poortinga, R. Bos, W. Norde, H.J. Busscher, Electric double layer interactions in bacterial adhesion to surfaces, Surface Science Reports. 47 (2002) 1–32. https://doi.org/10.1016/S0167-5729(02)00032-8.

[67] H.H. Tuson, D.B. Weibel, Bacteria-surface interactions, Soft Matter. 9 (2013) 4368–4380. https://doi.org/10.1039/c3sm27705d.

[68] V.M. Villapún, L.G. Dover, A. Cross, S. González, Antibacterial metallic touch surfaces, Materials. 9 (2016). https://doi.org/10.3390/ma9090736.

[69] A. Jesline, N.P. John, P.M. Narayanan, C. Vani, S. Murugan, Antimicrobial activity of zinc and titanium dioxide nanoparticles against biofilm-producing methicillin-resistant Staphylococcus aureus, Applied Nanoscience (Switzerland). 5 (2015) 157–162. https://doi.org/10.1007/s13204-014-0301-x.

[70] X. Jiang, B. Lv, Y. Wang, Q. Shen, X. Wang, Bactericidal mechanisms and effector targets of TiO2 and Ag-TiO2 against Staphylococcus aureus, Journal of Medical Microbiology. 66 (2017) 440–446. https://doi.org/10.1099/jmm.0.000457.

[71] M. Lorenzetti, I. Dogša, T. Stošicki, D. Stopar, M. Kalin, S. Kobe, S. Novak, The Influence of Surface Modification on Bacterial Adhesion to Titanium-Based Substrates, ACS Applied Materials and Interfaces. 7 (2015) 1644–1651. https://doi.org/10.1021/AM507148N.

[72] R.M. Sabino, K. Kauk, L.Y.C. Madruga, M.J. Kipper, A.F. Martins, K.C. Popat, Enhanced

hemocompatibility and antibacterial activity on titania nanotubes with tanfloc/heparin polyelectrolyte multilayers, Journal of Biomedical Materials Research - Part A. 108 (2020) 992–1005. https://doi.org/10.1002/jbm.a.36876.

[73] Z. Khatoon, C.D. McTiernan, E.J. Suuronen, T.F. Mah, E.I. Alarcon, Bacterial biofilm formation on implantable devices and approaches to its treatment and prevention, Heliyon. 4 (2018) 1067. https://doi.org/10.1016/j.heliyon.2018.e01067.

[74] V. Nandakumar, S. Chittaranjan, V.M. Kurian, M. Doble, Characteristics of bacterial biofilm associated with implant material in clinical practice, Polymer Journal. 45 (2013) 137–152. https://doi.org/10.1038/pj.2012.130.

[75] J. Hasan, Y. Xu, T. Yarlagadda, M. Schuetz, K. Spann, P.K.D.V. Yarlagadda, Antiviral and Antibacterial Nanostructured Surfaces with Excellent Mechanical Properties for Hospital Applications, ACS Biomaterials Science and Engineering. 6 (2020) 3608–3618. https://doi.org/10.1021/acsbiomaterials.0c00348.

[76] S.W.M.A.I. Senevirathne, J. Hasan, A. Mathew, M. Woodruff, P.K.D.V. Yarlagadda, Bactericidal efficiency of micro- And nanostructured surfaces: A critical perspective, RSC Advances. 11 (2021) 1883–1900. https://doi.org/10.1039/d0ra08878a.

5.1 Introduction

Over a million total hip and knee replacement procedures are performed every year in the United States out of which more than 37,000 are revision surgeries [1]. These procedures are performed on people suffering from degenerative and inflammatory diseases that leads to osteoarthritis, chondromalacia, and rheumatoid arthritis due to aging [2,3]. In recent years, studies have shown that younger people (< 65 years) are also suffering from advance arthritis, and the demand for improved mobility has led to greater increase in demand for total hip and knee replacement procedures [4]. Previously, stainless steel and cobalt chromium were used for hip/knee joint implants, bone plates and screws; but over time revision surgeries were required due to infection and wear of the implant [5,6]. Hence, titanium and its alloys were preferred to make these implants due to their excellent biocompatibility with the bone tissue, low modulus, and excellent corrosion resistance [7–10]. Although the bulk properties of titanium and its alloys are well suited for orthopedic implants, their bio-inertness and poor wear resistance often leads to failure of these implants [11–13]. Further, inappropriate interaction of the implant surface with the proteins and cells results in complications such as infection, inflammation, and reduced osseointegration, resulting in implant rejection and subsequent revision surgeries [14–16]. Hence, there is an unmet need to modify the surfaces of titanium based orthopedic implants so that the interaction with the bone tissue can be improved resulting in enhanced osseointegration and reduction in the need for revision surgeries. [1]

Various surface modification techniques have been explored commercially as well as at research stage to enhance osseointegration and promote longer implant life. Currently the implants available in the market are coated with inorganic calcium phosphate and hydroxyapatite using plasma spray coating technique [17]. Studies have shown that these coatings enhance bioactivity as they chem-

[1]This work was published in Elsevier Materials Science and Engineering: C and is reproduced in modified form here with permission

ically bond with bone tissues [18,19]. However, the high temperature processes result in phase transformations of calcium phosphate resulting in adverse effects on bone growth [20]. Hydroxyapatite has shown to enhance tissue regeneration for the first four weeks but longer exposure to bodily fluids leads to degradation of its intermolecular bonds [5]. Chemical coating by immobilizing peptides found in the extracellular matrix (ECM) of bone tissue on the implant surface has shown improved cell adhesion. However, these coating lose integrity over long periods of time [6]. One major drawback with coatings in general is that they delaminate over time resulting in loosening of implants that can only be fixed through revision surgery [21]. Several techniques have been explored at research level including, alloying and dealloying at the implant surface, surface modification using sand blasting, electrophoretic deposition, anodization, and hydrothermal treatments [11–14]. Studies have shown that some of these techniques that provide topographical surface modifications influences cell adhesion and proliferation [19–21]. For example, nanofibers, nanotubes, nanopores resemble the nanostructure of the bone tissue have shown enhanced interaction with osteoblasts (bone cells) [26,27]. However, till date there are very limited approaches to produce surfaces that are easy to fabricate, are robust and promote long term osseointegration.

In this study, a simple hydrothermal treatment was used to form nanostructures on the surface of titanium with the goal of enhancing long term osseointegration. The hydrothermal treatments with sodium hydroxide (NaOH) and sulfuric acid (H_2SO_4) led to two different surface topographies. Further, these fabricated surfaces with nanostructures are robust and do not have delamination issues like other coatings. The fabricated surfaces were characterized for wettability using a goniometer, morphology using a Scanning Electron Microscope (SEM), chemical composition using an X-Ray photoelectron Spectroscopy (XPS), and crystallinity using an X-ray Diffraction (XRD). Generally, bone derived mesenchymal stem cells (BMSCs) are used to evaluate surface's ability to promote cell adhesion, proliferation, and differentiation for bone regeneration. This is due to the ability BMSCs to differentiate into osteoblast [28–30]. However, extraction of BMSCs is highly invasive procedure and their yield rate is low [31]. Recently, adipose derive stem cells (ADSCs) were identified as a multi-potent stem cells that can also differentiate to osteoblasts [32,33]. ADSCs

can be obtained from the highly abundant adipose tissue, their extraction doesn't need an invasive procedure, and their yield rate is very high [34,35]. Studies have shown that ADSCs can adhere and proliferate in in-vitro conditions [13]. Hence, in this studies ADSCs were used to evaluate the potential of the modified surfaces. The modified surfaces were evaluated for cell toxicity after 1 day of culture with ADSCs. Cell adhesion, viability, proliferation and morphology on modified surfaces was investigated after 1, 4 and 7 days of culture with ADSCs. After 7 days of culture, differentiation towards osteoblastic lineage was induced. The modified surfaces were evaluated for ALP activity, calcium deposition and osteocalcin expression after 14 and 28 days of culture with ADSCs. The result indicated that the hydrophilicity is important for the cells to adhere. However, in long term, cell adhesion and their interaction with the surface nanotopography influences their morphology, differentiation, and mineralization. In summary, a simple hydrothermal treatment produces nanostructured surfaces on titanium that promotes ADSCs adhesion, proliferation and differentiation, and thus that have the potential of being used for orthopedic implants.

5.2 Materials and Methods

5.2.1 Fabrication of nanoporous titanium surfaces

Commercially available pure titanium (CpTi – Grade 2, purchased from Titanium Joe, Canada) were cut into 30 mm X 20 mm X 5 mm substrates. The substrates were polished gradually using SiC abrasive sheets (400, 600, 800, 1000, 1200). The substrates were then cleaned ultrasonically in acetone for 10 mins. This was followed by rinsing with deionized (DI) water and subsequent drying with nitrogen gas. Two different hydrothermal treatments [36] parameters were used to fabricate nanoporous titanium surfaces.

- Cleaned substrates were immersed in a 0.5 M sulfuric acid solution in an inert polytetrafluoroethylene (PTFE) container and placed inside a hot air oven at 80°C for a duration of 8 hrs. The modified substrates were rinsed with DI water and were annealed for 1 hr at 300°C.

- Cleaned substrates were immersed in a 5 M sodium hydroxide alkaline solution in an inert polytetrafluoroethylene (PTFE) container and placed inside a hot air oven at 80°C for a duration of 24 hrs. The modified substrates were rinsed with DI water and were annealed for 1 hr at 300 °C.

After hydrothermal treatments, all substrates were again cleaned ultrasonically in DI water for a duration of 10 mins and dried with nitrogen gas. The modified substrates were stored in a desiccator. The following notation has been used in the manuscript for different surfaces: Ti for unmodified titanium surfaces (control), $Ti_{H_2SO_4}$ for sulfuric acid modified surfaces, and Ti_{NaOH} for sodium hydroxide modified surfaces.

5.2.2 Surface characterization

Surface morphology

JEOL 6500 field emission scanning electron microscopy was used to characterize the surface morphology. The surfaces were coated with 10 nm gold before imaging for improved conductivity. The surfaces were imaged at magnifications of 500X, 2000X, 5000X and 30000X. The SEM was operated at an accelerating voltage of 15 kV.

Surface wettability

Rame-hart 260F4 goniometer was used to characterize surface wettability by measuring the contact angles. The surface wettability was determined by measuring the apparent contact angle with DI water (θ*) at ambient temperature using the sessile drop method. Images were captured 3 secs after 10 μL droplet of DI water was placed on the surface.

Surface chemistry

PHI-5800 spectrometer X-ray photo-electron spectroscopy was used to characterize the surface chemistry. A monochromatic Al-K X-ray source operated at 15 kV was used for the study and the

emitted photoelectrons were collected at a take-off angle of ≈ 45° relative to the sample surface. Survey spectra were collected from 0 to 1100 eV with a pass energy of 187.85 eV. Multipak software was used to measure the elemental composition and Origin software was used to subtract the baseline and plot the survey graph.

Surface crystallinity

Bruker D8 discover DaVinci Powder X-ray diffraction was used to characterize the surface crystallinity. The presence of alpha-titanium crystal phase and anatase TiO_2 phase on different surfaces was characterized by comparing with that available in the literature. XRD scans were collected at $\theta = 1.5°$, and 2θ ranges was chosen based on significant peak intensities. Detector scans were run at a step size of 0.01 with a time per step of 1 s.

5.2.3 Adipose derived stem cell culture on different nanoporous surfaces

Adipose derived stem cells (ADSCs) were isolated by Prof. Cox-York lab from Department of Food Science and Human Nutrition, Colorado State University, and generously donated for these studies. ADSCs were taken from abdominal and femoral subcutaneous adipose tissue biopsy surfaces as described previously [37]. The approved protocol for ADSCs isolation from healthy individuals by Colorado State University Institutional Review Board was followed. All procedures were performed in compliance with the National Institutes of Health's "Guiding Principles for Ethical Research". Informed consents were taken from human participants before the procedure. When ready for culturing, the ADSCs (passage 4) were thawed and expanded using standard cell culture techniques. The cells were expanded using growth media (MEM Alpha Modification, HyCloneTM) with 10% fetal bovine serum and 1% penicillin/streptomycin. Growth media was changed every other day until cells reached > 80% confluence. Confluence was achieved after 7 days of culture. Following expansion, ADSCs were detached using 0.25% Trypsin–EDTA and suspended in growth media for further culture on different surfaces.

Prior to cell culture, the surfaces were further cut into 0.5 mm X 0.5 mm substrates and were

sterilized by rinsing them with 70% ethanol, DI Water and phosphate buffered saline (PBS). The surfaces were then exposed to UV light for 15 mins for further sterilization. ADSCs were seeded on all the surfaces in a 48 well plate. Growth media (300 μL) with a concentration of 20,000 cells/mL was pipetted on each substrate. The well plates were incubated at 37°C and 5% CO_2 for the duration of study. Growth media was changed every other day, and cell adhesion and proliferation were characterized after 1, 4 and 7 days of culture.

After 7 days of culture, osteogenesis was induced by switching the growth media to osteogenic media. The osteogenic media consisted of growth media supplemented with 10 nM dexamethasone, 5.4 mM β–glycerolphosphate, and 300 μM ascorbic acid. This osteogenic media was changed every other day, and cell differentiation was characterized after 14 and 28 days of culture (i.e., 7 and 21 days after supplementing with osteogenic media).

5.2.4 Cytotoxicity on different surfaces

Cytotoxicity of different surfaces was characterized using lactate dehydrogenase (LDH) assay. After 1 day of culture, Substrate exposed growth media (100 μL) and LDH reaction solution (100 μL) were added to each well of a 96 well plate. The well plate was incubated at 37°C and 5% CO_2 for 30 mins. Absorbance of the resulting solution was measured at 490 nm wavelength using a plate reader. The protocol given by the manufacturer was followed and cell toxicity was calculated. To evaluate the highest possible amount of LDH enzyme that can be secreted from cells in a well, they were lysed using 10% Triton-X100 and the lysate was used with the assay (negative control). To evaluate the lowest possible amount of LDH enzyme that can be secreted from cells due to apoptosis, cells were grown in a well without any substrate (positive control).

5.2.5 Cell Viability on different surfaces

Cell viability on different surfaces was characterized using CellTiter-Blue® assay. After the desired culture time (after 1, 4 and 7 days), the growth media was aspirated. Growth media (270 μL) and

CellTiter-Blue dye (30 μL) were added to each well of a 96 well plate. The well plate was incubated at 37°C and 5% CO_2 for 7 hrs. Absorbance of the resulting solution was measured at 570 nm and 600 nm wavelength using a plate reader. The protocol given by the manufacturer was followed and cell viability was calculated.

5.2.6 Cell adhesion and proliferation on different surfaces

Cell adhesion and proliferation on different surfaces was characterized using the fluorescence microscopy. After the desired culture time (after 1, 4 and 7 days), the growth media was aspirated. The surfaces were gently rinsed with PBS three times to remove any unadhered cells. The surfaces were fixed using 3.7% formaldehyde for 15 mins at room temperature, followed by three rinses with PBS. The cells were permeabilized using 1% Triton-X for 3 mins, followed by four rinses with PBS. The cells were stained using 2% rhodamine-phalloidin (300 μL) for 30 mins and 3% 4,6-diamidino-2-phenylindole (DAPI) stain stock solution (100 μL) in the last 5 mins. The rhodamine-phalloidin stains the cytoskeleton and DAPI stains the nucleus of the cell. The surfaces were rinsed three times with PBS and then imaged using Zeiss Fluorescence microscope. The number of adhered cells on different surfaces were determined by counting the cells in DAPI stained 10X magnification images and ImageJ software.

Cell morphology on different surfaces was characterized using SEM. After the desired culture time (after 1, 4 and 7 days), the growth media was aspirated. The surfaces were gently rinsed with PBS three times to remove the unadhered cells. There surfaces were fixed using 3% glutaraldehyde, 0.1 M sodium cacodylate, and 0.1 M sucrose in DI water for 40 mins followed by a buffer solution for 10 mins. This was followed by incubation in 35%, 50%, 70% and 100% ethanol for 10 mins each. The surfaces were air-dried and imaged using SEM.

5.2.7 Cell differentiation on different surfaces

Cell differentiation was characterized using three different assays: micro-BCA assay, alkaline phosphatase (ALP) assay and calcium reagent assay. Cells were permeabilized using 0.2 % Triton-X for 20 mins on a shaker plate to remove all the intracellular proteins and the lysate was used for further analysis for micro-BCA and ALP assay. The surfaces after removing the lysate were used for calcium reagent assay.

Total protein content of all the cells on different surfaces was determined using micro-BCA protein assay kit. Equal proportions of cell lysate (150 μL) of and working reagent (150 μL) were added to each well of a 96 well plate. The resulting solution was incubated at 37°C and 5% CO_2 for 2 hrs. Absorbance was measured at 562 nm wavelength using a plate reader. The protocol given by the manufacturer was followed and total protein content was calculated.

ALP activity of all the cells on different surfaces was determined using QuantiChromTM Alkaline Phosphate Assay Kit. In a 96 well plate, cell lysate (50 μL) and 150 μL of working reagent were added. Absorbance of the resulting solution was measured at 405 nm wavelength after t = 0 min and t = 4 mins using a plate reader. The protocol given by the manufacturer was followed and ALP concentration was calculated. The ALP concentration was further normalized by dividing it with respective total protein content from the surface to account for variation in cell numbers on different surfaces.

Calcium deposition on all surfaces was evaluated using calcium reagent assay. The deposited calcium on the surface was extracted by immersing the surfaces in 500 μL of 6 N hydrochloric acid for 2 hrs and 20 μL of this calcium-acid solution was added to 1 mL of working reagent in each well of a 96 well plate. Absorbance of the resulting solution was measure at 570 nm wavelength using a plate reader. The protocol given by the manufacturer was followed and the calcium concentration was calculated. The calcium concentration was further normalized by dividing it with respective total protein content from the surface to account for variation in cell numbers on different surfaces.

The osteogenic differentiation of ADSCs on all surfaces was also evaluated using immunofluorescence microscopy. After 7 and 14 days of culture in osteogenic media, the surfaces were gently rinsed with PBS three times to remove the unadhered cells. The surfaces were fixed using 3.7% formaldehyde for 15 mins at room temperature, followed by three rinses with PBS. Cells were permeabilized using 1% Triton-X for 3 mins, followed by four rinses with PBS. The surfaces were moved to a new well plate and non-specific binding sites were blocked by incubating in 10% bovine serum albumin (BSA) for 30 mins. osteocalcin primary antibody of 1:100 dilution was added to the surfaces for 60 mins at room temperature and the surfaces were rinsed three times with PBS. FITC secondary antibody of 1:200 dilution was then added to the surfaces for 45 mins at room temperature and the surfaces were rinsed twice with PBS. ADSCs were further stained using The cells were stained using 2% rhodamine-phalloidin (300 μL) for 30 mins and 3% 4,6-diamidino-2-phenylindole (DAPI) stain stock solution (100 μL) for the last 5 mins. The rhodamine-phalloidin stains the cytoskeleton and DAPI stains the nucleus of the cell. The surfaces were rinsed three times with PBS. They were then imaged using Zeiss Fluorescence microscope. The area covered by osteocalcin and the number of cells present on different surfaces and was determined by counting the cells in DAPI stained 10X magnification images and ImageJ software.

Cell morphology on different surfaces was characterized using SEM. After the desired culture time (after 14 and 28 days), the osteogenic media was aspirated. The protocol discussed in Section 2.6 for SEM was followed. Mineral deposition from the cells (calcium and phosphorus) on different surfaces was characterized using Energy Dispersive Spectroscopy (EDS) at 20 kV accelerating voltage.

5.2.8 Statistical Analysis

Surface characterization was repeated for at least three different surfaces from each group. Fluorescence images, SEM images and contact angle measurements were taken at three different locations on each sample (n_{min} = 9). The LDH, cell proliferation, adhesion and differentiation assays were repeated at least two times with at least three different samples of each surface (n_{min} = 6). The

quantitative results were analyzed using a two-way analysis of variance (ANOVA) test using the R software. The results were stared if statistically significant with a (p-value < 0.05).

5.3 Results and Discussion

Patients suffering from diseased or fractured bones are usually treated by replacing the damaged bone with an implant [38,39]. These implants are mostly made up of metals and alloys as their mechanical properties are appropriate for load bearing tissue such as bone [40,41]. However, there are other implant characteristics such as bio-inertness, wear and surface properties that dictates the long-term fate of the implants [42,43]. Titanium has proven to have excellent biocompatibility and corrosion resistance for bone applications [44,45]. However, its surface without any modification doesn't promote cell adhesion, proliferation, and differentiation [46,47]. This is mainly due to the lack of surface topography that resembles the porous surface architecture of the extracellular matrix of bone [48]. Hence, there is a need to develop implants with improved surface properties and topography to enhance their integration with the bone tissue. Several studies have shown that implants with surface topography at nano-level can improve cell functionality [49,50]. Different techniques such as laser patterning, anodization, sand blasting and hydrothermal treatments have been explored to develop nanostructured surfaces [50–56]. In this study, hydrothermal treatment of titanium using two different solutions was performed to understand the influence of wettability and topography on the osteogenic pathway of ADSCs by measuring the cell adhesion, proliferation and differentiation.

The morphology of different surfaces was imaged using a SEM. Ti did not show any unique topography but rather showed scratches due to the material processing and polishing (**Figure 5.1**). After the H_2SO_4 treatment, the surfaces were etched and indicated presence of micro- to nano-hierarchical structures. The presence of grain boundaries was also revealed well as they normally get etched faster than the grain itself due to the disordered atomic arrangement and mismatch of atomic orientation between two adjacent grains [57]. Further, the information of

uniform nano pit like structures was also revealed. Overall, $Ti_{H_2SO_4}$ has more etching of the grain boundaries compared to the grain itself, resulting in 3D-like microscale pyramidical structures that have nanoscale topography. The following reactions takes place when the Ti surfaces are exposed to 0.5M sulfuric acid:

$$TiO_2 + 2H_2SO_4 \longrightarrow Ti(SO_4)_2 + 2H_2O \tag{5.1}$$

$$Ti + 2H_2SO_4 \longrightarrow Ti(SO_4)_2 + 2H_2 \tag{5.2}$$

$$Ti + H_2 \longrightarrow TiH_2 \tag{5.3}$$

The acid reacts with Ti and TiO_2 on the surface and forms titanium sulfate and hydrogen gas (eq. 5.1, 5.2). This hydrogen gas again reacts with the titanium and forms titanium hydride (eq. 5.3).

In contrast, NaOH treatment led to etching of the surfaces with nanostructure. The images (**Figure 5.1**) show the presence of grain boundaries as they normally get etched faster than the grain, however, the surface is much more uniform compared to the $Ti_{H_2SO_4}$. Overall Ti_{NaOH} has uniform etching of the grain boundaries and the grains, resulting in 2D-like microscale planar structures that have nanoscale porous topography. The following reactions takes place when the Ti surfaces are exposed to 5M NaOH base solution:

$$3Ti + 4NaOH + 4H_20 \longrightarrow 2Na_2TiO_3 + TiO_2 + 6H_2 \tag{5.4}$$

$$TiO_2 + 2NaOH \longrightarrow Na_2TiO_3 + H_2O \tag{5.5}$$

The base reacts with Ti and TiO_2 on the titanium surface and forms sodium titanate. The reaction between titanium and sodium hydroxide is dependent on the concentration of the alkaline

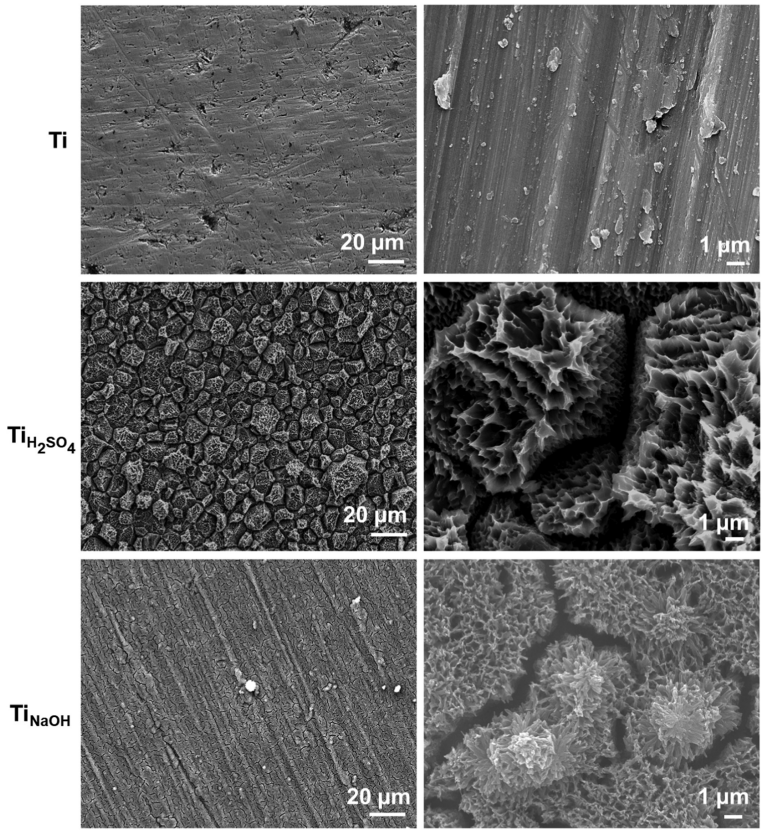

Figure 5.1: Representative SEM images of the developed surface morphology after hydrothermal treatment. The images were taken at 500X and 10, 000X magnification.

solution and temperature. This slow reaction leads to formation of stable oxide layers on the surface.

Surface wettability was characterized by measuring the apparent contact angle (θ^*) using a goniometer. Surface wettability plays a major role in protein adsorption and cell adhesion [58–61]. Studies have shown that hydrophilic surfaces ($\theta^* < 90°$) promote cell adhesion while hydrophobic surfaces ($\theta^* > 90°$) prevent cells from adhering to the surface [62]. Surface wettability is dictated by the surface chemistry, surface charge and surface roughness [63,64]. Apparent contact angles were measured with DI water. Results (**Figure 5.2**) showed that all the surfaces were hydrophilic with the following trend for θ^*: Ti < Ti_{NaOH} < $Ti_{H_2SO_4}$.The θ^* for Ti was higher (66.27°) compared to that for the Ti_{NaOH} and $Ti_{H_2SO_4}$ (17° and 10.14°) respectively. Ti is hydrophilic due presence of the oxide layer on the surface. Further modification with H_2SO_4 and NaOH results in increase in surface area due to the surface topography (nanopits and nanopores) as shown in **Figure 5.1** along

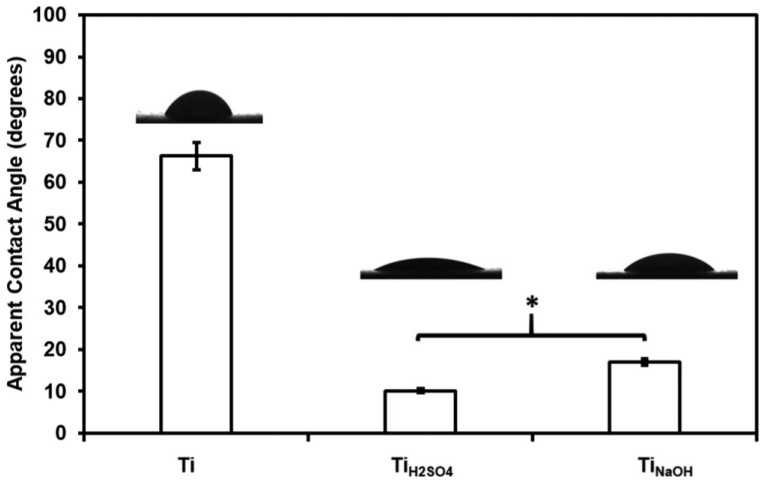

Figure 5.2: Apparent contact angles measured with DI water on different surfaces. The result indicates that the modified surfaces are significantly hydrophilic compared to Ti ($*p < 0.05$). The error bar represents the standard deviation.

with increased oxidation that made the surfaces even more hydrophilic. $Ti_{H_2SO_4}$ had the lowest θ^* due to the micro-nano hierarchical topography on the surface, followed by Ti_{NaOH} that just had nanotopography.

Surface chemistry was characterized using an XPS. The surface chemistry plays major role in long term success of implant surface integration with the natural tissue and hence was investigated. Survey scans on all surfaces (**Figure 5.3**) showed peaks for Ti_{2p} (458.5 eV), O_{1s} (529 – 530 eV) and C_{1s} (284.8 eV). The presence of C_{1s} was due to the impurities on the surface and in the XPS chamber. The survey scans also indicated that the $Ti_{H_2SO_4}$ and Ti_{NaOH} had higher titanium and oxygen content on the surface due to respective surface reactions (eq. 5.1, 5.2, 5.3, 5.4, and 5.5). However, the surfaces had lower carbon content compared to Ti (**Table 5.1**) since the treatment with $Ti_{H_2SO_4}$ and Ti_{NaOH} removed some of the surface impurities. Further, Ti_{NaOH} also showed the presence of Na1s (1071 eV) peak on the surface, confirming the presence of sodium titanate (eq. 5.4 and 5.5).

Surface crystallinity was characterized using XRD. The surface crystallinity plays major role in cellular attachment and proliferation and studies have shown different cells respond to surface crystallinity differently [65]. Studies have also shown that these lattice structures and their morphology

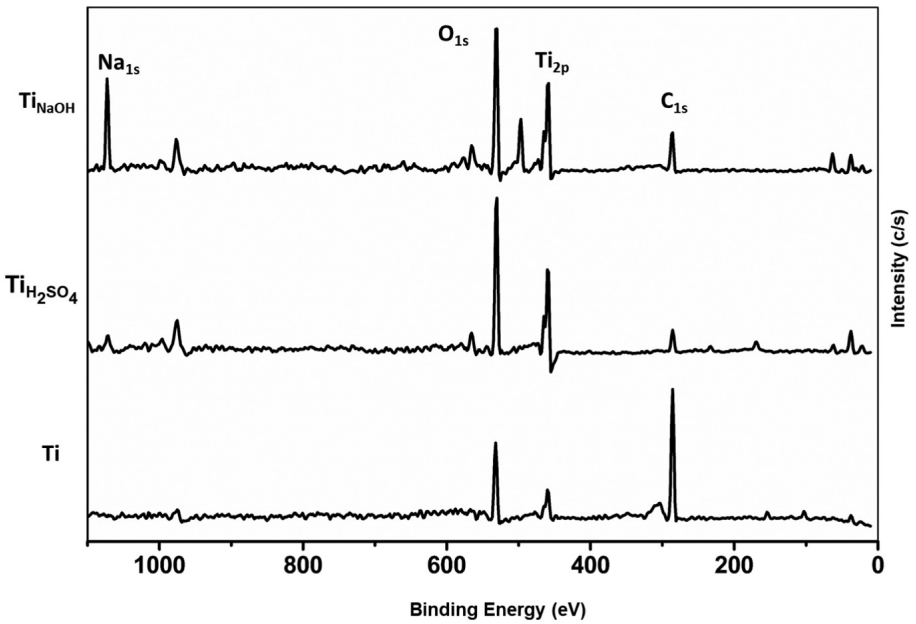

Figure 5.3: XPS survey scans for different surfaces. Survey spectra were collected from 0 to 1100 eV with a pass energy of 187.85 eV.

Table 5.1: XPS elemental composition calculated from the survey scans for different surfaces.

Surface	C1s (%)	O1s (%)	Ti2p (%)	Others (%)
Ti	69.31	21.05	3.74	5.91
$Ti_{H_2SO_4}$	20.16	58.04	17.84	3.94
Ti_{NaOH}	13.53	59.7	20.27	6.55

can dictate the interaction between water and the surface, and also the water-water interaction between the water molecules absorbed in the surface [66]. Hence, crystallinity was investigated. Intensity peaks (**Figure 5.4**) at$35°(100)$, $32°(002)$, $40°(101)$ and $53°(102)$ corresponds to metallic alpha phase Ti. Intensity peaks at $24°(101)$ and $62°(204)$ correspond to the TiO_2 anatase phase. Intensity peaks at $27°(110)$ and $76°(110)$ corresponds to the rutile phase titanium oxide (TiO_2). Intensity peaks at $41°(200)$ and $71°$ (311) corresponds to the TiH_2 presence on the surface. The Ti surface showed higher presence of metallic Ti α-phase. After the treatment, Ti_{NaOH} surface had higher rutile and anatase phase indicating that the surface was oxidized. The Ti_{NaOH} surface also showed higher metallic phase when compared to $Ti_{H_2SO_4}$ and Ti surface. There was no difference seen between the $Ti_{H_2SO_4}$ and Ti surface. However, there was phase transformation between metal-

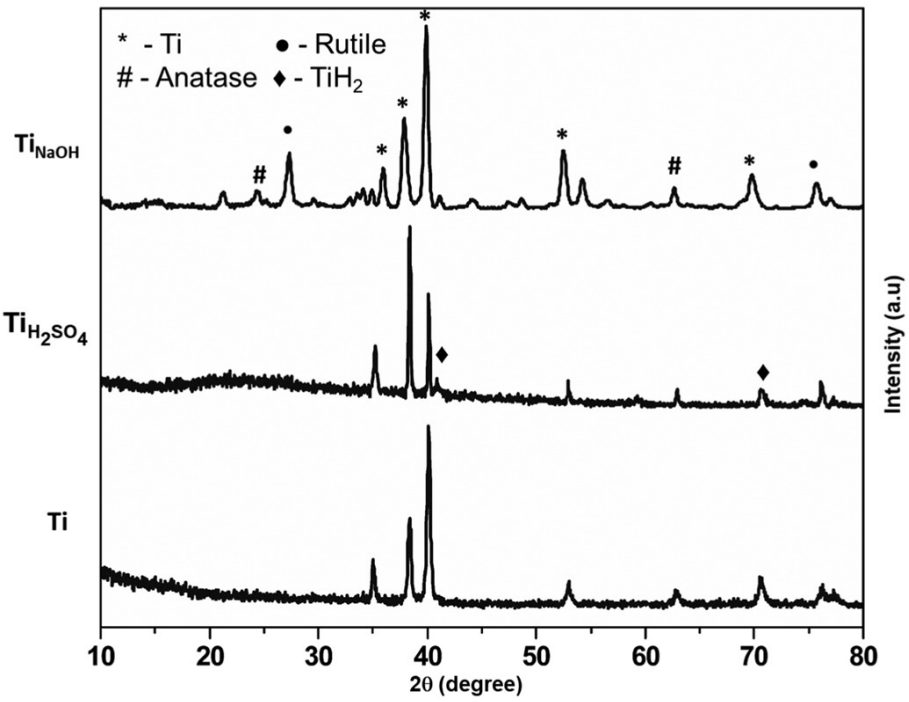

Figure 5.4: XRD scans for different surfaces. XRD scans were collected at θ = 1.5° and 2θ ranges were chosen based on significant peak intensities.

lic α-phase titanium on $Ti_{H_2SO_4}$ surface when compared to Ti surface, 101 lattice structure peaks were higher in Ti surface and 002 lattice structures were high on $Ti_{H_2SO_4}$ surface. This indicates that various planes are etched by the two different medium exposed. The presence of titanium hydride was verified by the intensity peaks at 41º and 71º [67]. The surface crystallinity is analyzed to identify the different lattice structure of different elements present on the surface. TiO_2 comprises of two different structures, anatase and rutile structures. Studies have shown that anatase structure is more stable than rutile [68].

Recently, studies have shown that adipose derived stem cells are cell source for tissue engineering and regenerative medicine [12,13]. ADSCs are mesenchymal stem cells that are derived from the adipose tissue. They have multi-lineage capacity and can maintain, repair, or enhance different tissues. Similar to bone marrow derived mesenchymal stem cells, they can differentiate into osteoblast cells leading to bone formation [12]. Typically, BMSCs are widely used to study osteointegration and osteogenesis for orthopedic application. However, their harvest protocol is

a highly invasive procedure, and their yield rate is low. While, ADSCs have proven to be easily accessible with minimal invasive procedure and can be extracted from discarded fat tissues, fast in proliferation, available in large quantity and they adhere, proliferate and differentiate easily In-vitro. Hence, ADSCs are used to evaluate surface for bone tissue regeneration.

Cytotoxicity was characterized using commercially available LDH assay. Hydrothermal treatment modifies the surface chemistry and topography. Thus, it is essential to evaluate whether these modifications induce any toxicity to the cells on the surfaces. Cells when influenced by a toxic element, stop growing and eventually die [69]. Hence, it is important to evaluate if the host body can tolerate the implant without any exclusion and cell deaths. Before dying, the cells breakdown by losing their membrane integrity and release an enzyme from the cytoplasm called LDH into the growth media [70]. After the 1 day of culture, the substrate exposed to growth media was used to determine the cytotoxicity with the commercially available LDH assay. Higher LDH activity in the growth media (**Figure 5.5**) indicated more cells have lost their cell membrane integrity and the surface is cytotoxic. The results indicate that negative control had highest LDH activity as all the cells were intentionally lysed to release maximum possible LDH in the growth media. Whereas, different surfaces and the positive control had significantly lower LDH activity when compared with negative control. Further, there was no significant difference between LDH activity on different surfaces and the positive control, indicating that hydrothermal treatment of surfaces does not cause any cytotoxic effects to the cells.

Cell viability was characterized after culturing different surfaces with ADSCs for 1,4 and 7 days. Hydrothermal treatment modifies the surface chemistry and topography that directly influences cell proliferation. Thus, it is important to evaluate whether these surface modifications inhibit the cells in contact with the surface to proliferate or not. When cells are induced to bioinert environment, healthy cells proliferate due to cytokinesis [71]. Hence, cell proliferation assays can also be used to assess the viability of the cells on the surface. In this assay, the metabolically active cells in growth media react with the resazurin present in the assay reagent and reduces it to resorufin. Higher

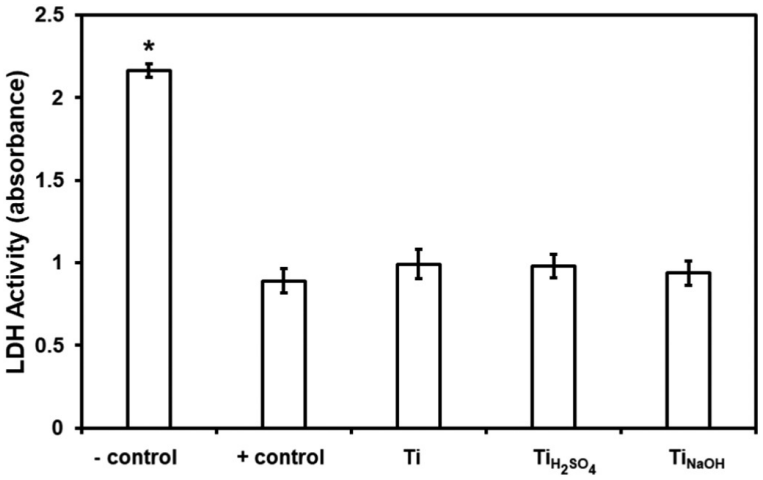

Figure 5.5: Cell cytotoxicity for ADSCs exposed to different surfaces measured using the LDH assay. The results indicate no significant differences in the LDH activity on all of the surfaces and positive control (100% live cells), whereas the LDH activity for the negative control (100% dead cells) was significantly different than other surfaces ($*p < 0.05$). The error bar represents the standard deviation.

resorufin in the resulting solution (**Figure 5.6**) indicates more viable cells. The absorbance of the solution was measured at 573 nm (maximum absorbance of resorufin) and 605 nm (maximum absorbance of resazurin). Cell viability was calculated using manufacturer provided protocol. After 1 day of culture, the results indicate no significant differences in cell viability for all the surfaces. However, Ti_{NaOH} has the highest cell viability and $Ti_{H_2SO_4}$ has the lowed cell viability. Similarly, after 4 and 7 days of culture, the results indicate no significant differences in the cell viability for all the surfaces. Thus, the results indicate that all surfaces had high metabolic activity and there were no significant differences in the cell viability due to the hydrothermal of the surface.

Cell adhesion and proliferation were characterized after culturing different surfaces with ADSCs for 1, 4 and 7 days. Hydrothermal treatment modifies the surface chemistry and topography. It is important to evaluate whether this modification affects cell adhesion and subsequent cell proliferation since it will eventually lead to osteogenic differentiation, faster bone growth and implant long-term stability [37]. Cell adhesion and proliferation were characterized using fluorescence microscopy. The number of adhered cells on different surfaces were determined by counting the cells on DAPI stained fluorescence microscopy images using ImageJ software. After 1 day of culture,

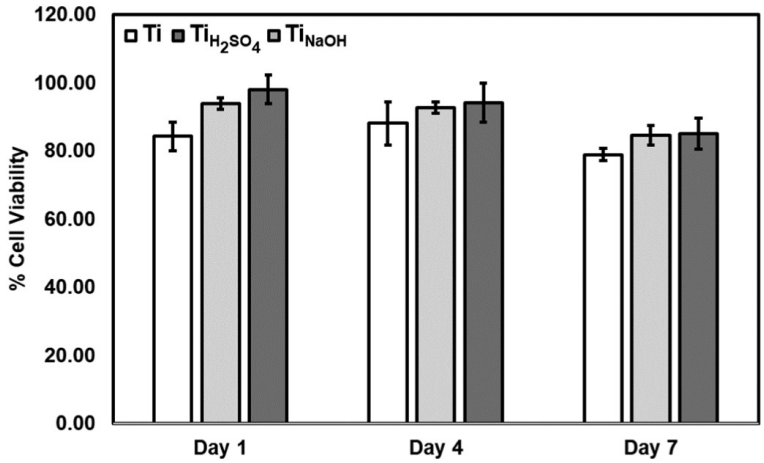

Figure 5.6: Cell viability of ADSCs exposed to different surfaces measured using Cell-Titer assay. The results indicate no significant differences in the cell viability on all the surfaces. The error bar represents the standard deviation.

the images (**Figure 5.7a**) indicated increased cell spreading on Ti$_{NaOH}$ compared to Ti and Ti$_{H_2SO_4}$. There were no significant differences in cells adhered (**Figure 5.7b**) on different surfaces. After 4 days of culture, the images indicate cells have proliferated and higher degree of cell spreading on Ti$_{NaOH}$ and Ti compared to Ti$_{H_2SO_4}$. There were no significant differences in cell proliferation on different surfaces. Ti$_{NaOH}$ had highest cell adhesion followed by Ti and Ti$_{H_2SO_4}$. This may be due to the surface morphology of Ti$_{NaOH}$ surface, the porous hydrophilic surface allows cells to attach and spread well. After 7 days of culture, the images indicated that 50% of all the surfaces were covered with ADSCs. However, Ti$_{H_2SO_4}$ and Ti$_{NaOH}$ showed more cell adhesion as compared to the Ti surfaces and Ti$_{NaOH}$ surface had significantly higher ASDCs compared to Ti. Studies have shown that cell need to attain a certain size to divide [72,73]. Thus, the results indicate Ti$_{NaOH}$ surface morphology influences the cells to spread and proliferate faster the Ti surface.

Cell morphology was characterized after culturing different surfaces with ADSCs for 1, 4 and 7 days. Hydrothermal treatment modifies the surface topography at a micro and nano-level. Thus, it is important to evaluate the effect of surface topography on cell spreading and morphology. After 1 day of culture, similar to fluorescence microscopy images, the SEM images (**Figure 5.8**) indicate the cells are attached on all the surfaces and are also interacting with the nano topography.

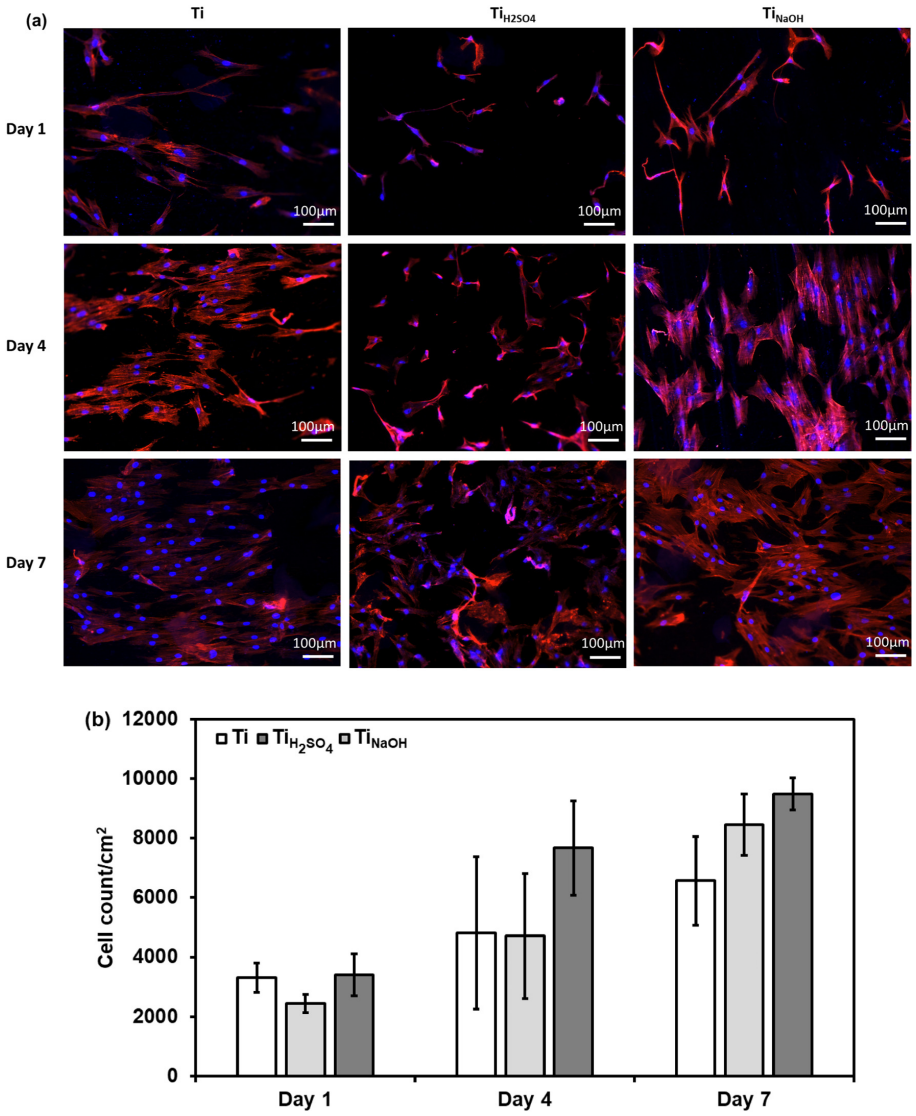

Figure 5.7: (a) Representative fluorescence microscope images of ADSCs stained with DAPI and rhodamine phalloidin on different surfaces. The results indicate cell adhesion and proliferation on all surfaces. (b) Number of cells adhered to the surface stained with DAPI calculated using ImageJ. The results indicate no significant differences in the cell viability on all the surfaces. The error bar represents the standard deviation.

However, the cells on the Ti_{NaOH} were anisotropically spread compared to those on Ti and $Ti_{H_2SO_4}$ [74] . After 4 days of culture, the SEM images indicate the more cell spreading on Ti and Ti_{NaOH} compare to $Ti_{H_2SO_4}$. On $Ti_{H_2SO_4}$, the cells are only able to attach on the grain surface due to more surface area, however they are not able to cross over the grain due to grain boundaries, thus resulting in restricted spreading. The cells are only able to attach at the grain boundaries as there is more surface area for adhesion. The spreading after adhesion is restricted by the surface topography present on the grain. Hence, that prevented the cells from spreading and restricted further cell-cell interactions. After 7 days of culture, the SEM images indicate the cells were even more spread on Ti surface compare to day 4. However, the cell spreading was localized to certain areas of the substrate. In contrast, the cells were uniformly spread on $Ti_{H_2SO_4}$ and Ti_{NaOH}. However, similar to day 4, cell spreading was restricted between the grain boundaries on $Ti_{H_2SO_4}$. Further, cells were even more spread and interacting with the nanoporous features on Ti_{NaOH}. Thus, results indicate that the surface morphology plays a major role in cell spreading and cell morphology.

After 7 days of ADSCs proliferation, the cells were supplemented with differentiation media (growth media with ascorbic acid, dexamethasone, and -glycerol phosphate). Ascorbic acid promotes collagen type I secretion. Dexamethasone promotes transcription factor (RUNX2) activity for osteoblast differentiation [75]. β-glycerol phosphate promotes hydroxyapatite production as it is the source for phosphate [76]. Cell differentiation is required for bone tissue regeneration and long-term stability of the implant and it is influenced by the cell adhesion, proliferation, and differentiation [77]. Hence, it is important to evaluate if the implant surface can also promote cell differentiation.

Alkaline Phosphate (ALP) deposition on different surfaces was characterized after culturing different surfaces with ADSCs for 14 and 28 days. ALP is an enzyme found in a healthy human bone tissue. Its activity peaks before mineralization and helps in converting organophosphate to inorganic phosphate [13]. This inorganic phosphate travels back into the vesicle and helps in hydroxyapatite formation. Therefore, ALP is a considered as an early marker for ADSCs differentiated to osteoblast

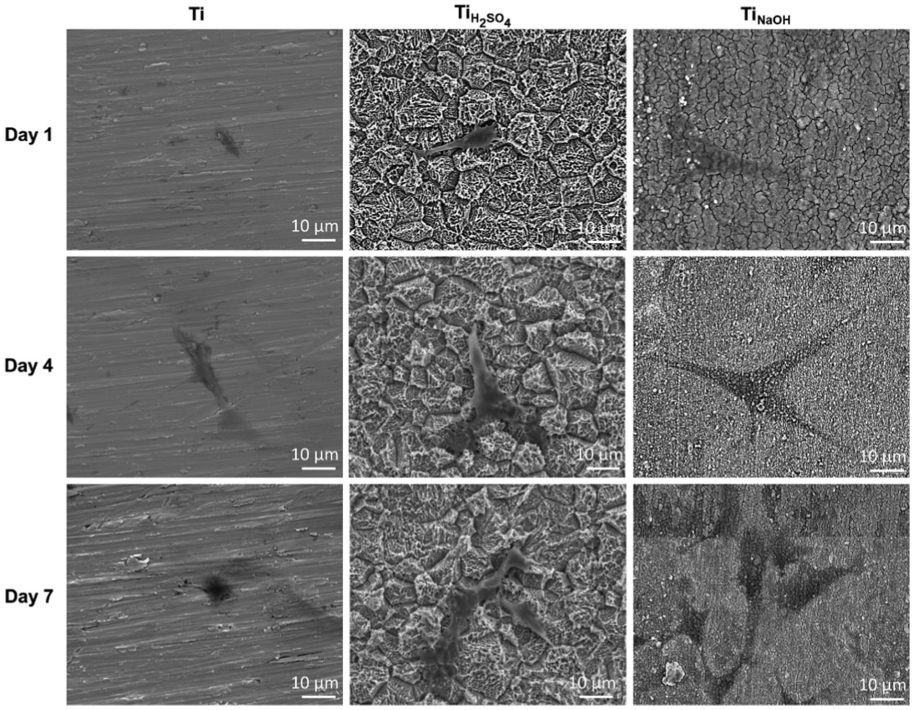

Figure 5.8: Representative SEM images of adhered cell on different surfaces. Images show a higher cell spreading on Ti_{NaOH} surfaces when compared to other surfaces. Images were taken at 1000X magnifications.

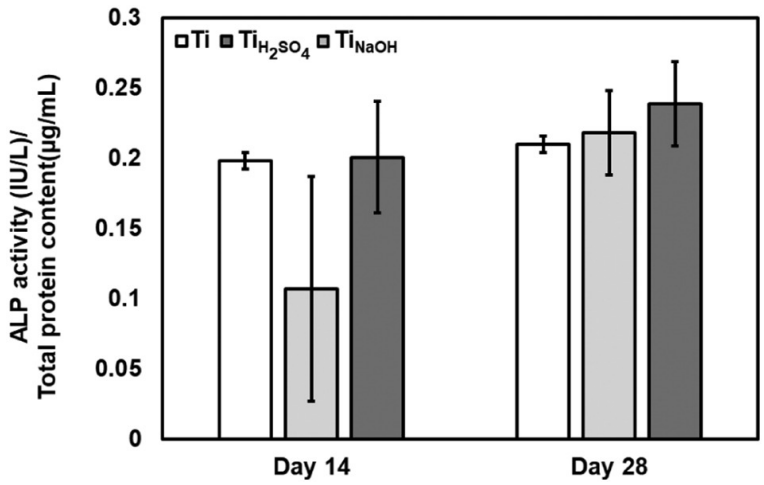

Figure 5.9: ALP activity of different surfaces was quantified and normalized by total protein content. ALP and BCA assays were performed after 14 and 28 days of culture.

cells [77,78]. ALP activity for cells on different surfaces was measured using QuantiChromTM Alkaline Phosphate Assay Kit. After 14 days of culture (i.e., after 7 days of inducing osteogenesis), the results (**Figure 5.9**) indicate no significant differences in ALP activity for all the surfaces. However, ALP activity on $Ti_{H_2SO_4}$ surface was lower than that on Ti and Ti_{NaOH}. After 28 days of culture (i.e., after 21 days of inducing osteogenesis), the results indicate no significant differences in ALP activity for all the surfaces, however, the ALP activity was higher compared to when measured after 14 days of culture. This indicates that the cells are differentiating. Several studies in literature have shown that Ti surfaces promote ADSCs differentiation into osteoblasts when provided with correct differentiation cues, and thus the results here indicate that the hydrothermal surface modification have not prevented ADSCs from differentiating into osteoblastic phenotype.

Calcium deposition on different surfaces was characterized after culturing different surfaces with ADSCs for 14 and 28 days. ADSCs after differentiating into osteoblast deposit calcium into the extracellular matrix and presence of calcium is considered as a late marker for differentiation [79,80]. Osteoblasts also play a major role in transporting the Calcium from the extracellular matrix to the osteoid and binds with the phosphate from ALP to form hydroxyapatite [81]. Hence, calcium plays a major role in bone formation. In this study, calcium secreted by the cells and deposited on

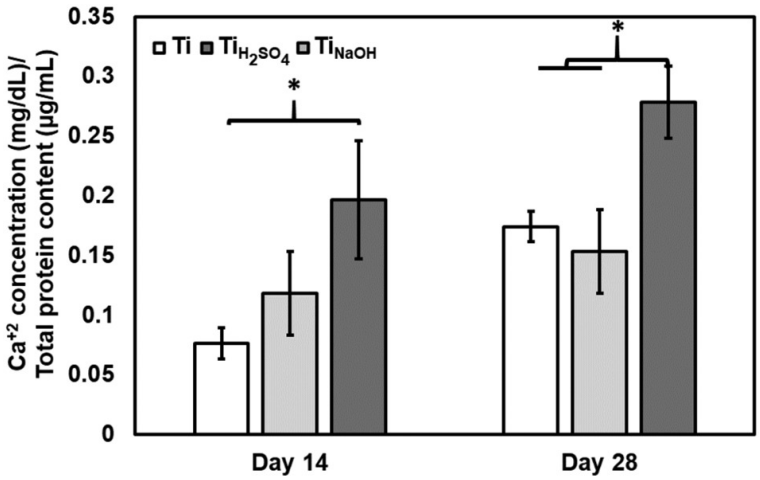

Figure 5.10: Calcium deposition by ADSCs on different surfaces was quantified and normalized by total protein content. Calcium and BCA assays were performed after 14 and 28 days of culture. The results indicate Ti_{NaOH} surface has higher calcium deposition compared to other surfaces ($*p < 0.05$). The error bar represents the standard deviation.

different surfaces was measured using a calcium reagent kit. The calcium from the cells reacts with the reagent (cresolphthalein complexone in 8-hydroxyquinoline) and form purple colored solution. After 14 days of culture, Ti_{NaOH} surface (**Figure 5.10**) had significantly higher calcium than that on Ti. After 28 days of culture, Ti_{NaOH} again had significantly higher calcium than the Ti and $Ti_{H_2SO_4}$ surfaces. Ti_{NaOH} surfaces showed higher calcium due to the cell morphology. As the cells were well spread out, they were able to transport more calcium from the extra cellular matrix [82,83]. Thus, the modified surfaces which encourage cell spreading promote higher mineralization making the surface improve long term stability of the implant.

Osteocalcin deposition on different surfaces was characterized after culturing with ADSCs for 14 and 28 days. Osteoblast cells secrete various noncollagenous and collagenous proteins [77]. Osteocalcin is one of the noncollagenous protein secreted into the bone micro-environment [84,85]. It changes its alignment to bind with the calcium ions in hydroxyapatite and initiate the formation of hydroxyapatite crystals. Hydroxyapatite crystals along with type I collagen matrix form bone tissue [86]. Hence, osteocalcin protein plays major role in binding the bone matrix and minerals. Osteocalcin expression by ADSCs on different surfaces was characterized using

immunofluorescence microscopy. The percentage area covered by osteocalcin was normalized by the number of cells. After 14 days of culture, the images (**Figure 5.11a**) show that most of the surface was covered with cells and there are small visual traces of osteocalcin. There was no significant difference (**Figure 5.11b**) on osteocalcin deposition seen between on all surfaces. This is because the cells were just induced to osteogenic differentiation and osteocalcin is one the late markers for osteoblast. However, the modified surfaces showed higher osteocalcin compared to Ti. After 28 days, the images (**Figure 5.11a**) show that all surfaces were completely covered with cells and the presence of osteocalcin was higher when compared to day 14. There was significant increase (**Figure 5.11b**) in osteocalcin on Ti_{NaOH} surface compared to Ti. Thus, the modified surfaces promote mineralization and improve bone growth.

Cell morphology and mineral deposition on different surfaces were characterized after culturing with ADSCs for 14 and 28 days. After 14 days of incubation, cells were more spread on all the surfaces compared to those after day 7 (**Figure 5.12**), however, no visual evidence of any of mineralization was seen. Further, the EDS results (**Table 5.2**) indicated presence of calcium and phosphorous only on Ti_{NaOH} indicating initiation of mineralization. After 28 days of incubation, all surfaces were completely covered with the cells with presence of minerals deposits. The EDS results also indicated absence of titanium on Ti_{NaOH} and $Ti_{H_2SO_4}$ surface indicating the surface was completely covered with cells. Further, the EDS results indicated higher concentrations of calcium and phosphorous compare to that after day 14. However, the Ti_{NaOH} surface had the highest concentration of calcium and phosphate indicating further progression of mineralization compare to day 14. Further, the Ca/P ratio on Ti and Ti_{NaOH} was closer to that of hydroxyapatite (1.67) [43]. However, the amount of Ca and P presence on Ti was significantly lower compare to Ti_{NaOH}. Thus, the results indicate that the Ti_{NaOH} with uniform nanoporous architecture could be better option for bone tissue integration.

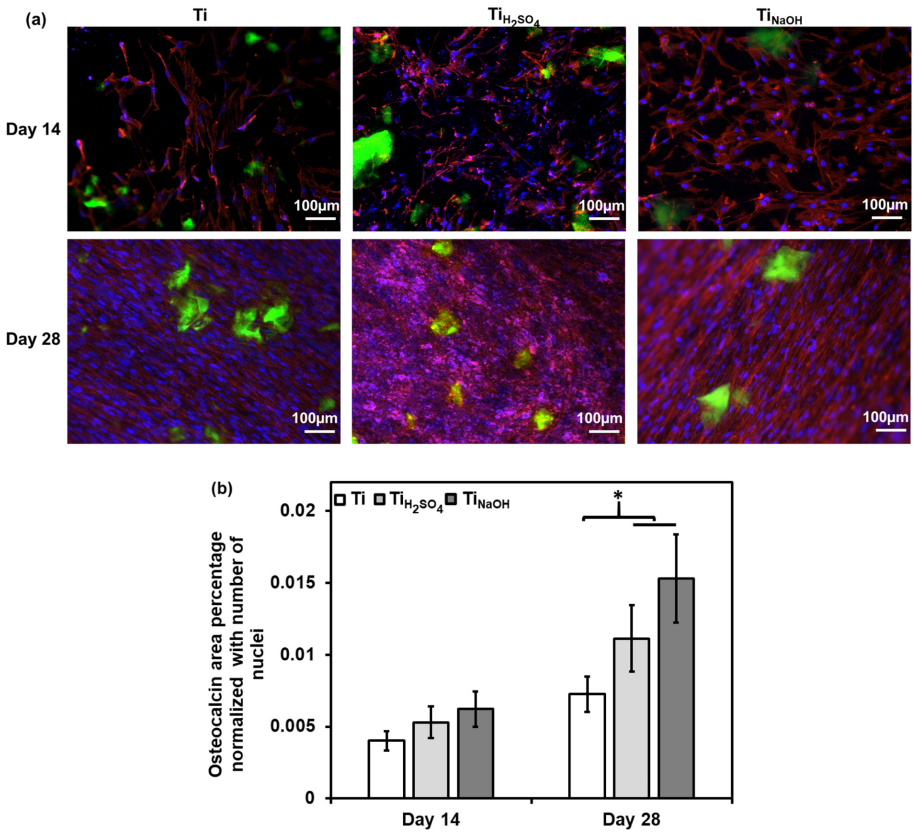

Figure 5.11: (a) Representative fluorescence microscope images of ADSCs along with osteocalcin stained with FITC, DAPI and rhodamine phalloidin on different surfaces. The results indicate cell proliferation and osteocalcin expression (green stain) on all surfaces. (b) Percentage area coverage of osteocalcin normalized by number of nuclei after 14 and 28 days of culture. Number of cells adhered to the surface stained with DAPI calculated using ImageJ. The area covered by osteocalcin expression was calculated using ImageJ. The results indicate significant differences on both modified surfaces ($*p < 0.05$) after 28 days of incubation. The error bar represents the standard deviation.

Table 5.2: EDS elemental composition of the SEM images was calculated after 28 days of incubation.

Surface	Ti (%)		Ca (%)		P (%)		Ca/P ratio	
	Day 14	Day 28	Day 14	Day 28	Day 14	Day 28	Day 14	Day 28
Ti	84.83	48.20	0.02	7.9	0	4.8	0	1.65
$Ti_{H_2SO_4}$	84.8	9.2	0	17.1	0	12.1	0	1.41
Ti_{NaOH}	40.1	7.8	5.1	21.1	3.1	12.7	1.64	1.66

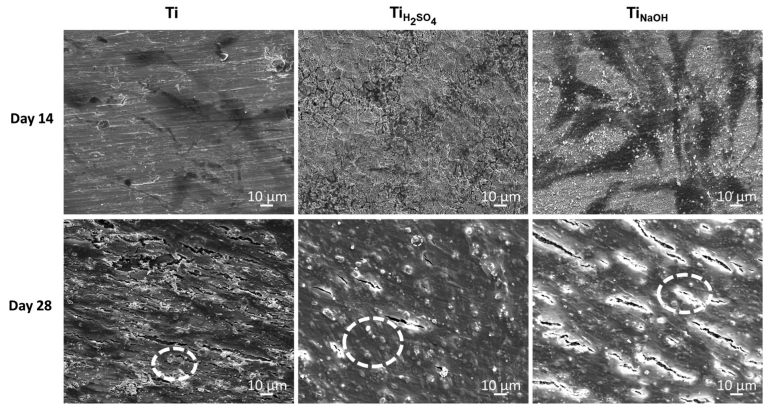

Figure 5.12: Representative SEM images of adhered cell on different surfaces after 14 and 28 days of incubation. Images were taken at 500X magnifications.

5.4 Conclusion

In this study, a simple hydrothermal technique was used to treat titanium surface with sulfuric acid and sodium hydroxide. Results showed that the treatment led to two unique nanostructures. The sulfuric acid treatment led to 3D-like microscale pyramidical structures that have nanoscale pits. Whereas, the sodium hydroxide treatment led to 2D-like microscale planar structures that have nanoscale porous topography. The surfaces were characterized for wettability, surface chemistry and crystallinity. The modified surfaces were significantly more hydrophilic compared to the Ti surface. The modified surfaces had higher presence of oxygen, and titanium compared to Ti surface. The potential for orthopedic application was evaluated by measuring surface cytotoxicity, cell viability, adhesion, proliferation, and differentiation. The surfaces showed no toxic effect after 24 hrs of ADSCs incubation. The surfaces did not affect the cell viability and adhesion significantly, however, results showed that after 7 days of studies, both modified surfaces had improved cell proliferation and adhesion because of improved hydrophilicity and surface features. $Ti_{H_2SO_4}$ surface showed improved cell spreading while the surface topography of $Ti_{H_2SO_4}$ hindered cell spreading due to the micron level grain structures hindering the cells from spreading easily. Cell differentiation was characterized by measuring ALP activity, calcium deposition and osteocalcin expression. Ti_{NaOH} and $Ti_{H_2SO_4}$ surface showed no significant difference in alkaline phosphates activity but induces

higher calcium deposition, and osteocalcin expression compared with Ti. Simultaneously, Ti_{NaOH} surface with dense nanoporous structures proved to be a better substitute for bone tissue implants compared to planar Ti and $Ti_{H_2SO_4}$ as the surface features interacted well with cells and promoted cell spreading, differentiation and bone tissue formation (Ca^{+2}) and this can improve implant long term durability. Thus, this study reveals that hydrophilic surfaces enhance cell adhesion, but the surface morphology plays a major in cell adhesion, spreading and differentiation.

5.5 References

[1] W.A. Steiner C, Andrews R, Barrett M, HCUP Projections: Mobility/Orthopedic Procedures 2003 to 2012. 2012. HCUP Projections Report 2012-03. 2012 Sep 20. U.S. Agency for Healthcare Research and Quality., 2015.

[2] L. Sokoloff, joint disease — Description, Types, Symptoms, Treatment — Britannica, (2020). https://www.britannica.com/science/joint-disease (accessed February 23, 2021).

[3] V.B. Vad, D.R. Adin, J. Solomon, Knee osteoarthritis, Critical Reviews in Physical and Rehabilitation Medicine. 16 (2004) 211–231. https://doi.org/10.1615/CritRevPhysRehabilMed.v16.i3.30

[4] Y. Zhang, J.M. Jordan, Epidemiology of osteoarthritis, Clinics in Geriatric Medicine. 26 (2010) 355–369. https://doi.org/10.1016/j.cger.2010.03.001.

[5] K.A. Pacheco, Allergy to Surgical Implants, (2016). https://doi.org/10.1007/s12016-018-8707-y.

[6] W.Z.W. Teo, P.C. Schalock, Metal Hypersensitivity Reactions to Orthopedic Implants, Dermatology and Therapy. 7 (2017) 53–64. https://doi.org/10.1007/s13555-016-0162-1.

[7] H.J. Rack, J.I. Qazi, Titanium alloys for biomedical applications, Materials Science and Engineering C. 26 (2006) 1269–1277. https://doi.org/10.1016/j.msec.2005.08.032.

[8] M. Geetha, A.K. Singh, R. Asokamani, A.K. Gogia, Ti based biomaterials, the ultimate choice for orthopaedic implants - A review, Progress in Materials Science. 54 (2009) 397–425. https://doi.org/10.1016/j.pmatsci.2008.06.004.

[9] M. Kaur, K. Singh, Review on titanium and titanium based alloys as biomaterials for orthopaedic applications, Materials Science and Engineering C. 102 (2019) 844–862. https://doi.org/10.1016/j.msec.2019.04.064.

[10] P. Hameed, V.K. Manivasagam, M. Sankar, K.C. Popat, G. Manivasagam, Nanofibers and nanosurfaces, in: Springer Series in Biomaterials Science and Engineering, Springer Science and Business Media Deutschland GmbH, 2021: pp. 107–130. https://doi.org/10.1007/978-981-33-6252-94.

[11] V. Leszczak, B.S. Smith, K.C. Popat, Hemocompatibility of polymeric nanostructured surfaces, Journal of Biomaterials Science, Polymer Edition. 24 (2013) 1529–1548. https://doi.org/10.1080/09205063.2013.777228.

[12] R.M. Sabino, G. Mondini, M.J. Kipper, A.F. Martins, K.C. Popat, Tanfloc/heparin polyelectrolyte multilayers improve osteogenic differentiation of adipose-derived stem cells on titania nanotube surfaces, Carbohydrate Polymers. 251 (2021) 117079. https://doi.org/10.1016/j.carbpol.2020.117079.

[13] K. Cowden, M.F. Dias-Netipanyj, K.C. Popat, Adhesion and Proliferation of Human Adipose-Derived Stem Cells on Titania Nanotube Surfaces, Regenerative Engineering and Translational Medicine. 5 (2019) 435–445. https://doi.org/10.1007/s40883-019-00091-9.

[14] J. Vishnu, V. K Manivasagam, V. Gopal, C. Bartomeu Garcia, P. Hameed, G. Manivasagam, T.J. Webster, Hydrothermal treatment of etched titanium: A potential surface nano-modification technique for enhanced biocompatibility, Nanomedicine: Nanotechnology, Biology, and Medicine. 20 (2019). https://doi.org/10.1016/j.nano.2019.102016.

[15] J. Vishnu, M. Sankar, H.J. Rack, N. Rao, A.K. Singh, G. Manivasagam, Effect of phase transformations during aging on tensile strength and ductility of metastable beta titanium alloy Ti–35Nb–7Zr–5Ta-0.35O for orthopedic applications, Materials Science and Engineering A. 779 (2020) 139127. https://doi.org/10.1016/j.msea.2020.139127.

[16] M. Geetha, A.K. Singh, R. Asokamani, A.K. Gogia, Ti based biomaterials, the ultimate choice for orthopaedic implants - A review, Progress in Materials Science. 54 (2009) 397–425. https://doi.org/10.1016/j.pmatsci.2008.06.004.

[17] R.B. Heimann, Plasma-Sprayed Hydroxylapatite Coatings as Biocompatible Intermediaries Between Inorganic Implant Surfaces and Living Tissue, Journal of Thermal Spray Technology. 27 (2018) 1212–1237. https://doi.org/10.1007/s11666-018-0737-8.

[18] R.B. Heimann, Plasma-Sprayed Hydroxylapatite Coatings as Biocompatible Intermediaries Between Inorganic Implant Surfaces and Living Tissue, Journal of Thermal Spray Technology. 27

(2018) 1212–1237. https://doi.org/10.1007/s11666-018-0737-8.

[19] D. Arcos, M. Vallet-Regí, Substituted hydroxyapatite coatings of bone implants, Journal of Materials Chemistry B. 8 (2020) 1781–1800. https://doi.org/10.1039/c9tb02710f. [20] K. Duan, R. Wang, Surface modifications of bone implants through wet chemistry, Journal of Materials Chemistry. 16 (2006) 2309–2321. https://doi.org/10.1039/b517634d.

[21] A. Somersalo, J. Paloneva, H. Kautiainen, E. Lönnroos, M. Heinänen, I. Kiviranta, Increased mortality after upper extremity fracture requiring inpatient care, Acta Orthopaedica. 86 (2015) 553–557. https://doi.org/10.3109/17453674.2015.1043833.

[22] R.G. Richards, The effect of surface roughness on fibroblast adhesion in vitro, Injury. 27 (1996) S/C38-S/C43. https://doi.org/10.1016/0020-1383(96)89031-0.

[23] M.F. Dias-Netipanyj, K. Cowden, L. Sopchenski, S.C. Cogo, S. Elifio-Esposito, K.C. Popat, P. Soares, Effect of crystalline phases of titania nanotube arrays on adipose derived stem cell adhesion and proliferation, Materials Science and Engineering C. 103 (2019).
https://doi.org/10.1016/j.msec.2019.109850.

[24] M.T. Tavares, M.B. Oliveira, J.F. Mano, J.P.S. Farinha, C. Baleizão, Bioactive silica nanoparticles with calcium and phosphate for single dose osteogenic differentiation, Materials Science and Engineering C. 107 (2020). https://doi.org/10.1016/j.msec.2019.110348.

[25] J. Vishnu, M. Sankar, H.J. Rack, N. Rao, A.K. Singh, G. Manivasagam, Effect of phase transformations during aging on tensile strength and ductility of metastable beta titanium alloy Ti–35Nb–7Zr–5Ta-0.35O for orthopedic applications, Materials Science and Engineering A. 779 (2020) 139127.
https://doi.org/10.1016/j.msea.2020.139127.

[26] K.C. Popat, R.H. Daniels, R.S. Dubrow, V. Hardev, T.A. Desai, Nanostructured surfaces for bone biotemplating applications, Journal of Orthopaedic Research. 24 (2006) 619–627.
https://doi.org/10.1002/jor.20105.

[27] S. Bauer, J. Park, K. von der Mark, P. Schmuki, Improved attachment of mesenchymal stem cells on super-hydrophobic TiO2 nanotubes, Acta Biomaterialia. 4 (2008) 1576–1582.

https://doi.org/10.1016/j.actbio.2008.04.004.

[28] Y. Qin, J. Guan, C. Zhang, Mesenchymal stem cells: Mechanisms and role in bone regeneration, Postgraduate Medical Journal. 90 (2014) 643–647. https://doi.org/10.1136/postgradmedj-2013-132387.

[29] A. Oryan, A. Kamali, A. Moshiri, M. Baghaban Eslaminejad, Role of Mesenchymal Stem Cells in Bone Regenerative Medicine: What Is the Evidence?, Cells Tissues Organs. 204 (2017) 59–83. https://doi.org/10.1159/000469704.

[30] S.C. Huo, B. Yue, Approaches to promoting bone marrow mesenchymal stem cell osteogenesis on orthopedic implant surface, World Journal of Stem Cells. 12 (2020) 545–561. https://doi.org/10.4252/wjsc.v12.i7.545.

[31] P. Tropel, N. Platet, J.-C. Platel, D. Noël, M. Albrieux, A.-L. Benabid, F. Berger, Functional Neuronal Differentiation of Bone Marrow-Derived Mesenchymal Stem Cells, Stem Cells. 24 (2006) 2868–2876. https://doi.org/10.1634/stemcells.2005-0636.

[32] V.V. Miana, E.A. Prieto González, Adipose tissue stem cells in regenerative medicine, Ecancermedicalscience. 12 (2018). https://doi.org/10.3332/ecancer.2018.822.

[33] P.A. Zuk, M. Zhu, P. Ashjian, D.A. De Ugarte, J.I. Huang, H. Mizuno, Z.C. Alfonso, J.K. Fraser, P. Benhaim, M.H. Hedrick, Human adipose tissue is a source of multipotent stem cells, Molecular Biology of the Cell. 13 (2002) 4279–4295. https://doi.org/10.1091/mbc.E02-02-0105.

[34] C.T. Gomillion, K.J.L. Burg, Stem cells and adipose tissue engineering, Biomaterials. 27 (2006) 6052–6063. https://doi.org/10.1016/j.biomaterials.2006.07.033.

[35] B.A. Bunnell, M. Flaat, C. Gagliardi, B. Patel, C. Ripoll, Adipose-derived stem cells: Isolation, expansion and differentiation, Methods. 45 (2008) 115–120. https://doi.org/10.1016/j.ymeth.2008.03.006.

[36] V.K. Manivasagam, K.C. Popat, In Vitro Investigation of Hemocompatibility of Hydrothermally Treated Titanium and Titanium Alloy Surfaces, ACS Omega. (2020). https://doi.org/10.1021/acsomega.0c00281.

[37] K.A. Cox-York, C.B. Erickson, R.I. Pereira, D.H. Bessesen, R.E. Van Pelt, Region-specific

effects of oestradiol on adipose-derived stem cell differentiation in post-menopausal women, Journal of Cellular and Molecular Medicine. 21 (2017) 677–684. https://doi.org/10.1111/jcmm.13011.

[38] D. Clark, M. Nakamura, T. Miclau, R. Marcucio, Effects of Aging on Fracture Healing, Current Osteoporosis Reports. 15 (2017) 601–608. https://doi.org/10.1007/s11914-017-0413-9.

[39] A. Somersalo, J. Paloneva, H. Kautiainen, E. Lönnroos, M. Heinänen, I. Kiviranta, Increased mortality after upper extremity fracture requiring inpatient care, Acta Orthopaedica. 86 (2015) 553–557. https://doi.org/10.3109/17453674.2015.1043833.

[40] D.R. H Hermawan, Biomedical Engineering: From Theory to Applications, in: Biomedical Engineering, InTech, Rijecka, n.d.: p. 411.

[41] B.D. Ratner, Surface Properties and Surface Characterization of Biomaterials, in: Biomaterials Science: An Introduction to Materials: Third Edition, Elsevier Inc., 2013: pp. 34–55. https://doi.org/10.1016/B978-0-08-087780-8.00005-X.

[42] B.D. Ratner, F.J. Schoen, The Concept and Assessment of Biocompatibility, in: Biomaterials Science: An Introduction to Materials: Third Edition, Elsevier Inc., 2013: pp. 588–592. https://doi.org/10.1016/B978-0-08-087780-8.00052-8.

[43] D.R. H Hermawan, Biomedical Engineering: From Theory to Applications, in: Biomedical Engineering, InTech, Rijecka, n.d.: p. 411.

[44] M. Long, H.J. Rack, Titanium alloys in total joint replacement - A materials science perspective, Biomaterials. 19 (1998) 1621–1639. https://doi.org/10.1016/S0142-9612(97)00146-4.

[45] H.J. Rack, J.I. Qazi, Titanium alloys for biomedical applications, Materials Science and Engineering C. 26 (2006) 1269–1277. https://doi.org/10.1016/j.msec.2005.08.032.

[46] D. Hara, Y. Nakashima, T. Sato, M. Hirata, M. Kanazawa, Y. Kohno, K. Yoshimoto, Y. Yoshihara, A. Nakamura, Y. Nakao, Y. Iwamoto, Bone bonding strength of diamond-structured porous titanium-alloy implants manufactured using the electron beam-melting technique, Materials Science and Engineering C. 59 (2016) 1047–1052. https://doi.org/10.1016/j.msec.2015.11.025.

[47] B.D. Ratner, Surface Properties and Surface Characterization of Biomaterials, in: Biomaterials Science: An Introduction to Materials: Third Edition, Elsevier Inc., 2013: pp. 34–55.

https://doi.org/10.1016/B978-0-08-087780-8.00005-X.

[48] A. Boyde, Scanning electron microscopy of bone, in: Methods in Molecular Biology, Humana Press Inc., 2019: pp. 571–616.

https://doi.org/10.1007/978-1-4939-8997-$3_3$1.

[49] E. Gongadze, D. Kabaso, S. Bauer, T. Slivnik, P. Schmuki, U. van Rienen, A. Iglič, Adhesion of osteoblasts to a nanorough titanium implant surface., International Journal of Nanomedicine. 6 (2011) 1801–1816.

[50] K.C. Popat, R.H. Daniels, R.S. Dubrow, V. Hardev, T.A. Desai, Nanostructured surfaces for bone biotemplating applications, Journal of Orthopaedic Research. 24 (2006) 619–627.

https://doi.org/10.1002/jor.20105.

[51] M. Kulkarni, A. Mazare, J. Park, E. Gongadze, M.S. Killian, S. Kralj, K. von der Mark, A. Iglič, P. Schmuki, Protein interactions with layers of TiO2 nanotube and nanopore arrays: Morphology and surface charge influence, Acta Biomaterialia. 45 (2016) 357–366.

https://doi.org/10.1016/j.actbio.2016.08.050.

[52] C. Yao, E.B. Slamovich, T.J. Webster, Enhanced osteoblast functions on anodized titanium with nanotube-like structures, Journal of Biomedical Materials Research Part A. 85A (2008) 157–166. https://doi.org/10.1002/jbm.a.31551.

[53] Y. V. Kolen'ko, K.A. Kovnir, A.I. Gavrilov, A. V. Garshev, J. Frantti, O.I. Lebedev, B.R. Churagulov, G. Van Tendeloo, M. Yoshimura, Hydrothermal synthesis and characterization of nanorods of various titanates and titanium dioxide, Journal of Physical Chemistry B. 110 (2006) 4030–4038. https://doi.org/10.1021/jp055687u.

[54] S. Ban, Y. Iwaya, H. Kono, H. Sato, Surface modification of titanium by etching in concentrated sulfuric acid, Dental Materials. 22 (2006) 1115–1120.

https://doi.org/10.1016/j.dental.2005.09.007.

[55] E. Gongadze, D. Kabaso, S. Bauer, T. Slivnik, P. Schmuki, U. van Rienen, A. Iglič, Adhesion of osteoblasts to a nanorough titanium implant surface., International Journal of Nanomedicine. 6 (2011) 1801–1816.

[56] R.M. Sabino, K. Kauk, L.Y.C. Madruga, M.J. Kipper, A.F. Martins, K.C. Popat, Enhanced hemocompatibility and antibacterial activity on titania nanotubes with tanfloc/heparin polyelectrolyte multilayers, Journal of Biomedical Materials Research - Part A. 108 (2020) 992–1005. https://doi.org/10.1002/jbm.a.36876.

[57] L. Beaunier, CORROSION OF GRAIN BOUNDARIES: INITIATION PROCESSES AND TESTING, Le Journal de Physique Colloques. 43 (1982) C6-271-C6-282 https://doi.org/10.1051/jphyscol:1982624.

[58] M. Lampin, R. Warocquier-Clrout, C. Legris, M. Degrange, M.F. Sigot-Luizard, Correlation between substratum roughness and wettability, cell adhesion, and cell migration, Journal of Biomedical Materials Research. 36 (1997) 99–108. https://doi.org/10.1002/(SICI)1097-4636(199707)36:1¡99::AID-JBM12¿3.0.CO;2-E.

[59] C.H. Kim, M.S. Khil, H.Y. Kim, H.U. Lee, K.Y. Jahng, An improved hydrophilicity via electrospinning for enhanced cell attachment and proliferation, Journal of Biomedical Materials Research Part B: Applied Biomaterials. 78B (2006) 283–290. https://doi.org/10.1002/jbm.b.30484.

[60] K. Webb, V. Hlady, P.A. Tresco, Relative importance of surface wettability and charged functional groups on NIH 3T3 fibroblast attachment, spreading, and cytoskeletal organization, Journal of Biomedical Materials Research. 41 (1998) 422–430. https://doi.org/10.1002/(SICI)1097-4636(19980905)41:3¡422::AID-JBM12¿3.0.CO;2-K.

[61] R.M. Sabino, K. Kauk, S. Movafaghi, A. Kota, K.C. Popat, Interaction of blood plasma proteins with superhemophobic titania nanotube surfaces, Nanomedicine: Nanotechnology, Biology and Medicine. 21 (2019) 102046. https://doi.org/10.1016/J.NANO.2019.102046.

[62] K. Webb, V. Hlady, P.A. Tresco, Relative importance of surface wettability and charged functional groups on NIH 3T3 fibroblast attachment, spreading, and cytoskeletal organization, Journal of Biomedical Materials Research. 41 (1998) 422–430. https://doi.org/10.1002/(SICI)1097-4636(19980905)41:3¡422::AID-JBM12¿3.0.CO;2-K.

[63] J. Lahann, S. Mitragotri, T.N. Tran, H. Kaido, J. Sundaram, I.S. Choi, S. Hoffer, G.A. Somorjai, R. Langer, A reversibly switching surface, Science. 299 (2003) 371–374.

https://doi.org/10.1126/science.1078933.

[64] J.J. Nairn, W.A. Forster, R.M. van Leeuwen, Quantification of physical (roughness) and chemical (dielectric constant) leaf surface properties relevant to wettability and adhesion, Pest Management Science. 67 (2011) 1562–1570. https://doi.org/10.1002/ps.2213.

[65] H. Cui, P.J. Sinko, The role of crystallinity on differential attachment/proliferation of osteoblasts and fibroblasts on poly (caprolactone-co-glycolide) polymeric surfaces, Frontiers of Materials Science. 6 (2012) 47–59. https://doi.org/10.1007/s11706-012-0154-8.

[66] K. Bourikas, C. Kordulis, A. Lycourghiotis, Titanium Dioxide (Anatase and Rutile): Surface Chemistry, Liquid–Solid Interface Chemistry, and Scientific Synthesis of Supported Catalysts, Chemical Reviews. 114 (2014) 9754–9823. https://doi.org/10.1021/cr300230q.

[67] P. Wang, X. Yi, Y. Lu, H. Yu, J. Yu, 5. In-situ synthesis of amorphous H2TiO3-modified TiO2 and its improved photocatalytic H2-evolution performance, Journal of Colloid and Interface Science. 532 (2018) 272–279. https://doi.org/10.1016/j.jcis.2018.07.139.

[68] T. Luttrell, S. Halpegamage, J. Tao, A. Kramer, E. Sutter, M. Batzill, Why is anatase a better photocatalyst than rutile? - Model studies on epitaxial TiO2 films, Scientific Reports. 4 (2015) 1–8. https://doi.org/10.1038/srep04043.

[69] P.B. Tchounwou, C.G. Yedjou, A.K. Patlolla, D.J. Sutton, Heavy metal toxicity and the environment, EXS. 101 (2012) 133–164. https://doi.org/10.1007/978-3-7643-8340-4_6.

[70] P.B. Tchounwou, C.G. Yedjou, A.K. Patlolla, D.J. Sutton, Heavy metal toxicity and the environment, EXS. 101 (2012) 133–164. https://doi.org/10.1007/978-3-7643-8340-4_6.

[71] T. Riss, A. Niles, R. Moravec, N. Karassina, J. Vidugiriene, Cytotoxicity Assays: In Vitro Methods to Measure Dead Cells, Eli Lilly Company and the National Center for Advancing Translational Sciences, 2004.

[72] F.T. Lewis, The correlation between cell division and the shapes and sizes of prismatic cells in the epidermis of cucumis, The Anatomical Record. 38 (1928) 341–376. https://doi.org/10.1002/ar.1090380305.

[73] E. Wood, P. Nurse, Sizing up to Divide: Mitotic Cell-Size Control in Fission Yeast, Annual

Review of Cell and Developmental Biology. 31 (2015) 11–29. https://doi.org/10.1146/annurev-cellbio-100814-125601.

[74] L.C. Palmer, C.J. Newcomb, S.R. Kaltz, E.D. Spoerke, S.I. Stupp, Biomimetic systems for hydroxyapatite mineralization inspired by bone and enamel, Chemical Reviews. 108 (2008) 4754–4783. https://doi.org/10.1021/cr8004422.

[75] A. Rakngarm, Y. Miyashita, Y. Mutoh, Formation of hydroxyapatite layer on bioactive Ti and Ti-6Al-4V by simple chemical technique, Journal of Materials Science: Materials in Medicine. 19 (2008) 1953–1961. https://doi.org/10.1007/s10856-007-3285-1.

[76] F.E. Freeman, H.Y. Stevens, P. Owens, R.E. Guldberg, L.M. McNamara, Osteogenic Differentiation of Mesenchymal Stem Cells by Mimicking the Cellular Niche of the Endochondral Template, Tissue Engineering - Part A. 22 (2016) 1176–1190. https://doi.org/10.1089/ten.tea.2015.0339.

[77] F.E. Freeman, H.Y. Stevens, P. Owens, R.E. Guldberg, L.M. McNamara, Osteogenic Differentiation of Mesenchymal Stem Cells by Mimicking the Cellular Niche of the Endochondral Template, Tissue Engineering - Part A. 22 (2016) 1176–1190. https://doi.org/10.1089/ten.tea.2015.0339.

[78] S. Lee, Y.-Y. Chang, J. Lee, S.K. Madhurakkat Perikamana, E.M. Kim, Y.-H. Jung, J.-H. Yun, H. Shin, Surface engineering of titanium alloy using metal-polyphenol network coating with magnesium ions for improved osseointegration, Biomaterials Science. (2020). https://doi.org/10.1039/d0bm00566e.

[79] C. Shen, C. Yang, S. Xu, H. Zhao, Comparison of osteogenic differentiation capacity in mesenchymal stem cells derived from human amniotic membrane (AM), umbilical cord (UC), chorionic membrane (CM), and decidua (DC), Cell and Bioscience. 9 (2019) 17. https://doi.org/10.1186/s178-019-0281-3.

[80] F.M.P. Tonelli, A.K. Santos, K.N. Gomes, L.O. Ladeira, R.R. Resende, D.A. Gomes, S.L. Da Silva, Stem cells and calcium signaling, Advances in Experimental Medicine and Biology. 740 (2012) 891–916. https://doi.org/10.1007/978-94-007-2888-$2_4$0.

[81] R. Florencio-Silva, G.R.D.S. Sasso, E. Sasso-Cerri, M.J. Simões, P.S. Cerri, Biology of Bone Tissue: Structure, Function, and Factors That Influence Bone Cells, BioMed Research International.

2015 (2015).
https://doi.org/10.1155/2015/421746.
[82] M.A. Schwartz, Spreading of human endothelial cells on fibronectin or vitronectin triggers elevation of intracellular free calcium, Journal of Cell Biology. 120 (1993) 1003–1010. https://doi.org/10.1083/jcb.120.4.1003.
[83] N. Itano, S. ichi Okamoto, D. Zhang, S.A. Lipton, E. Ruoslahti, Cell spreading controls endoplasmic and nuclear calcium: A physical gene regulation pathway from the cell surface to the nucleus, Proceedings of the National Academy of Sciences of the United States of America. 100 (2003) 5181–5186. https://doi.org/10.1073/pnas.0531397100.
[84] A.M.F.S. Mohamed, An overview of bone cells and their regulating factors of differentiation, Malaysian Journal of Medical Sciences. 15 (2008) 4–12.
[85] M.S. Razzaque, Osteocalcin: A pivotal mediator or an innocent bystander in energy metabolism, Nephrology Dialysis Transplantation. 26 (2011) 42–45.
https://doi.org/10.1093/ndt/gfq721.
[86] L.C. Palmer, C.J. Newcomb, S.R. Kaltz, E.D. Spoerke, S.I. Stupp, Biomimetic systems for hydroxyapatite mineralization inspired by bone and enamel, Chemical Reviews. 108 (2008) 4754–4783. https://doi.org/10.1021/cr8004422.

CHAPTER 6: SELECTIVE IN-VITRO ENDOTHELIALIZATION ON HYDROTHERMALLY TREATED TITANIUM FOR CARDIOVASCULAR APPLICATION

6.1 Introduction

Cardiovascular diseases (CVDs) continue to be the leading cause of the death in the United States and worldwide. According to the Global Burden of Disease study, 17.8 million deaths globally are due to CVDs [1]. Coronary artery disease (CAD) is the most common type of CVD, caused by plaque buildup on the walls of arteries. This plaque is mostly made of cholesterol deposits. Arteries play a major role in circulating blood inside our body and this plaque buildup narrow down the blood vessels and limits blood flow in our body. This disease is also called atherosclerosis and a common treatment for this disease is either coronary artery bypass surgery (CABG) or percutaneous heart intervention (PCI) [2]. During CABG, a graft will be attached to the affected artery to restore the blood flow. This is an extensive surgical and invasive procedure, and this procedure can lead to hemorrhage, infection and pneumonia. During PCI, a stent is placed on the affected region of the artery to restore the blood flow. This is a nonsurgical and noninvasive technique, and the procedure can lead to inflammation and hemorrhage. Recovery time from CABG is higher than PCI. Hence, PCI is preferred over CABG due to its simplicity. However, patients with multiple blocks are still treated with a CABG procedure [3].

Bare metal stents (BMS) were the first kind of stents used in the 1980s and 1990s. These are mostly made of nickel-titanium, stainless steel and cobalt-chromium alloy for their excellent strength and corrosion. The major limitation of BMS is restenosis. Restenosis is a gradual re-narrowing of the vessel in the stented area [4]. In-stent restenosis is a complex process involving tissue repair after vessel injury during stent implantation leading to neo-intimal hyperplasia where the smooth muscle cells proliferate and migrate into the internal layer [5]. These smooth muscle cells interact with the implant surface and dedifferentiate and initiate proliferation. This will reduce the lumen

diameter obstructing the blood flow. Hence, it's vital to develop an implant surface that prevents smooth muscle cell adhesion and proliferation. Because BMS had high potential for early stage restenosis, the development of drug eluding stents (DES) had emerged. DES are commonly used as they have molecular therapy to reduce restenosis, inflammation and initial thrombus formation. DES in the clinical market is mostly made of nitinol, stainless or cobalt-chromium base covered with polymer overlayer containing specific drugs such as sirolimus, paclitaxel, everolimus and zotarolimus [6]. However, the side effect of this drug is impaired endothelial regeneration and over time the drug is depleted, and late thrombosis is seen in patients with DES which is comparable to BMS. Thrombosis is acute syndrome where the blood clots in the surface of the stent and, once the clotting cascade begins, it spreads rapidly, and this increase the chances of mortality [7]. Hence, it's vital to develop an implant surface that prevents thrombosis. Regardless of the kind of stents in market, endothelization is not happening to promote blood flow without clotting. Therefore, there is a crucial need to develop a stent surface which can selectively prevent smooth muscle cell adhesion and proliferation (restenosis), simultaneously promote endothelialization for enhancing blood compatibility.

In a healthy individual, the endothelial lining in blood vessels prevent adhesion of cells and clotting proteins to maintain hemostasis, a similar strategy can be adopted to develop new implant surfaces that promote endothelial cells adhesion, proliferation, and differentiation [8]. Researchers have taken various approaches to develop hemocompatible surfaces for cardiovascular implant application. Studies have demonstrated the influence of surface properties such as morphology, chemistry, and wettability on cell and blood interaction. Hence, researchers have either modified surface morphology or surface chemistry or both for enhancing hemocompatibility and simultaneously improve endothelization. Anodization is one of the surface modification technologies which has been extensively researched as it leads to higher hemocompatibility with decreased platelet and smooth muscle cell adhesion as well as enhanced endothelial cell growth through the formation of nanotubes in the presence of hydrofluoric (HF) acid and oxygen plasma treatment. Further, studies carried out on nanotubes coated with zinc and polymers, showed lower smooth muscle cell

adhesion and higher endothelial cells. However, nanotubes and coatings are prone to delamination and oxidation. Researchers have also explored surface coating for improving endothelization on titanium surface, ECM derived adhesion sequences c[RGDfK], SIKVAV, and VGVAPG realized using functionalized mussel-derived peptides showed enhanced endothelial cell adhesion and differentiation[9]. Similarly, Poly(4-methyl-1-pentene) (PMP) gas-exchange membranes coated on titanium during, using the pulsed vacuum cathodic arc plasma deposition (PVCAPD) technique, showed to develop a stable endothelial surface without promoting inflammation and the thrombogenicity [10]. Hence, there is a critical demand to develop a stable surface with selective endothelial adhesion and preventing smooth muscle cells.

To address this research gap, in this study, two novel micro/nano surface morphology were developed on titanium surface using hydrothermal treatment with sodium hydroxide and sulfuric acid. The surfaces were characterized for morphology using a Scanning Electron Microscope (SEM) and the wettability was evaluated through contact angle measurement with water using a goniometer. Cytocompatibility of the developed surfaces were assessed by evaluating cytotoxicity, cell viability, adhesion, proliferation, morphology, and differentiation using smooth muscle cells and endothelial cells. Results indicated that hydrothermal treatment with sodium hydroxide and sulfuric acid led to the formation of two unique surface morphologies. Further, surface wettability studies showed that both the surfaces were significantly hydrophilic compared to polished titanium surface. Cytotoxicity studies revealed that both modified surfaces did not induce any toxicity on both smooth muscle cells and endothelial cells after incubation for 24 hrs. Cell studies indicated that the micro-nano surface morphology developed by sulfuric treatment selectively prevented smooth muscle cell adhesion and promoted endothelial cell adhesion and proliferation.

6.2 Materials and Methods

Commercial pure medical Grade II titanium sheets were cut into 5 cm X 3 cm X 0.02 cm surfaces . These surfaces were mechanically polished using Silicon-Carbide dry abrasive sheets. The grit

size of the abrasive sheets was gradually increased (400, 600, 800, 1000, 1200) to attain a polished surface. Polished surfaces were sonicated for 10 mins in an acetone medium and these surfaces were subsequently rinsed with water and air dried.

6.2.1 Fabrication of nanoporous structures on titanium surfaces

Sodium hydroxide treatment

Cleaned surfaces were submerged in a sodium hydroxide base solution (5 M) and hydrothermally treated at 80 °C in a hot air oven for 8 hrs. Experimental parameters such as temperature, solution concentration and duration of experiment was tweaked to develop different surface morphology and tested for hemocompatibility. The surface with the highest hemocompatibility as explained in the author's previous work was used in this manuscript. After being treated, the modified substrates were annealed for one hour at 300 °C.

Sulfuric acid treatment

Cleaned surfaces were submerged in a sulfuric acid solution (0.5 M) and hydrothermally treated at 80 °C in a hot air oven for 8 hrs. Experimental parameters are optimized for surface morphology as explained in the author's previous work. After treatment, the modified substrates were annealed for one hour at 300°C.

Hydrothermally modified surfaces were further sonicated for 10 mins in DI water to remove debris and dried using compressed air. These modified surfaces were stored in a desiccator until further studies. For cell studies, polished and hydrothermal surfaces were further cut down into smaller square surfaces (0.5 cm X 0.5 cm). The following notations were used to refer the treated titanium surfaces: Ti for unmodified titanium surfaces (control), $Ti_{H_2SO_4}$ for sulfuric acid modification, and Ti_{NaOH} for sodium hydroxide modification.

Surface Characterization

Morphology of control and modified surfaces was visualized using a JEOL 6500 field emission scanning electron microscopy (FE-SEM). The specimen chamber was maintained at a pressure of 10^{-5} Pa and operated at 15Kv accelerating voltage. Images were taken at different magnification 500x, 2000x and 10000x. The advancing contact angle (θ*) of different surfaces with Milli-Q water was calculated using a Ramé-hart 260F4 goniometer at room temperature. The advancing contact angle was measured by placing a Milli-Q water droplet and the volume was increased in a controlled manner using a micro syringe until the contact angle value saturates.

6.2.2 HUVEC and SMC culture

Human Umbilical Vascular Endothelial Cells (HUVECs, passage 4) were suspended in endothelial cell basal media with supplement kit in a 75ml cell culture flask. Human Aortic Smooth Muscle Cells (HASMCs, passage 5) were suspended in smooth muscle cell growth media with supplement kit in a 75ml cell culture flask. The cells were cultured inside a 37 °C and 5% CO_2 incubator. Cell growth media was changed every other day until 90% confluence was attained. After the cell confluence was attained, cells were detached from the culture flask using TrypLE. The cell concentration was diluted to 20,000 cells/ml before cell seeding. In a 48 well plate, sterilized surfaces were placed and 300 μl of diluted cell solution was pipetted into each well. The well plates were stored inside a 37°C and 5% CO_2 incubator for the duration of each individual study. Cell media was changed every other day for the entire duration of the study.

6.2.3 Cytocompatibility

Cytocompatibility of modified surfaces was quantified using lactate dehydrogenase (LDH) assay. After 24 hrs of incubation with HUVEC and SMC cells, 100μl of incubated cell growth media was used to evaluate the LDH expression. Protocol provided by the manufacturer was followed, a mixture of 100 µl of assay reaction solution and 100 µl of incubated cell growth media was

incubated in a 37 °C and 5% CO_2 incubator for 30 mins. After incubation, 50 μl of stop solution was added and the absorbance of the resulting solution at 490nm was measured using an UV spectrophotometer. Maximum LDH expression was measured by lysing cells using 10% Triton X-100 solution and spontaneous LDH expression was measured by using cell solution from cells incubated in a blank well.

6.2.4 Cell viability

Cell viability of modified surfaces was quantified using CellTiter-Blue Assay. After 1, 3 and 5 days of incubation with HUVEC and SMC, cell media was aspirated and 300 μl of fresh cell media and 10% CellTiter-Blue was added to each well. The surfaces were further incubated in a 37°C and 5% CO_2 incubator for 7 hours. Absorbance of the resulting solution 570 nm and 600 nm using an UV spectrophotometer. Cell media was changed after each time point of study. Protocol provided by the manufacturer was followed to calculate the cell viability.

6.2.5 Cell adhesion and Proliferation

Cell adhesion and proliferation on modified surfaces were visualized and quantified using fluorescence microscopy. After 1, 3 and 5 days of incubation with HUVEC and SMC, cell media was aspirated, and surfaces were gently rinsed with PBS thrice. The surfaces were fixed using a fixative solution (3.7% formaldehyde) for 15 mins and the surfaces were gently rinsed with PBS thrice. The cells were permeabilized using membrane permeability solution (1 % Triton X-100) for 3 mins and surfaces were gently rinsed with PBS thrice. F-actin, actin filaments and nucleus of the fixed cells were incubated in a staining solution (2% rhodamine-phalloidin) for 25 mins and followed by a nucleus staining solution (3% 4,6-diamidino-2-phenylindole) for 5 mins. Surfaces were gently rinsed with PBS thrice and the surfaces were imaged using Zeiss fluorescence microscopy. Cells were quantified using ImageJ software.

6.2.6 Cell morphology

Cell morphology of modified surfaces were visualized and quantified using SEM. After 1, 3 and 5 days of incubation with HUVEC and SMC, cell media was aspirated, and surfaces were gently rinsed with PBS three times. Further, the surface was fixed using a fixative solution (3 % glutaraldehyde, 0.1 M sodium cacodylate, and 0.1 M sucrose) for 45 mins followed by buffer solution (0.1 M sodium cacodylate, and 0.1 M sucrose) for 10 mins. The surfaces were consequently dried by incubating with 35%, 50%, 70% and 100% ethanol for 10 mins each. Surfaces were coated with gold 5nm and imaged using SEM.

6.2.7 Cell differentiation

Cellular differentiation and expression of marker proteins of modified surfaces were visualized and quantified using fluorescence microscopy. After 7 and 10 days of incubation with HUVEC and SMC, cell media was aspirated, and surfaces were gently rinsed with PBS thrice. Adhered cells were fixed as described earlier. Later, the surfaces were incubated in 10% bovine serum albumin (BSA) for 30 mins. This is followed by incubation with primary antibody (anti-VE-cadherin and anti-von Willebrand Factor for HUVEC; calponin and myosin heavy chain 11 for SMC) for 60 mins. The surfaces were incubated with secondary antibody-FITC for 45 mins, followed by incubation in rhodamine phalloidin and DAPI, as described earlier, and then imaged using fluorescence microscopy.

6.2.8 Statistical analysis

Surface characterization was repeated for at least three different surfaces from each group. Contact angle measurements, fluorescence microscopy and SEM imaging was done at three different locations on each sample (nmin = 9). Cytocompatibility, cell proliferation, adhesion and differentiation assays were repeated at least two times with at least three different surfaces from each group (nmin = 6). The quantitative results were analyzed using a two-way analysis of variance (ANOVA) test

using R software. The results are presented with * with statistically significant and a p-value < 0.05.

6.3 Results and Discussion

Humans diagnosed with heart diseases like atherosclerosis are operated to implant mechanical stents for free flow of blood. These stents are commonly made of metals such as stainless steel, titanium, and other alloys, owning to their excellent mechanical properties and biocompatibility [11], [12]. However, on implantation, the stent interact with the inner layer of the blood vessel and damage the endothelial lining. This phenomenon is called endothelial denudation. This causes the smooth muscle cells inside the blood vessels to interact with the stent surface, leading to de-differentiation and proliferation causing restenosis [13]. Researchers explored various surface level physical/chemical modification techniques to improve surface hemocompatibility of these stent materials and developed DES. DES has shown to prevent restenosis. However, after 5-6 months of implantation, the drug on the surface is exhausted and the surface interacts with the blood and leads to late thrombosis [14]. The key to prevent thrombosis is to promote endothelization. In this manuscript, a simple cost-effective hydrothermal treatment process was explored to modify the surface physically, using different alkaline/acidic solutions. Modified surfaces were assessed for in-vitro endothelization as this is found to prevent blood clotting and smooth muscle adhesion/proliferation as this is found to prevent restenosis.

Surface morphology of the treated surfaces was visualized using a SEM. Polished Ti surfaces have planar surfaces and at high magnification polishing scratches were observed (**Figure 6.1**). After sodium hydroxide treatment, Ti_{NaOH} surface exhibited nanofibrous microstructure on the surface [15]. The formation of nanofibrous structure is attributed to the different etching rates between the grain and grain boundaries. The grain boundaries with weaker bonds were etched significantly higher than the grain surface. The etching inside the grain led to a fibrous structure. In contrast, after sulfuric acid treatment, $Ti_{H_2SO_4}$ surface showed multi-scalar features, and this was

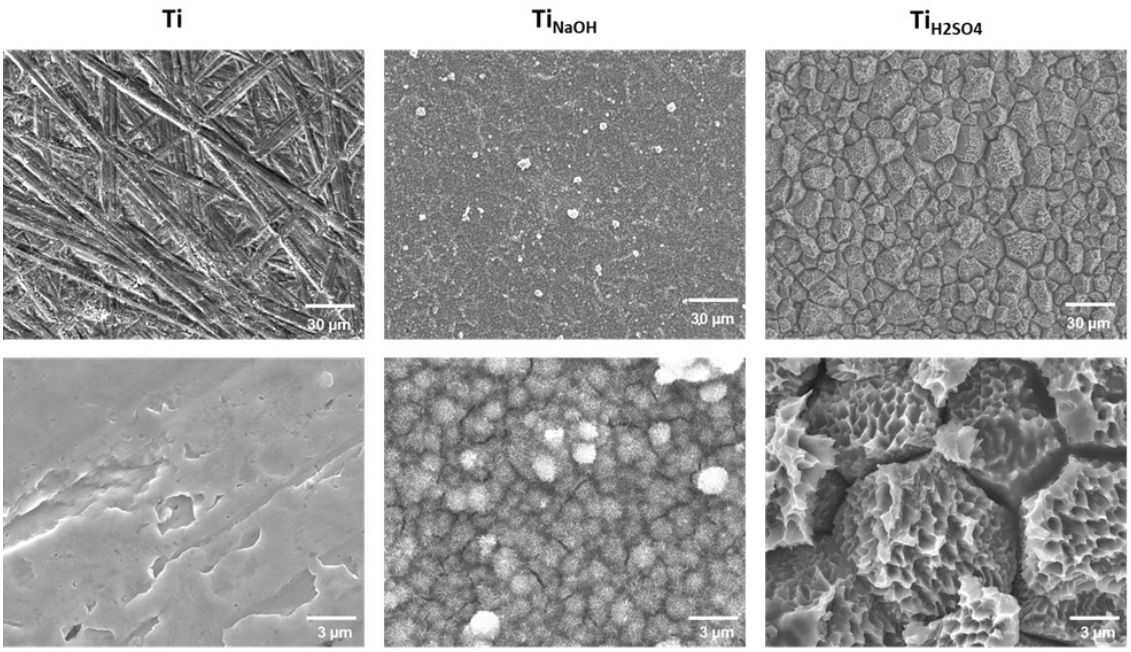

Figure 6.1: FESEM Images of polished and modified surfaces at two different magnification.

due to gradient etching. The etching rate was higher towards the grain boundaries and gradually decreased towards the center of the grain. The presence of highly disoriented atoms in the grain boundaries have led to the formation of 3D pyramid like micron structures [16]. In addition, unidirectional etching perpendicular to the surface has led to nano-pits.

Surface wettability was characterized using a goniometer. Surface wettability plays a major role in protein adsorption and cell adhesion and hence was investigated. Advancing contact angle (θ_{adv}) was measured using Milli-Q water. Advancing contact angle is the highest contact angle in the free energy range. Results indicated that all surfaces are hydrophilic (<90°) with the trend for θ_{adv}: Ti < Ti$_{NaOH}$ < Ti$_{H_2SO_4}$ (**Figure 6.2**). The advancing angle of Ti was significantly higher than Ti$_{NaOH}$ and Ti$_{H_2SO_4}$. Surface chemistry was analyzed in our previous works, results indicates that the treatment removed the carbon impurities in the surface and oxidized the surface.

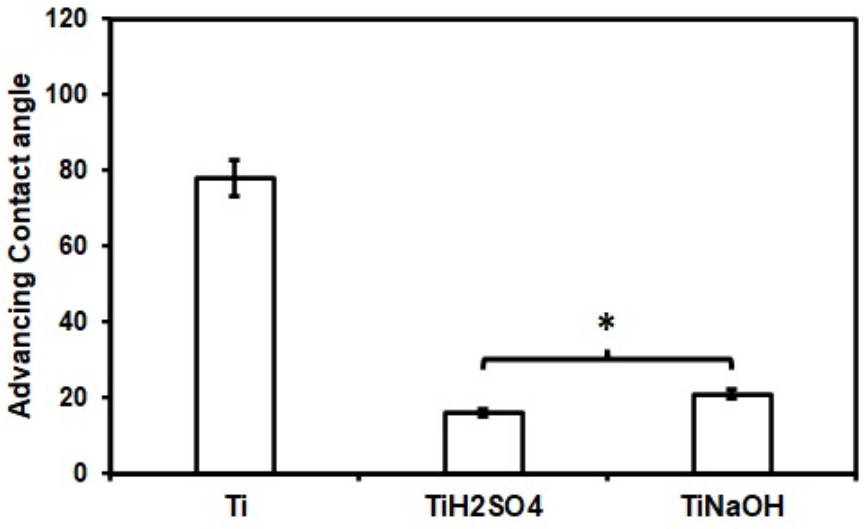

Figure 6.2: Advancing contact angle of different surfaces. The error bar represents the standard deviation. (*p < 0.05).

6.3.1 Endothelial cell interaction with modified surfaces

The main functionality of endothelial cells inside a blood vessel is to regulate blood flow by regulating diameter of the blood vessel, inflammation and coagulation. Endothelial cells can produce molecules like thrombomodulin and tissue factor pathway inhibitor (TFPI) that help to inhibit coagulation, while producing von Willebrand factor, which promotes platelet aggregation [17]. Endothelial glycocalyx is a layer of sugar molecules that surrounds the endothelial cells and lines the inner surface of the blood vessels. This layer is composed of a complex mixture of glycosaminoglycans, glycoproteins and proteoglycans. The endothelial glycocalyx plays a crucial role in regulating blood flow by influencing the mechanical and chemical properties of the blood vessels[18]. In this study, HUVECs are used to model the surface interaction with endothelial cells as they have similar behavior.

Hydrothermal treatment modifies surface properties such as morphology, chemistry, and wettability. Hence, it's vital to evaluate surface induced toxicity. HUVECs when induced to toxic environment, stop proliferating and slowly die. During this process, cells will lose membrane integrity and release various enzymes into the medium. LDH is a dominant enzyme found when

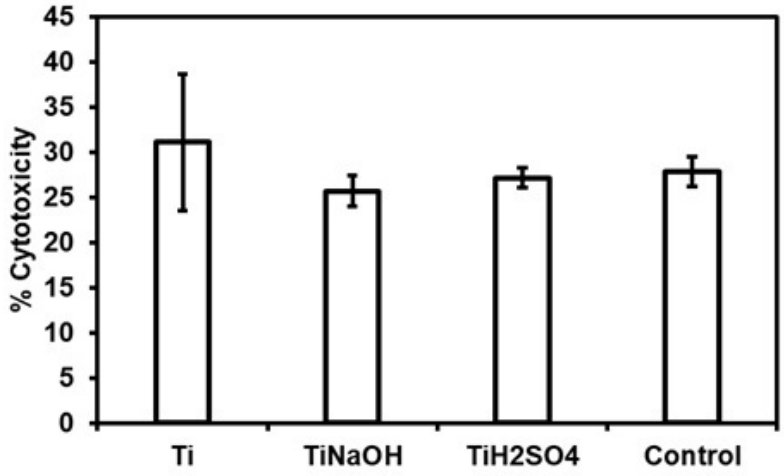

Figure 6.3: Cell cytotoxicity for HUVECs exposed to different surfaces after 24 hrs measured using the LDH assay. The error bar represents the standard deviation. (*p < 0.05)

cells die due to apoptosis and necrosis. Apoptosis is due to natural cell death as part of an organ growth. Necrosis is due to environment induced cell death [19]. Modified surfaces were evaluated for cytocompatability after incubating with HUVECs for 24hrs using commercially avialable LDH assay. Results indicated that hydrothermal treatment did not induce toxicity as there was no significant difference between the toxicity levels with cells incubated with Ti, blank (polystyrene well), Ti_{NaOH} and $Ti_{H_2SO_4}$ (**Figure 6.3**).

Surfaces were evaluated for cell viability after incubating with HUVECs for 1, 3 and 5 days using commercially available CellTiter-Blue assay. Hydrothermal treatment modifies surface properties such as morphology, chemistry, and wettability. Hence, it's vital to evaluate modified surface inhibits cell adhesion and proliferation. Metabolically active cells will interact with resazurin present in the reagent and reduces to resorufin. Higher resorufin in the resulting solution indicates more viable cells [20]. Results indicate that after 1 day of incubation, no significant difference was seen between Ti, Ti_{NaOH} and $Ti_{H_2SO_4}$. Similarly, no significant difference was seen after 3 and 5 days of incubation. However, $Ti_{H_2SO_4}$ had a significant increase cell proliferation after 3 and 5 days

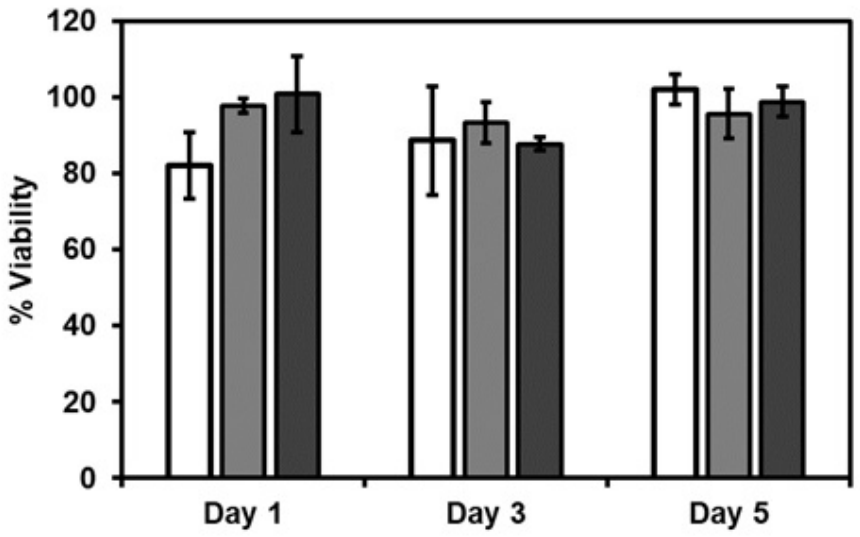

Figure 6.4: Cell viability for HUVECs exposed to different surfaces measured after day 1,3 and 5 using the cell viability assay. The error bar represents the standard deviation. (*p < 0.05)

of incubation (**Figure 6.4**). Ti_{NaOH} showed the fastest growth between 1 and 3 days of incubation.

Cell adhesion and proliferation of the modified surfaces after incubating with HUVECs for 1, 3 and 5 days were evaluated using a fluorescence microscope. Hydrothermal treatment modifies surface properties such as morphology, chemistry, and wettability and this in turn modifies the cell adhesion and proliferation [21]. Hence, it's vital to evaluate if modified surfaces promote cell adhesion and proliferation as they can prevent early thrombosis and restenosis. Results indicate that after 1 day of incubation, Ti_{NaOH} showed significantly higher cell adhesion compared to $Ti_{H_2SO_4}$ and Ti surface. Similar trend was observed after 3 and 5 days of incubation. However, all surfaces showed significant increase in cell coverage between the different time points(**Figure 6.5a**). Cell count studies showed that Ti_{NaOH} had significantly higher cell on day 1 and 3 compared to $Ti_{H_2SO_4}$ and Ti. However, cell count studies after 5 days of incubation showed that $Ti_{H_2SO_4}$ had higher cells compared to $Ti_{NaOH}$and Ti. This is mainly due to the interaction of cells with different surface morphology (**Figure 6.5b**), endothelial cells are smaller in size and cuboidal (roughly square under a microscope)). Hence, the hydrophilic $Ti_{H_2SO_4}$ surface with the micro-nano features promotes cell adhesion and proliferation growth although its micro-nano surface prevents cell spreading (**Figure**

6.5c). Thus, after 5 days of incubation, $Ti_{H_2SO_4}$ has a higher cell count with lower cell coverage compared to Ti_{NaOH}.

Surfaces were evaluated for cell morphology after incubating with HUVECs for 1, 3 and 5 days using a SEM. Hydrothermal treatment modifies the surface properties such as morphology, chemistry, and wettability. Hence, it's vital to evaluate if modified surfaces influence cell morphology. Results indicated that Ti surface enables the cells to spread and Ti_{NaOH} surface with planar fibrous nano structures promote higher cell spreading (**Figure 6.6**). However, the $Ti_{H_2SO_4}$ surface with micron scale pyramid features prevents cell spreading significantly and this corroborates with the cell adhesion and proliferation results.

Surfaces were evaluated for cell differentiation after incubating with HUVECs for 5,7 and 10 days using an immunofluorescence staining assay. Hydrothermal treatment modifies surface properties such as morphology, chemistry, and wettability. Hence, it's vital to evaluate if modified surfaces influence cell differentiation. Although implant surface have to adhere and assist cell proliferation, it's crucial for the developed surface to support cell differentiation to mimic healthy blood vessels. HUVECs during differentiation express certain proteins such as vascular endothelial cadherin (VE-cadherin), and von Willebrand factor (vWF). Hence, the presence of such protein markers confirms cells differentiation. VE-cadherin is a type of cadherin protein that is expressed after endothelization. It is important for maintaining the integrity of the blood vessels by holding the endothelial cells together and preventing the leakage of blood from the vessels. It also plays a role in the formation and stability of the blood vessels during development and tissue repair.

VE-cadherin can modulate the activity of intracellular signaling pathways that control the smooth muscle cells, altering the diameter of the blood vessels. Results indicated Ti_{NaOH} and $Ti_{H_2SO_4}$ initiated faster cell differentiation (**Figure 6.7a**). After 7 days of incubation, there was a significant increase in endothelization on both Ti_{NaOH} and $Ti_{H_2SO_4}$. After 10 days of incubation, the cells have changed to cuboidal shapes on all surfaces, cuboidal shape of endothelial cells allows for a high surface-to-volume ratio, which is important for the many physiological functions. Thus,

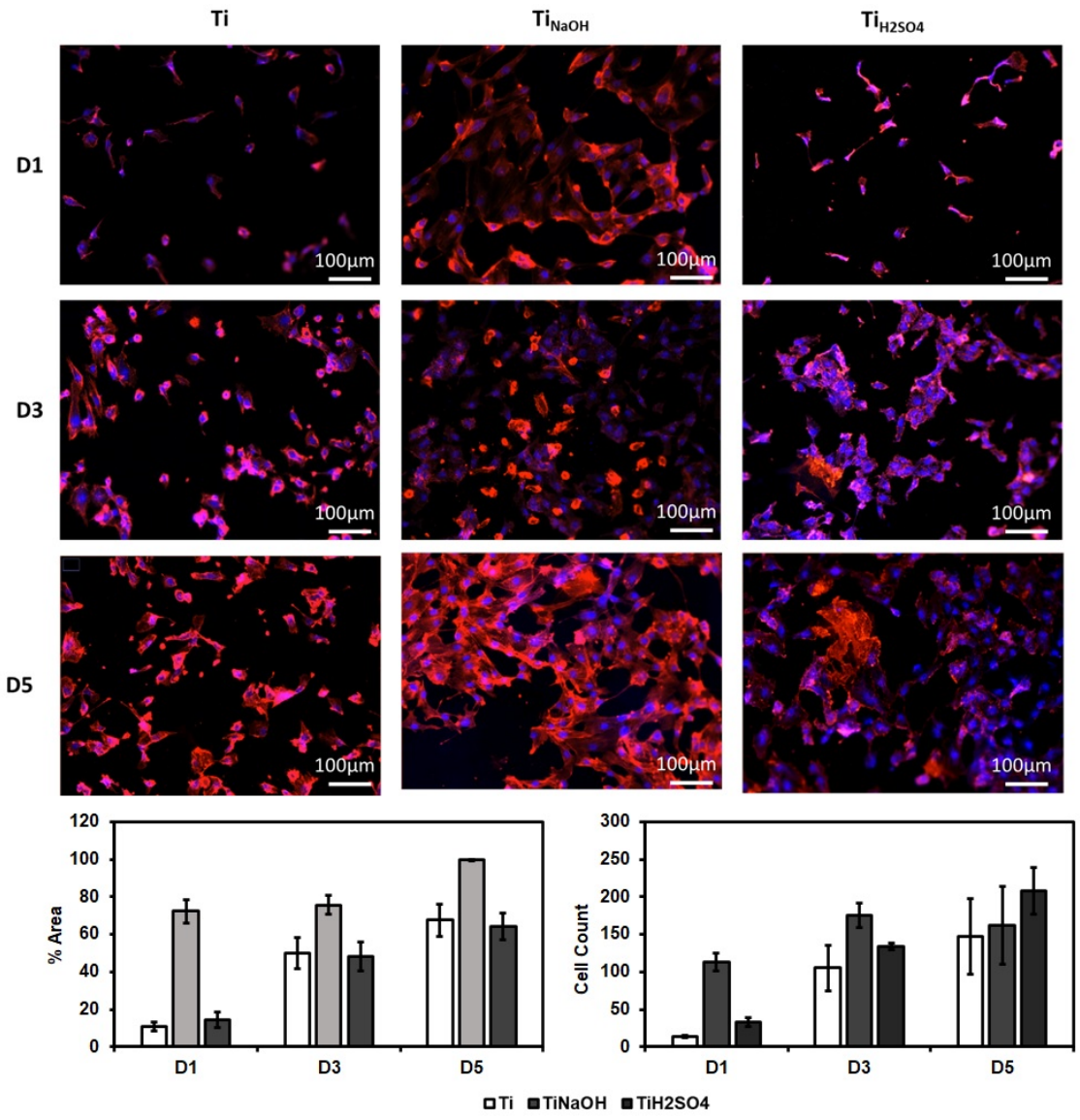

Figure 6.5: a)Fluorescence microscope images HUVECs stained with DAPI and rhodamine–phalloidin on different surfaces after day 1,3 and 5 of incubation. b) Percentage area coverage of cells on different surfaces after 1,3 and 5 of incubation. c) Number of cells adhered to the surface stained with DAPI calculated using ImageJ. The error bar represents the standard deviation. (*$p < 0.05$)

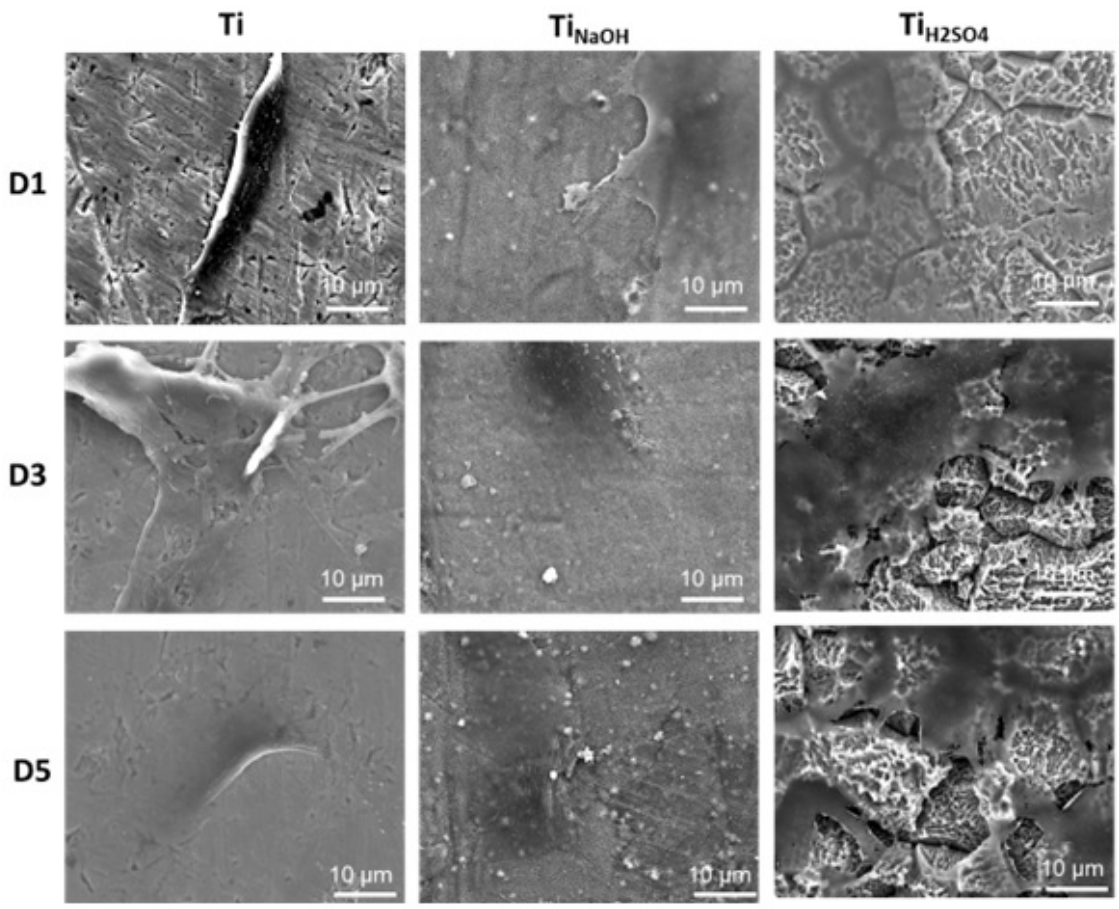

Figure 6.6: SEM images of adhered cells on different surfaces after day 1,3 and 5 of incubation. Images were taken at 1000× magnifications.

the studies shows that all surfaces are able to differentiate the HUVECs completely.

vWF is a glycoprotein that plays a crucial role in blood clotting. vWF is produced during endothelization and stored in the endothelial cells and platelets and is released into the bloodstream in response to injury or inflammation. During a blood vessel injury, the exposed subendothelial collagen activates platelets, which in turn release vWF from their storage granules. vWF acts as a bridge between platelets and the collagen, helping platelets to stick to the site of injury and aggregate to form a platelet plug. vWF also acts as a carrier protein for clotting factor VIII, which is essential for the formation of a stable clot. Results indicated Ti$_{H_2SO_4}$ initiated faster cell differentiation. After 10 days of incubation, the cells have changed to cuboidal shapes on all surfaces, cuboidal

shape of endothelial cells allows for a high surface-to-volume ratio, which is important for the many physiological functions(**Figure 6.7b**). Thus, the studies shows that all surfaces are able to differentiate the HUVECs completely.

6.3.2 SMC toxicity interaction with modified surfaces

The main functionality of SMCs in a blood vessel is to repair vasculature after injury. However, these properties can act disadvantageous by reacting abnormally to post injuries and lead to restenosis. Hence, surfaces which promote SMCs adhesion and proliferation can alleviate restenosis. Thus, it is crucial for researchers to develop surface that selectively prevent SMCs adhesion and promote ECs adhesion for implant longevity.

Surfaces were evaluated for cytocompatability after incubating with SMCs for 24hrs using commercially avialable LDH assay. Results indicated that hydrothermal treatment did not induce toxicity as there was no significant difference between the toxicity levels with cells incubated with Ti, blank (polystyrene well), Ti_{NaOH} and $Ti_{H_2SO_4}$ (**Figure 6.8**).

Surfaces were evaluated for cell viability after incubating with HUVECs for 1, 3 and 5 days using commercially avialable CellTiter-Blue assay. Results indicate that after 1, 3 and 5 days of incubation, no significant difference was seen between Ti, Ti_{NaOH} and $Ti_{H_2SO_4}$. Similarly, no significant difference was observed between the different points (**Figure 6.9**). This implies that SMCs growth rate on different surfaces was in par with cell growth with the blank well(polystyrene).

Surfaces were evaluated for cell adhesion and proliferation after incubating with HUVECs for 1, 3 and 5 days using a fluorescence microscope. Results indicate that after 1 day of incubation, Ti_{NaOH} showed significantly higher cell adhesion compared to $Ti_{H_2SO_4}$ and Ti surface (**Figure 6.10a**). Similar trend was observed after 3 and 5 days of incubation. Similarly, the Ti surface showed a significant increase in cell coverage between the different time points (**Figure 6.10b**). However, $Ti_{H_2SO_4}$ showed no significant increase in cell count between different time points (**Figure**

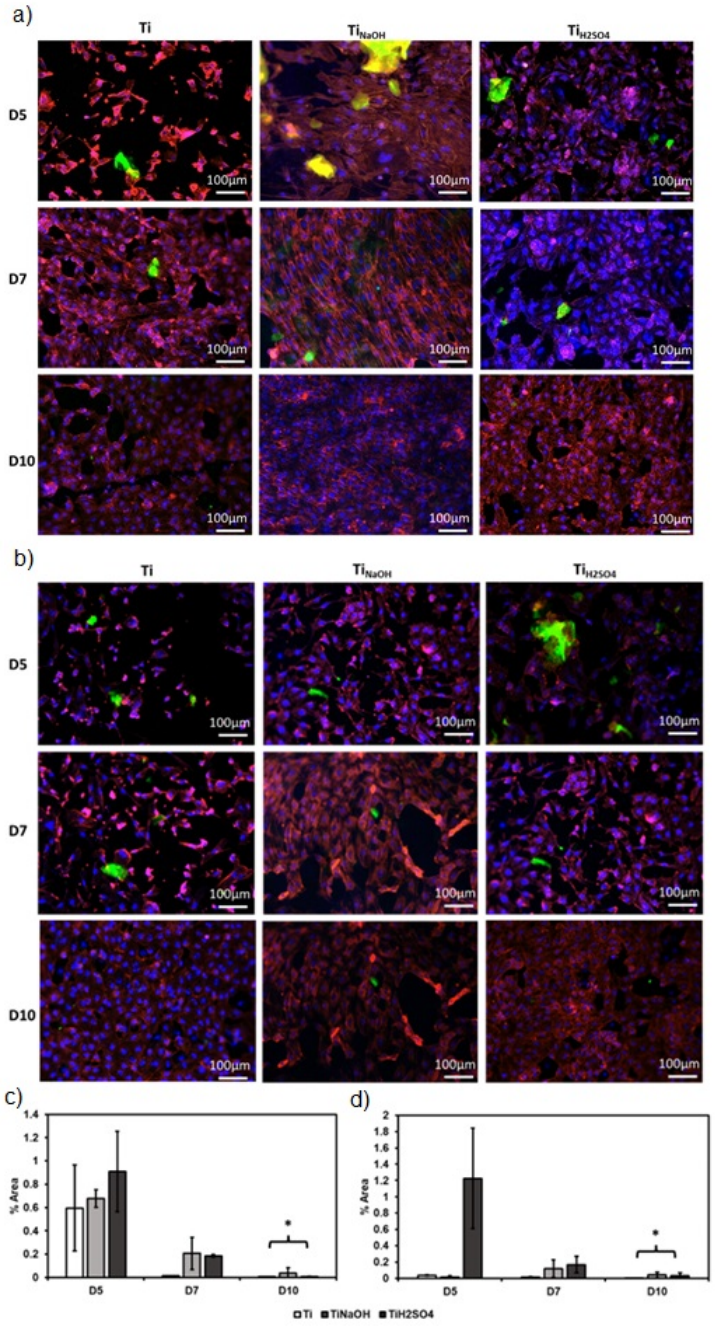

Figure 6.7: a) Fluorescence microscope images of HUVECs along with VE-Cadherin after day 5,7 and 10 of incubation. (b) Fluorescence microscope images of HUVECs along with vWF after day 5,7 and 10 of incubation.. (c) Percentage area coverage of VE- cadherin after day 5,7 and 10 of incubation. (d) Percentage area coverage of vWF after day 5,7 and 10 of incubation.

6.10c). Cell count studies showed that cells had significantly higher cells on day 1,3 and 5 compared to $Ti_{H_2SO_4}$ and Ti. $Ti_{H_2SO_4}$ surface had the lowest cells compared to TiNaOH and Ti. This is mainly

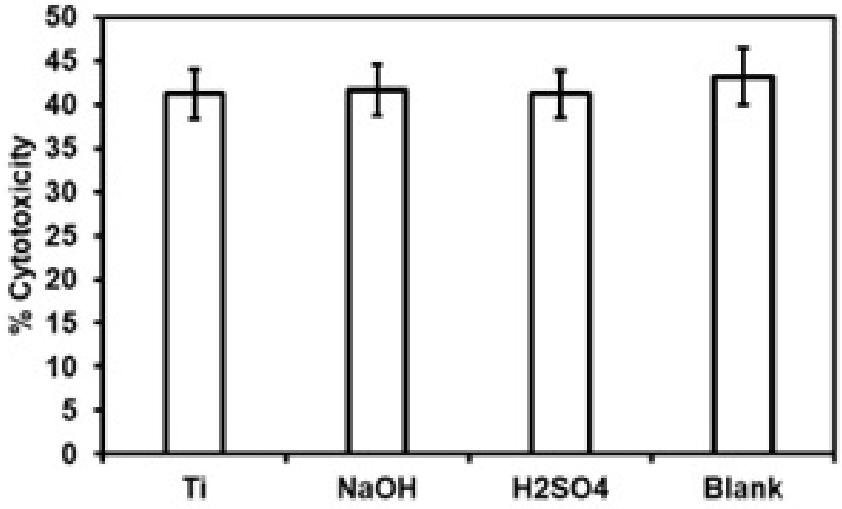

Figure 6.8: Cell cytotoxicity for SMCs exposed to different surfaces after 24 hrs measured using the LDH assay. The error bar represents the standard deviation.

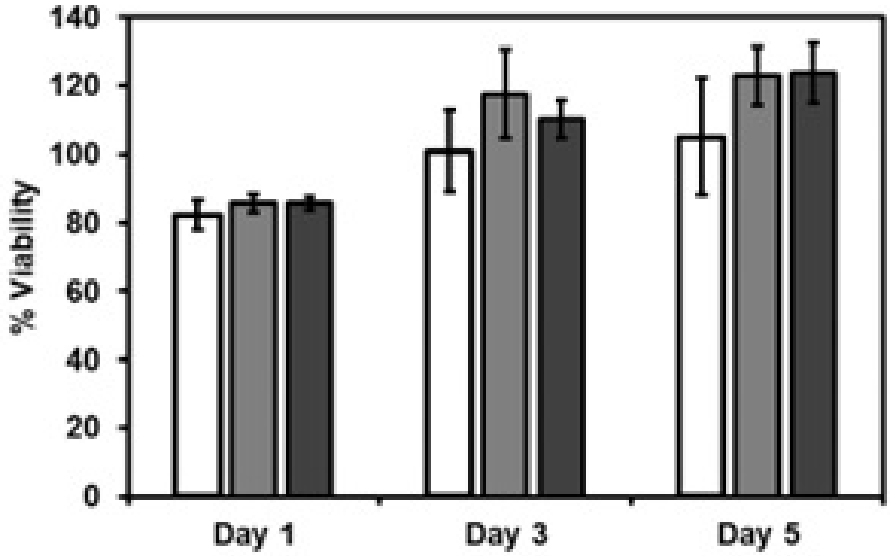

Figure 6.9: Cell viability for SMCs exposed to different surfaces measured after day 1,3 and 5 using the cell viability assay. The error bar represents the standard deviation.

due to the interaction of cells with different surface morphology, $Ti_{H_2SO_4}$ with the micro-nano surface features prevents SMCs spreading and proliferation. This is because SMCs are larger in size, and they need to adhere and spread to proliferate and $Ti_{H_2SO_4}$ micron scale polygon features prohibit spreading. Thus, $Ti_{H_2SO_4}$ has the lowest SMCs adhesion and proliferation compared to

Ti_{NaOH} and Ti.

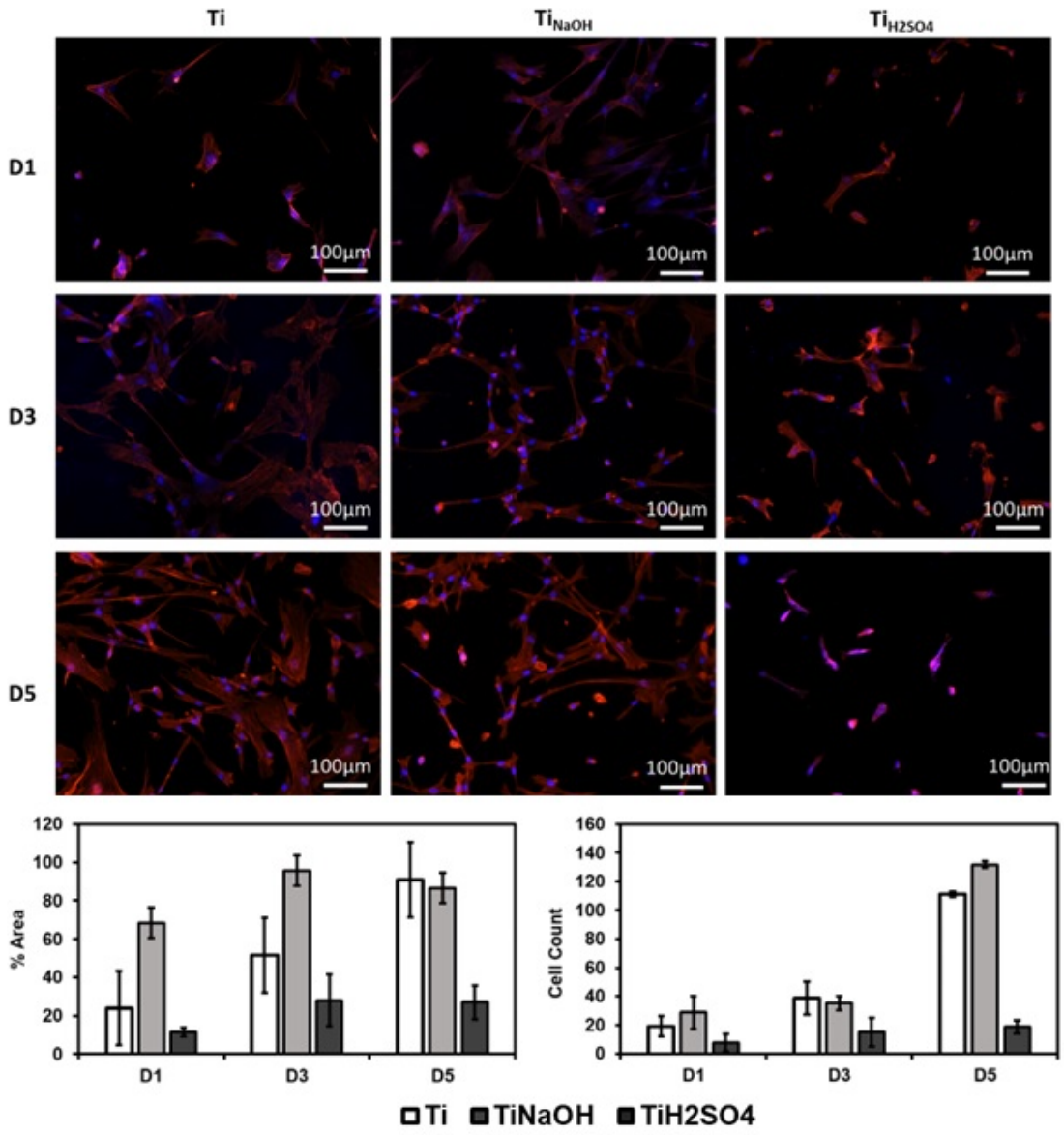

Figure 6.10: a)Fluorescence microscope images SMCs stained with DAPI and rhodamine–phalloidin on different surfaces after day 1,3 and 5 of incubation. b) Percentage area coverage of cells on different surfaces after 1,3 and 5 of incubation. c) Number of cells adhered to the surface stained with DAPI calculated using ImageJ. The error bar represents the standard deviation. (*$p < 0.05$)

Surfaces were evaluated for cell morphology after incubating with HUVECs for 1, 3 and 5 days using a SEM. Results indicated that Ti surface enables the cells to spread and Ti_{NaOH} surface with

planar fibrous nano structures promotes higher cell spreading. However, the $Ti_{H_2SO_4}$ surface with micron scale pyramid features restricted cell spreading significantly and this corroborates with the cell adhesion and proliferation results (**Figure 6.11**).

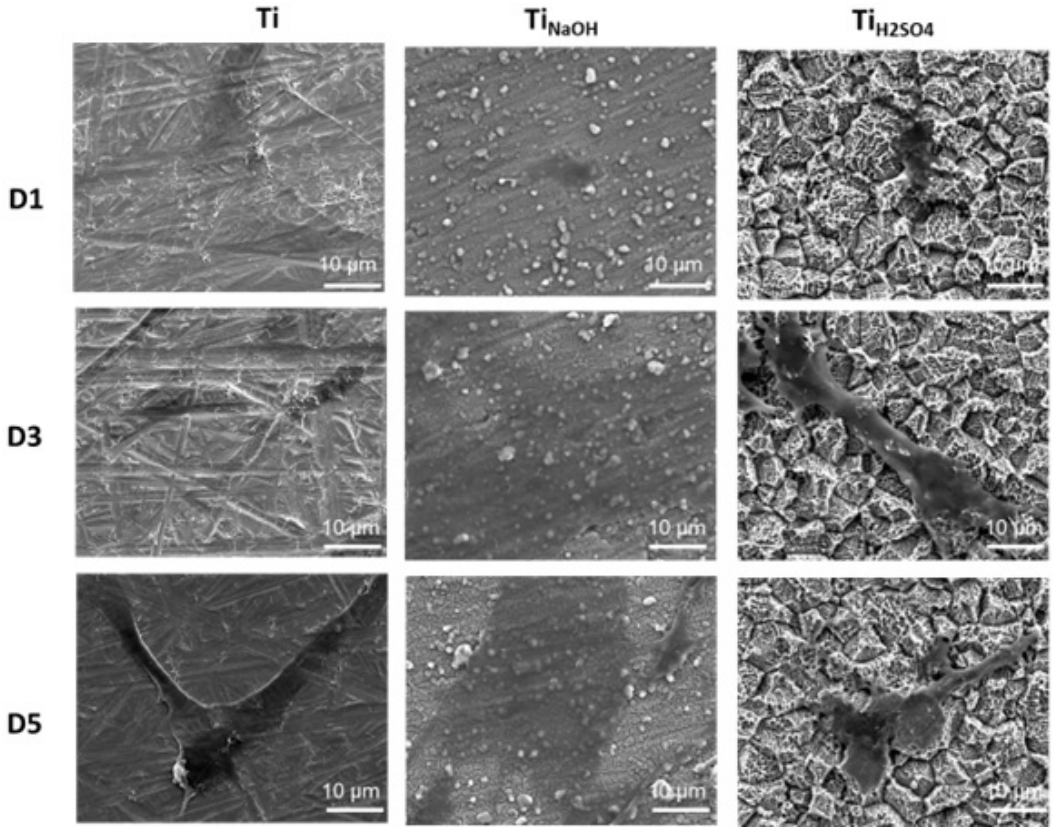

Figure 6.11: SEM images of adhered cells on different surfaces after day 1,3 and 5 of incubation. Images were taken at 1000× magnifications.

Surfaces were evaluated for cell differentiation after incubating with SMCs for 5,7 and 10 days using an immunofluorescence staining assay. Recent genetic lineage tracing studies have shown that SMCs phenotypic switching directly promotes atherosclerosis. Calponin is a protein that is found abundant in smooth muscle cells, it regulates cell contraction and it's considered a reliable marker for SMC differentiation. Myosin Heavy Chain (MYH) is a cytoplasmic structural protein present in SMCs, it influences the mechanical properties of the cells. This is expressed during SMCs development and differentiation. Results indicated TiNaOH initiated faster cell differentiation

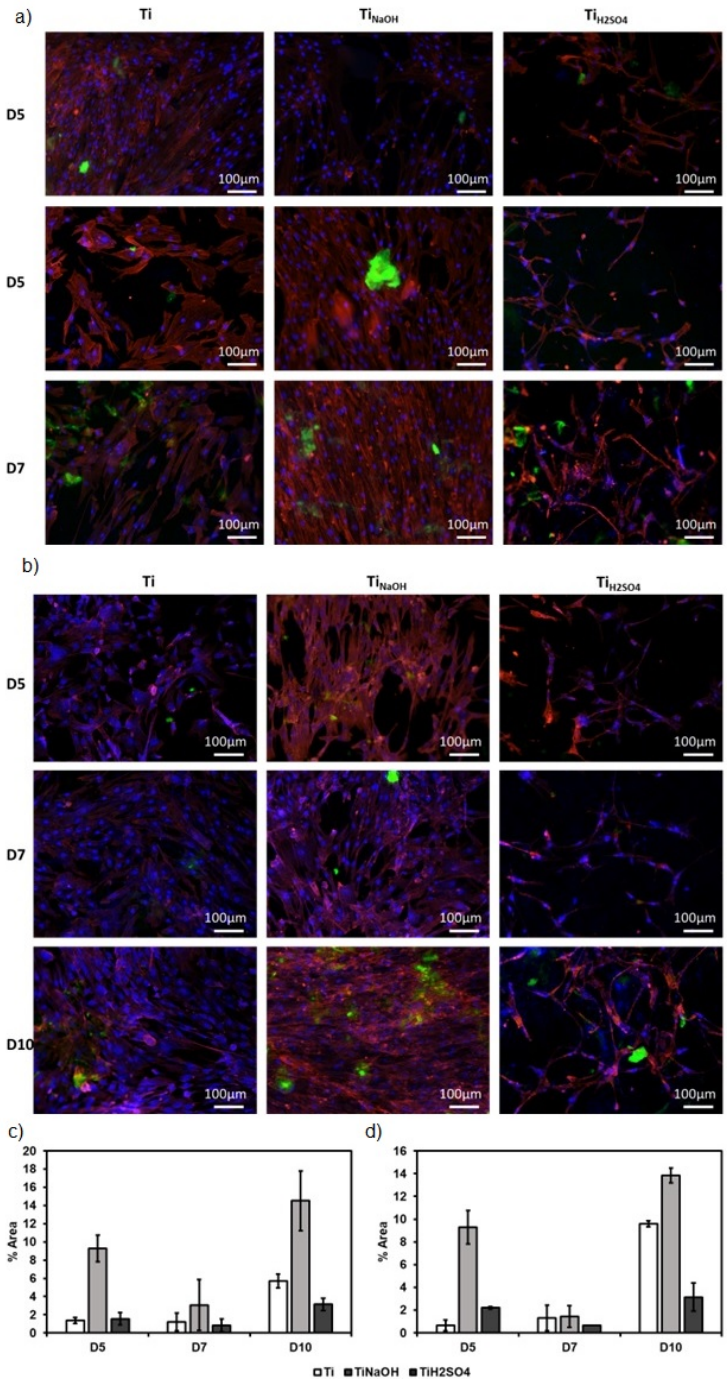

Figure 6.12: a) Fluorescence microscope images of SMCs along with calponin after day 5,7 and 10 of incubation. b) Fluorescence microscope images of SMCs along with MYH after day 5,7 and 10 of incubation. (c) Percentage area coverage of calponin after day 5,7 and 10 of incubation. (d) Percentage area coverage of MYH after day 5,7 and 10 of incubation.

throughout the entirety of the study (**Figure 6.12a and Figure 6.12b**). $Ti_{H_2SO_4}$ had the lowest expression of both calponin and MYH at different timepoints compared to Ti_{NaOH} and Ti(Figure 6.12c and Figure 6.12d).

6.4 Conclusion

The single layer of endothelial cells lining the blood vessels plays a major role in maintaining vascular hemostasis. After stenting procedure, significant injuries are done to the endothelial cell layer. These injuries leads to inflammation and development of neointimal hyperplasia. Restenosis after stent implantation has been primarily due to smooth muscle cell proliferation. Hence, it's crucial to develop an implant surface which prevents smooth cell adhesion and proliferation. Previous work by the author has shown improved antithrombogenic properties, with reduced platelet adhesion and activation compared to smooth titanium surface, which indicates they are promising candidates for cardiovascular implant applications. Titanium surfaces hydrothermally treated with sodium hydroxide and sulfuric acid separately to develop two different surface morphologies. Titanium treated with sodium hydroxide solution led to a planar fibrous surface with etched grain boundaries. Titanium treated with sodium hydroxide solution led to a 3D-like microscale pyramidical structures with nanoscale pits. Surface wettability studies showed that both hydrothermally treated surfaces were significantly hydrophilic compared to control titanium surface. Surfaces were evaluated for cytocompatability, cell viability, adhesion, proliferation, and differentiation with both endothelial cells and smooth muscle cells. Modified surfaces did not induce any toxicity after 24 hrs of HUVECs and SMCs incubation. Cell adhesion and proliferation studies showed that sulfuric acid treatment prevented smooth muscle cells proliferation. However, this surface promoted endothelial cell adhesion and proliferation as the morphology didn't influence smaller endothelial cells. Differentiation studies showed that the sulfuric acid treated surface had higher endothelial cell differentiation on the surface with morphologically changed cells. Hence, this surface proves to be a great fit for cardiovascular implants.

6.5 References

[1] "2020 Heart Disease and Stroke Statistical Update Fact Sheet: Global Burden of Disease," American Heart Association, 2020, doi: 10.1161/CIR.0000000000000757.

[2] C. C. Zwack, C. Smith, V. Poulsen, N. Raffoul, and J. Redfern, "Information Needs and Communication Strategies for People with Coronary Heart Disease: A Scoping Review," International Journal of Environmental Research and Public Health 2023, Vol. 20, Page 1723, vol. 20, no. 3, p. 1723, Jan. 2023, doi: 10.3390/IJERPH20031723.

[3] M. Faisaluddin et al., "Cardiovascular Outcomes of Redo-Coronary Artery Bypass Graft Versus Percutaneous Coronary Intervention of Index Bypass Grafts Among Acute Coronary Syndrome: Regression Matched National Cohort Study: Running Title: PCI vs. Redo-CABG in ACS With Prior CABG," Curr Probl Cardiol, p. 101580, Jan. 2023, doi: 10.1016/J.CPCARDIOL.2022.101580.

[4] D. Buccheri, D. Piraino, G. Andolina, and B. Cortese, "Understanding and managing in-stent restenosis: a review of clinical data, from pathogenesis to treatment," J Thorac Dis, vol. 8, no. 10, p. E1150, 2016, doi: 10.21037/JTD.2016.10.93.

[5] C. Chaabane, F. Otsuka, R. Virmani, and M. L. Bochaton-Piallat, "Biological responses in stented arteries," Cardiovasc Res, vol. 99, no. 2, pp. 353–363, Jul. 2013, doi: 10.1093/CVR/CV15.

[6] B. E. Claessen, J. P.S. Henriques, and G. D. Dangas, "Clinical studies with sirolimus, zotarolimus, everolimus, and biolimus A9 drug-eluting stent systems," Curr Pharm Des, vol. 16, no. 36, pp. 4012–4024, Jan. 2010, doi: 10.2174/138161210794454941.

[7] T. F. Lüscher et al., "Drug-Eluting Stent and Coronary Thrombosis," Circulation, vol. 115, no. 8, pp. 1051–1058, Feb. 2007, doi: 10.1161/CIRCULATIONAHA.106.675934.

[8] O. F. Khan and M. v. Sefton, "Endothelialized biomaterials for tissue engineering applications in vivo," Trends Biotechnol, vol. 29, no. 8, p. 379, Aug. 2011, doi: 10.1016/J.TIBTECH.2011.03.004.

[9] F. Clauder, A. S. Czerniak, S. Friebe, S. G. Mayr, D. Scheinert, and A. G. Beck-Sickinger, "Endothelialization of Titanium Surfaces by Bioinspired Cell Adhesion Peptide Coatings," vol. 18, p. 32, 2019, doi: 10.1021/acs.bioconjchem.9b00573.

[10] M. Pflaum et al., "Endothelialization and characterization of titanium dioxide-coated gas-exchange membranes for application in the bioartificial lung," Acta Biomater, vol. 50, pp. 510–521, Mar. 2017, doi: 10.1016/J.ACTBIO.2016.12.017.

[11] V. K. Manivasagam, R. M. Sabino, Prem Kantam, and K. C. Popat, "Surface modification strategies to improve titanium hemocompatibility: a comprehensive review," Mater Adv, vol. 2, no. 18, pp. 5824–5842, Sep. 2021, doi: 10.1039/D1MA00367D.

[12] P. Hameed, V. K. Manivasagam, M. Sankar, K. C. Popat, and G. Manivasagam, "Nanofibers and nanosurfaces," in Springer Series in Biomaterials Science and Engineering, vol. 16, Springer Science and Business Media Deutschland GmbH, 2021, pp. 107–130. doi: 10.1007/978-981-33-6252-9_4.

[13] A. Cornelissen and F. J. Vogt, "The effects of stenting on coronary endothelium from a molecular biological view: Time for improvement?," J Cell Mol Med, vol. 23, no. 1, p. 39, Jan. 2019, doi: 10.1111/JCMM.13936.

[14] J. Zong, Q. He, Y. Liu, M. Qiu, J. Wu, and B. Hu, "Advances in the development of biodegradable coronary stents: A translational perspective," Mater Today Bio, vol. 16, p. 100368, Dec. 2022, doi: 10.1016/J.MTBIO.2022.100368.

[15] J. Vishnu et al., "Hydrothermal treatment of etched titanium: A potential surface nano-modification technique for enhanced biocompatibility," Nanomedicine, vol. 20, Aug. 2019, doi: 10.1016/j.nano.2019.102016.

[16] V. K. Manivasagam, G. Perumal, H. S. Arora, and K. C. Popat, "Enhanced antibacterial properties on superhydrophobic micro-nano structured titanium surface," J Biomed Mater Res A, 2022, doi: 10.1002/JBM.A.37375.

[17] J. W. Yau, H. Teoh, and S. Verma, "Endothelial cell control of thrombosis," BMC Cardiovasc Disord, vol. 15, no. 1, Oct. 2015, doi: 10.1186/S12872-015-0124-Z.

[18] S. Reitsma, D. W. Slaaf, H. Vink, M. A. M. J. van Zandvoort, and M. G. A. Oude Egbrink, "The endothelial glycocalyx: composition, functions, and visualization," Pflugers Archiv , vol. 454, no. 3, p. 345, Jun. 2007, doi: 10.1007/S00424-007-0212-8.

[19] S. L. Fink and B. T. Cookson, “Apoptosis, pyroptosis, and necrosis: Mechanistic description of dead and dying eukaryotic cells,” Infection and Immunity, vol. 73, no. 4. American Society for Microbiology (ASM), pp. 1907–1916, Apr. 2005. doi: 10.1128/IAI.73.4.1907-1916.2005.

[20] V. Kuete, O. Karaosmanoğlu, and H. Sivas, “Anticancer Activities of African Medicinal Spices and Vegetables,” Medicinal Spices and Vegetables from Africa: Therapeutic Potential Against Metabolic, Inflammatory, Infectious and Systemic Diseases, pp. 271–297, Jan. 2017, doi: 10.1016/B978-0-12-809286-6.00010-8.

[21] V. K. Manivasagam et al., “Surface-modified WE43 magnesium alloys for reduced degradation and superior biocompatibility,” In vitro models, vol. 1, no. 3, pp. 273–288, Jun. 2022, doi: 10.1007/s44164-022-00016-x.